

Discovery and Characterization of the Highest Proper Motion Stars

A DISSERTATION

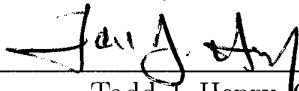
Presented in Partial Fulfillment of Requirements for the
Degree of Doctor of Philosophy
in the College of Arts and Sciences
Georgia State University

2004

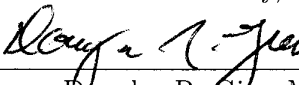
by

Wei-Chun Jao

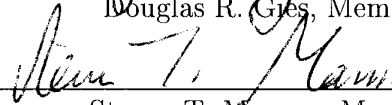
Committee:



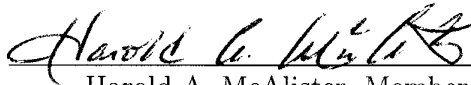
Todd J. Henry, Chair



Douglas R. Gies, Member



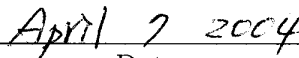
Steven T. Manson, Member



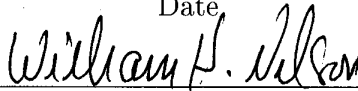
Harold A. McAlister, Member



Paul J. Wiita, Member



Date



William H. Nelson, Chair

Department of Physics and Astronomy

Abstract

This dissertation presents methods and results of searching for missing stars in the solar neighborhood based on a rigorous selection of the highest proper motion stars. The MOTION sample of stars discussed in this work includes all systems with proper motions greater than $1''0/\text{yr}$. As of January 1, 2003, there are 549 systems and 653 individual stars in the sample. We characterize all of these systems astrometrically, photometrically and spectroscopically.

Data supporting this investigation have been taken as part of CTIOPI (Cerro Tololo Inter-American Observatory Parallax Investigation), for which data acquisition and reduction techniques are discussed. In addition to the production of trigonometric parallaxes, proper motions, and *VRI* photometry, atmospheric refraction is addressed in detail for the astrometric observations, and the photometry is used to convert the relative parallaxes to absolute parallaxes. We report first ever parallax measurements for 46 MOTION systems. Five of these are new RECONS (Research Consortium on Nearby Stars) systems within 10 pc of the Sun — LHS22, LHS145, LHS263, LHS337, and DENI1048–3956. An additional 25 systems are within the 25 pc NStars horizon. These parallax results cover more than 50% of the MOTION systems that previously had no trigonometric parallaxes. We also provide *VRI* photometry for 86 MOTION systems that previously had incomplete or no such photometry. Of these, 15 systems are photometrically estimated to be within 25 pc. In addition, we give new spectroscopy results for 43 MOTION systems.

Because of the inherent kinematic bias in the sample, a full $\sim 15\%$ (82) of the MOTION systems prove to be subdwarfs, an important sample that will be useful for future investigations. In this sample we have identified the first M-type subdwarf binary, LHS189AB, and the first subdwarf/white dwarf binary, LHS193AB. Finally, nine new companions have been confirmed as proper motion companions to stars observed during CTIOPI. Five of these (LHS193B, LHS206B, LHS225B, LHS300B and LHS463B) are members of MOTION systems.

Dedication

This disseration is dedicated to my dad, mom, wife, two lovely children and my sister. Their constant love and caring are every reason for where I am and what I am. My gratitude and my love to them are beyond words.

Acknowledgements

There are a lot of people who helped to make this dissertation a reality. This is an opportunity for me to thank them all for their assistance.

The greatest thanks goes to my advisor, Todd Henry. I thank him for introducing me to this nearby stars world. Although I have never had a chance to ride that famous spaceship with him to wander around the solar neighborhood, at least I can observe these little twinkling stars under his kind guidance. Virgo like me is “meticulous and reliable” but I am only one millionth of Todd. Aside from his help in my research, I have learned how to being a cautious and trustworthy scientist. Thanks to him for treating me like a member of his family and letting me feel he is like my brother who I have never had. I am proud to be his first ever student. Thank you, muchas gracias and hsieh-hsieh.

Building the astrometry pipeline is a difficult task for a student without any astrometry experience. However, I am lucky to know two of the greatest astronomers, Phil Ianna and Barbara McArthur. I am most grateful to Phil, a national treasure of astrometry. It is my honor to meet and learn the beauty of astrometry from him. I thank Barbara for assisting me in building the parallax pipeline after exchanging hundreds of emails.

This study would not be possible without the great teamwork from the Georgia State RECONS members. I need to give my deepest thanks to John Subasavage, Misty Brown, Jennifer Winters, Thom Beaulieu and Charlie Finch. Thanks for their great assistance in reducing more than 150GB of data and finding all kinds of bugs of my pipelines. I also want to thank our two Chilean collaborators, Edgardo Costa and Rene Mendez for their suggestions to improve my reduction manual.

I give my deep appreciation to Douglas Gies, Hal McAlister, Steven Manson and Paul Wiita for agreeing to be members of my dissertation committee and for reading my dissertation thoroughly and giving me valuable suggestions. Friendly and helpful professors are a true necessity to the success of a dissertation and I am grateful for

their help.

Collecting the MOTION list would not have been easy without the pioneering work of Christina Williams. I thank her for generating the beta version of the MOTION list. Other individuals who also have earned my great appreciation for their guidance and assistance include Mike Begam (DCR refraction), Fritz Benedict (Gaussfit), Don McCarthy (Kuiper Telescope), Doug Mink (WCStools), Dave Monet (Astrometry) and Myles Standish (DE405). Their generous assistance led to the wonderful scientific results included here.

Of course, I want to thank the humorous, lovely, and knowledgeable graduate students in Astronomy at Georgia State University. They always gave me appropriate suggestions for my research, when using the computers, in helping me understand the culture of this country, or even being the best moving crews. Studying here as a foreigner would have been hard without them. Finally, another group of people who also were of great help throughout my research is the staff at CTIO, and the lovely and generous Chileans.

Contents

List of Tables	x
List of Figures	xii
1 Introduction	1
1.1 Surveys for High Proper Motion Objects	2
1.1.1 LHS and NLTT Catalogs	2
1.1.2 Lowell Proper Motion Survey	5
1.1.3 Wroblewski/Torres/Costa Southern Proper Motion Survey	6
1.1.4 SUPERBLINK Survey	7
1.1.5 Liverpool-Edinburgh High Proper Motion Survey	8
1.1.6 Southern Proper Motion Survey by Scholz <i>et al.</i>	8
1.1.7 Calán-ESO Proper Motion Survey	9
1.2 The MOTION Sample	12
1.2.1 Notes on Individual Objects	14
1.2.2 MOTION Stars Distribution	17
1.2.3 Organization of this Dissertation	17
2 Astrometry	20
2.1 Parallax Observations	20
2.2 Parallax Displacement	22
2.2.1 Parallax Displacement in Ecliptic Coordinates	23
2.2.2 Parallax Displacements in the RA and DEC Directions	25
2.2.3 The Uncalibrated Coordinate Problem	28
2.3 Differential Color Refraction	28
2.3.1 Measuring DCR Empirically	33
2.3.2 The Final DCR Model for CTIOPI	34

2.4	Astrometric Reductions	38
2.4.1	Initial Steps	38
2.4.2	Least Squares Reduction of Images Taken at Many Epochs . .	40
2.5	Conversion of Relative to Absolute Parallax	42
2.6	CTIOPI Parallax Calibration Stars and Quality Check	43
2.7	Parallax Results for MOTION Stars	46
2.7.1	Notes on Individual Stars	47
3	Photometry for MOTION Stars	52
3.1	<i>VRI</i> Photometric Observations	52
3.2	Photometry Reductions	53
3.3	MOTION Sample <i>VRI</i> Photometry Results	54
3.4	Reliability Checks and Comparison with Other Observations	55
3.5	MOTION Sample <i>JHK_s</i> Photometry	63
3.6	MOTION Sample Photometric Parallaxes	63
3.7	Reduced Proper Motion Diagram	66
4	Spectroscopy for MOTION Stars	70
4.1	Spectroscopic Observations	70
4.2	Spectroscopic Data Reduction and Results	71
4.3	Subdwarfs Confirmed by Spectroscopy	81
4.4	Subdwarfs Reconfirmed via the HR Diagram and the Reduced Proper Motion Diagram	82
4.5	Subdwarf Spectroscopic Subtypes	86
4.6	Estimated Spectral Types for Additional MOTION Stars	88
4.7	Notes on Individual Objects	90
5	New MOTION stars components	92
5.1	Companion Search	92
5.2	Astrometric Confirmation of New Doubles	94
5.3	Differential Photometry	104
5.4	New Component for LHS206	109
6	Discussion	110
6.1	Probabilities that MOTION Stars are Nearby	110
6.2	Space Distribution of MOTION Stars of Different Luminosity Classes	113
6.3	Tangential Velocity Distribution of MOTION Stars	114

6.4	Subdwarf Multiplicity	118
6.5	The Mass-Luminosity Relation for Subdwarfs	120
6.6	Summary	122
A	Complete List of MOTION Sample	123
B	MOTION Stars Parallax, Photometry and Spectroscopy	145
C	Least Squares Method for DCR	161
D	CTIOPI Photometry Reduction Manual	164
D.1	Before It Starts	166
D.2	Organize Your Processed Data	166
D.3	Standard Stars	167
D.3.1	Modify Parameters in <i>PHOT</i> Task	168
D.3.2	Make Observation Files	169
D.3.3	Make a Master List of Instrumental Magnitudes	169
D.3.4	Make Configure File and Standard <i>VRI</i> Magnitude Table . . .	169
D.3.5	Final Steps for Standard Stars	172
D.4	Science Stars	172
D.4.1	Examine Science Images	178
D.4.2	Remove Cosmic Rays	179
D.4.3	Tag Isolated Stars in an Crowd Field	179
D.4.4	Apply Aperture Correction	179
D.4.5	Get Instrumental Magnitudes for Science Stars	180
D.4.6	Make Science Star Observation Files and Master List Files . .	180
D.4.7	Calculate Apparent Magnitude	180
D.5	Transformation Equations	181
D.6	Remark	182
E	CTIOPI Parallax Reduction Manual	183
E.1	Introduction	185
E.2	Install <i>redpi</i> Package	185
E.2.1	<i>redpi</i> Package Usage Guide	185
E.2.2	Reduce the Raw Data	189
E.3	SExtractor – Get the Centroid	189
E.3.1	Install SExtractor	189

E.3.2	Brief Introduction to SExtractor	190
E.3.3	Configuration and Parameter File	190
E.3.4	Running SExtractor	191
E.4	<i>VRI</i> Photometry Stars	197
E.5	JPL DE405	198
E.6	Generate Lots of Files	198
E.7	Running Gaussfit	200
E.8	Finalize the Parallax Reduction	202
E.9	Concerning gauss.uty and the IDL Program	206

List of Tables

1.1	Statistics for the HPM surveys discussed.	11
1.2	The MOTION sample statistics on the sky	18
1.3	The new MOTION stars added after 2003 January 1.	19
2.1	The parallax standard stars from CTIOPI.	44
2.2	CTIOPI MOTION parallax results	50
3.1	MOTION <i>VRI</i> photometry results	59
3.2	The details of photometric parallax relations from RECONS and white dwarf sample	65
3.3	Photometric distance estimates for MOTION stars	67
4.1	MOTION stars spectroscopy results	75
4.2	Wavelength ranges for certain spectroscopic indices	81
4.3	MOTION subdwarfs spectroscopic indices	84
5.1	Astrometry data for CTIOPI resolved systems	101
5.2	Magnitude difference for CTIOPI resolved systems	107
5.3	Astrometry and photometry results for LHS206AB	109
6.1	Probability of MOTION stars within 10pc	112
6.2	MOTION systems spatial distribution in different luminosity classes .	114
6.3	The number of MOTION systems with $V_{tan} > 200$ km/sec	117
6.4	Multiplicity comparison between dwarfs and subdwarfs	119
A.1	MOTION Samples	124
B.1	MOTION stars Parallax, Photometry and Spectroscopy	146
D.1	The apparent magnitude for different aperture size	182

E.1	The input and output files from redpi package.	187
E.2	Parallax data reduction quick reference 1	208
E.3	Parallax data reduction quick reference 2	209
E.4	Parallax data reduction quick reference 3	210

List of Figures

1.1	Proper motion comparison from LHS, LOB, Hipparcos and BSN-LHS	4
1.2	NLTT catalogue distribution	5
1.3	Lowell proper motion survey distribution	6
1.4	WT and SUPERBLINK HPM distribution	7
1.5	Liverpool-Edinburgh HPM Survey	9
1.6	Calán-ESO and Scholz <i>et al.</i> distribution	10
1.7	A MOTION finder chart example	16
1.8	MOTION sample distribution	17
2.1	Parallactic displacement	22
2.2	Parallax in right ascension and declination	24
2.3	The example of parallax factor in the RA and DEC	26
2.4	The discussion of stellar paths with different proper motion.	29
2.5	Stellar coordinate refracted by the Earth atmosphere	30
2.6	Wide passband and normalized spectral energy distribution	32
2.7	The mean refraction for different colors of stars	36
2.8	DCR fitting plots for V , R and I band	37
2.9	Example plot with and without DCR correction	39
2.10	The CTIOPI parallax standard comparison plot	45
2.11	Parallax error vs. time coverage	46
2.12	MOTION parallax results statistics	48
3.1	MOTION VRI results statistics	55
3.2	The VRI photometry S/N and standard star errors	57
3.3	The RECONS VRI photometry comparison with published results	58
3.4	The reduced proper motion H_K vs. $(V - K)$ plot for MOTION stars without parallax	69

4.1	MOTION stars spectroscopy statistics	73
4.2	Spectroscopy from CTIOPI compared with other published results . .	74
4.3	The CaH band indices vs. TiO5 band index	83
4.4	Subdwarfs location on the HR diagram	85
4.5	Re-confirm subdwarfs by reduced proper motion diagram	86
4.6	The spectra comparison between G1191, LHS272, and G1203	87
4.7	The spectra comparison between LHS161, G1356, G1367, G1784, G1825 and G1879	89
4.8	Other MOTION stars without spectra types	90
5.1	New companions finder charts	93
5.2	Histogram of CTIOPI images FWHM analysis	95
5.3	New components searching limit	96
5.4	The CPM pairs confirmation	98
5.5	New components separation from primary stars	99
5.6	Errors in the magnitude differences between 23 companions and their primaries are plotted against separation.	106
5.7	LHS206 finder chart	109
6.1	Distance distributions of MOTION stars of various luminosity classes and proper motions	115
6.2	Tangential velocity histogram of MOTION systems	116
6.3	MOTION dwarfs with $V_{tan} > 200$ km/sec	118
6.4	Mass-Luminosity Relation for M dwarfs	121
D.1	Parameters example for setairmass, phot and photpars	170
D.2	Parameters examples for datapars, centerpars and fitskypars	171
D.3	Parameters for mkimsets and the output file format	173
D.4	Standard star configuration example	174
D.5	Parameters examples for fitparam, mkapfile and evalfit	175
D.6	Output file example from evalfit.pl and standard.pl	176
D.7	Fitparam fitting plot example.	177
E.1	SExtractor configuration file	192
E.2	The example plot from the parallax.stats.pro IDL program	203
E.3	The flow chart of parallax data reduction.	205
E.4	Parallax reduction recording sheet	207

List of Abbreviations

2MASS	Two Micron All Sky Survey
BD	Bonner Durchmusterung
ADS	NASA Astrophysics Data System
AU	astronomical unit
BPMS	Bruce Proper Motion Survey
CDS	Centre de Données astronomiques de Strasbourg
CE	Prefix to star's Calán-ESO Proper Motion Survey catalog number
CNS3	Preliminary version of the third Catalogue of Nearby Stars
CHARA	The Center for High Angular Resolution Astronomy
CTIO	Cerro Tololo Inter-American Observatory
CPM	Common Proper Motion
CTIOPI	Cerro Tololo Inter-American Observatory
DEC	Declination
DENIS	Deep Near Infrared Survey
ESO	European Southern Observatory
FGS	Fine Guidance Sensors
FWHM	Full-width Half-maximum
Gl(GJ)	Prefix to star's CNS3 number
HD	Prefix to star's Henry Draper Catalogue number
HIP	Prefix to star's Hipparcos catalog number
HPM	High Proper Motion
HST	Hubble Space Telescope
IDL	Iterative Data Language
IPAC	Infrared Processing and Analysis Center
IRAF	Image Reduction and Analysis Facility
JPL	Jet Propulsion Laboratory
KPNO	Kitt Peak National Observatory

LHS	Luyten Half-Second Catalog
LOB	Lowell HPM survey from Lowell Observatory Bulletin
NASA	National Aeronautics and Space Administration
NSF	National Science Foundation
NLTT	New Luyten Two Tenth Arcsecond Catalog
NOAO	National Optical Astronomy Observatory
Perl	Practical Extraction and Reporting Language
POSS-I	The National Geographic Society, Palomar Observatory Sky Atlas
POSS-II	The Second Palomar Observatory Sky Survey
RA	Right Ascension
RECONS	Research Consortium on Nearby Stars
S/N	Signal to noise ratio
SCR	Prefix to stars's SuperCOSMOS RECONS survey
SIMBAD	Astronomical database administered by the CDS (France)
SMARTS	Small and Moderate Aperture Research Telescopes System
WT	Wroblewski and Torres Southern Proper Motion Survey
YPC	Yale Parallax Catalog

Chapter 1

Introduction

The solar vicinity provides astronomers with the foundation of stellar astronomy and much of our understanding of the Galactic population, and holds a special attraction for the general public. A wide range of astrophysical problems are addressed by studying the nearby star population, including such diverse fields as star formation, stellar evolution and mass transfer, the stellar luminosity and mass functions, Galactic dynamics, and recently, searches for planetary systems. All of these problems rely at least in part on an accurate census of nearby stars.

In the early 1940s, the most complete sample of nearby stars was collected by the astrometry pioneer Peter van de Kamp (1940). This list included only 34 systems within 5 pc of the Sun. A turning point in nearby star research occurred when the first 20 pc compendium was finished by Gliese (1957), with later updates reaching to 25 pc by Gliese (1969) and Gliese and Jahreiß (1979, 1980). Advancements in observational techniques and telescopes have led astronomers to continue identification of more nearby stars, typically those that are intrinsically faint. In 1991, Gliese and Jahreiß (1991) compiled data from the available sources and released the Third Catalogue of Nearby Stars (CNS3). This catalog contains 3803 stars within 25 pc of the Sun and depends primarily on the unpublished preliminary version of the new *General Catalogue of Trigonometric Parallaxes* prepared by van Altena and collaborators.

However, a recent nearby star census indicates that $\sim 35\%$ of stellar systems are still “missing” within 10 pc of the Sun (Henry et al. 1997), which implies that even more systems are missed beyond 10 pc. To discover and characterize the missing members, NASA and NSF launched the NStars Project in 1998. The primary goal of NStars is to provide the most complete census of stars within 25 pc of the Sun, so that astronomers will have a comprehensive, volume-limited sample that can be

used to investigate the true nature of our solar neighborhood.

Historically, nearby stars have been found using two methods — high proper motions and photometric distance estimates. In many ways, the high proper motion (HPM) samples offer the best source lists for nearby star searches simply because given the random motions of stars in the Galaxy, those that are closest will appear to have the largest proper motions.

The subject of this thesis is the collection of available and new data on all objects with proper motions greater than $1''0/\text{yr}$, and the scientific investigation (proper motions, parallaxes, $VRIJHK_s$ photometry, and optical spectroscopy) of the entire sample. The following section will outline the various HPM catalogs used to generate the sample.

1.1 Surveys for High Proper Motion Objects

1.1.1 LHS and NLTT Catalogs

Among the current HPM catalogs, the most extensive is that compiled by Willem Luyten. The second edition of the *Luyten Half-Second Catalogue* (hereafter, LHS) was published by Luyten (1979a). It supersedes the “*Catalogue of Stars with Motions exceeding $0''.5/\text{yr}$ annually*” published by Luyten (1955). LHS contains 3601 stars with annual proper motions greater than $0''.5$ and 869 stars with lower proper motions. It is based on a long-term effort to discover HPM objects using pairs of photographic plates from the Palomar Survey, which covers declinations north of -33° and can reach $m_{pg} \sim 21.1$ and $m_R \sim 19.4$. South of the Palomar declination limit, the Bruce Proper Motion Survey (Luyten 1963, hereafter, BPMS) is the main source of HPM stars. However, the BPMS provides only blue-band photographic photometry, and only reaches to $m_{pg} \sim 15.5$ or 16.0 . In addition to the Palomar and BPMS Surveys, a small southern area survey taken by the Palomar Schmidt Telescope from 1963 to 1973, often called the “Whiteoak extension”, covers a region between 21^h45^m and 4^h in right ascension and south to -45° . Finder charts for many of the HPM stars from the three efforts are found in the *LHS Atlas*, by Luyten and Albers (1979).

The completeness of LHS for the Palomar region ($\delta \geq -33^\circ$ and $|b| > 10^\circ$) has been discussed by Dawson (1986), who reached several important conclusions. First, he found that north of -33° , the LHS is $\sim 90\%$ complete for stars with $\mu > 0''.5/\text{yr}$ and brighter than $m_R = 18$. Second, he emphasized that Luyten had a $2''.5/\text{yr}$ threshold for his HPM star search, in order to minimize source confusion errors (except at the

north Galactic pole where the limit is $3''/\text{yr}$). Therefore, any faint stars ($m_R > 18.0$) with large proper motion ($\mu > 2''.5$) are missing from LHS. Third, they expected that ~ 40 binary systems with $\Delta m < 0.5$ mag and separation less than $10''$ were missed in LHS because the stellar images are elongated and companions were not seen during the blinking process. Finally, ~ 40 faint companions with $\Delta m > 3$ were also missed during the blinking process.

Many of the stars in LHS have had notoriously inaccurate coordinates, in large part because of Luyten's effort to keep his stars "hidden" (Roberta Humphreys, U. Minnesota, private communication). To remedy the coordinate problem, the entire LHS was recently refined by Bakos et al. (2002) (hereafter, BSN-LHS), who used the first Palomar Observatory Sky Survey (POSS-I, Abell (1959)) and the second Palomar Observatory Sky Survey (POSS-II, Reid et al. (1991)) plates to derive more accurate positions. For most of the brighter stars ($m_R \lesssim 12$), the positions and proper motion data have been replaced by the authors with accurate Tycho-2/Hipparcos data, which are typically accurate to $1''$ in position and a few tens of milliarcseconds per year in μ . For the fainter stars, the revised BSN-LHS positions typically have $2''$ error, but in a few cases the errors reach $\sim 8''$. This is a huge improvement over coordinates in LHS.

However, as shown in Gould and Salim (2003) and Hambly et al. (2004), the proper motions in BSN-LHS are inferior to Luyten's because accurate determinations of μ require a long time between plate epochs, and BSN often did not have sufficient time separation for a reliable result. Comparisons of proper motions from the original LHS, the Lowell Survey (which will be discussed in Section 1.1.2), Hipparcos, and BSN-LHS are shown in Figure 1.1. The top two plots show 219 stars from LHS, Hipparcos and BSN-LHS. The bottom two plots show 253 stars from LHS, the Lowell survey and BSN-LHS. These clearly show that the revised proper motions from BSN-LHS are consistent with other catalogs (as long as there are no flags or comments on the objects), but the differences are rather larger than desired.

Luyten cataloged additional HPM stars in his *New Luyten Catalogue of Stars with Proper Motions Larger than Two Tenths of an Arcsecond* (Luyten 1979b, hereafter, NLTT). This compendium includes 58,845 stars from more than 800 Palomar Proper Motion Survey plates found to have relative annual proper motions exceeding $0''.18$. Because the NLTT is an extension of the LHS, it has a similar declination limit, resolution limit, and magnitude limits ($m_{pg} \sim 21.2$ and $m_R \sim 19.8$). The distribution of NLTT entries is shown in Figure 1.2. Clearly, this catalog has poor coverage within about 10° of the Galactic plane and south of -33° . Gould and Salim (2003) have

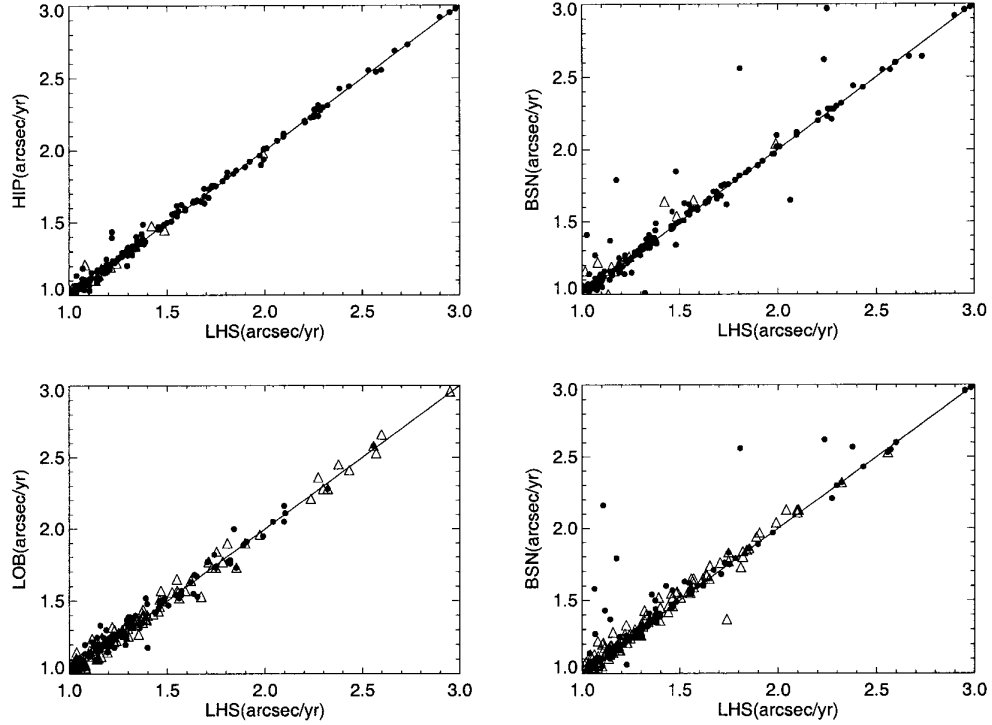


Figure 1.1: The top two plots show 202 stars (filled circles) with proper motions from LHS, Hipparcos and BSN-LHS. All 202 stars from BSN-LHS have flags which indicate various comments on the quality of plates. The extra 17 stars (triangles) have no comments in the BSN-LHS. The same definitions hold for the bottom plots from LHS, LOB (Lowell HPM Survey) and BSN-LHS for 253 stars (123 systems with comments and 130 systems without comments in the BSN-LHS).

discussed the completeness of the NLTT, and find it to be $\sim 100\%$ complete for $V \lesssim 11.5$ and $|b| > 15^\circ$, but only $\sim 75\%$ complete near the Galactic plane.

Gould and Salim (2003) and Salim and Gould (2003) have recently used the Two Micron All Sky Survey (2MASS) (Skrutskie et al. 1997) to improve the NLTT astrometry and to obtain JHK_s photometry for 61% of the entries in the NLTT catalog. Data for bright stars ($m_R \leq 14.0$) have been revised by matching NLTT entries to the Hipparcos (European Space Agency 1997), Tycho 2 (Høg et al. 2000), and Starnet (Röser 1996) catalogs. Faint stars have been matched to USNO-A (Monet 1996 and Monet 1998) and the 2MASS second release data.

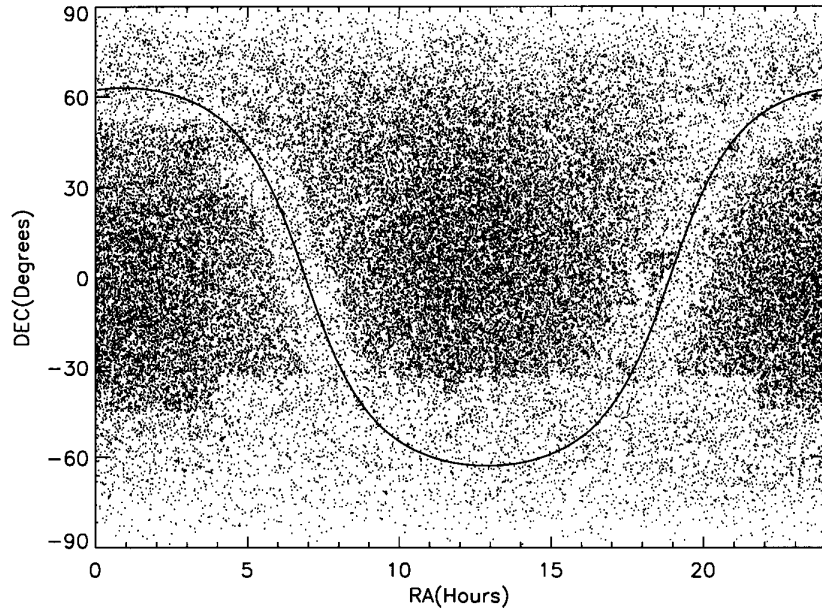


Figure 1.2: This plot shows the sky distribution of stars in the NLTT. The dark line indicates the Galactic plane. Coordinates are for equinox 1950.0.

1.1.2 Lowell Proper Motion Survey

The single other extensive list of HPM stars comes from the *Lowell Proper Motion Survey* (Giclas et al. 1971, 1978, hereafter, LOB), which was published in a series of Lowell Observatory Bulletins spanning three decades. This program is rooted in the theoretical work of Percival Lowell, who was intrigued by the possibility of trans-Neptunian planets. To search for such planets, a special 13-inch telescope was designed and built in Flagstaff, Arizona (where Pluto was, in fact, discovered in 1930). Photographic plates later used for the proper motion survey were first taken in 1929, and plate pairs have epoch differences of 28 to 48 years. The northern catalog (stars north of declination = 0) contains 8991 HPM stars with $\mu > 0''.26/\text{yr}$ (2 stars, G072-051 and G049-034 have only $\mu \sim 0''.2/\text{yr}$). The southern catalog (stars between declination = 0 and -40) contains 2,758 HPM stars with $\mu > 0''.20/\text{yr}$. Both catalogs have a photographic plate limit of $m_{pg} < 17$. The sky distribution of stars contained in the LOB is shown in Figure 1.3.

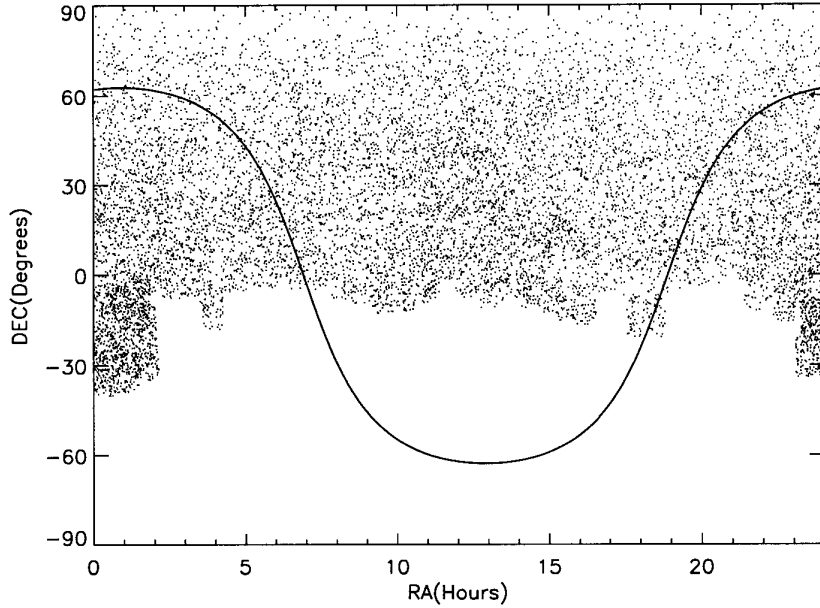


Figure 1.3: This plot shows the sky distribution of stars found in the Lowell Proper Motion Survey. The dark line indicates the Galactic plane. Coordinates are for equinox 1950.0.

1.1.3 Wroblewski/Torres/Costa Southern Proper Motion Survey

A third HPM survey has been carried out by Wroblewski and Torres from 1989 to 1998 and Wroblewski and Costa since 1999 (Wroblewski and Torres 1989, 1990, 1991, 1992, 1994, 1995, 1996, 1997, 1998, Wroblewski and Costa 1999, 2000, 2001, hereafter, WT for the entire body of work). The first epoch plates for the WT survey were taken in 1969-1970 using the 70/100/210 cm double-meniscus Maksutov Astrograph at Estación Astronómica de Cerro El Roble de la Universidad de Chile. In total, 164 plates were selected that had a sufficient number of galaxies that could be used as reference frames to calibrate coordinates in the plates. The second-epoch plates south of declination -40° began to be taken in 1985, thereby providing a ~ 15 year time span to detect HPM stars. The WT survey includes many more faint, fast moving objects at southern declinations than NLTT because the Astrograph reaches to $m_{pg} \approx 20$, while the BPMS portion of the NLTT has a limit of only $m_{pg} \approx 16$. The WT work not only revealed a large sample of new HPM stars (2,495), but recovered

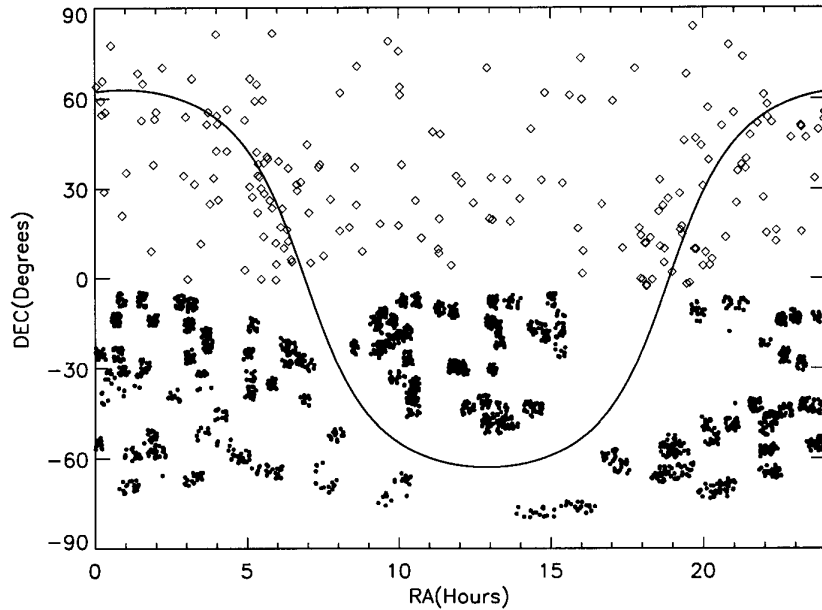


Figure 1.4: This plot shows the sky distribution of stars found in the WT (solid points) and new SUPERBLINK (open diamonds) surveys. The dark line indicates the Galactic plane. 1262 recovered NLTT stars from the WT survey are not shown. Coordinates are for equinox 2000.0.

many NLTT stars (1,262). The distribution of the new HPM stars from WT is plotted in Figure 1.4.

1.1.4 SUPERBLINK Survey

Lépine et al. (2002b) and Lépine et al. (2003c) have retrieved Digitized Sky Survey (DSS) images from the Space Telescope Science Institute archive to conduct a new survey of HPM stars. The first and second epoch images were from the Palomar Sky Survey red images, POSS-I and POSS-II, respectively. These plates were compared using an innovative method called SUPERBLINK, which rotates and distortion corrects the plate sets, then subtracts one image from another to reveal HPM objects. The search area covers 98% of the northern sky and reaches south to declination -2.8° . They have identified a total of 1,747 HPM stars in the range $0''.5/\text{yr} < \mu < 2''.0/\text{yr}$ and as faint as $m_R = 19.8$, the magnitude limit of the POSS-I plates. Of these, 1,540 stars were previously listed in the NLTT and LHS catalogs

while 198 are new HPM stars. The distribution of the new HPM stars is shown in Figure 1.4. The primary contribution of this survey is the significant list of new stars found in regions near the Galactic plane, which were neglected in other searches, as shown for the NLTT in Figure 1.2.

1.1.5 Liverpool-Edinburgh High Proper Motion Survey

The Liverpool-Edinburgh high proper motion Survey (hereafter, LEHPMS) has been conducted using the SuperCOSMOS digitized R-band ESO and UK Schmidt plates in 131 fields at the south galactic cap, and currently includes $\sim 7.5\%$ of the sky (Pokorny et al. 2003). The SuperCOSMOS Sky Survey (SSS) is carried out at the Royal Observatory in Edinburgh, Scotland (details can be found in Hambly et al. 2001). The purpose of SuperCOSMOS is to digitize Schmidt survey plates from the ESO, UK, and Palomar Schmidt (southern declinations) surveys with the SuperCOSMOS microdensitometer machine and make the data available on-line to the astronomical community. To date, the LEHPMS has retrieved 6,605 objects with $0''.18 < \mu < 20''.0$ and $9.0 \leq m_R \leq 19.7$ (see Figure 1.5). They are located in a region of $-87^\circ \leq DEC \leq -17^\circ$ and $19^h \leq RA \leq 6^h$. The blank portions in this search region represent areas where either the two images have a time base too short for reliable proper motion detections, or too few bright stars to calculate relative astrometry. Of the total, 399 objects are repeat detections from the overlapped regions on the plates. Therefore, 6,206 stars have been identified, of which 5,529 (84% of the original detections) are new ¹. This recent effort has not yet been carefully checked to be sure that all of the objects included are real. Our own work shows that many of the HPM objects are, in fact, not real objects.

1.1.6 Southern Proper Motion Survey by Scholz *et al.*

Scholz et al. (2000) reported about 100 new HPM stars in the region between 0^h and 7^h30^m in right ascension and -63° and -32° in declination with proper motions between $0''.3$ and $1''.0/\text{yr}$. Part of this survey overlaps with the “Whiteoak extension” discussed above. For this study, they scanned photographic plates for 40 United

¹Because the electronic version of the LEHPMS results from CDS does not contain information about which of the sample are the repeated objects (399), we have used a SIMBAD e-mail ID query to determine which objects are new or duplicated. If only the LEHPM name is shown (the name assigned for LEHPMS by SIMBAD), the star is considered to be a new HPM object.

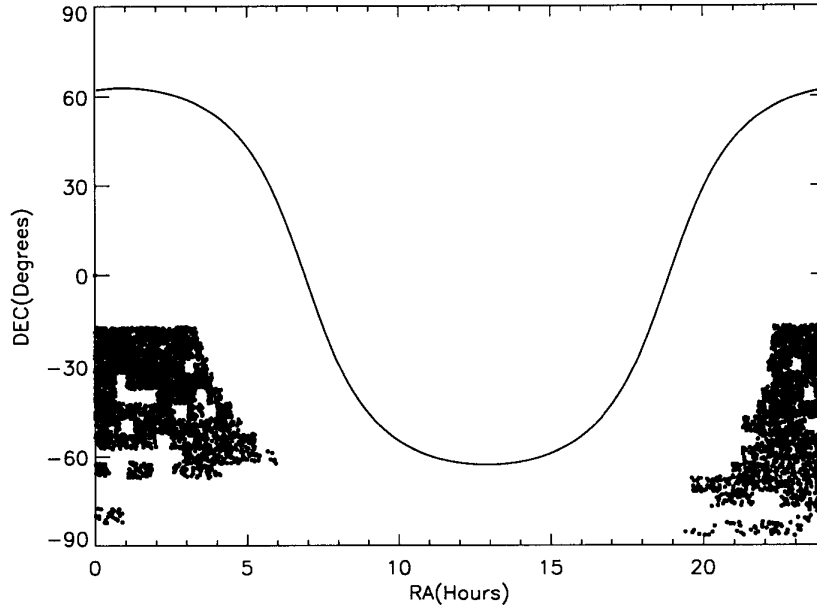


Figure 1.5: This plot shows the sky distribution for objects found in the Liverpool-Edinburgh High Proper Motion Survey. The dark line indicates the Galactic plane. Coordinates are for equinox 2000.0.

Kingdom Schmidt Telescope survey fields with the APM (Automatic Plate Measuring) machine. The epoch difference for most plate pairs is 15 years, with a few pairs separated by less than 10 years. The faintest objects found by this project form a common proper motion pair, APMPMJ0352-4127AB with $\mu = 0''.51/\text{yr}$ ($m_R^A = 19.7$, $m_R^B = 20.9$). Locations on the sky for these detections are shown in Figure 1.6.

1.1.7 Calán-ESO Proper Motion Survey

The Calán-ESO (European Southern Observatory) proper motion survey was carried out using photographic plates taken by the ESO Schmidt Camera with a time base of 6 to 16 years (Ruiz et al. 2001). Fourteen “random” fields were selected (avoiding the crowded Galactic plane region) that were of good quality and had a sufficiently long time base. The main intention of this survey was to find possible cool white dwarfs. In all, 542 HPM stars were found in the 14 fields, 381 of which were new HPM stars. The search parameters were $\mu > 0''.2/\text{yr}$ and $7.5 < m_R < 19.5$. Locations on the sky for these detections are plotted in Figure 1.6.

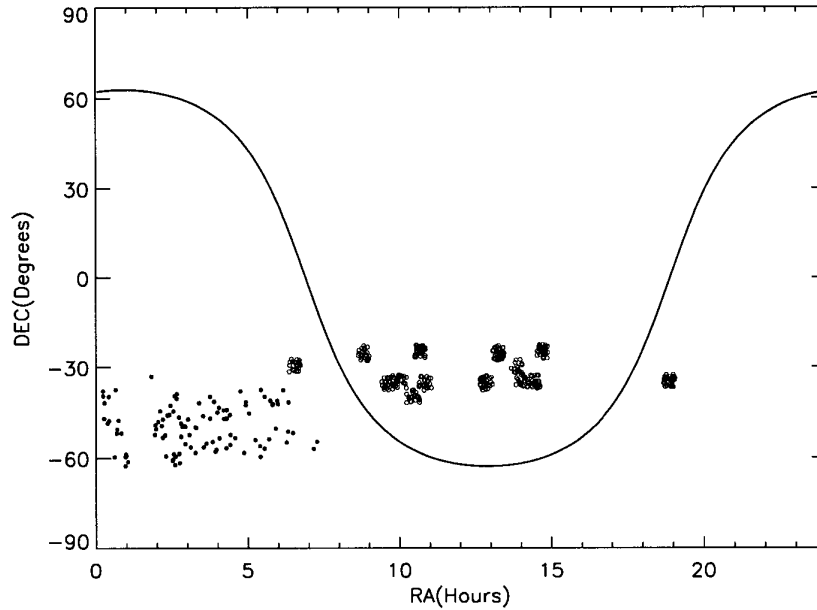


Figure 1.6: This plot shows the sky distribution of stars found in the Scholz (solid points) and Calán-ESO (open circles) surveys. The dark line indicates the Galactic plane. Coordinates are for equinox 2000.0.

Based on the large area HPM surveys discussed, the distributions of proper motion detections on the sky illustrated in Figure 1.2 to Figure 1.6, and the results given in Table 1.1, we conclude that

- All of these surveys have been accomplished by using photographic plates. Stars fainter than the photographic plate limits will be missed.
- At least two different plates are used for discovering HPM objects. If stars are detected on one plate but are too faint to be detected on a second plate (different emulsion, poor quality, blended image), the object will be missed.
- Samples of HPM stars remain incomplete near the galactic plane and in the southern sky.

Survey	Mag limit	DEC limit	μ Limit "/yr	Number of stars in proper motion bins ("/yr)							Category
				< 0.2	0.2~0.4	0.4~0.6	0.6~0.8	0.8~1.0	>1.0	total	
(1)	(2)	(3)	(4)	(5)	(6)	(7)	(8)	(9)	(10)	(11)	(12)
NLT	19.8	(e) $> -33^\circ$	$\mu > 0.18$	15956	36536	4229	1188	407	529	58845	fun
LOB	17.0	(e) $> -40^\circ$	$\mu > 0.26$	258	8206	2047	808	163	265	11747	dup
WT survey	21.0	(p) $< 0^\circ$	$\mu > 0.11$	1304	1058	104	24	3	2	2495	new
SUPERBLINK	19.8	(e) $> -2.8^\circ$	$2.0 > \mu > 0.5$	0	0	99	50	31	18	198	new
LEHPMS	19.7	(p) $-82.5^\circ \sim -22.5^\circ$	$20.0 > \mu > 0.18$	2053	3201	225	31	4	15	5529	new
Scholz	20.9	(p) $-63.0^\circ \sim -32.0^\circ$	$1.0 > \mu > 0.3$	0	83	88	24	6	3	204	dup
Calán-ESO	19.5	(p) $-22.0^\circ \sim -41.0^\circ$	$\mu > 0.2$	63	410	52	10	3	4	542	dup

Table 1.1: The summary of current HPM surveys discussed in this chapter. The number of stars listed includes duplicates with other catalogs in each bin (labeled in last column), except the WT, SUPERBLINK and Liverpool-Edinburgh catalogs. All 3 of the stars with $\mu > 1''/yr$ from Scholz et al. (2000) are previously known LHS stars. Only one star with $\mu > 1''/yr$ from Calán-ESO is new. The magnitude limits shown here are photographic plate magnitudes, typically m_R . Note—(e): entire north or south of that region; (p): part of the region; fun: fundamental reference; dup: some duplicates.

1.2 The MOTION Sample

The two primary goals of this thesis project are to (1) discover missing nearby stars in the published HPM survey catalogs and (2) characterize the complete sample of proper motion stars with $\mu > 1''0/\text{yr}$. In total, there are more than 66,000 HPM stars known, many of which have no follow-up observations. Given the correlation between HPM and proximity, many of the HPM stars remain “hidden” nearby stars simply because the necessary astrometric, photometric, and spectroscopic work needed to reveal members of the solar neighborhood has not been done. In order to restrict the sample to a manageable size, we concentrate on the very HPM stars that have annual proper motions greater than $1''0/\text{yr}$, otherwise known as the “MOTION” sample. The complete list of MOTION stars is given in Table A.1, which includes 549 stellar systems and 653 individual stars. Of these, 514 systems (93%) are from the fundamental HPM catalog, LHS. The selection criteria for the MOTION sample are:

1. All MOTION sample members have been published before 2003 January 1. Stars from the large area HPM surveys discussed above are included, except the Liverpool-Edinburgh High Proper Motion Survey. New components to known primaries published by Jao et al. (2003), Scholz et al. (2003), McCaughrean et al. (2004), and one unpublished object found by this project are included in the sample.
2. Stars from the BSN-LHS catalog are included unless they have flag “b”, which indicates “for some reason our proper motion measurement is not accurate (Bakos et al. 2002)”. Furthermore, if stars have $\mu < 0''8/\text{yr}$ in the LHS, they are not included in the MOTION sample even if BSN-LHS indicates that they are MOTION stars. There are three stars that are exceptional cases:
 - LHS1134 ($\mu = 1''10/\text{yr}$ (Bakos et al. 2002)) has a 14 year baseline between POSS-I and POSS-II that was used by BSN-LHS to determine the proper motion. There is no flag or comment for this object, so it is presumably accurate. It has been included in the MOTION sample even though LHS has $\mu = 0''744/\text{yr}$.
 - LHS1496 has flag “b” in BSN-LHS, but has $\mu > 1''0/\text{yr}$ as determined by Hipparcos (1997) and Giclas et al. (1971), so it is included.

- LHS1678 has flag “b” in BSN-LHS, but Reyl   et al. (2002) shows LHS1678 to have $\mu > 1''0/\text{yr}$, so it is included.

Various identifiers (ID) for the MOTION objects are given in Table A.1, indicating that there are often various sources of the proper motion. The proper motions (and position angles of proper motion) of MOTION sample members are selected based on the following criteria:

1. If stars with $\mu > 1''0/\text{yr}$ are in both Hipparcos and LHS, the μ from LHS is chosen (because the LHS motions are based on a longer time interval).
2. If stars with $\mu > 1''0/\text{yr}$ are in both LHS and LOB, the μ from LHS is chosen.
3. If stars are in Hipparcos, LHS, and LOB, but only LOB shows $\mu > 1''0/\text{yr}$, the μ from LOB is chosen (to include all reasonably likely MOTION members).
4. If stars are not in Hipparcos, LHS, LOB but in BSN-LHS, the μ from BSN-LHS is chosen, but the stars must abide by the selection criteria discussed above.
5. Other individual observations.

All coordinates for the MOTION sample members in Table A.1 have been manually identified from 2MASS using the OASIS program². The extracted coordinates are at the epoch of the 2MASS observations (within a few years of 2000) and have been converted to epoch and equinox J2000.0 coordinates using the proper motions given in Table A.1. For stars too faint to be detected in 2MASS, coordinates are from other sources, as noted.

The first two columns of Table A.1 are the coordinates of the MOTION stars. The third and fourth columns are the proper motions and proper motion position angles. The fifth column is the object name that will be used throughout this dissertation. The LHS ID is the primary ID that will be used. If CNS3 lists a sample member as a multiple system, but LHS does not have an ID for the secondary component(s), the CNS3 ID is used. If both LHS and CNS3 IDs are assigned to a primary star only, but a secondary has been discovered, the LHS ID is used for primary as well as the secondary. For stars without both LHS and CNS3 IDs, the ID shown in SIMBAD is used³.

²OASIS is a java program which can access various image catalogs at IPAC (Infrared Processing and Analysis Center) and is available online at <http://irsa.ipac.caltech.edu/applications/Oasis/>.

³USNO2101+0307 has a very unconventional ID shown in SIMBAD, [MFL2000] J210104.18+030705.1. Hence, the USNO ID is used for this particular object.

Finder charts for all MOTION stars are available locally at Georgia State University. The finder charts were created using a combination of SkyCat⁴, Perl (Practical Extraction and Reporting Language) and L^AT_EX. An example finder chart is shown in Figure 1.7.

1.2.1 Notes on Individual Objects

LHS106 can not be identified by blinking POSS-I and POSS-II plates. No such HPM star moves in this field. The source at the coordinates for LHS106 in BSN-LHS does not show any movement on the plates. This star currently is included in the MOTION sample because Luyten had it in his original sample, but we suspect that it does not exist.

LHS256, Gl766A and LHS3513 have Hipparcos IDs, but there are no proper motions available for them in the Hipparcos catalog.

LHS537 and LHS551 are listed as double stars in the WDC (Washington Double Star Catalog) as GAU20AB (WDS23096+0045) and BRT2519 (WDS23579+2321), respectively. However, the duplicity of LHS537 has not been confirmed and the companion to LHS551 has not been observed for over 20 years.

Gl732B was a companion with 12'' separation from Gl732A (CNS3). However, Gl732B can not be confirmed with common proper motion when using plates from different epochs. (Jahreiß2003, private communication). Also, a CCD image taken in CTIO 0.9-m has confirmed no such a companion exists. Thus, the companion is not listed in Table A.1.

HIP28442, HIP67593 and HIP107711 are all listed with $\mu > 1''0/\text{yr}$ in Hipparcos. However, HIP28442 = LHS1804 has $\mu = 0''.56/\text{yr}$ in LHS. HIP67593 (5''.83/yr) does not have common proper motion (CPM) with its supposed primary star HIP67594 (0''.05/yr). HIP107711 is in CNS3 with $\mu = 0''.342/\text{yr}$. Therefore, none of these three stars are included in the MOTION sample.

HIP70536, HIP72509, HIP73184, and HIP120005 have additional Hipparcos IDs — 70529, 72511, 73182, and 45343, respectively.

LSR1915+1609 has been the subject of spectroscopy by the RECONS group — it is a giant. Blinking POSS-I, POSS-II and 2MASS images confirms that LSR1915+1609 is very bright on the red plate and in 2MASS, while extremely faint on the blue plate. However, there is another nearby background star that is very

⁴SkyCat is a tool created by ESO that combines visualization of images and access to catalogs and archive data for astronomy. It is available at <http://archive.eso.org/skycat/>.

bright on the blue plate. We suspect that SUPERBLINK determined a false HPM by matching the blue and red objects, which are actually different sources, so the star is not included in the MOTION sample.

01:43:01.18 -67:18:34.70

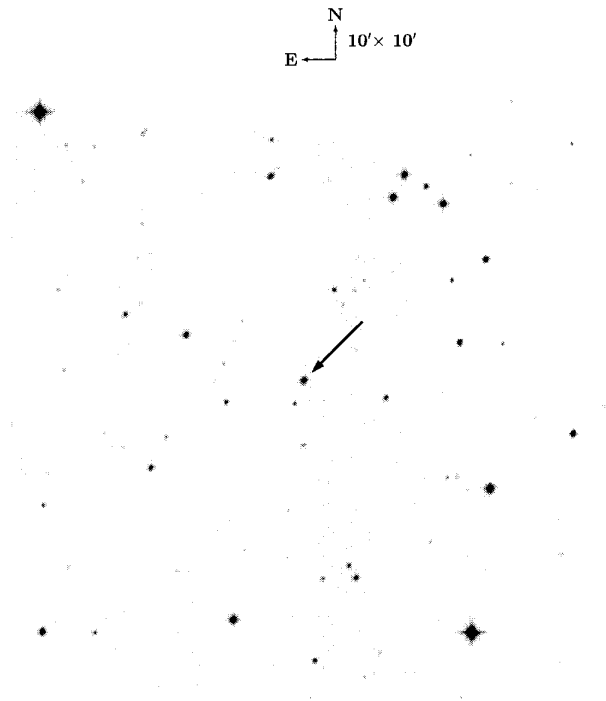
**LHS145**

Figure 1.7: A finder chart example for a MOTION sample member. Because these finder charts were created before the 2MASS All Sky data were released, the BSN-LHS catalog coordinates are used (equinox and epoch J2000.0). The image is from a POSS-I plate. Because of the HPM of LHS145 on the sky, a large shift is expected when using this finder chart at current time. This permits confident identification of the target when at the telescope.

1.2.2 MOTION Stars Distribution

The distribution of the MOTION systems on the sky is shown in Figure 1.8 and statistics of the sample distribution are given in Table 1.2. It is clear that if the surface density is the same for the southern and northern hemisphere subsamples, there are more southern MOTION stars missing from the sample. Furthermore, for MOTION stars within 10° of the Galactic plane, the southern sky density is less than in the north. The 15 new MOTION stars discovered since 2003 January 1 are also plotted in Figure 1.8. Details of these systems are given in Table 1.3.

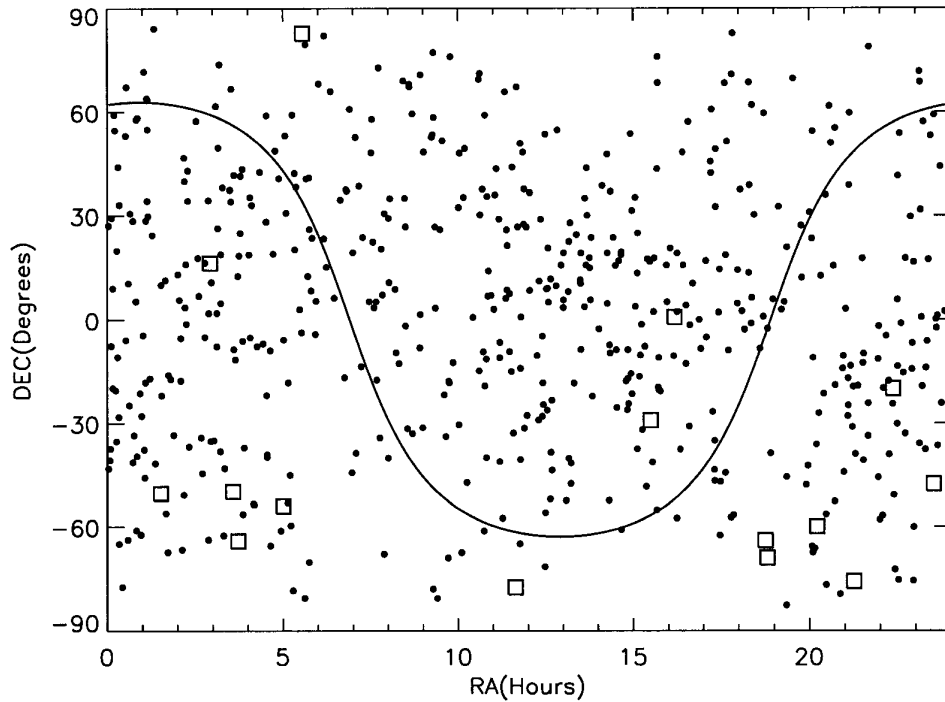


Figure 1.8: The MOTION sample distribution on the sky. Dots indicate the MOTION systems before 2003 January 1. Squares indicate the new members since 2003.

1.2.3 Organization of this Dissertation

Our comprehensive work on the MOTION sample includes astrometric, photometric, and spectroscopic work. Chapter 2 discusses the astrometric effort, including the

Table 1.2: The MOTION sample statistics on the sky.

	$-90^\circ \sim -30^\circ$	$-30^\circ \sim -00^\circ$	$00^\circ \sim 30^\circ$	$30^\circ \sim 90^\circ$	total
all sky (before 2003)	126	127	153	143	549
all sky (April 2004)	136	129	155	144	564
$ b < 10^\circ$ (April 2004)	23	9	16	36	85

analysis of parallaxes and proper motions. Chapter 3 outlines the photometric results, including both optical and near-infrared photometry. In addition, possible MOTION stars within 25 pc are revealed. Chapter 4 gives details about the spectroscopic nature of the MOTION members. Chapter 5 includes a discussion of the new companions found during this thesis work. Chapter 6 is a discussion of the entire MOTION sample.

There are 5 appendixes in this dissertation. Appendix A is the complete MOTION list with coordinates, proper motions and different IDs. Appendix B is the complete MOTION list with $VRIJHK_s$ photometry, weighted-mean parallax, and spectral types. Appendix C shows the differential color refraction (DCR) least squares fitting method used during astrometric reductions. Appendix D is the Cerro Tololo Inter-American Observatory Parallax Investigation (CTIOPI) photometry reduction manual and Appendix E is the CTIOPI parallax reduction manual.

Table 1.3: The new MOTION stars added after 2003 January 1.

RA (J2000.0)	DEC	Name	P.M. (" / yr)	P.A. (deg)	Note
01 31 04.12	−50 24 54.3	LEHPM1628	1.10	141.6	(a)
02 55 10.57	+16 17 01.1	TEE0255+1617	5.05	137.9	(e)
03 34 09.05	−49 53 38.2	LEHPM3396	2.41	78.7	(a)
03 42 56.40	−64 07 47.9	SCR0342−6407	1.07	141.4	(d)
05 00 15.36	−54 06 09.1	LEHPM3861	1.06	168.4	(a)
05 32 53.57	+82 46 45.1	2MA0532+8246	2.60	130.0	(g)
11 38 22.30	−77 21 54.2	SCR1138−7721	2.14	286.7	(d)
15 29 14.17	−29 07 22.8	LEHPM1529−2907	1.04	188.9	(b)
16 10 28.96	+00 40 54.0	LSR1610−0040	1.46	212.0	(f)
18 45 02.60	−63 57 52.0	SCR1845−6357	2.56	74.7	(d)
18 48 21.50	−68 55 25.3	SCR1848−6855	1.29	194.3	(d)
20 12 31.30	−59 56 40.1	SCR2012−5956	1.44	165.6	(d)
21 15 12.68	−75 41 39.5	LEHPM4051	1.10	144.0	(a)
22 21 10.39	−19 58 05.4	LEHPM4592	1.06	124.6	(a)
23 30 16.15	−47 36 45.2	APM0690	1.13	211.6	(u)
Probable refuted systems					
01 19 35.08	−57 10 57.9	LEHPM1428	4.68	218.3	(a), N
01 39 16.97	−45 58 54.0	LEHPM1756	6.95	172.8	(a), P
01 39 20.75	−46 12 09.6	LEHPM1757	7.51	342.3	(a), P
01 54 59.57	−34 09 48.1	LEHPM1998	4.54	94.0	(a), N
02 49 20.51	−36 14 10.4	LEHPM2802	10.73	20.5	(a), N
21 07 04.26	−72 14 27.6	LEHPM4028	5.46	172.4	(a), P
21 49 11.87	−41 33 32.5	L427-34	1.06	116.5	(c), N
22 48 30.58	−31 57 49.5	LEHPM5158	1.64	336.6	(a), P
23 15 54.12	−50 59 55.7	LEHPM5638	8.01	359.6	(a), P
23 37 41.96	−42 12 59.8	LEHPM6006	6.63	229.5	(a), P

Ref.-(a) Pokorny et al. (2003). (b) Pokorny et al. (2004). (c) Gould and Salim (2003); Salim and Gould (2003). (d) Hambly et al. (2004). (e) Teegarden et al. (2003). (f) Lépine et al. (2003a). (g) Burgasser et al. (2003). (u) Scholz (private communication, 2002)

Note – (N) indicates that this star can not be confirmed by manually blinking two epoch images. (P) indicates that either there is more than one object moving in the field or it is too faint to be confirmed. LEHPM1529−2907 does not have a SIMBAD identifier yet so a conventional name is used.

Chapter 2

Astrometry

The RECONS (Research Consortium On Nearby Stars) group is currently carrying out a southern sky parallax survey known as CTIOPI (Cerro Tololo Inter-American Observatory Parallax Investigation). This program was selected to be a NOAO Survey Program in 1999, and observations began in August of that year. With the success of the initial program, CTIOPI was continued as part of the SMARTS (Small and Moderate Aperture Research Telescope System) program beginning in 2003 February. The primary goals of CTIOPI are to discover and characterize nearby red, brown, and white dwarfs that remain unidentified in the solar neighborhood. In addition, as the observation time span is extended, RECONS is searching for long term perturbations caused by unseen companions pulling on the target stars.

2.1 Parallax Observations

Most of the target stars (hereafter, the “pi stars”) are selected for CTIOPI because available astrometric (e.g, high proper motion), photometric, or spectroscopic data indicate that they might be closer than 25 pc. Roughly 95% of the pi stars are red dwarfs and 30% are MOTION stars.

Although CTIOPI used both 0.9-m and 1.5-m telescopes during the NOAO Survey Program, the current results for MOTION stars are from the 0.9-m, where CTIOPI has been continued under SMARTS. The RECONS team at Georgia State University has been responsible for data reduction for the 0.9-m program, while data from the 1.5-m program is being analyzed by Edgardo Costa and Rene Mendez of the Universidad de Chile in Santiago.

The 0.9-m telescope is equipped with a 2048×2048 Tectronix CCD camera

with $0''.401/\text{pixel}$ plate scale (Jao et al. 2003). All observations were made using the central quarter of the chip, yielding a 6.8 square field of view, through V_J , R_C and I_C filters ¹. The dewar containing the CCD camera is mounted on the telescope with columns oriented in the north-south direction. A slight rotation relative to the sky is possible due to instrument flexure and repositioning during telescope maintenance. This rotation angle will be discussed in Section 2.4.1.

The observing procedures employed during CTIOPI mimic those used in the multi-decade parallax program at the Siding Spring Observatory parallax program in Australia, carried out by Philip Ianna (University of Virginia) who is a member of CTIOPI. When a star is observed for the first time, preliminary exposures are taken in the three different filters, V_J , R_C , and I_C , to find a suitable set of reference stars in the field. The parallax filter is selected to balance the brightness of the pi star with available potential reference stars, and that filter is used for all subsequent parallax frames. Because most of our pi stars are nearby stars, they are brighter than most of the field stars. We attempt to place the pi star on the chip so that 5 to 10 field stars of adequate flux can be included. Typically, a good reference star is not more than twice as bright as the pi star (in the few cases when the pi star is not the brightest star in the field), but has at least 1000 counts during a typical parallax exposure.

For each target star, a setup chart is made with the pi star and an initial set of reference stars marked. The pi star (x,y) position on the CCD chip is labeled so that all CTIOPI observers can place the pi star in approximately the same pixel position henceforth, thereby keeping the entire reference star set on the chip.

Bias frames and dome flats are taken at the beginning of each night to allow for basic data reduction calibrations. Parallax observations are usually made within ± 30 minutes of a pi star's transit in order to minimize the corrections required for differential color refraction (DCR), which is discussed in section 2.3. Some faint pi stars are observed with a wider hour angle tolerance, within one hour of the meridian, because frame acquisition takes longer. Because of the success of the DCR model, additional individual images (e.g. photometry frames taken far from the meridian in the filter used for parallax observations) are included even if the hour angle is as high as 3 hours. Exposure times for parallax frames typically provide a peak of at least $\sim 50,000$ counts for the pi star (saturation occurs at 65,535 counts), in an effort to maximize the number of counts available for pi star and reference star

¹Subscript: J=Johnson, C=Cousins. The central wavelengths for V_J , R_C and I_C are 5475Å, 6425Å and 8075Å, respectively. The filter curves are shown in Fig. 2.6.

centroiding. Usually, 2-10 frames are taken in each visit, depending primarily on the exposure time required. Multiple frames are taken to reduce the errors on the pi star and reference star positions at each observation epoch. Briefly, the typical set of observations required to determine a final parallax and proper motion includes four seasons of observations carried out over at least 2.5 years (further details in Section 2.6).

2.2 Parallax Displacement

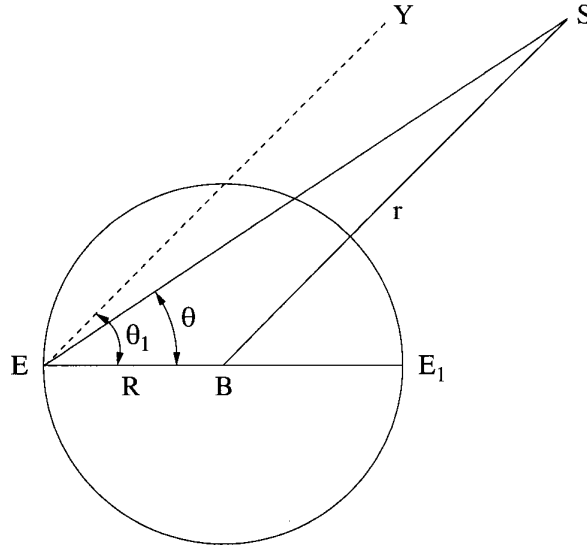


Figure 2.1: This plot indicates the parallactic displacement due to the Earth's revolution around the Sun.

Figure 2.1 shows the Earth's orbit, which we can treat as circular for this schematic (although the eccentricity of Earth's orbit is included in the astrometric reductions). B indicates the Solar System barycenter and R is the orbital radius². S denotes the position of a star at a distance r from B. We assume that the star is stationary with respect to B (i.e., no secular acceleration). On a given date, the Earth is located at E, and at E_1 six months later. The segment EY is parallel to BS and we denote the angles YEB and SEB by θ_1 and θ respectively. Therefore,

²The difference between the Earth-Sun distance and the Earth-Solar system barycenter distance is about 0.005 AU. The radius of the Earth can be ignored when compared to the Earth-Solar system barycenter distance.

$$\sin(\theta_1 - \theta) = \frac{R}{r} \sin \theta \quad (2.1)$$

The star's annual *trigonometric parallax*, Π , is defined by

$$\Pi = \frac{1}{r}. \quad (2.2)$$

Π is expressed in seconds of arc and r in parsecs, where 1 parsec = 206,265 AU. $R \sin \theta$ is the so called *parallax factor*. Because $\theta_1 - \theta$ is small even for the nearest star outside our Solar System, Proxima with $\Pi = 0''.77$, this equation can be simplified as,

$$\theta_1 - \theta = \Pi R \sin \theta. \quad (2.3)$$

In Figure 2.1, BS is the direction of the star as seen from the Solar System barycenter (the heliocentric direction), and ES is the direction of the star as seen from the Earth when observing (the geocentric direction). If the star were located at infinite distance, it would be found precisely in the EY direction. Clearly, the geocentric direction ES is displaced from EY *toward* the direction EB of the Solar System barycenter, and this displacement $\theta_1 - \theta$ is in the plane of EBS. We can project this parallactic displacement on the celestial sphere as shown in Figure 2.2 to provide a three-dimensional view on the celestial sphere.

2.2.1 Parallax Displacement in Ecliptic Coordinates

At any moment during the Earth's revolution around the Sun, the parallax displacement of a distant star is toward the Solar System barycenter, directed along the great circle tracing the BS arc. Therefore, the parallactic displacement in longitude and latitude are (van de Kamp (1967) and Smart (1977)):

$$\begin{aligned} x_\lambda &= \Pi R \sin \theta \sin \phi, \quad (longitude) \\ y_\beta &= -\Pi R \sin \theta \cos \phi, \quad (latitude) \end{aligned} \quad (2.4)$$

where ϕ is shown on Figure 2.2, λ and β are the longitude and latitude of S', and x and y are the displacements in the two directions. By applying spherical trigonometry, we derive

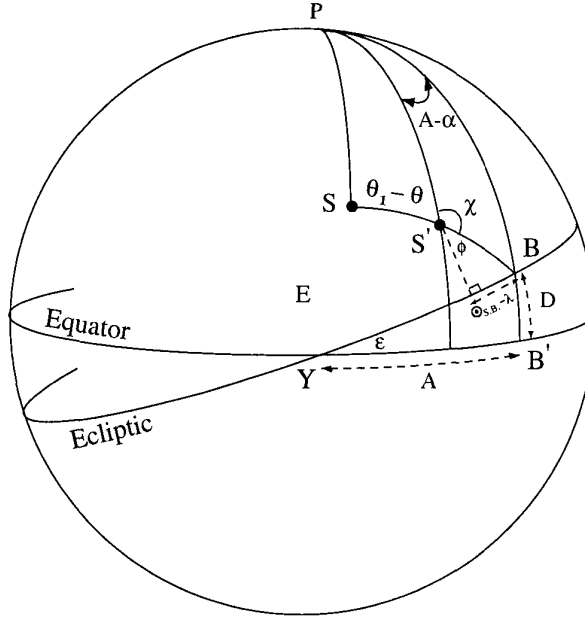


Figure 2.2: S is the star, B is the Solar System barycenter at coordinate (A,D). E is the Earth. Y is the vernal equinox. S' is the stellar position seen from the Earth. $\odot_{S,B}$ is the angle from Y to B along the ecliptic.

$$\begin{aligned}\sin \theta \sin \phi &= \sin(\odot_{S,B} - \lambda), \\ \sin \theta \cos \phi &= \cos(\odot_{S,B} - \lambda) \sin \beta,\end{aligned}\tag{2.5}$$

and thus find,

$$\begin{aligned}x_\lambda &= \Pi R \sin(\odot_{S,B} - \lambda), \\ y_\beta &= -\Pi R \cos(\odot_{S,B} - \lambda) \sin \beta.\end{aligned}\tag{2.6}$$

After eliminating the $(\odot_{S,B} - \lambda)$ term, we derive

$$\frac{x_\lambda^2}{\Pi^2 R^2} + \frac{y_\beta^2}{\Pi^2 R^2 \sin^2 \beta} = 1.\tag{2.7}$$

This is the equation of an ellipse, in this context known as the *parallactic ellipse*. The curve traced out by a star represents the reflex movement of the geocentric

position S' around the Sun throughout the year. The major axis of the parallactic ellipse is parallel to the ecliptic and the minor axis is perpendicular to the ecliptic. The semimajor axis is independent of the object's latitude and is equal to ΠR . If the star lies precisely on the ecliptic, the semiminor axis will vanish to zero.

2.2.2 Parallax Displacements in the RA and DEC Directions

Because of the small inclination of the ecliptic relative to the Earth's equator (which sets the RA and DEC coordinate system), the major portion of the parallactic displacement always occurs in the RA direction, while the minor portion occurs in the DEC direction. We can therefore rewrite the parallax factors in terms of the RA and DEC directions, which are illustrated in Figure 2.2 along the Equator line,

$$\begin{aligned} P_\alpha &= R \sin \theta \sin \chi, \quad (\text{in RA}) \\ P_\delta &= R \sin \theta \cos \chi, \quad (\text{in DEC}) \end{aligned} \quad (2.8)$$

where χ is shown on Figure 2.2. We can eliminate χ using the spherical triangle SBP :

$$\begin{aligned} \sin \theta \sin \chi &= \cos D \sin(A - \alpha), \\ \sin \theta \cos \chi &= \cos D \sin \delta \cos(A - \alpha) - \sin D \cos \delta. \end{aligned} \quad (2.9)$$

Using the spherical triangle YBB' gives

$$\begin{aligned} \cos B &= \cos A \cos D, \\ \sin B \sin \epsilon &= \sin D, \\ \sin B \cos \epsilon &= \sin A \cos D, \end{aligned} \quad (2.10)$$

where ϵ is the obliquity of the Solar System barycenter³ which is a function of time because of Earth's precession. By combining (2.8), (2.9) and (2.10) we find:

³The difference between the obliquity of the Solar System ecliptic and Solar System barycenter is about 1.05105×10^{-5} radian.

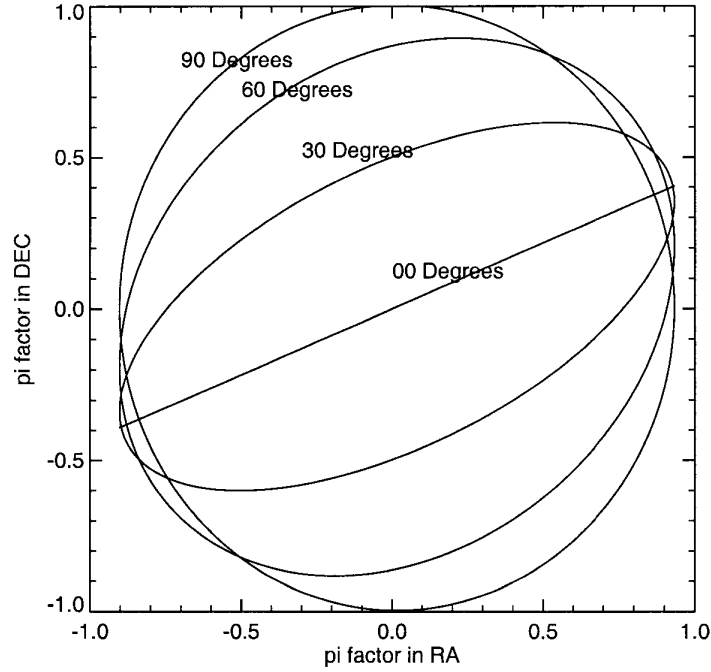


Figure 2.3: This plot shows parallaxic ellipses projected onto the RA/DEC plane for stars with $RA = 0^h$ located at various DEC. The ellipse vanishes for stars located on the ecliptic ($DEC = 0$). The tilt angle corresponds to the obliquity of the ecliptic relative to the RA/DEC grid. The distance to the Solar System barycenter has been normalized to 1.0 AU. In this case, the parallax factor in DEC can exceed 1.0 slightly because of the eccentricity of the Earth's orbit.

$$\begin{aligned} P_{\alpha} &= R(\cos \epsilon \cos \alpha \sin B - \sin \alpha \cos B), \\ P_{\delta} &= R[(\sin \epsilon \cos \delta - \cos \epsilon \sin \alpha \sin \delta) \sin B - \cos \alpha \sin \delta \cos B]. \end{aligned} \quad (2.11)$$

P_{α} and P_{δ} are the parallax factors in RA and DEC, which of course also trace out an ellipse. An example is shown on Figure 2.3. The shape of this ellipse will depend on the location of the star. Because this is the plot only for parallax factors, it will not reflect the real parallaxic movement in the celestial sphere. The actual movement of the object will be discussed later in this section.

We may modify Equation (2.11) by using the rectangular equatorial coordinate

system:⁴.

$$\bar{X} = R \cos B, \quad \bar{Y} = R \sin B \cos \epsilon, \quad \bar{Z} = R \sin B \sin \epsilon. \quad (2.12)$$

Consequently, Equation (2.11) becomes

$$\begin{aligned} P_\alpha &= \bar{Y} \cos \alpha - \bar{X} \sin \alpha, \\ P_\delta &= \bar{Z} \cos \delta - \bar{X} \cos \alpha \sin \delta - \bar{Y} \sin \alpha \sin \delta. \end{aligned} \quad (2.13)$$

We define (α_0, δ_0) as the set of coordinates of the star, S, at an established equinox and epoch (usually both J2000.0), and (α, δ) as the coordinates for S' at the time of observation using the same equinox as S, but at a different epoch. Then,

$$\begin{aligned} (\alpha_0 - \alpha) \cos \delta &= \Pi P_\alpha, \\ \delta_0 - \delta &= \Pi P_\delta. \end{aligned} \quad (2.14)$$

However, the position of the star in the sky is not stationary even if there is no parallactic displacement. The description of its stellar path must include a component for proper motion. Furthermore, because the image is taken using a CCD camera, it is convenient to work in terms of the rectangular coordinates on the CCD chip instead in celestial coordinates. Hence, the stellar displacement in the sky can be expressed as:

$$\begin{aligned} x &= x_0 + \mu_x t + \Pi P_\alpha, \\ y &= y_0 + \mu_y t + \Pi P_\delta, \end{aligned} \quad (2.15)$$

where $\mu_x = \mu_\alpha \cos \delta$ and $\mu_y = \mu_\delta$ represent the proper motions in RA and DEC, respectively, in units of seconds of arc per year, and t is the time difference between the established standard coordinate epoch and the time of observation, in years. A series of images is taken over a period of years to determine the parallax and proper motion of a star, so there will be more than one epoch of images for pi stars. This

⁴The $(\bar{X}, \bar{Y}, \bar{Z})$ rectangular coordinate system is from the most recent version of the JPL Planetary and Lunar Ephemerides, DE405. EY is the \bar{X} axis and EP is the \bar{Z} axis. \bar{Y} is chosen to complete a right-handed set. DE405 provides the location of the Earth to high precision, and is available through the ftp site at ssd.jpl.nasa.gov/pub/eph/export.

pair of time-dependent equations therefore forms the basis for the multi-epoch images used to determine a pi star’s relative parallax and proper motion, via reductions using least squares methods.

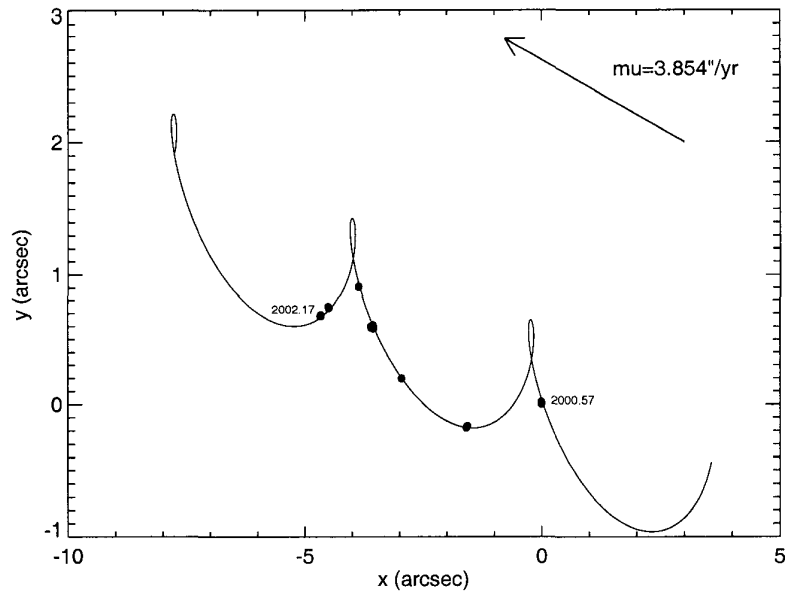
Figure 2.4 shows examples for stellar paths traced out by two stars with identical parallax but different proper motions. Figure 2.4(a) indicates the stellar path for Proxima based on 1.6 years of CTIOPI data. Error bars on the points are smaller than the dots in the plot. Figure 2.4(b) shows the same stellar path, split into two directions, x and y. The retrograde motion seen for Proxima is caused by its relatively high proper motion. If the proper motion for Proxima is artificially changed to zero, the stellar path traces out the curves shown in Figure 2.4(c), which is the standard parallax ellipse. Hence, the stellar path is determined by three factors: the star’s coordinates, its parallax, and its proper motion. Consequently, Equation (2.15) must include the proper motion terms.

2.2.3 The Uncalibrated Coordinate Problem

The established coordinate set, (α_0, δ_0) is located in the center of parallactic ellipse shown in Figure 2.4(c) for the zero proper motion case. Currently, the coordinates used for the MOTION sample are from the 2MASS All Sky Point Source Catalog, in which the astrometry has been reconstructed in the International Celestial Reference System (ICRS) via the Tycho 2 Catalog. The coordinates are accurate to 70–80 mas for stars with magnitudes $9 < K_s < 14$ mag. The astrometric accuracy of brighter sources is approximately 120 mas. However, the 2MASS coordinates do not consider the slight shift from the true “zero point” coordinates of each star caused by its parallax. Presently, except Hipparcos catalog, other astrometry catalogs do not consider this effect. Therefore, the coordinates for each star include an “unavoidable error” that has not yet been calibrated. This error can be ignored for ground based parallax observations due to their relatively low accuracy. However, this error must be considered for the Space Interferometry Mission (SIM), which has a goal of determining parallaxes to one microarcsecond.

2.3 Differential Color Refraction

An additional factor that affects ground based trigonometric parallax determinations is atmospheric refraction. As shown in Figure 2.5, the position of star X on the celestial sphere is refracted by the Earth’s atmosphere toward the zenith to a position



(a) Stellar path for Proxima

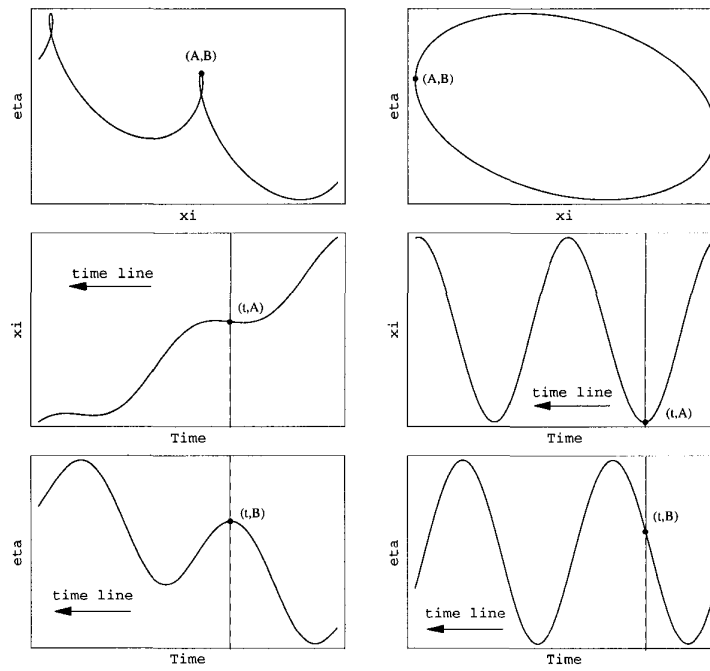
(b) An example of a stellar path in the x and y directions over 2 years for a star with $\mu \neq 0$.(c) An example of a stellar path in the x and y directions over 2 years for a star with $\mu=0$.

Figure 2.4: Stellar path examples.

X' along the ZX arc (assuming the light is monochromatic). The observer's site is at latitude ϕ . The arc $X'Y$ is a small portion of the circle centered at the celestial pole, P . Because XX' is very small, we consider the spherical triangle YXX' as a plane triangle with right angle at Y .

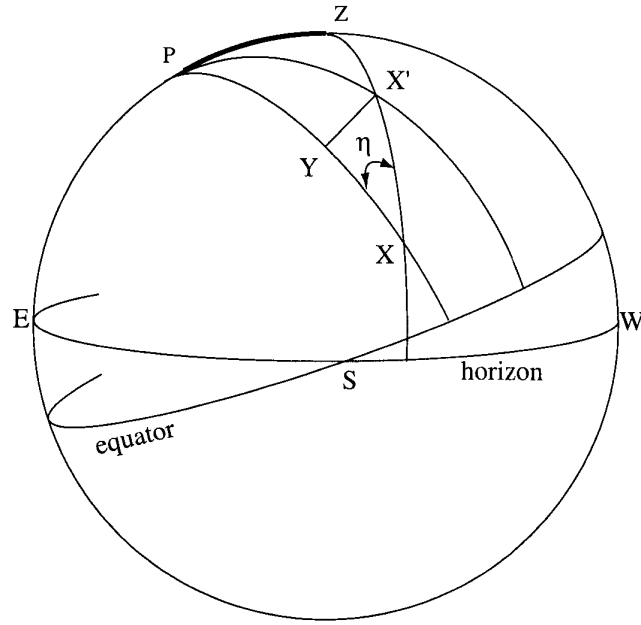


Figure 2.5: This plot outlines the shift in position of a star that is refracted by the Earth's atmosphere. X indicates the true position without refraction and X' is the position after refraction.

The amount of atmospheric refraction is given by $XX' = -\kappa \tan \zeta$, where $\zeta = ZX'$ is the zenith angle, and κ is the atmosphere's index of refraction. The index of refraction is a function of wavelength, temperature, humidity, and atmospheric pressure (Stone 1996). The projections of the total refraction onto the celestial sphere are

$$\begin{aligned} X'Y &= XX' \sin \eta, \\ XY &= XX' \cos \eta, \end{aligned} \tag{2.16}$$

where η is the parallactic angle. Using the law of sines for triangle ZPX , we can derive $\sin \eta$ to be

$$\sin \eta = \frac{\sin HA}{\sin \zeta} \sin(90^\circ - \phi),$$

where HA is the star's hour angle. Therefore,

$$X'Y = \frac{\kappa \tan \zeta \sin HA \cos \phi}{\sin \zeta} = \frac{\kappa \sin HA \cos \phi}{\cos \zeta} = (\alpha - \alpha') \cos \delta'. \quad (2.18)$$

Using the law of cosines for triangle ZPX , we can derive $\cos \eta$ via

$$\cos(90^\circ - \phi) = \cos \zeta \cos(90^\circ - \delta) + \sin \zeta \sin(90^\circ - \delta) \cos \eta,$$

to be

$$\cos \eta = \frac{\sin \phi - \cos \zeta \sin \delta}{\sin \zeta \cos \delta}.$$

Therefore,

$$\begin{aligned} XY &= \delta - \delta' = XX' \cos \eta \\ &= \kappa \tan \zeta \frac{\sin \phi - \cos \zeta \sin \delta}{\sin \zeta \cos \delta} \\ &= \kappa \frac{\sin \phi - \cos \zeta \sin \delta}{\cos \zeta \cos \delta} \\ &= \kappa (\sin \phi \sec \zeta \sec \delta - \tan \delta). \end{aligned} \quad (2.20)$$

Equation (2.18) shows that when a star transits (i.e. $X'Y = HA = 0$), its position is refracted directly toward to the zenith.

Filippenko (1982) showed that at an altitude of $\sim 2\text{km}$ (similar to many observatories), a latitude of $\sim \pm 30^\circ$, an atmospheric pressure of $\approx 600\text{ mm Hg}$, a temperature $T \approx 7^\circ\text{C}$, and for $\sec Z = 1.5$, the amounts of refraction for monochromatic light at $\lambda = 3000\text{\AA}$, 4000\AA , 5000\AA , 6000\AA , 7000\AA , 8000\AA and 9000\AA are $2''.37$, $0''.71$, $0''.00$, $-0''.37$, $-0''.60$, $-0''.74$ and $-0''.84$, respectively. The wavelength at which zero refraction occurs has been defined to be monochromatic 5000\AA light. As expected, these results clearly show that blue light is refracted more than red light when passing through the Earth's atmosphere.

In reality, because starlight spreads across all wavelengths and filters with pass-bands ranging from $\sim 200\text{\AA}$ to $\sim 2000\text{\AA}$ are used when observing, a mean refraction

must be considered when calculating the amount of refraction caused by the Earth's atmosphere. Figure 2.6 shows the three filter passbands utilized in CTIOPI, along with the normalized spectral energy distributions for A0 V and M5 V type stars, taken from Gunn and Stryker (1983). As can be seen for each filter passband in the plot, there is more short wavelength light from the A0 V star than from the M5 V star. This causes the effective wavelength of the A0 V star's light to be shifted to shorter wavelengths than for the M5 V star. Thus, A0 V type stars (or in general, blue stars) will experience more refraction than M5 V type (red) stars. The effective wavelength difference is greatest in the V filter and smallest in the I filter. This offset in the refraction caused by the different colors of stars is known as *differential color refraction* (DCR).

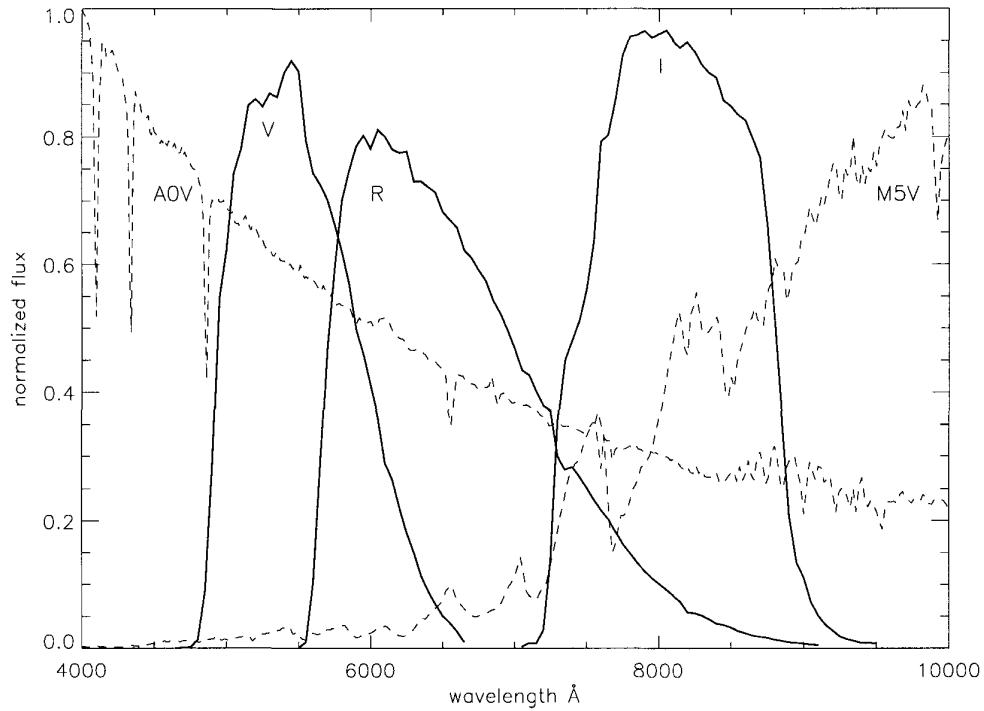


Figure 2.6: The Johnson *V* and Cousins *RI* passbands for filters used at the CTIO 0.9-m telescope are shown along with two normalized spectral energy distributions for A0 V and M5 V type stars.

Stone (1996) has shown that the κ in equations (2.18) and (2.20) for monochromatic light can be replaced by the mean refraction R_m , which is described by

$$R_m = \frac{\int_0^\infty S(\lambda)E(\lambda)A(\lambda)L(\lambda)F(\lambda)Q(\lambda)\kappa(\lambda)d\lambda}{\int_0^\infty S(\lambda)E(\lambda)A(\lambda)L(\lambda)F(\lambda)Q(\lambda)d\lambda}, \quad (2.21)$$

where $S(\lambda)$ is the spectral energy distribution of the star, $E(\lambda)$ is the transmission of interstellar dust along the line of sight, $A(\lambda)$ is the transmission of the atmosphere at the airmass being observed, $L(\lambda)$ is the transmission of the telescopes, $F(\lambda)$ describes the wavelength dependence of the filter passband, and $Q(\lambda)$ is the quantum efficiency of the detector.

2.3.1 Measuring DCR Empirically

Different observing and reduction methods used to measure DCR have been discussed by Monet et al. (1992), Tinney (1993), Stone (1996), and Stone (2002). Here we use both the theoretical methods proposed by Stone (1996) and the empirical methodology proposed by Monet et al. (1992) to measure DCR for the CTIOPI program, and to make final corrections during astrometric reductions.

DCR observations were made by the author during four photometric nights in December 2002 using the 0.9-m telescope at CTIO. This is the identical combination of telescope, filters, and CCD camera used during the parallax program. Ten different fields spread from zenith to low altitude that contained blue ($V - I = 0.57$) to red ($V - I = 3.22$) stars were selected and observed through the V , R and I filters. Four to five fields were each observed four to five times per night through hour angles of $\sim \pm 4$ hours. Exposure times were chosen to be the same as used in the parallax program for each field so that the faintest reference stars could be analyzed for DCR. In total, 72 stars were included in the final DCR analysis. Although refraction is, in general, a function of temperature, pressure, and humidity, due to the stable observing conditions throughout this run, these factors can be ignored, as discussed in Monet et al. (1992) and Stone (2002).

In order to provide a zero point reference frame for the DCR calculation, one set of images must be taken when the field transits. In other words, we assume there is no refraction in either the RA and DEC directions when the hour angle is zero. However, there is some amount of unknown refraction toward the zenith, so equation (2.20) needs to be modified to be:

$$\begin{aligned}
XY_{new} &= XY - XY_0 \\
&= R_m \frac{\sin \phi - \cos \zeta \sin \delta}{\cos \zeta \cos \delta} - R_m \frac{\sin \phi - \cos \zeta_0 \sin \delta}{\cos \zeta_0 \cos \delta} \\
&= R_m \frac{\sin \phi}{\cos \delta} \left(\frac{1}{\cos \zeta} - \frac{1}{\cos(\phi - \delta)} \right) \\
&= R_m \frac{\sin \phi}{\cos \delta} (\sec \zeta - \sec(\phi - \delta)). \tag{2.22}
\end{aligned}$$

From Equations (2.18) and (2.22), the components of refraction in the RA and DEC directions are

$$(\alpha - \alpha') \cos \delta = \frac{R_m \sin HA \cos \phi}{\cos \zeta} = R_m \cos \phi \sin HA \sec \zeta = R_m Z_x \tag{2.23}$$

$$\delta - \delta' = R_m S \sin \phi \sec \delta (\sec \zeta - \sec(\phi - \delta)) = R_m Z_y, \tag{2.24}$$

where $S = 1$ if $(\phi - \delta) \geq 0$ and $S = -1$ if $(\phi - \delta) < 0$.

These empirical measurements assume that the refraction R_m is a polynomial function of $(V - I)$ color as discussed in Stone (1996). Therefore, we have determined the V , R , and I magnitudes for all 72 stars used to calculate the DCR.

2.3.2 The Final DCR Model for CTIOPI

The images taken for the DCR model were reduced in a manner identical to the parallax frames, as discussed in Section 2.4.1. Briefly, after the frames are bias subtracted and flat-fielded, SExtractor (Bertin and Arnouts 1996) is used to determine centroids for all stars of interest. Because each field was observed in the V_J , R_C and I_C filters, there is one frame each night that has the smallest hour angle. Those frames were selected as trail plates (or standard plates, which are considered to have no DCR) for each filter. Plate constants are calculated by using the GaussFit (Jefferys et al. 1987) program. A total of six plate constants were solved for, as discussed in Section 2.4.2 so that telescope shifts (translation movement) could be removed. We ignore any effects of source proper motion or parallax during the four nights of DCR observations because they are negligible on that time scale. Consequently, after calculating the plate constants, the only shifts in stellar centroids are due to atmospheric refraction. The amount of centroid shift from the trail plate in the X direction is a direct

measure of the refraction, as represented by the quantity on the left side of Equation (2.23). Monet et al. (1992) showed that because the refraction in the Y direction has been redefined as shown in equation (2.22) (effectively removing any shift in the Y direction for zero hour angle), the X shift (Z_x) will have more variation than the Y shift (Z_y) when the hour angle is different from zero. Therefore, we concentrate on the RA direction to determine the empirical polynomial function for R_m .

To determine the functional form of R_m , first the hour angle and Z_x for every useful star in the 10 DCR test fields are derived. Then, based on the centroid shift and Z_x for each star observed during the observing run, the slope of R_m versus Z_x can be found. Figure 2.7 shows an example for LHS0158 and a reference star in the field. The field was observed from 1.47 hours east of the meridian to 3.71 hours west, including seven sets of *VRI* observations at different hour angles. A linear fit was made to each star independently to determine R_m as a function of Z_x . Of course, as discussed above, the mean refraction is also a function of stellar color. So, the same method is applied for all 72 stars selected in the 10 different fields in order to provide an ensemble of refraction curves, R_m , which are functions of Z_x and stellar ($V - I$) color.

We set the zero point for DCR to be $R_m = 0$ when $(V - I) = 0$. Thus, the 0th order coefficient for each field is slightly different from the others and this offset can be computed by a least squares fit for a polynomial function, which is discussed in Appendix C. By combining the R_m slopes and the $(V - I)$ values for all 72 stars, we generate the plots in Figure 2.8, showing the empirical fits with solid curves.

The theoretical curves for all three filters⁵ from Stone (1996) were also calculated and are shown in Figure 2.8 as dashed lines. A hypothetical field at DEC = -26° , “observed” during a night with temperature $T = 12^\circ\text{C}$ and 40% humidity was chosen to generate the model curves. These conditions are similar to those encountered during CTIOPI observations. Twelve stars with spectral types of A0 V to M5 V were selected for the model, and were “observed” at positions that were 0 to 3 hours from the meridian.

The mean empirical refraction functions are,

⁵The FORTRAN code was kindly provided by M. Begam from the Siding Spring Observatory parallax project, led by P. Ianna.

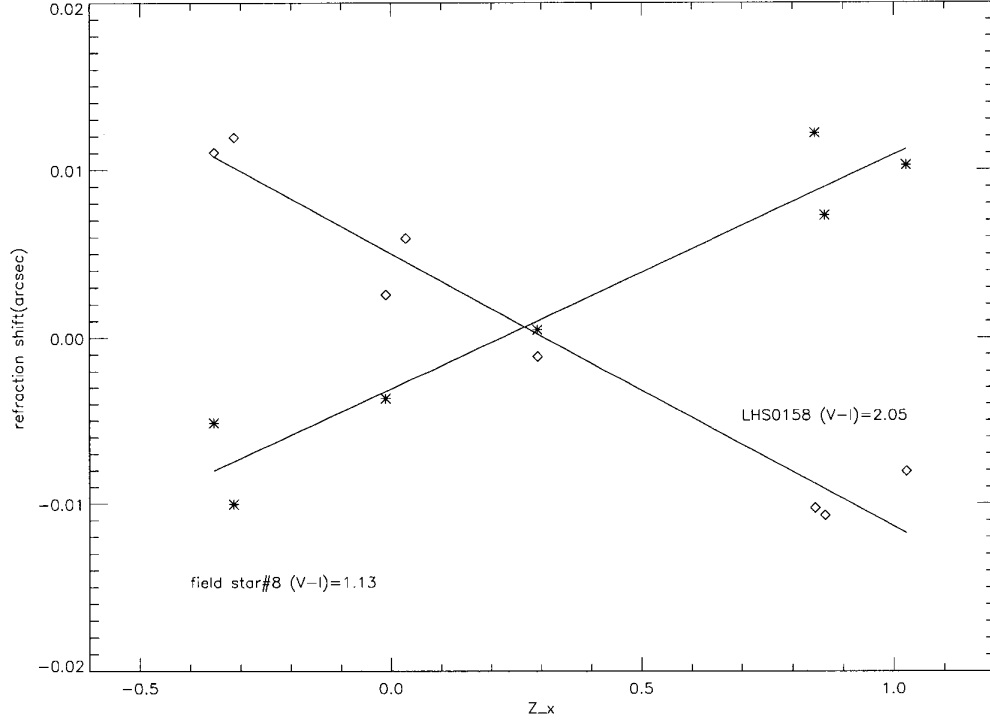


Figure 2.7: This plot illustrates examples of atmospheric refraction for two stars having different colors. The slope for LHS0158 is -0.016 , while the slope for field star #8 is 0.014 . Eight sets of VR frames were taken during eight visits spanning $HA = 1.47$ east to 3.71 west of the meridian. Field star #8 is deleted at $Z_x \approx 0.02$ due to the poor image quality.

$$\begin{aligned}
 F_V &= -0.0407(V - I) + 0.0941(V - I)^2, \\
 F_R &= -0.0417(V - I) + 0.0482(V - I)^2 - 0.0245(V - I)^3 \\
 &\quad + 0.0036(V - I)^4, \\
 F_I &= +0.0007(V - I)
 \end{aligned} \tag{2.25}$$

As expected, Figure 2.8 shows that I band has the least DCR of the three filters. In all three filters the average difference between the model and the empirical curve is less than 6 mas if the star's $(V - I)$ is less than 3.22. Because our DCR sample is deficient in very red stars, the difference increases at the red end of the R band

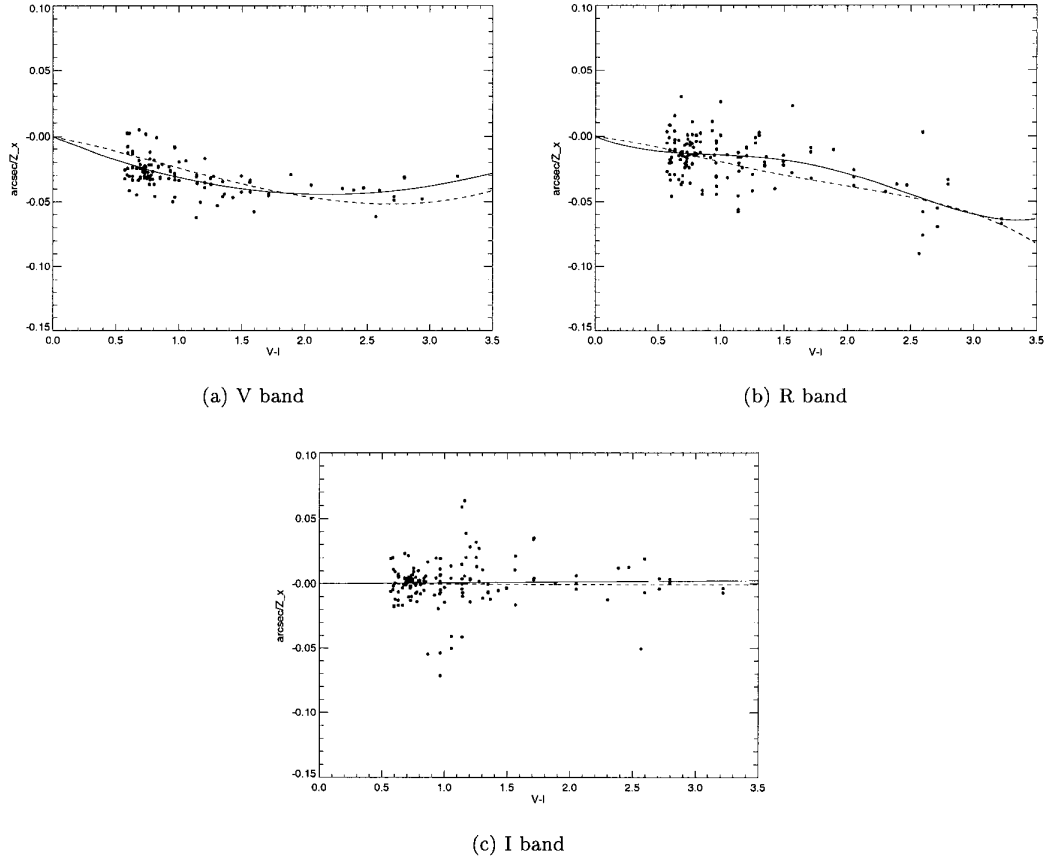


Figure 2.8: These three plots illustrate the empirical DCR data and the least squares fits (solid lines) used in the final astrometric reductions for all three filters used in CTIOPI: (a) is for the V filter, with a third order fit; (b) is for the R filter, with a fourth order fit; and (c) is for the I filter, with a first order fit. The curves from the theoretical models of Stone (1996) are plotted as dashed lines.

calibration. Note that when the stellar color is redder than $(V - I) = 2.6$, stars observed through the R filter will actually experience more refraction than they will when observed through the V filter. This result can be explained because we are discussing “differential” color refraction, i.e., the amount of refraction is affected by the assumption of zero refraction at zero color, even though two different filters are used.

A valuable comparison of astrometry reductions with and without DCR correction is shown in Figure 2.9. A series of high hour angle measurements were taken in mid-2003 to test our DCR protocol, as indicated by the points with HA between -100 and -200 minutes. The effects of DCR correction are clearly seen when comparing the right two panels in (a) to the right two panels in (b). In the case of no DCR correction, the (b) panels, the X direction residuals show a very deep “valley” and the Y direction residuals show a large scatter. After the DCR corrections are applied, the X residuals flatten out, and the Y residuals are reduced and more symmetric around zero.

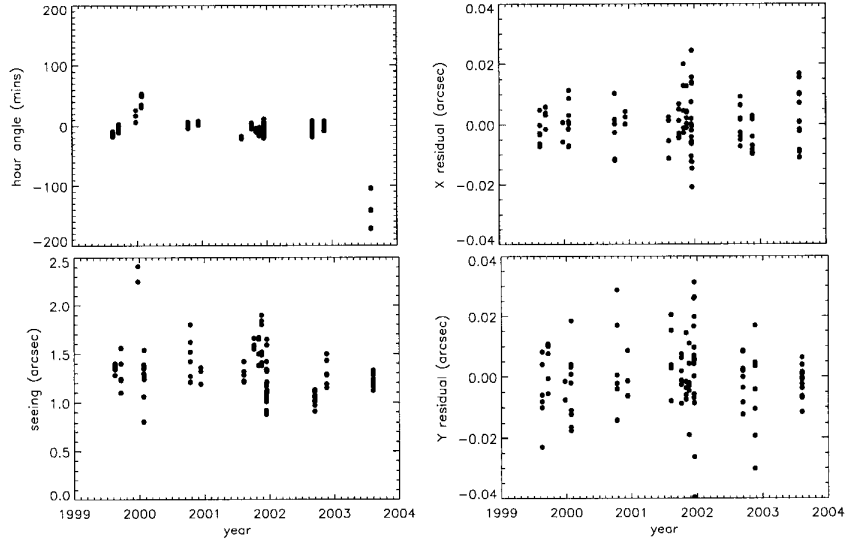
2.4 Astrometric Reductions

2.4.1 Initial Steps

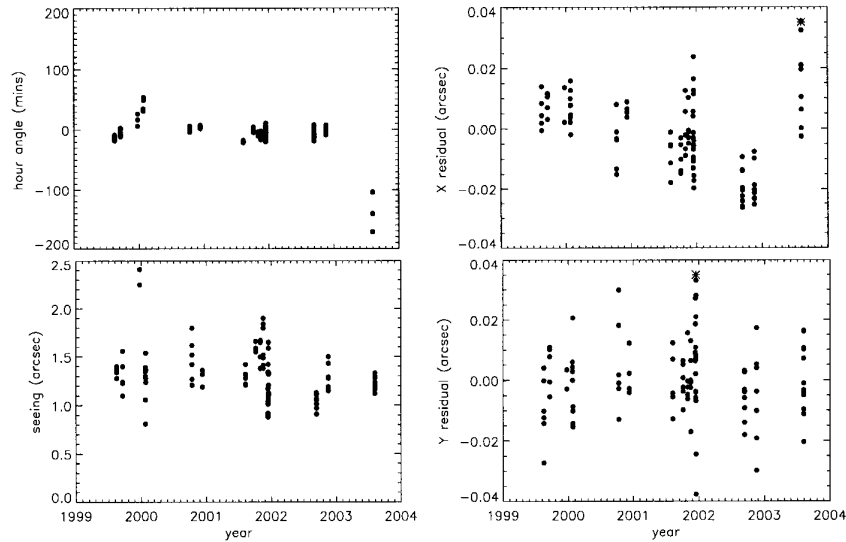
A flowchart outlining the astrometric data reduction pipeline is given in Appendix E (where instructions for those reducing astrometric data are given their entirety), Figure E.3. The basic data reduction for the astrometry CCD frames includes over-scan correction, bias subtraction, and flat-fielding, performed using an IRAF package called *redpi*, which was created by the author⁶. After processing the raw data, frames are sorted into storage directories by object until there are enough parallax frames and time coverage (e.g. 2.5 years coverage and 40 frames) to derive an astrometric solution.

When sufficient frames are available, *SExtractor* is used to determine centroids for each pi star and all pre-selected reference stars. The selection criteria for these reference stars are discussed in Appendix E. Before doing a parallax reduction, we check the *VRI* photometry so that DCR corrections and the correction from relative to absolute parallax can be carried out. We discuss photometry reductions in Chapter 3.

⁶Because our science stars are mostly red dwarfs, this package is called “*redpi*”.



(a) Example plot with DCR correction



(b) Example Plot without DCR correction

Figure 2.9: The effects of DCR corrections in the GJ1061 field are illustrated for both the X and Y directions. The improvement in the X and Y residuals is evident in the two sets of panels to the right in (a) and (b), especially in the X direction. In each set of four panels, the upper-left plot shows the hour angles of the observations vs. time and the lower-left plot represents the seeing vs. time. The * is a warning sign that at least one point at a given epoch has a residual greater than 30 mas.

Using the 2MASS coordinates for α_0 and δ_0 , the parallax factors for the pi star(s) and *all* of the reference stars are computed by the FORTRAN program, *genpif*. In addition to parallax factors, *genpif* also calculates the Julian date in the middle of exposure from information in the image header, applies the DCR corrections for the selected parallax filter, and selects a few high quality reference frames, called *trail plates*. The selection criteria for a trail plate are discussed in Appendix E. Usually, the best/final trail plate is the one with the smallest HA and best seeing among the high quality frames selected by *genpif*.

The rotation angle of the definitive trail plate is calculated relative to the Guide Star Catalog 2.2 (GSC2.2) using WCSTools/imwcs⁷. This program has been included in the *redpi/wcsangle* IRAF task. Our parallax images are usually deeper than GSC2.2, so stellar objects with apparent magnitudes brighter than 18.0 and FWHM smaller than 2".5 (but larger than 0".6 to avoid poor centroiding on 0".401 pixels) are used. Once the rotation angle is determined, the parallax factors and centroids for all reference stars and pi stars are recalculated by the FORTRAN program, *pltrotate*.

2.4.2 Least Squares Reduction of Images Taken at Many Epochs

The trail plate is used as a fundamental reference frame to which all other images are compared to remove any rotation and translation. The relationship between a frame and the trail plate is based on the measured positions of pre-selected reference stars. A new set of coordinates is derived as a function of the trail plate coordinates and a set of constants:

$$\begin{aligned}\xi &= Ax + By + C, \\ \eta &= Dx + Ey + F,\end{aligned}\tag{2.26}$$

where (ξ, η) denotes the set of coordinates after the transformation of this standard coordinate set and A–F are the *plate constants*. This six-constant model allows for a different scale in both the x and y directions, and compensates for different amounts of translation in both directions as well. The higher order plate constants (radial

⁷WCSTools is available at <http://tdc-www.harvard.edu/software/wcstools/>.

distortion: $Rx(x^2 + y^2)$, coma: Smx (m is magnitude), and decentering distortion: $P(x^2 + y^2)$ (Eichhorn, 1974) are not included in the current calculations because parallax results from our standard stars are within 2σ of all other observations and no systematic differences are seen (discussed in section 2.6).

Even a star located at 500 pc has a trigonometric parallax equal to $0''.002$, which is similar to the error in our final parallaxes. As discussed previously, analysis of the stellar path of the pi star must take into account both the proper motion and parallax, but each reference star also experiences both motions on the sky. Because it is very rare to know accurate proper motions and parallaxes for each of our pre-selected reference stars, we assume that the reference grid has $\sum_i \Pi_i = 0$ and $\sum_i \mu_i = 0$ (van Altena et al. 1986, Benedict et al. 1999). Hence, a set of constants for each frame can be calculated from the reference stars using:

$$\begin{aligned}
 A^1 x_1^1 + B^1 y_1^1 + C^1 + \mu_{x1} t + \Pi_1 P_{\alpha 1} &= \xi_1^t \\
 A^1 x_2^1 + B^1 y_2^1 + C^1 + \mu_{x2} t + \Pi_2 P_{\alpha 2} &= \xi_2^t \\
 A^1 x_3^1 + B^1 y_3^1 + C^1 + \mu_{x3} t + \Pi_3 P_{\alpha 3} &= \xi_3^t \\
 &\dots\dots\dots \\
 A^1 x_n^1 + B^1 y_n^1 + C^1 + \mu_{xn} t + \Pi_4 P_{\alpha n} &= \xi_n^t
 \end{aligned}
 \tag{2.27}$$

where superscripts indicate frame numbers, subscripts indicate the ID numbers of reference stars, and ξ_n^t represents the x coordinate for the trail plate. The plate constants, A , B , and C can be calculated from these equations using least squares methods which are constrained by the conditions of reference star parallaxes and proper motions summing to zero. A similiar set of equations can be applied for the y direction (plate constants D , E , and F in equation 2.26). After the plate constants and star constants (μ and Π) are acquired for the set of reference stars, μ and Π (and their errors) are computed for the pi star. Gaussfit typically requires three iterations to minimize χ^2 .

Currently, the Gaussfit program⁸ is used to run the least squares calculation. Where necessary, the input parallax model is a modified version of that used by the University of Texas HST Astrometry Team. The image quality of each frame and

⁸This is a program for least squares and robust estimation which is available from the Hubble Space Telescope (HST) Astrometry Team <ftp://clyde.as.utexas.edu/pub/gaussfit/manual/>.

the reliability of reference stars are determined using the results of the initial run of Gaussfit. Any pre-selected reference stars with high proper motion, parallax, residuals or high photometric parallax (discussed in Section 2.5) are deleted. Entire frames with high residuals are also removed. Additional details concerning the removal of bad reference stars and frames are given in Appendix E. The Gaussfit program is executed again to get the final pi star μ and Π after poor frames and reference stars have been removed.

2.5 Conversion of Relative to Absolute Parallax

The trigonometric parallax we have measured reflects the distance of the pi star relative to the set of reference stars. As discussed in van Altena (1974) and van Altena et al. (1988), there are (at least) three different ways to correct the *relative parallax* to true *absolute parallax* — using statistical methods, spectroscopic parallaxes for the reference stars, or photometric parallaxes for the reference stars.

Statistical methods rely on a model of the Galaxy for the disk and halo. By adopting a Galactic model and knowing the apparent magnitudes and Galactic coordinates of the reference stars, distances (and hence, parallaxes) can be estimated for the reference stars. No reference star color information is used. For example, van Altena et al. (1988) concludes that faint halo stars have ($14.5 < V < 15.5$) with a narrow distribution in their parallaxes for fields near the north Galactic pole. However, bright disk stars ($10.5 < V < 11.5$) exhibit a wide range of parallaxes. Therefore, faint reference stars have smaller mean parallaxes and require a small correction for the relative to absolute parallax conversion, while brighter reference stars require larger corrections. As discussed in Appendix E, the reference stars chosen for CTIOPI are the brightest available in the target fields (in order to obtain better centroids), so we do not use a statistical methodology for the conversion of relative to absolute parallax.

Using spectroscopic parallaxes is the most reliable method to determine the correction from relative to absolute parallax. In this method, the spectral type and luminosity class of every reference star are determined. This allows us to distinguish main sequence stars from giants and subdwarfs, and to apply correct $M_V - color$ relations for each class of star. However, this method requires a significant amount of observing time, and is not practical for CTIOPI, in which several hundred stars are observed, with an average of ~ 10 reference stars each.

Instead, we use the photometric parallax method to convert the pi star’s relative

parallax to its absolute parallax. *VRI* magnitudes for the pi star and all reference stars have already been acquired for the DCR correction, so the same data can be used to estimate a distance to each reference star. However, due to the lack of information about the luminosity class of these stars, this correction assumes that all of the reference stars are main-sequence stars. Additional corrections for the contamination by giants and because reddening has not been included will require further work.

The fundamental relations between M_V and color used in CTIOPI are based on the RECONS sample of stars within 10 pc (Henry 2004). Close multiple stars, subdwarfs, evolved stars, and stars with poor trigonometric parallaxes have been deleted from this sample to provide reliable $M_V - color$ relations. Three different colors, $(V - R)$, $(V - I)$, and $(R - I)$, are used to calculate the mean photometric parallax for each reference star. The error on the photometric parallax for an individual star is taken to be the average difference between the mean photometric parallax and the parallax from each color. The weighted mean photometric parallax of the entire set of reference stars is then calculated, and represents the final correction from relative to absolute parallax. The error in the final correction is determined from

$$\frac{err^1/\pi_1^{phot} + err^2/\pi_2^{phot} + \dots + err^n/\pi_n^{phot}}{n} \times \pi_{weighted-mean} \quad (2.28)$$

where n is the number of reference stars (not an exponent), err is the photometric parallax error of each star and π is the weighted mean photometric parallax of the ensemble of reference stars. We note that the mean absolute parallax correction for all MOTION stars from CTIOPI is 1.42 mas with 0.16 mas error.

2.6 CTIOPI Parallax Calibration Stars and Quality Check

Seven parallax standard stars were chosen to check the reliability of CTIOPI results. All but one, LHS1777, are within 10 pc, and they were selected so that different parts of the sky were represented. Of the seven stars, six currently have final parallax determinations with more than 60 frames spanning more than 2.9 years. The results for these stars are shown in Table 2.1 and Figure 2.10. Note that CTIOPI parallax errors are within 2σ of all other observations, indicating that the current parallax pipeline, DCR corrections, and conversion from relative to absolute parallax produce

reliable results.

Table 2.1: The parallax standard stars from CTIOPI.

	CTIOPI	Hipparcos	YPC	others
Proxima [†]	0.77425±0.00208	0.77230±0.00240	0.76980±0.00610	0.76991±0.00054 ^a
G10440 [†]	0.21507±0.00203	0.21640±0.00210	0.21830±0.00670	...
G10465 [†]	0.11027±0.00246	0.11250±0.00250	0.11250±0.00590	...
G10555	0.15846±0.00262	0.16350±0.00280	0.15760±0.00790	...
G10581 [†]	0.15466±0.00262	0.15950±0.00230	0.15790±0.00560	...
LHS1731	0.10870±0.00215	0.10786±0.00295
LHS1777	0.07520±0.00191 ^b	0.07700±0.00270

Note.— The numbers indicate $\pi \pm \text{error}$ in arcseconds. †: the available parallax has been improved during CTIOPI, and the star is in the MOTION sample. (a) The parallax error from HST is slightly different from Benedict et al. (1999) due to the improvement in the absolute parallax calculation (Benedict, private communication). (b) Because no *VRI* data are available for absolute parallax correction, the relative parallax is presented

The final parallax error is a combination of many factors, including (1) the accuracy of the coordinates, (2) the quality of the reference star frame (brightness, distribution), (3) the accuracy of the (x,y) centroids, (4) the total number of parallax images, (5) the time span, (6) parallax factor coverage, (7) the DCR correction, and (8) the correction of relative to final absolute parallax. The first three factors can not easily be modified after they are chosen. However, the duration and number of observations can be controlled, and depends only on the resources, staffing, and stamina of the CTIOPI Team. At present, a parallax target is considered “finished” when all of the following criteria are met⁹.

- the relative parallax error is less than 3 mas
- the target has been observed for 4 or more seasons (one season includes 2~3 months of continuous observations)
- the target has been observed for at least 2.5 years
- there are at least 40 frames of the field
- *VRI* photometry has been obtained for the field

In practice, an extended time span results in meeting most of these criteria, so it is perhaps the best single benchmark to be used to evaluate parallax errors for the entire

⁹Some objects are continuing to be observed because long-term perturbation searches have commenced.

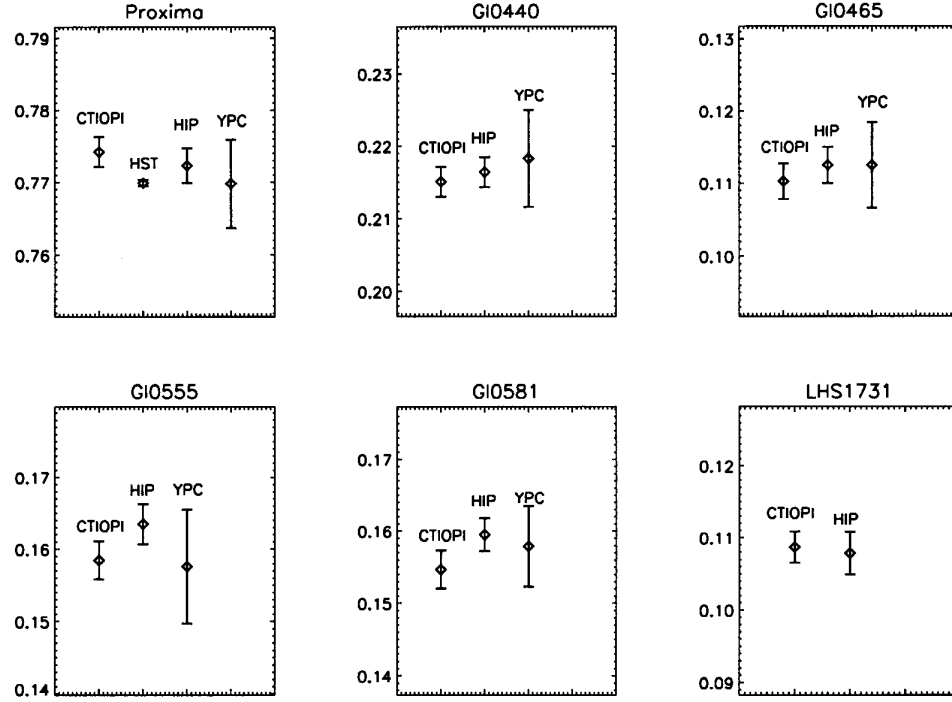


Figure 2.10: Comparison of CTIOPI parallaxes to parallaxes measured from the ground (YPC = Yale Parallax Catalog), and space (HIP = Hipparcos, HST = Hubble Space Telescope). Note that the CTIOPI parallaxes generally have smaller errors than those from YPC and have errors comparable to HIP.

survey. Figure 2.11 illustrates how time coverage affects the relative parallax error for 10 different stars within 10 pc (six are calibration stars and four are additional CTIOPI targets). Parallax reductions were executed using various subsets of the complete datasets (each star indicated with a symbol). A few stars show only ~ 2 mas error after only about one year of observations. In these cases, the parallaxes determined can be quite inaccurate, but a good fit with minimal formal error can be made to the proper motion and parallactic motion even though they have not yet been adequately decoupled. When key high parallax factor images are taken later, a different stellar path is determined and the error represents reality. The mean error for the 10 fields shown is 2.45 mas, which is reached at a time point 2.32 years into an observing sequence. We therefore conclude that 2.5 years of coverage is sufficient to determine accurate parallaxes with acceptable final errors. This is consistent with

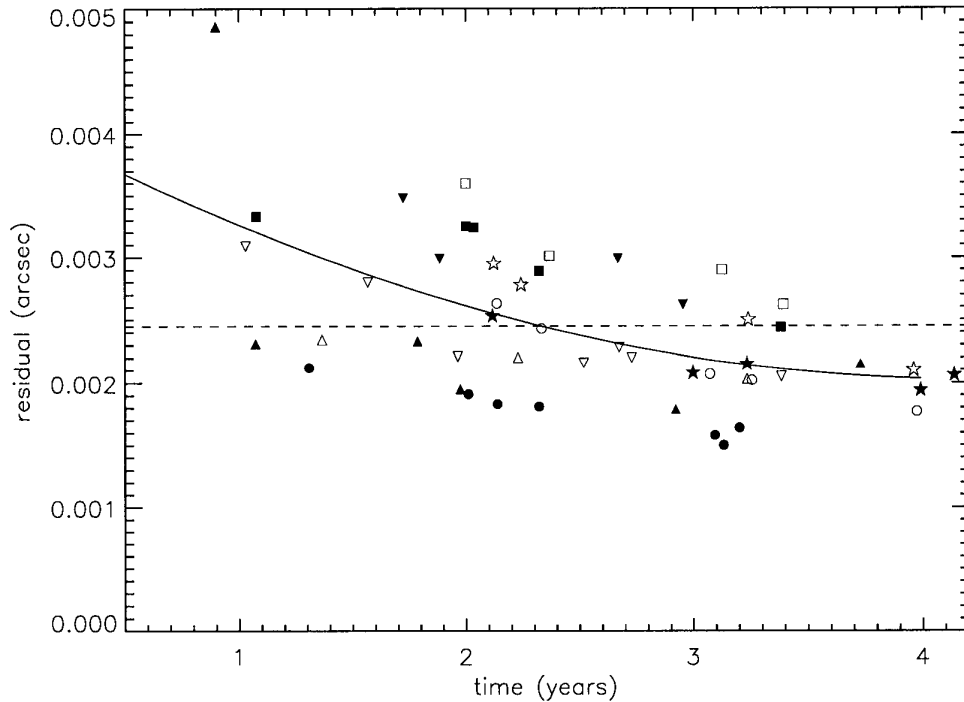


Figure 2.11: This plot shows the relation between relative parallax error and time coverage. The parallax errors for 10 nearby stars are plotted using different symbols. The dashed line indicates the mean error for these 10 fields. The crossover point of the decreasing errors and the mean error is at 2.32 years.

the results of Dahn et al. (2002), who find that the USNO parallaxes are stable after about 2 years observation. Note also that the final errors decrease negligibly after ~ 3 years.

2.7 Parallax Results for MOTION Stars

Parallax results for stars in the MOTION sample are presented in Table 2.2, broken into three blocks of data. The first block includes “definitive parallaxes”, which are for targets meeting the observational criteria discussed above. No more frames are being taken on these stars unless they are within 10 pc or show suspicious data, in which case they are targeted for perturbation studies. The second block includes “nearly definitive parallaxes”. Stars in this block need one more set of observations to

meet the minimum requirements. The third block includes “preliminary parallaxes” for stars which need either several more visits, or for which there is not yet any *VRI* photometry. The first three columns are the RA, DEC, and object name (some names have been abbreviated; full names can be found in Table A.1). The fourth, fifth, and sixth columns provide observational statistics, including the total number of seasons observed, the total frames used in the reductions, and the time coverage. The seventh column is the number of reference stars used for the reductions. The eighth column gives the relative parallax and error in mas, while the ninth column gives the absolute parallax correction (discussed in Section 2.5), and the tenth column gives the final absolute parallax. The eleventh and twelfth columns are the proper motion and position angle of the proper motion. The thirteenth column is the tangential velocity¹⁰ measured with respect to the Sun. The last column has a “!” if there are notes in the text relating to the object.

Figure 2.12 shows the statistics of the parallaxes now available for the MOTION sample. Of the 549 MOTION systems, 67 (12%) are currently included in CTIOPI. Of these, (a) 46 systems have first parallax determinations by CTIOPI, (b) 8 systems have improved parallaxes, (c) 4 currently do not have enough frames for definitive parallax determinations, and (d) 9 stars have been observed at the 1.5-m and we await final results from our Chilean collaborators. The dark gray region in the “no pi” histogram (38 systems) represents stars that are accessible to CTIOPI but which are not on the current program. Of these, 23 are brighter than $V=19.0$ and many will be added to CTIOPI.

2.7.1 Notes on Individual Stars

Definitive Parallaxes

LHS440 It has a mean Y-residual is larger than X-residual. Further investigation is necessary.

LHS463AB This is a close binary system with separation $1''.42$ (Jao et al. 2003). All 105 available frames were examined manually, and 59 images with good seeing were selected to permit parallax reductions for both components. The seeing diagnostics do not reflect the true seeing for the target system, so the FWHM has been set manually to prevent both pi stars being automatically removed from the reductions. The final absolute parallax errors are high for both

¹⁰ $V_{tan} = 4.74 * \mu / \pi$

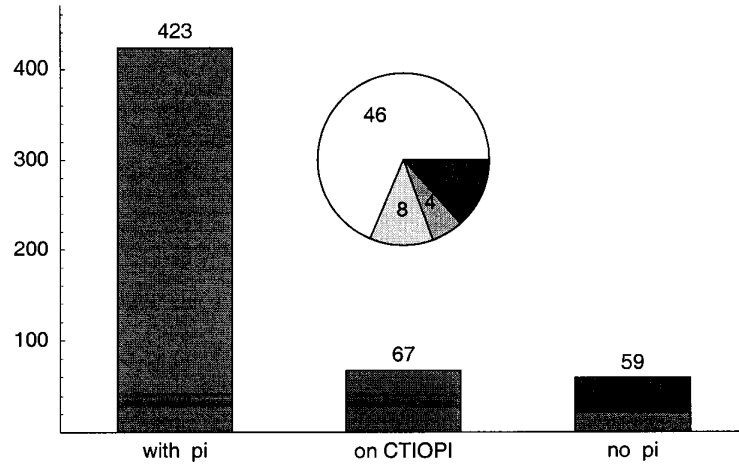


Figure 2.12: The current trigonometric parallax statistics from CTIOPI for MOTION stars (in number of systems). The dark gray portion of the “no pi” histogram represents 38 systems south of DEC +30 degrees that are accessible to CTIOPI. Details concerning the pie chart portion can be found in the text.

components because of their small separation. Position angles and separations have been calculated for the observations, but even though we have 3.11 years of observations, no orbital motion has been detected (which is consistent with the result in Jao et al. 2003).

Nearly Definitive Parallaxes

LHS157 This star has a very weak reference frame, so the reduction includes several stars that have fewer than 100 peak counts.

LHS193AB This is a relatively wide binary system with separation $12''.59$ (Jao et al. 2003). LHS0193B was reduced with all 68 frames available even though there are 37 frames with LHS0193B having fewer than 100 peak counts. Field star #3 in the frame has $\pi = 0''.02729 \pm 0''.00171$ (36.6pc), $\mu = 0''.0354/\text{yr}$, and $(V - I) = 2.71$.

LHS273 There is insufficient parallax factor coverage for this star for a definitive parallax, although it has more than 40 frames over 2.02 years.

LHS288 If the single image in 2002 is removed, there is a 1.5 year gap in between images.

LHS475 It has more than 40 frames over more than 2 years, but only one frame in the last epoch, 2003.2. Without the last frame, the coverage is only 1.96 years.

Preliminary Parallaxes

LHS124 There are only three portions of the parallactic ellipse that have significant coverage.

LHS164 The parallax star is on the edge of the CCD field and the parallax factor coverage is poor.

LHS225AB This is a close binary system with separation $2''.45$ (Jao et al. 2003). The available data covers only three epochs in 2.2 years. Because of the binary nature, images with ellipticity greater than 0.2 are included in the data reductions.

LHS263 There were only two frames taken in 2000. If those are removed, the coverage is only 2.7 years.

LHS272 There was only one image taken at epoch 2002.9. If it is removed, the coverage is only 1.14 years.

LHS300AB This is a binary system with separation $4''.28$ (Jao et al. 2003). There is a possible perturbation on component A. Additional data and further investigation are necessary.

LHS382 This star shows a curving trend in the Y-residuals. If frames 1-7 are removed, the curved feature decreases, but these frames have the highest parallax factors among all the frames. No suspicious features are seen in the X-residuals. This star is close to the ecliptic, so the semiminor axis of the parallactic ellipse is small in the Y-direction. There is strong nebulosity in the field.

LHS423 There was only one image taken in 2002. If it is removed, there is a 1.5 year gap.

J2231-7514AB This is a wide visual binary. No trail plate rotation has yet been applied for this field.

LHS532 This is an extremely preliminary result because there are only three epochs of data, and two of the three epochs only have one night of data.

LHS4058 If the first image is removed, the coverage is only 2.24 years.

Table 2.2: CTIOPI MOTION parallax results

RA (J2000.0)	DEC (2)	Name	Nsea	Nfrn	ΔT (yrs)	Nref	π (rel) (mas)	π (corr) (mas)	π (abs) (mas)	μ (mas/yr)	P.A. (deg)	V_{tan} (km/s)	Note
(1)	(2)	(3)	(4)	(5)	(6)	(7)	(8)	(9)	(10)	(11)	(12)	(13)	(14)
Definitive Parallaxes													
01 43 01.02	-67 18 30.3	LHS 145	4c	90	3.20	9	101.36 \pm 1.64	0.71 \pm 0.05	102.07 \pm 1.64	1074.2 \pm 1.3	198.7 \pm 0.12	47.0	
04 10 28.15	-53 36 08.2	LHS 22	5c	76	3.96	8	142.39 \pm 1.92	1.03 \pm 0.12	143.42 \pm 1.92	2553.5 \pm 1.6	199.1 \pm 0.06	84.4	
13 13 09.35	-41 30 39.7	ER2	4c	49	2.94	8	82.28 \pm 1.58	1.30 \pm 0.10	83.58 \pm 1.58	1027.6 \pm 1.8	271.7 \pm 0.15	58.3	
14 20 07.36	-09 37 13.4	LHS 369†	4c	49	3.16	9	71.02 \pm 1.38	0.50 \pm 0.03	71.52 \pm 1.38	1020.7 \pm 1.2	216.8 \pm 0.14	67.6	
17 18 25.59	-43 26 37.6	LHS 440	4s	85	2.94	9	35.19 \pm 2.14	1.71 \pm 0.47	36.90 \pm 2.20	1080.4 \pm 2.2	233.8 \pm 0.23	138.8	!
17 28 07.33	-62 27 14.2	LHS 3292	4s	67	2.72	10	59.37 \pm 1.50	1.74 \pm 0.16	61.11 \pm 1.50	959.3 \pm 1.6	197.4 \pm 0.18	74.4	
18 20 57.18	-01 02 58.0	LHS 463A	4c	59	3.11	10	37.31 \pm 5.27	5.12 \pm 0.26	42.43 \pm 5.27	1091.6 \pm 4.4	207.8 \pm 0.45	121.9	!
18 20 57.18	-01 02 58.0	LHS 463B	4c	59	3.11	10	26.27 \pm 6.14	5.12 \pm 0.26	31.39 \pm 6.14	1095.9 \pm 5.2	208.3 \pm 0.52	165.5	!
19 20 47.97	-45 33 29.7	LHS 60†	5c	121	4.06	9	166.76 \pm 1.52	2.27 \pm 0.32	169.03 \pm 1.55	2960.7 \pm 1.1	167.5 \pm 0.03	83.0	
20 27 42.08	-56 27 25.2	LHS 492	4c	87	2.87	12	48.13 \pm 2.13	2.40 \pm 0.18	50.53 \pm 2.14	1298.7 \pm 2.8	161.3 \pm 0.22	121.8	
20 28 03.81	-76 40 15.9	LHS 493	4c	68	2.95	7	76.96 \pm 2.24	2.06 \pm 0.17	79.02 \pm 2.24	1426.6 \pm 2.2	149.6 \pm 0.17	85.6	
20 55 37.11	-14 03 54.8	LHS 501B†	4c	70	3.00	9	81.07 \pm 1.54	0.88 \pm 0.05	81.95 \pm 1.54	1490.4 \pm 1.4	108.1 \pm 0.10	86.2	
20 55 37.76	-14 02 08.1	LHS 501A†	4c	70	3.00	9	76.71 \pm 1.49	0.88 \pm 0.05	77.59 \pm 1.49	1492.3 \pm 1.4	108.0 \pm 0.09	91.2	
21 30 47.66	-40 42 29.5	LHS 510	4c	56	3.11	8	82.44 \pm 2.52	1.16 \pm 0.14	83.60 \pm 2.52	1723.9 \pm 2.4	143.1 \pm 0.16	97.7	
21 38 43.65	-33 39 55.3	LHS 512	4c	63	3.13	8	80.34 \pm 2.10	1.68 \pm 0.06	82.02 \pm 2.10	1151.1 \pm 1.9	116.7 \pm 0.18	66.5	
22 27 59.21	-30 09 32.8	LHS 521	4c	68	3.15	11	20.60 \pm 1.59	1.00 \pm 0.07	21.60 \pm 1.59	1008.8 \pm 2.2	136.8 \pm 0.24	221.4	
23 10 42.16	-19 13 34.9	LHS 538	4c	62	3.12	8	40.15 \pm 2.31	0.99 \pm 0.06	41.14 \pm 2.31	1428.1 \pm 2.5	178.2 \pm 0.15	164.5	
23 15 51.60	-37 33 30.6	LHS 539	4c	54	2.89	8	51.93 \pm 2.01	0.92 \pm 0.07	52.85 \pm 2.01	1311.2 \pm 3.0	78.4 \pm 0.22	117.6	
23 36 52.30	-36 28 51.8	LHS 547	4c+	53	2.88	7	85.17 \pm 2.03	1.06 \pm 0.05	86.23 \pm 2.03	1168.9 \pm 2.2	87.0 \pm 0.16	64.3	
Nearly Definitive Parallaxes													
01 00 56.37	-04 26 56.5	LHS 130	3c+	44	2.36	6	86.61 \pm 2.46	0.57 \pm 0.05	87.18 \pm 2.46	1318.8 \pm 4.2	70.4 \pm 0.33	71.7	
02 39 50.71	-34 07 57.5	LHS 157	3c	66	2.13	6	90.68 \pm 4.41	1.42 \pm 0.43	92.10 \pm 4.43	1678.0 \pm 4.8	160.4 \pm 0.29	86.4	!
02 42 02.85	-44 30 58.7	LHS 158	3c	61	2.07	8	25.39 \pm 1.95	1.73 \pm 0.12	27.12 \pm 1.95	1009.5 \pm 2.4	86.9 \pm 0.22	176.4	
04 32 36.96	-39 02 14.6	LHS 193B	3c	68	2.20	8	25.39 \pm 3.42	2.21 \pm 0.21	28.81 \pm 3.42	1017.0 \pm 5.4	43.4 \pm 0.60	167.3	!
04 32 36.55	-39 02 03.4	LHS 193A	3c	68	2.20	8	29.99 \pm 1.70	2.21 \pm 0.21	32.20 \pm 1.71	998.3 \pm 2.9	44.8 \pm 0.33	147.0	!
08 59 05.30	-31 13 26.6	LHS 258	3c	50	2.15	11	53.11 \pm 1.84	1.41 \pm 0.11	54.52 \pm 1.84	1092.3 \pm 2.0	140.0 \pm 0.21	95.0	
09 44 47.34	-18 12 48.9	LHS 273	3c	45	2.02	8	88.49 \pm 2.97	1.70 \pm 0.13	90.19 \pm 2.97	1600.0 \pm 2.1	264.1 \pm 0.12	84.1	!
10 05 54.93	-67 21 31.2	WT0248	3c+	50	3.10	11	37.43 \pm 2.47	1.12 \pm 0.08	38.55 \pm 2.47	1209.9 \pm 2.0	265.2 \pm 0.15	148.8	
10 14 51.79	-47 09 24.1	LHS 281	3c	45	2.15	10	85.30 \pm 2.05	0.62 \pm 0.03	85.92 \pm 2.05	1127.0 \pm 2.2	291.7 \pm 0.20	62.2	
10 43 02.81	-09 12 40.8	WT1827	3c+	56	3.23	8	79.19 \pm 2.45	0.52 \pm 0.10	79.71 \pm 2.45	1961.1 \pm 2.2	280.0 \pm 0.11	116.6	
10 44 21.28	-61 12 35.5	LHS 288†	3c+	45	3.19	9	204.06 \pm 3.35	1.21 \pm 0.16	205.27 \pm 3.35	1644.7 \pm 2.5	347.9 \pm 0.15	38.0	!

Table 2.2: continued

RA (1)	DEC (2)	Name (3)	Nsea (4)	Nfrm (5)	ΔT (yrs) (6)	Nref (7)	π (rel) (mas) (8)	π (corr) (mas) (9)	π (abs) (mas) (10)	μ (mas/yr) (11)	P.A. (deg) (12)	V_{tan} (km/s) (13)	Note (14)
10 48 14.58	-39 56 07.0	DEN1048-3956	3c+	55	2.80	8	249.39 \pm 1.74	1.07 \pm 0.11	250.46 \pm 1.74	1532.4 \pm 2.1	229.0 \pm 0.16	29.0	
11 31 08.38	-14 57 21.3	LHS 306	3s	54	2.15	8	87.64 \pm 1.72	1.04 \pm 0.15	88.68 \pm 1.72	1430.3 \pm 2.4	163.2 \pm 0.17	76.5	
13 09 20.41	-40 09 27.0	LHS 346	3c	52	2.16	9	59.28 \pm 1.11	1.97 \pm 0.13	61.25 \pm 1.11	1231.5 \pm 1.4	143.6 \pm 0.13	95.3	
15 43 18.33	-20 15 32.9	LHS 406	3c+	42	2.72	10	45.72 \pm 1.72	1.75 \pm 0.28	47.47 \pm 1.74	1160.2 \pm 2.1	194.7 \pm 0.17	115.8	
19 20 54.37	-82 33 16.1	LHS 475	3c+	57	2.67	8	75.74 \pm 2.25	1.88 \pm 0.33	77.62 \pm 2.27	1269.1 \pm 2.2	164.7 \pm 0.16	77.5	!
Preliminary Parallaxes													
00 19 36.59	-28 09 38.8	LHS 110	3c	48	2.97	8	28.82 \pm 1.94	
00 19 37.02	-28 09 45.7	LHS 111	3c	48	2.97	8	29.90 \pm 2.00	
00 49 29.04	-61 02 32.7	LHS 124	4c	28	2.64	6	46.00 \pm 5.54	1.12 \pm 0.15	47.12 \pm 5.54	1120.0 \pm 5.4	94.8 \pm 0.46	112.7	!
00 50 17.09	-39 30 08.3	LHS 125	3s	28	1.90	5	15.95 \pm 5.63	2.06 \pm 0.16	18.01 \pm 5.63	1037.0 \pm 6.4	172.1 \pm 0.56	272.9	
03 01 40.57	-34 57 56.5	LHS 164	3c	44	1.99	9	32.48 \pm 6.84	!
07 04 45.84	-38 36 07.5	LHS 225A	3c	59	2.24	9	57.93 \pm 3.10	1.96 \pm 0.10	59.89 \pm 3.10	1206.8 \pm 3.4	103.0 \pm 0.27	95.5	!
07 04 45.84	-38 36 07.5	LHS 225B	3c	58	2.24	9	42.13 \pm 4.52	1.96 \pm 0.10	44.09 \pm 4.52	1222.5 \pm 4.9	103.3 \pm 0.39	131.4	!
09 17 05.33	-77 49 23.4	LHS 263	3s+	27	3.72	11	119.45 \pm 2.54	2.57 \pm 0.18	122.02 \pm 2.55	1040.2 \pm 2.5	141.8 \pm 0.28	40.4	!
09 43 46.17	-17 47 06.2	LHS 272	2s+	55	1.80	10	77.21 \pm 1.93	1.14 \pm 0.11	78.35 \pm 1.93	1437.4 \pm 3.2	279.5 \pm 0.21	87.0	!
11 11 13.70	-41 05 32.7	LHS 300AB	3c	43	1.98	12	30.61 \pm 2.31	1.65 \pm 0.17	32.26 \pm 2.31	1245.4 \pm 2.8	264.2 \pm 0.20	183.0	!
12 25 50.74	-24 33 17.8	LHS 327	3s	38	2.15	9	10.64 \pm 2.10	0.84 \pm 0.11	11.48 \pm 2.10	979.5 \pm 2.7	262.8 \pm 0.25	404.4	
12 29 34.54	-55 59 37.1	LHS 332	3c	38	2.09	10	72.30 \pm 1.54	2.89 \pm 0.88	75.19 \pm 1.77	1199.4 \pm 2.4	227.8 \pm 0.23	75.6	
12 38 49.11	-38 22 53.8	LHS 337	2c	33	0.96	14	150.52 \pm 3.57	1.41 \pm 0.14	151.93 \pm 3.57	1466.0 \pm 7.4	206.3 \pm 0.52	45.7	
13 10 01.80	+22 30 05.3	LHS 347	4c+	29	2.36	5	17.78 \pm 4.90	0.99 \pm 0.09	18.77 \pm 4.90	1163.6 \pm 4.7	232.5 \pm 0.47	293.8	
14 50 41.22	-16 56 30.8	LHS 382	3c	38	2.32	7	20.58 \pm 2.58	0.83 \pm 0.11	21.41 \pm 2.58	1427.1 \pm 3.0	244.0 \pm 0.23	315.9	!
16 35 40.40	-30 51 20.2	LHS 423	2c+	38	2.09	13	48.44 \pm 3.28	2.05 \pm 0.22	50.49 \pm 3.29	1158.1 \pm 3.1	223.6 \pm 0.31	108.7	!
22 20 26.97	-24 21 49.5	LHS 518	2+	52	1.34	11	21.68 \pm 5.38	
22 30 33.55	-75 15 24.2	J2231-7515	2c	29	1.43	10	65.55 \pm 5.16	!
22 30 40.00	-75 13 55.3	J2231-7514	2c	30	1.43	10	69.77 \pm 4.78	!
22 56 24.66	-60 03 49.2	LHS 532	2c+	38	1.81	9	58.03 \pm 1.36	!
23 59 51.38	-34 06 42.5	LHS 4058	4c+	36	3.44	9	60.80 \pm 4.47	!

Note -!: Notes are discussed in the text. !: Improved MOTION parallaxes; all others are the first parallaxes for the targets.

Nsea: c \Rightarrow seasons are compact; s \Rightarrow seasons are scattered or evenly distributed; + \Rightarrow only 1 or 2 frames at one epoch (included in the numbers given in the

Nsea column).

Chapter 3

Photometry for MOTION Stars

As discussed in the previous chapter, the minimum duration for the measurement of a reliable parallax is a sequence of observations over at least 2.5 years. The integrated observing time required to determine a final parallax amounts to roughly one night/star over the 2.5 year period. In order to utilize efficiently the limited staffing, observing, and financial resources, it is highly desirable to produce a list of probable nearby stars from high proper motion stars catalogs, i.e., the MOTION sample. One of the best ways to prioritize stars within the MOTION sample is to estimate a photometric distance for each star using optical and/or infrared photometry. Therefore, this chapter will discuss important photometric observations made for MOTION stars that were carried out for several reasons, including (1) to determine photometric distance estimates, (2) to characterize this important astrophysical sample (e.g. separating the rare high velocity subdwarfs from normal main sequence stars), and (3) to provide the photometry required for DCR corrections and conversions of relative to absolute parallaxes.

3.1 *VRI* Photometric Observations

All of the results in this chapter are from observations taken between November 1999 and December 2003. The *VRI* photometry for MOTION stars was acquired at two different sites. Southern hemisphere stars were observed at CTIO, and the northern stars were observed at the Kuiper Telescope of Steward Observatory, located on Mount Bigelow near Tucson, Arizona. The observations made at CTIO were made with the same telescope (0.9-m), instrument, and filter setup as was used for the parallax frames (discussed in Section 2.1).

The Kuiper Telescope used for the northern MOTION stars was equipped with a 2K×2K CCD imager (0".15/pixel and 5' field of view). Observations were made through the Harris *V*, Harris *R*, and Arizona *I* filters¹. Eight nights of observations were initially scheduled. However, because of non-photometric weather and forest fires that required the evacuation of observers from Mount Bigelow, only two nights of data are presented here.

Bias and dome flat images were acquired every night and used for basic science frame calibration. Most target stars were observed at $\sec z < 1.8$ or less (a few were between 1.8 and 2.0 airmasses). Various exposure times were used to reach $S/N \geq 100$ for each target star. Standard stars from Landolt (1992) and/or E-regions from Graham (1982) were observed to derive transformation coefficients. Each night at least one field with several reliable standard stars was observed at three different airmasses and was always within four hours of the meridian to provide an extinction curve. In addition, one or two very red standard stars fields were observed in order to get the second order transformation term. Typically, 4–5 standard star fields were observed 2–3 times per night depending on the length of the night. In addition, MOTION stars with reliable photometry in Bessell (1990) and Weis (1996) were also observed so that comparisons could be made between our photometry and theirs to check for any systematic offsets.

3.2 Photometry Reductions

The same data reduction package used for parallax frames, *IRAF/redpi*, was used for photometry frames taken at CTIO. A modified *IRAF/redpi* package was used for frames taken at the Kuiper Telescope, which had different CCD characteristics (e.g. size).

During reduction, stars of interest (science stars, reference stars for astrometry reductions, and photometric standard stars) are tagged within the *redpi/apercorr* task. If there are no background stars near a star of interest, a 7" radius aperture size is applied. After removing any prominent cosmic rays, the instrumental magnitude is determined by adding all the counts for all pixels falling in that aperture (i.e. aperture photometry). A 7" radius aperture size was always used for the standard stars, matching the aperture used by Landolt (1992). In the few cases where a

¹Harris *V* and *R* filters are the same as the *V* and *R* filters used at CTIO. However, according to the telescope manual, "Arizona *I* has a bluer central wavelength than *I_c*, but should match with the standard filter when convolved with the CCD on the 61-inch".

contaminating source is within the 7'' aperture, an aperture correction² is performed within the *redpi/apercorr* task. A sky annulus with 20'' inner radius and 3'' width was applied to calculate the sky background counts.

The second-order transformation equation for apparent magnitude is

$$m_{standard} = m_{inst} + a_1 + a_2x + a_3(color) + a_4(color)x, \quad (3.1)$$

where m_{inst} is the instrumental magnitude from *IRAF/DAOPHOT*, a_1 through a_4 are the transformation coefficients, *color* is the color term (which may have various permutations using *VRI* magnitudes), x is the airmass and $m_{standard}$ is the standard magnitude from Landolt (1992). The *IRAF/fitparam* task is used to compute these coefficients via a least squares method. To generate the final *VRI* magnitudes, the transformation equation is applied using a custom-made Perl task, *evalfit.pl* developed by the author. The advantage of this Perl script over the *IRAF/evalfit* task is that the output file contains not only the *VRI* apparent magnitudes, but image names, magnitude errors, and the date of data reduction. These output files are then concatenated into a large master photometry database for future access.

Additional details of the full photometry data reduction pipeline and the usage of the *evalfit.pl* script are discussed in Appendix D.

3.3 MOTION Sample *VRI* Photometry Results

Before this thesis project began, 154 (28%) of the 549 MOTION systems were without complete *VRI* photometry. We provide here new *VRI* photometry for 86 (56%) of these systems, and new observations for an additional 35 systems that already had published *VRI* photometry. Of the remaining 68 systems without photometry, 23 are north of +30 degrees and are not observable from CTIO. The remaining 45 systems are on the CTIO photometry observing list of the RECONS Team. The statistics for *VRI* photometry for the complete MOTION sample are illustrated in Figure 3.1.

Complete *VRI* photometry results for the MOTION sample are given in Table 3.1. The first three columns give the RA, DEC, and names. The next three blocks of data are the *VRI* photometry, signal-to-noise ratio (S/N) error, and the errors from the calibration of the standard stars. The S/N errors come directly from

²The aperture correction is the magnitude difference between the asymptotic magnitude as aperture size increases and the magnitude at the given aperture.

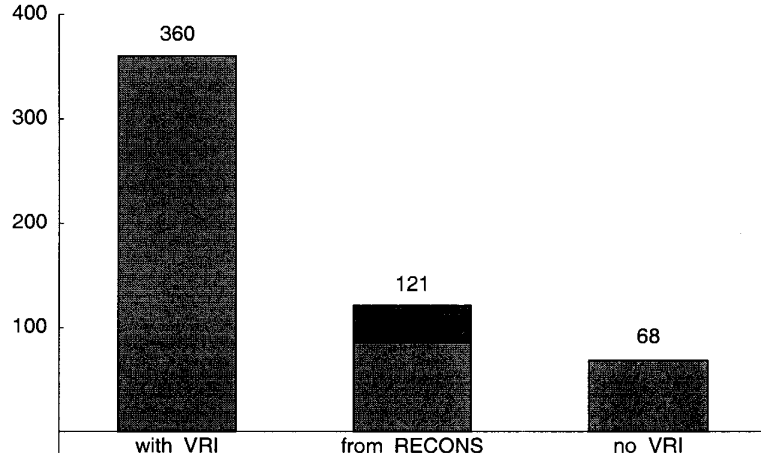


Figure 3.1: Of the 549 MOTION sample systems, 121 have been observed by RECONS. Of these, 86 are new *VRI* photometry and 35 are revised/repeated observations (shown as the dark segment of the RECONS bar).

the *IRAF/DAOPHOT* task. This error is usually very small because our observations normally have very high S/N. The standard star errors are determined using the residuals to the least squares fits of the standard stars. All of the science stars observed during a single night will have the same standard star error in a given filter. We do not yet have a sufficient database to determine accurately the night-to-night variations in the *VRI* photometry (e.g. due to stellar variability), although future work will concentrate on this aspect of the photometry.

The thirteenth column lists the number of nights each star was observed, and the fourteenth column indicates the observatory site. The fifteenth column indicates the aperture size (diameter in arcsec) applied for *VRI* images, respectively. If two different aperture sizes were used for different nights, a “va” is listed for various apertures. The final column shows references for *VRI* photometry published by other groups, again for *VRI*, respectively.

3.4 Reliability Checks and Comparison with Other Observations

Figure 3.2 shows the S/N errors and standard star errors for all MOTION stars in this work, except two binaries separated by less than a few arcseconds, LHS300AB

and Gl473AB. The S/N error plot shows that errors increase for fainter stars. It is not a surprise that the standard star errors are less than 0.03 magnitudes for all three filters. Mean standard star errors for *VRI* are 0.015, 0.014, 0.017 magnitudes, respectively. The S/N error is usually much less than the standard star error, unless the apparent magnitude is fainter than magnitude ~ 16 . We conclude that we have achieved a photometric accuracy of 0.03 magnitudes at *VRI* for all but the faintest stars.

A check on the reliability of our measurements can be made by comparing our values to published observations. The *VRI* MOTION photometric data have been compared with four sources, including Bessell (1990), Weis (1996)³, Patterson et al. (1998), and the USNO parallax program. In order to increase the number of stars in the comparisons, stars observed by RECONS but not in the MOTION sample have been added. The results of the comparisons are displayed in Figure 3.3. The differences in magnitudes (delta magnitude, in the sense RECONS–published) in the different filters are plotted with various symbols. There is a systematic difference ~ 0.03 magnitude (average for all three filters) from Bessell (1990). However, it is clear that our photometric data exhibit no systematic differences from Weis (1996) which has 14 stars in common to our sample. A trend is apparent in the comparison with Patterson et al. (1998), especially in the I band. This is caused by the omission of the color-dependent term in the transformation equation used by Patterson et al. (1998). Finally, in the lower right panel, observations for 17 MOTION stars are compared to USNO *V* band measurements (only the *V* band has been reported by USNO). There is no systematic difference between the MOTION and USNO photometry at *V*. Some of the differences may be explained by stellar variability.

³ *R* and *I* magnitudes from Weis (1996) have been converted to *R* and *I* on the Cousins systems.

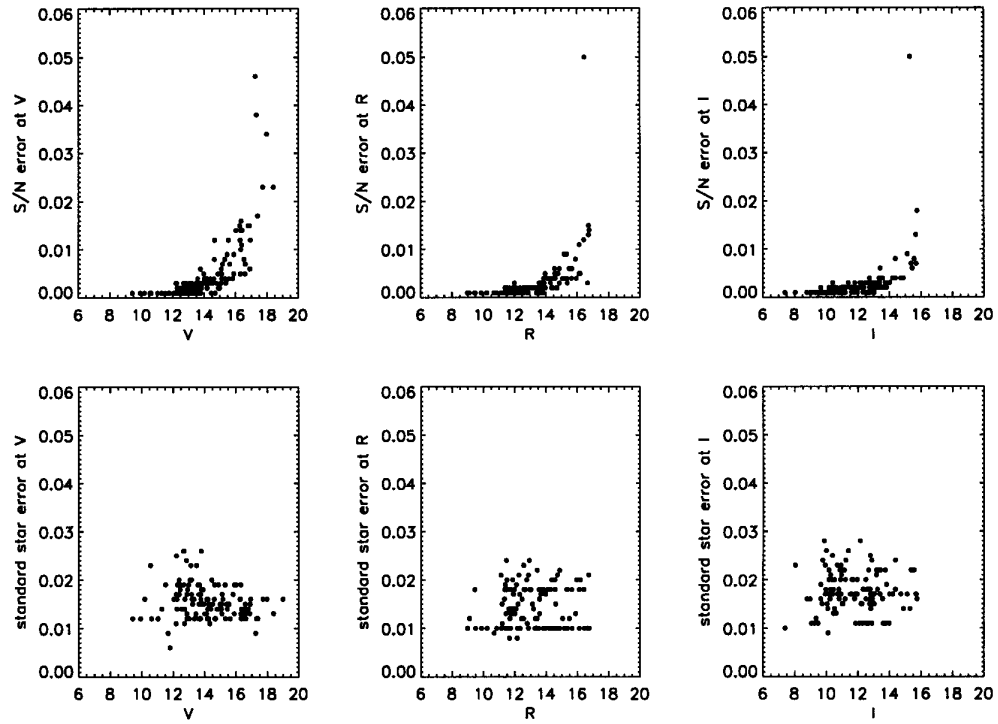


Figure 3.2: The top three plots show the S/N errors for MOTION *VRI* photometry. The bottom three plots show the standard star errors for the three filters. Stars observed in the same night have the same standard star errors at each filter.

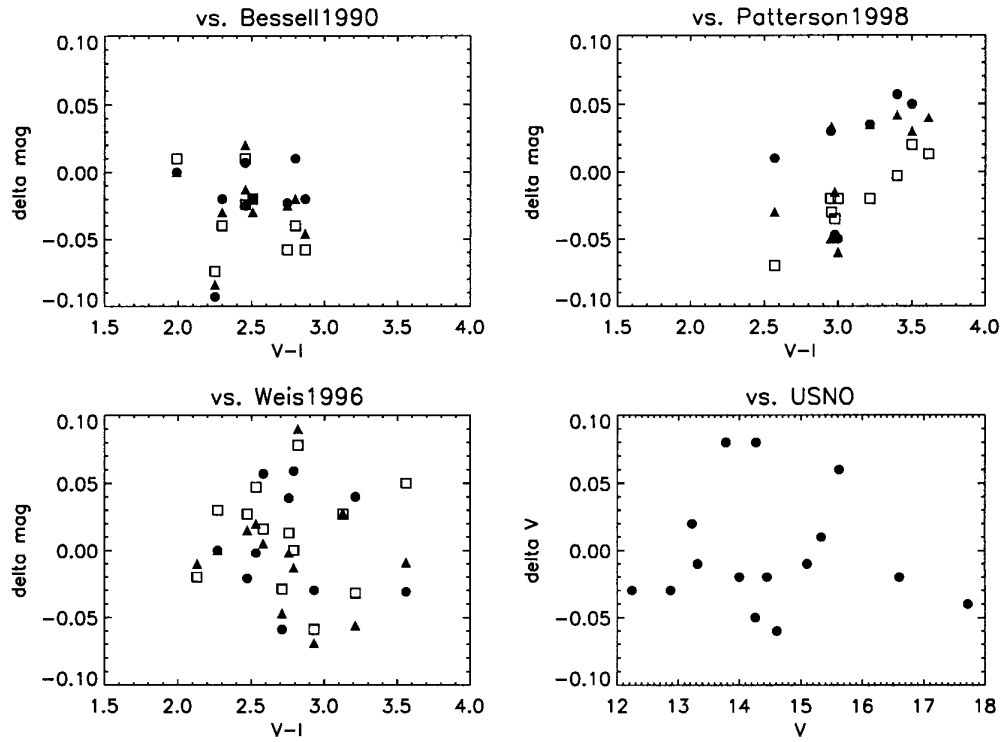


Figure 3.3: The differences in VRI magnitudes between RECONS measurements and those published by other authors are shown as a function of $(V-I)$ color (in the sense RECONS–published). The symbols for VRI are filled circles, filled triangles and open squares, respectively. The lower right panel shows ΔV vs. V for MOTION and USNO observations.

Table 3.1: MOTION V/R/I photometry results

RA (J2000.0)	DEC (2)	Name (3)	V (mag) (4)	$\sigma_{err}^{S/N}$ (mag) (5)	σ_{std}^{std} (mag) (6)	R (mag) (7)	$\sigma_{err}^{S/N}$ (mag) (8)	σ_{std}^{std} (mag) (9)	I (mag) (10)	$\sigma_{err}^{S/N}$ (mag) (11)	σ_{std}^{std} (mag) (12)	N (13)	site (14)	aper (") (15)	Refs (16)
00 04 36.45	-40 44 02.7	LHS 102	12.87	0.001	0.017	11.66	0.001	0.008	10.11	0.001	0.009	1	C	14.14,14	
00 09 16.46	+09 00 41.9	LHS 104	13.73	0.002	0.012	12.87	0.001	0.010	12.09	0.002	0.011	1	S	14.14,14	19,
00 09 17.31	-19 42 31.6	LHS 105	15.56	0.004	0.015	14.36	0.002	0.020	12.68	0.001	0.022	1	C	14.14,14	
00 11 31.82	+59 08 39.9	LSR0011+5908	14.65	0.012	0.012	13.89	0.003	0.010	11.85	0.002	0.011	1	S	14.14,14	
00 49 29.04	-61 02 32.7	LHS 124	12.18	0.001	0.011	11.19	0.001	0.015	9.93	0.001	0.017	2	C	14.14,14	
00 50 17.09	-39 30 08.3	LHS 125	14.33	0.003	0.011	13.59	0.002	0.018	12.92	0.002	0.016	1	C	14.14,14	
00 55 43.89	-21 13 07.1	LHS 127	15.81	0.004	0.017	14.87	0.003	0.022	13.73	0.003	0.022	1	C	14.14,14	
01 00 56.37	-04 26 56.5	LHS 130	13.35	0.001	0.012	12.08	0.001	0.014	10.52	0.001	0.014	2	CS	14.14,14	
01 31 30.82	+10 01 29.8	LHS 1257	16.38	0.011	0.012	15.21	0.004	0.010	13.77	0.002	0.011	1	S	14.14,14	19,
01 38 49.04	+11 21 36.7	LHS 144	16.32	0.010	0.012	15.21	0.004	0.010	13.98	0.003	0.011	1	S	14.14,14	
01 43 01.02	-67 18 30.3	LHS 145	13.83	0.002	0.015	13.55	0.002	0.018	13.23	0.002	0.018	2	C	14.14,14	3,3,3
02 39 50.71	-34 07 57.5	LHS 157	11.79	0.001	0.006	10.68	0.001	0.009	9.35	0.001	0.012	1	C	14.14,14	
02 42 02.85	-44 30 58.7	LHS 158	13.64	0.003	0.015	12.66	0.002	0.018	11.60	0.002	0.017	2	C	14.14,14	4,
02 46 14.92	-04 59 20.6	LHS 17	16.32	0.010	0.012	14.67	0.002	0.010	12.68	0.001	0.011	1	S	14.14,14	17,
02 46 34.74	+16 25 10.2	LHS 1443	17.31	0.038	0.012	15.17	0.009	0.010	12.88	0.003	0.011	1	S	14.14,14	
02 52 45.51	+01 55 50.5	LHS 161	14.64	0.008	0.019	13.70	0.003	0.018	12.78	0.003	0.018	1	C	14.14,14	
02 56 13.21	-35 08 26.9	LHS 162	15.38	0.003	0.015	14.44	0.002	0.020	13.43	0.002	0.022	1	C	14.14,14	
03 16 26.79	+38 05 55.8	LHS 170	10.62	0.001	0.012	9.87	0.001	0.010	9.25	0.001	0.011	1	S	14.14,14	3,3,3
03 28 53.11	+37 22 56.7	LHS 173	11.03	0.001	0.012	10.22	0.001	0.010	9.48	0.001	0.011	1	S	14.14,14	
03 35 38.61	-08 29 22.7	LHS 176	15.89	0.009	0.019	14.29	0.003	0.018	12.32	0.001	0.018	1	C	14.14,14	3,3,3
04 03 38.44	-05 08 05.4	LHS 186	14.87	0.005	0.019	13.85	0.004	0.018	12.73	0.004	0.018	1	C	14.14,14	
04 10 28.15	-53 36 08.2	LHS 22	13.62	0.001	0.017	12.21	0.001	0.015	10.44	0.001	0.013	2	C	14.14,14	
04 31 43.99	-21 50 44.3	LHS 1676	16.01	0.014	0.019	14.57	0.005	0.018	12.71	0.003	0.018	1	C	14.14,14	
04 32 42.63	-39 47 12.4	LHS 1678	12.49	0.002	0.019	11.46	0.001	0.018	10.26	0.001	0.018	1	C	14.14,14	
04 32 35.96	-39 02 14.6	LHS 193 B	17.25	0.046	0.009	16.45	0.050	0.010	15.30	0.050	0.014	2	C	14.14,14	
04 32 36.55	-39 02 03.4	LHS 193	11.67	0.001	0.009	10.84	0.001	0.010	10.09	0.001	0.014	2	C	14.14,14	
04 37 47.41	-08 49 10.6	LHS 194	13.75	0.002	0.017	13.43	0.002	0.022	13.17	0.003	0.022	1	C	14.14,14	
05 07 57.10	-53 01 56.5	LHS 202	12.27	0.002	0.019	11.36	0.001	0.018	10.45	0.001	0.018	1	C	14.14,14	
05 13 05.36	-59 38 44.4	LHS 204	9.42	0.001	0.012	9.10	0.001	0.012	8.77	0.001	0.016	1	C	14.14,14	11,
05 48 00.20	+08 22 14.0	LHS 211	14.13	0.004	0.016	13.20	0.002	0.014	12.25	0.003	0.015	2	CS	14.14,14	
06 27 33.30	+06 16 58.9	LSR0627+0616	16.30	0.014	0.019	15.32	0.009	0.018	14.37	0.008	0.018	1	C	14.14,14	
07 04 45.84	-38 36 07.5	LHS 225	12.87	0.003	0.012	11.85	0.002	0.014	10.51	0.002	0.013	1	C	2, 2, 2	
07 04 45.84	-38 36 07.5	LHS 225 B	13.02	0.003	0.012	11.99	0.003	0.014	10.63	0.002	0.013	1	C	2, 2, 2	

Table 3.1: continued

RA (1)	DEC (2)	Name (3)	V (mag) (4)	$\sigma_{err}^{S/N}$ (mag) (5)	σ_{err}^{std} (mag) (6)	R (mag) (7)	$\sigma_{err}^{S/N}$ (mag) (8)	σ_{err}^{std} (mag) (9)	I (mag) (10)	$\sigma_{err}^{S/N}$ (mag) (11)	σ_{err}^{std} (mag) (12)	N (13)	site (14)	aper (") (15)	Refs (16)
07 13 40.58	-13 27 57.1	LHS 227	14.45	0.001	0.020	13.59	0.001	0.013	12.78	0.001	0.025	1	c	14,14,14	5, ,
07 16 27.70	+23 42 10.4	LHS 228	15.53	0.012	0.015	14.56	0.006	0.020	13.34	0.004	0.022	1	c	14,14,14	
07 35 46.32	+03 29 36.0	LHS 232	13.68	0.002	0.019	13.00	0.002	0.018	12.38	0.002	0.018	1	c	14,14,14	
08 01 29.01	+10 43 04.2	LHS 1970	17.72	0.023	0.016	16.72	0.013	0.010	15.66	0.013	0.017	1	c	14,14,14	13, 13
08 59 05.30	-31 13 26.6	LHS 258	13.79	0.001	0.018	12.56	0.001	0.012	10.95	0.001	0.021	2	c	14,14,14	
09 17 05.33	-77 49 23.4	LHS 263	13.16	0.002	0.017	11.86	0.002	0.020	10.16	0.001	0.020	3	c	va,va,va	
09 20 21.93	+26 43 43.0	LHS 266	15.62	0.007	0.012	14.19	0.004	0.010	12.51	0.003	0.011	1	s	14,14,14	5, ,
09 20 57.94	+03 22 06.5	LHS 267	13.32	0.002	0.016	12.17	0.001	0.010	10.70	0.001	0.017	1	c	9,14,14	5,3,3
09 29 11.09	+25 58 09.3	LHS 269	16.41	0.014	0.013	14.78	0.005	0.010	12.81	0.003	0.014	2	cs	14,14,14	6,6,6
09 38 53.83	-33 48 45.4	CE89	16.87	0.015	0.013	15.34	0.004	0.018	13.38	0.003	0.017	1	c	14,14,14	
09 42 46.36	-68 53 06.1	LHS 271	12.74	0.002	0.016	11.39	0.002	0.019	9.65	0.002	0.019	3	c	14,14,14	
09 43 46.17	-17 47 06.2	LHS 272	13.16	0.001	0.020	12.10	0.001	0.019	10.89	0.001	0.020	2	c	14,14,14	18,18,18
09 44 47.34	-18 12 48.9	LHS 273	12.39	0.002	0.017	11.20	0.001	0.011	9.64	0.001	0.016	2	c	va,va,va	
10 05 54.93	-67 21 31.2	WTT0248	14.52	0.003	0.015	13.40	0.001	0.010	11.95	0.001	0.017	2	c	va,va,va	15,15,15
10 14 51.79	-47 09 24.1	LHS 281	13.49	0.002	0.023	12.26	0.001	0.021	10.69	0.001	0.023	2	c	14,14,14	
10 36 03.10	-14 42 29.1	LHS 284	16.79	0.015	0.014	15.49	0.006	0.012	13.81	0.002	0.019	3	c	14,14,14	
10 43 02.81	-09 12 40.8	WTT1827	15.11	0.005	0.017	13.57	0.003	0.016	11.61	0.002	0.020	2	c	14,14,14	15,15,15
10 44 21.28	-61 12 35.5	LHS 288	13.90	0.003	0.018	12.31	0.001	0.017	10.27	0.001	0.021	3	c	va,va,va	
10 48 14.58	-39 56 07.0	DEN11048-3956	17.39	0.017	0.012	15.06	0.004	0.012	12.57	0.001	0.018	3	c	14,14,14	,7
10 52 04.25	+13 59 51.4	LHS 295	12.71	0.001	0.014	11.54	0.001	0.010	10.05	0.001	0.015	1	c	14,14,14	3,3,3
11 10 08.38	+28 56 50.8	LHS 297	13.23	0.003	0.016	12.23	0.001	0.010	10.93	0.001	0.017	1	c	14,14,14	8, ,
11 11 22.68	-06 31 56.4	LHS 299	14.78	0.003	0.014	13.85	0.002	0.010	12.94	0.002	0.015	1	c	14,14,14	
11 11 13.70	-41 05 32.7	LHS 300AB	13.17J	0.001	0.012	12.28J	0.001	0.012	11.47J	0.001	0.016	1	c	14,14,14	
11 28 00.49	-09 10 56.6	LHS 2412	12.37	0.001	0.020	11.43	0.001	0.013	10.38	0.001	0.025	1	c	14,14,14	2,2,2
11 31 08.38	-14 57 21.3	LHS 306	14.19	0.002	0.014	12.80	0.001	0.011	11.05	0.001	0.015	2	c	14,14,14	
11 45 42.96	-64 50 29.7	LHS 43	11.51	0.001	0.019	11.34	0.001	0.016	11.20	0.001	0.020	2	c	va,va,va	1,1,1
11 52 32.09	+27 30 51.3	LHS 2467	12.24	0.003	0.014	11.70	0.002	0.010	11.18	0.002	0.016	1	c	14,14,14	5, ,
11 53 12.43	-31 23 56.1	LHS 317	13.65	0.002	0.012	12.42	0.001	0.012	10.81	0.001	0.016	1	c	14,14,14	
11 56 54.87	+26 39 56.3	LHS 318	15.45	0.009	0.014	14.49	0.004	0.010	13.56	0.004	0.016	1	c	14,14,14	
12 02 33.66	+08 25 50.7	LHS 320	14.00	0.004	0.013	13.03	0.002	0.018	11.87	0.002	0.017	1	c	14,14,14	8, ,
12 17 30.18	-29 02 20.7	LHS 323	16.93	0.012	0.016	15.66	0.006	0.010	14.00	0.003	0.017	1	c	14,14,14	
12 23 56.21	-27 57 46.4	LHS 325a	18.39	0.023	0.013	16.42	0.012	0.018	14.20	0.004	0.017	1	c	14,14,14	
12 24 26.81	-04 43 36.7	LHS 326	14.90	0.002	0.014	13.97	0.002	0.010	13.03	0.001	0.015	1	c	14,14,14	

Table 3.1: continued

RA (1)	DEC (2)	Name (3)	V (mag) (4)	σ_{err}^{std} (mag) (5)	R (mag) (7)	σ_{err}^{std} (mag) (8)	I (mag) (10)	σ_{err}^{std} (mag) (11)	N (13)	site (14)	aper (") (15)	Refs (16)
12 24 52.49	-18 14 32.2	LHS 45	11.27	0.001	10.23	0.001	8.97	0.001	1	c	14,14,14	2,2,2
12 25 50.74	-24 33 17.8	LHS 327	12.71	0.001	12.15	0.001	11.60	0.001	1	c	14,14,14	
12 29 34.54	-55 59 37.1	LHS 332	13.23	0.001	12.02	0.001	10.41	0.003	2	c	14,14,14	3,3,3
12 33 17.41	+09 01 15.7	Gl 473 AB	12.46J	0.002	10.88J	0.001	8.92J	0.001	2	c	14,14,14	2,2,2
12 34 15.78	+20 37 05.7	LHS 334	17.97	0.034	16.76	0.014	15.12	0.009	1	c	14,14,14	
12 34 53.18	+05 03 54.1	LHS 335	16.60	0.007	15.64	0.004	14.71	0.004	1	c	14,14,14	5, ,
12 38 49.11	-38 22 53.8	LHS 337	12.73	0.001	11.42	0.001	9.73	0.001	1	c	14,14,14	15,15,15
12 40 24.19	-23 17 43.8	LHS 339	16.53	0.008	16.12	0.011	15.74	0.018	1	c	14,14,14	
13 08 39.57	+08 04 21.9	LHS 345	15.07	0.003	13.82	0.001	12.19	0.002	1	c	14,14,14	9, ,
13 09 20.41	-40 09 27.0	LHS 346	12.86	0.002	11.73	0.001	10.24	0.001	2	c	14,14,14	3,3,3
13 10 01.80	+22 30 05.3	LHS 347	12.44	0.001	11.76	0.001	11.14	0.002	3	cs	14,14,14	17, ,
13 13 09.35	-41 30 39.7	ER2	12.91	0.001	11.61	0.001	9.96	0.001	1	c	14,14,14	15,15,15
13 39 15.35	+15 40 57.9	LHS 2774	14.27	0.003	13.13	0.002	11.70	0.002	2	cs	14,14,14	8, ,
13 46 55.52	+05 42 56.4	LHS 360	15.16	0.007	14.27	0.004	13.41	0.006	1	c	14,14,14	
14 18 20.43	-52 24 12.6	LHS 367	13.20	0.003	12.34	0.002	11.51	0.002	1	c	14,14,14	
14 20 07.36	-09 37 13.4	LHS 369	12.84	0.001	11.69	0.001	10.15	0.001	2	c	14,14,14	
14 20 52.95	+36 57 17.2	LHS 370	16.28	0.012	14.73	0.005	12.87	0.003	1	s	14,14,14	
14 35 08.89	+16 53 54.4	LHS 376	15.08	0.006	13.96	0.005	12.49	0.003	2	cs	14,14,14	
14 47 25.35	-17 42 15.8	LHS 378	16.34	0.016	15.89	0.008	15.44	0.006	1	c	14, 8, 8	1,1,1
14 50 41.22	-16 56 30.8	LHS 382	15.30	0.008	14.61	0.004	13.17	0.002	2	c	14,14,14	18,18,18
14 55 35.83	-15 33 44.0	LHS 385	14.61	0.004	16.67	0.003	12.78	0.003	2	c	14,14,14	4, ,
15 03 24.59	+03 46 57.3	LHS 389	12.04	0.001	11.14	0.001	10.22	0.001	2	c	14,14,14	3,3,3
15 06 14.27	-37 25 20.2	LHS 390	12.53	0.002	11.73	0.001	11.01	0.002	1	c	14,14,14	
15 14 54.41	-31 50 13.8	LHS 3045	14.39	0.004	13.53	0.002	12.74	0.002	1	c	14,14,14	
15 19 26.83	-07 43 20.3	LHS 394	10.55	0.001	9.44	0.001	8.04	0.001	2	c	14,14,14	2,2,2
15 28 13.99	+16 43 10.8	LHS 3073	14.12	0.003	12.96	0.002	12.79	0.003	1	c	14,14,14	8, ,
15 39 39.06	-55 09 10.0	LHS 401	12.72	0.002	11.87	0.002	11.11	0.002	1	c	14,14,14	
15 40 03.59	+43 29 39.4	LHS 402	12.24	0.001	11.12	0.001	9.77	0.001	1	s	5, 5, 5	18,18,18
15 40 03.81	+43 29 35.3	LHS 403	14.22	0.004	12.87	0.002	11.23	0.002	1	s	5, 5, 5	18,18,18
15 43 18.33	-20 15 32.9	LHS 406	13.06	0.003	12.07	0.002	10.93	0.002	2	c	14,14,14	
16 14 32.64	+19 06 10.8	LHS 55	12.87	0.003	11.77	0.001	10.32	0.002	1	c	14,14,14	8,3,3
16 08 14.96	-10 26 14.4	LHS 412	14.69	0.001	13.43	0.001	11.78	0.001	1	c	14,14,14	
16 25 13.95	+15 40 54.2	LHS 418	13.44	0.003	12.59	0.002	11.81	0.003	1	c	14,14,14	12,12,12

Table 3.1.: continued

RA (1)	DEC (2)	Name (3)	V (mag) (4)	$\frac{S}{N}$ σ_{err}^{std} (mag) (5)	σ_{err}^{std} (mag) (6)	R (mag) (7)	$\frac{S}{N}$ σ_{err}^{std} (mag) (8)	σ_{err}^{std} (mag) (9)	I (mag) (10)	$\frac{S}{N}$ σ_{err}^{std} (mag) (11)	σ_{err}^{std} (mag) (12)	N (13)	site (14)	aper (15)	Refs (16)
16 35 40.40	-30 51 20.2	LHS 423	12.66	0.001	0.019	11.58	0.001	0.018	10.16	0.002	0.022	1	c	14,14,14	
16 37 05.42	-01 32 00.5	LHS 424	14.17	0.002	0.012	13.31	0.002	0.012	12.50	0.003	0.016	1	c	14,14,14	
16 42 04.33	+10 25 58.7	LHS 425	15.10	0.004	0.013	14.10	0.004	0.018	12.94	0.002	0.017	1	c	14,14,14	8
17 18 25.59	-43 26 37.6	LHS 440	12.98	0.002	0.019	11.98	0.001	0.018	10.86	0.001	0.022	2	c	14,14,14	
17 28 07.33	-62 27 14.2	LHS 3292	12.74	0.003	0.016	11.54	0.002	0.010	9.95	0.001	0.017	1	c	14,14,14	3,3,3
17 58 22.91	+14 17 37.8	LSR1758+1417	16.30	0.005	0.013	16.12	0.005	0.018	15.69	0.007	0.017	1	c	14,14,14	
18 09 50.14	-02 47 43.2	LSR1809-0247	16.25	0.015	0.016	14.87	0.006	0.010	13.04	0.003	0.017	1	c	14,14,14	
18 17 06.49	+13 28 25.0	LSR1817+1328	15.88	0.005	0.013	15.37	0.003	0.010	14.88	0.004	0.014	2	cs	14,14,14	
18 35 43.20	-08 16 06.2	LHS 466	13.78	0.003	0.026	12.93	0.002	0.024	12.14	0.003	0.028	1	c	14,14,14	8,
18 41 36.37	+00 55 13.8	LHS 467	12.19	0.003	0.017	11.33	0.001	0.016	10.52	0.002	0.020	2	s	14,14,14	14,3,14
18 48 44.87	-02 33 45.7	LHS 468	13.57	0.004	0.019	12.57	0.002	0.023	11.39	0.003	0.026	2	cs	14,14,14	17,
18 53 39.92	-38 36 44.5	LHS 469	12.65	0.002	0.026	11.46	0.002	0.024	9.87	0.001	0.028	1	c	14,14,14	
19 20 54.37	-82 33 16.1	LHS 475	12.68	0.003	0.026	11.50	0.002	0.020	10.00	0.001	0.026	2	c	14,14,14	
19 46 48.61	+12 04 59.3	LHS 479	14.26	0.003	0.012	13.29	0.002	0.010	12.28	0.002	0.011	1	s	8, 8, 8	8,
20 00 05.70	+30 57 32.2	LSR2000+3057	16.62	0.007	0.012	14.72	0.002	0.010	12.63	0.001	0.011	1	s	14,14,14	
20 19 04.57	+12 35 04.1	LHS 489	15.33	0.004	0.012	11.43	0.002	0.010	13.60	0.002	0.011	1	c	14,14,14	10,
20 27 42.08	-56 27 25.2	LHS 492	12.20	0.001	0.025	11.19	0.001	0.015	9.93	0.001	0.023	1	c	14,14,14	3,3,3
20 28 03.81	-76 40 15.9	LHS 493	13.96	0.005	0.015	12.76	0.002	0.020	11.11	0.001	0.022	1	c	14,14,14	
21 01 04.80	+03 07 04.7	USNO2101+0307	18.99	0.120	0.016	16.72	0.015	0.021	14.37	0.004	0.024	1	s	14,14,14	
21 30 47.66	-40 42 29.5	LHS 510	13.12	0.001	0.023	11.92	0.001	0.017	10.34	0.001	0.020	1	c	14,14,14	
22 30 40.00	-75 13 55.3	J2231-7514	16.59	0.005	0.015	15.95	0.004	0.020	15.36	0.007	0.022	1	c	14,14,14	16,16,16
22 30 33.55	-75 15 24.2	J2231-7515	16.90	0.006	0.015	16.19	0.005	0.020	15.56	0.008	0.022	1	c	14,14,14	16,16,16
22 53 16.75	-14 15 49.2	LHS 530	10.19	0.001	0.016	8.98	0.001	0.010	7.39	0.001	0.010	2	c	14,14,14	2,2,2
23 09 32.95	+00 42 39.5	LHS 537	9.92	0.001	0.012	9.49	0.001	0.010	9.06	0.001	0.011	1	c	14,14,14	17,
23 15 51.60	-37 33 30.6	LHS 539	14.98	0.002	0.015	13.66	0.001	0.017	11.96	0.001	0.020	2	c	14,14,14	
23 36 52.30	-36 28 51.8	LHS 547	13.76	0.006	0.016	12.46	0.001	0.016	10.79	0.001	0.018	3	c	14,14,14	

Note: -J indicates joint photometry. c indicates data are from CTIO and s denotes data are from Steward Observatory. The "var" indicates a different aperture size is used for two or more different observations. The three codes separated by comma in the final column indicate the references for other published VRI magnitudes. Refs: - (1) Bergeron et al. (2001), (2) Bessell (1990), (3) CNS3-website (2004), (4) Dahn et al. (1982), (5) Dahn et al. (1988), (6) Dawson and Forbes (1989), (7) Delfosse et al. (2001), (8) Harrington and Dahn (1980), (9) Hartwick et al. (1984), (10) Harrington et al. (1985) (11) European Space Agency (1997), (12) Landolt (1992), (13) Monet et al. (1992), (14) Leggett (1992), (15) Patterson et al. (1998), (16) Scholz et al. (2002), (17) SIMBAD, (18) Weis (1996), (19) YPC

3.5 MOTION Sample JHK_s Photometry

The Two Micron All Sky Survey (2MASS) provides the astrometry for the MOTION sample as well as broad band near-infrared photometry over the entire sky. 2MASS observations employed the J , H , and K_s filters. The J ($1.25\ \mu\text{m}$) and H ($1.65\ \mu\text{m}$) passbands match the standard Johnson system, while the K_s ($2.17\ \mu\text{m}$) passband is truncated at long wavelengths to avoid terrestrial H_2O absorption. The 2MASS all-sky point source catalog was released in early 2003, so all MOTION sample members could be manually identified using the OASIS and GATOR tools provided by IPAC. The results are given in Appendix B.

3.6 MOTION Sample Photometric Parallaxes

The distances to MOTION stars without trigonometric parallaxes can be estimated photometrically using the acquired optical and infrared photometry. Photometric distances for stars are derived by estimating the absolute magnitude (here M_K) from available colors, then comparing the absolute magnitude to the observed apparent magnitude in the selected filter. The photometric distance relations presented here have been calibrated by Henry (2004), who used single main-sequence stars within 10 pc with reliable $VRIJHK_s$ photometry ($\sigma_{mag} < 0.04\ \text{mag}$), and trigonometric parallaxes ($\sigma_\pi < 5\ \text{mas}$)⁴. Of the 15 possible colors that can be generated from the six filter passbands, 12 are reliable enough to be used for photometric distance estimates. The color combinations from JHK_s alone are not used because these colors do not have sufficient color baselines to distinguish different spectral types. The final photometric parallax is the mean distance from the 12 different color combinations⁵. When used in combination, the resulting photometric parallaxes are accurate to 10%, determined by running the stars used in the calibrations back through the set of $color - M_K$ relations and comparing the photometric distances to the known trigonometric distances. The main weaknesses in this technique are that (1) these relations do not take into account the intrinsic scatter in the Hertzsprung-Russell diagram, which is caused by different ages and metallicity, and (2) distances can only be estimated reliably for main sequence stars and not for the many subdwarfs in-

⁴Some non-RECONS stars redder than M6.0 V were included to bolster the relations at the red ends. The number of very red stars added to the RECONS sample for each relation is given in column 4 of Table 3.2.

⁵No interstellar reddening corrections were made in these distance estimations.

cluded in the MOTION sample. Photometric distances can *only* be used for selecting probable nearby stars — accurate distances still need to be acquired by trigonometric parallax observations. The coefficients for the 12 different color-magnitude relations are given in Table 3.2 from columns 5–9 in the sense:

$$M_K = c1 \times (color)^4 + c2 \times (color)^3 + c3 \times (color)^2 + c4 \times (color) + c5, \quad (3.2)$$

where c1 through c5 are the coefficients given in Table 3.2.

A similar technique has been developed by Subasavage (2004) for white dwarf photometric distance estimates based on 58 known white dwarfs. Relations from three different colors, $V - I$, $V - K_s$ and $R - K_s$ are used. These relations have been generated using $VRIJHK_s$ ⁶ photometry for white dwarfs with trigonometric distances within 25 pc included in Bergeron et al. (2001). Photometry of close multiple systems has not been used. The derived photometric distance accuracy is $\sim 12\%$, although the error is likely rather larger because various white dwarf types (DA, DB, DC, DQ, DZ) have been mixed to boost the number of stars available for the relations. The relations for these four white dwarfs are similar to Eqn. 3.2, but they relate to M_V not M_K .

⁶The near-infrared photometry in Bergeron et al. (2001) has been converted from the CIT system to the 2MASS system.

Main Sequence Stars									
color	Applicable range	# RECONS stars	# very red stars	coeff #1 $\times (\text{color})^4$	coeff #2 $\times (\text{color})^3$	coeff #3 $\times (\text{color})^2$	coeff #4 $\times (\text{color})$	coeff #5 constant	
(1)	(2)	(3)	(4)	(5)	(6)	(7)	(8)	(9)	
(V - R)	0.53 to 2.40	117	6	+ 2.76693	- 17.24135	+ 35.98897	- 25.18740	+ 9.73235	
(V - I)	0.93 to 4.81	119	14	+ 0.04506	- 0.67147	+ 3.29678	- 4.49041	+ 6.10812	
(V - J)	2.51 to 8.00	115	14	+ 0.02876	- 0.60720	+ 4.50752	- 12.74588	+ 17.28992	
(V - H)	3.59 to 8.27	100	14	+ 0.02840	- 0.69348	+ 6.05707	- 21.24400	+ 31.25703	
(V - K)	2.27 to 9.27	119	14	+ 0.01050	- 0.25848	+ 2.18966	- 6.40267	+ 10.21108	
(R - I)	0.43 to 2.35	117	7	- 1.51526	+ 8.00469	- 14.14203	+ 12.55690	+ 0.70329	
(R - J)	1.64 to 5.53	114	7	+ 0.06666	- 1.05939	+ 5.84873	- 11.69482	+ 12.85838	
(R - H)	2.68 to 6.36	99	7	+ 0.10640	- 1.96263	+ 12.94836	- 34.69467	+ 38.01063	
(R - K)	1.62 to 6.97	117	7	+ 0.01786	- 0.37670	+ 2.64174	- 5.89391	+ 8.33916	
(I - J)	0.88 to 3.43	115	19	+ 0.57405	- 4.62672	+ 12.12269	- 8.89098	+ 6.07128	
(I - H)	1.67 to 4.23	100	19	+ 0.11981	- 1.07228	+ 2.15577	+ 4.39635	- 3.71087	
(I - K)	1.07 to 4.83	119	19	+ 0.19428	- 2.40789	+ 10.02965	- 14.05193	+ 10.24214	
White Dwarfs									
color	Applicable range	# WD stars		coeff #1 $\times (\text{color})^4$	coeff #2 $\times (\text{color})^3$	coeff #3 $\times (\text{color})^2$	coeff #4 $\times (\text{color})$	coeff #5 constant	
(V - I)	0.00 to 1.50	58	- 0.70526	+ 1.15815	+ 2.19882	+ 12.57192	
(V - K)	-0.80 to 2.40	58	+ 0.13966	- 0.28985	+ 1.33524	+ 12.78686	
(R - K)	-0.90 to 1.60	58	+ 0.31635	- 0.32807	+ 1.56047	+ 12.78686	

Table 3.2: The details of color vs. M_K relations for RECONS main sequence samples and colors vs. M_V for white dwarfs.

Results for Main Sequence Stars We estimate photometric distances to 28 red dwarfs among the 59 MOTION systems that do not have trigonometric parallax measurements and on CTIOPI observing (see Chapter 2 and Appendix B). The results are shown in Table 3.3. The 31 MOTION systems not included in this main sequence sample either do not have *VRI* photometry, or are known white dwarfs, or corrupted stars (e.g., close binaries). Eleven of the 28 systems with new distance estimates are possibly closer than the CNS3/NStars horizon at 25 pc. Four stars have photometric distances beyond 100 pc. These stars, along with those having no reliable spectral types, are analyzed using the reduced proper motion plot shown in Figure 3.4, and discussed below. The standard deviations for the photometric distances are given in parentheses in column 5. These “errors” represent a measure of the consistency of the photometric distances derived from the relations. The known subdwarfs in Table 3.3 do exhibit larger “error” values, which can be used to separate the subdwarfs from the main sequence stars.

Results for White Dwarfs Four of the remaining 31 systems without trigonometric parallaxes have been spectroscopically confirmed to be white dwarfs. The photometric distance estimates for these white dwarfs are given at the end of Table 3.3. The standard deviations are also given in column 5. All four white dwarfs are probably within 25 pc.

3.7 Reduced Proper Motion Diagram

The concept of reduced proper motion, H , was introduced by Luyten (1939) as an alternative to using absolute magnitude when constructing an HR Diagram. The advantage of using reduced proper motions is that stars can be placed on a pseudo-HR Diagram without knowing their distances. Instead, the proper motion is used as a proxy for the parallax. The basic assumption is that the inverse proper motion ($1/\mu$) is proportional to the distance, i.e., stars with high proper motion are assumed to be close. Furthermore, it assumes stars all have the same velocity dispersion and that the proper motion measures most of the space velocity vector. Although this is an “ideal” assumption, it can still be used effectively (although not perfectly) to separate stars of different luminosity classes. The reduced proper motion can be expressed as,

RA (J2000) (1)	DEC (2)	Name (3)	Spect. (4)	D_{phot} (pc) (5)	# (6)	$d < 25pc$ (7)	Spectral Refs. (8)
main sequence stars							
00 09 17.31	-19 42 31.6	LHS 105	M4.5 V	27(2.9)	12		(T)
00 11 31.82	+59 08 39.9	LSR0011+5908	M5.5 V	11(1.3)	12	✓	(5)
01 31 30.82	+10 01 29.8	LHS 1257	M— VI	97(8.8)	12		(T)
02 10 35.44	+46 42 04.8	LHS 1349	M— V	27(2.4)	12		(REPM)
03 35 38.61	-08 29 22.7	LHS 176	M5.0 V	13(0.5)	12	✓	(T)
04 31 43.99	-21 50 44.3	LHS 1676	M5.0 V	27(3.8)	12		(T)
04 32 42.63	-39 47 12.4	LHS 1678	M1.5 V	27(0.8)	12		(7)
08 03 06.12	+34 56 54.8	LHS 243	M— V?	42(3.0)	12		(REPM)
08 54 12.34	-08 05 00.2	LHS 254	M6.5 V	25(4.7)	12	✓	(3)
09 29 11.09	+25 58 09.3	LHS 269	M— V	17(0.9)	12	✓	(REPM)
09 38 53.83	-33 48 45.4	CE89	M5.5 V	28(3.2)	12		(T)
10 09 16.90	+35 14 52.2	LHS 279	M5.5 V	35(10.7)	12		(1)
10 36 03.10	-14 42 29.1	LHS 284	M4.5 V	67(8.7)	12		(T)
11 56 54.87	+26 39 56.3	LHS 318	M— VI	190(9.5)	9		(REPM)
12 02 40.13	+36 36 06.8	LHS 321	M0.5 V	36(1.4)	12		(2)
12 17 30.18	-29 02 20.7	LHS 323	M3.0 V?	78(10.2)	12		(8,REPM)
12 23 56.21	-27 57 46.4	LHS 325a	M6.0 V	21(1.3)	12	✓	(T)
12 24 26.81	-04 43 36.7	LHS 326	M— VI	140(7.6)	9		(REPM)
12 32 32.17	-26 10 14.3	LHS 2573	M3.0 V	33(1.8)	12		(T)
14 15 16.04	+47 47 26.2	LHS 365	M— VI	210(11.0)	11		(REPM)
14 20 52.95	+36 57 17.2	LHS 370	M5.0 V	23(2.4)	12	✓	(1)
15 14 54.41	-31 50 13.8	LHS 3045	K5.0 V?	150(8.5)	9		(2,REPM)
18 09 50.14	-02 47 43.2	LSR1809-0247	M5.0 V	36(5.1)	12		(5)
18 26 11.06	+30 14 18.9	LSR1826+3014	M8.5 V	15(1.4)	9	✓	(6)
20 00 05.70	+30 57 32.2	LSR2000+3057	M6.0 Ve	14(1.6)	12	✓	(5)
21 01 04.80	+03 07 04.7	USNO2101+0307	M7.0 V	13(0.8)	11	✓	(T)
21 58 53.18	-57 56 03.5	LHS 3740	M3.0 V	22(0.3)	3	✓	(T)
23 06 35.80	+71 43 25.5	LHS 534	M2.5 V	20(0.5)	12	✓	(4)
white dwarfs							
10 37 02.71	+71 10 58.8	LHS 285	DK—	21(1.1)	3	✓	(9)
12 40 24.19	-23 17 43.8	LHS 339	DA—	23(0.5)	3	✓	(9)
17 58 22.91	+14 17 37.8	LSR1758+1417	DA10.0	20(5.9)	3	✓	(10)
18 17 06.49	+13 28 25.0	LSR1817+1328	DA10.0	14(0.6)	3	✓	(10)

Table 3.3: Photometric distance estimates for MOTION stars. Numbers inside parentheses in column 5 are the standard deviations of photometric distance estimates from the number of color relations given in column 6. Column 7 marks the possible systems within 25pc. Refs.-(REPM) reduced proper motion diagram; (T) this work; (1) Bessell (1991); (2) Bidelman (1985); (3) Gizis (1997); (4) Hawley et al. (1996); (5) Lépine et al. (2003b); (6) Lépine et al. (2002a); (7) Reid et al. (1995); (8) Reylé et al. (2002); (9) McCook and Sion (1999); (10) Lépine et al. (2003b)

$$\begin{aligned}
H &= m + 5 - 5 \log d \\
&= m + 5 + 5 \log \mu,
\end{aligned} \tag{3.3}$$

where H is the reduced proper motion, m is the apparent magnitude, d is the distance, and μ is the proper motion.

The open symbols in Figure 3.4 represent MOTION stars with known spectral types (main-sequence stars, white dwarfs, and low metallicity subdwarfs). The V and K_s photometry and proper motions can be found in Appendix B. Close multiple systems with joint photometry are not included in the plot, nor are stars with flags on the K_s photometry. Three different regions separating the three types of stars can be distinguished, and the separation of the white dwarfs is particularly noteworthy. The lack of clear separation between the main sequence stars and the subdwarfs highlights imperfections in the reduced proper motion diagram technique.

Black filled circles represent 9 stars with photometric distances greater than 100 pc or without spectral types in Table 3.3. This figure clearly shows that the four stars (LHS318, LHS326, LHS365 and LHS3045) with large photometric distances are located in the subdwarf region⁷. Thus, the photometric distances computed for these systems are not reliable because the relations assume that the stars are on the main-sequence. LHS323 is classified as M3.0 V by Reyl   et al. (2002), but the type is not definitive. Details on the spectroscopy of MOTION sample members will be discussed in the next chapter. The three other stars (LHS243, LHS269, LHS1349) have no spectral types but are probably main-sequence stars. LHS1257 shows weak subdwarf features obtained by this work (details discussed in the next chapter), but has high standard deviation and large photometric distance. It is probably a subdwarf.

⁷LHS3045 has been classified as K5.0 V by Bidelman (1985), but is probably a subdwarf.

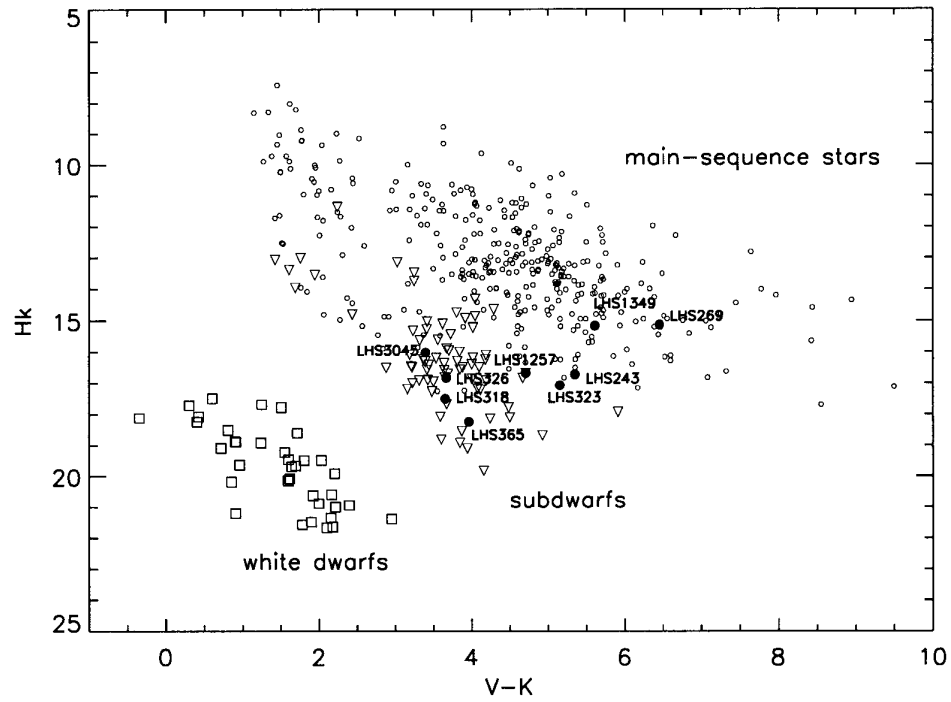


Figure 3.4: The reduced proper motion diagram (H_K vs. $V - K$) is shown for the MOTION stars. Open circles represent known main-sequence stars, triangles are known subdwarfs, and boxes are known white dwarfs. Stars without trigonometric parallaxes are shown in solid circles.

Chapter 4

Spectroscopy for MOTION Stars

In order to understand the different types of stars that comprise the solar neighborhood sample, spectroscopic observations are needed in addition to astrometric and photometric observations. Spectroscopic results are particularly useful in identifying nearby star candidates that are actually giants much further away. Eliminating giants from the CTIOPI target list frees up valuable observing time for stars that are truly nearby.

4.1 Spectroscopic Observations

Spectroscopic observations were made using the CTIO 4.0-m and 1.5-m telescopes. At the 4.0-m, the R-C spectrograph with a Loral 3K×1K CCD was used with the #181 grating (in first order) at tilt 58.8°. Order-blocking filter OG515 was used, resulting in spectra covering the range from 5500Å to 10000Å with a resolution of 6Å. These observations were made from 2002 March 31 to April 2. Additional observations were made using the CTIO 1.5-m in March, July, October, and December 2003. For these observations, the R-C spectrograph with a Loral 1200×800 CCD camera was used with the #32 grating (in first order) at tilt 15.1°. Order-blocking filter OG570 was used, resulting in spectra covering the range from 6000Å to 9500Å with a resolution of 8.6Å.

Bias frames and dome flats (and sky flats at the 1.5-m) were taken at the beginning of each night. At least two frames were taken for each object to permit cosmic ray rejection. If stars were faint, three or more observations were sometimes made, but no exposure was longer than 1200 seconds. A 10 second Ne+He+Ar or Ne only arc lamp spectrum was recorded after each target to permit wavelength calibration.

Several spectroscopic flux standard stars found in the *IRAF* spectroscopy reduction packages were observed during each observing run, usually nightly.

4.2 Spectroscopic Data Reduction and Results

The raw spectroscopic data were reduced using *IRAF* (Massey et al. 1992). Spectra acquired at both telescopes exhibit spectral fringes caused by thin-film interference effects in the CCD detectors, especially at wavelengths longer than $\sim 8000\text{\AA}$. Because no sky flats were taken at the 4.0-m telescope, the fringes were removed by cross-correlation using dome flat field images. The fringes from the 1.5-m data have been effectively removed using the combination of dome and sky flats (Beaulieu 2004).

Definitive spectral types were assigned using an IDL program, ALLSTAR, which matches a target spectrum to each spectrum in a database of more than 100 spectral standards of K and M dwarfs previously published by RECONS (Henry et al. 2002 and Beaulieu 2004, in preparation). The advantage of this technique is that it compares the entire spectrum, including both spectral features due to stellar atmospheric composition and the overall spectral slope, with standard spectra over the entire 6500\AA to 9000\AA range. Additional information about the technique is available in Henry et al. (2002). The best spectral type match, i.e., the one with the lowest residual value, from the standard spectra database is assigned. Because *only* main-sequence stars are included in the current standard star database, subdwarfs, white dwarfs, and giants cannot be assigned definitive spectral types. Therefore, for the MOTION sample members discussed here, only main sequence stars have assigned spectral types including subtypes, e.g. M2.0 V. For the remaining stars, only coarse spectral types of “VI”, “wd”, or “giant” are given.

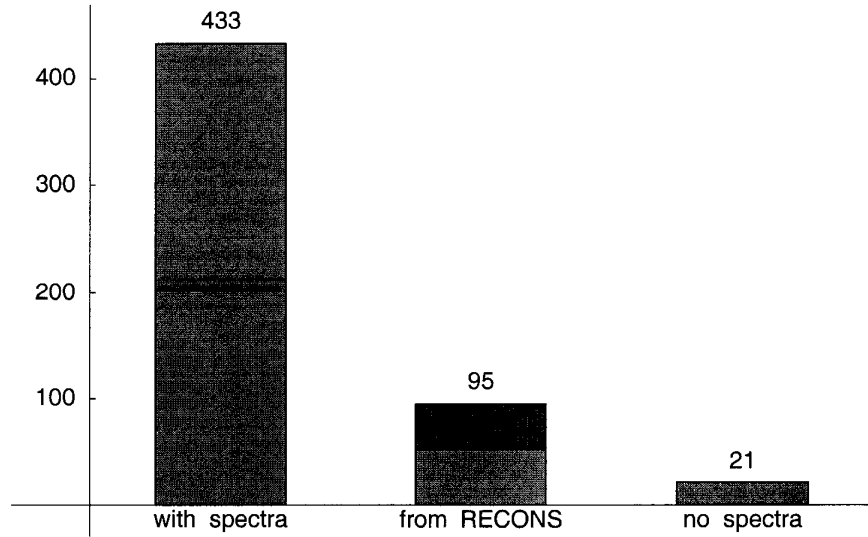
Spectral types for MOTION stars are listed in Table 4.1 (and the complete list can be found in Appendix B). The number of nights on which the star was observed is given in the fourth column. Most of the objects were observed on only one night. Previously published spectral types for MOTION stars are listed in the seventh column. The telescope codes are listed in the last column, where “1.5” and “4.0” represent the CTIO 1.5-m and 4.0-m telescopes, respectively.

Figure 4.1(a) shows the statistical results for MOTION sample systems. Before this thesis project, 116 (21%) of the MOTION systems were without definitive spectral types. We provide here new spectral types for 43 of these systems (52 systems have RECONS types that are improvements of earlier published types). Of the remaining 21 systems without spectral types, 11 are north of DEC +30 degrees and are

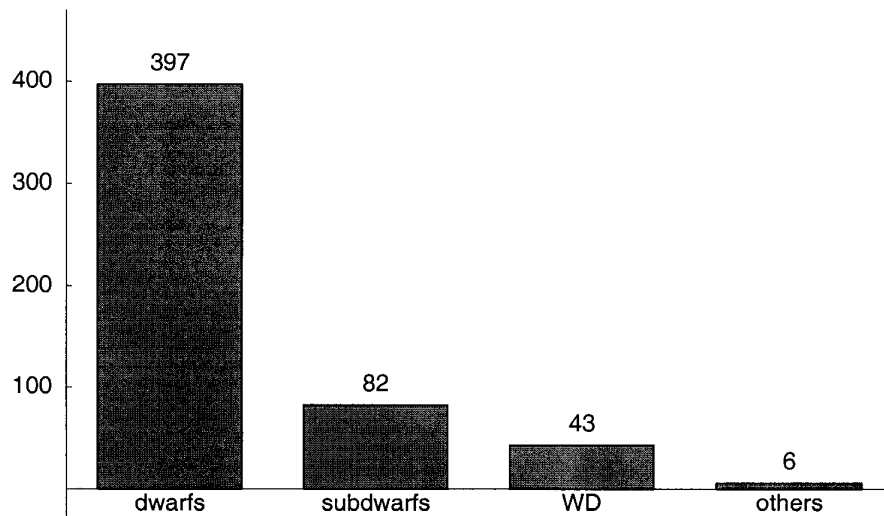
not observable from CTIO. The remaining 10 systems are on the CTIO spectroscopy observing list of the RECONS team¹. When the MOTION sample members with known spectral types are sorted by luminosity class (counts are done based upon the primary star in multiple systems), as shown in Figure 4.1(b), 75% of the 528 systems are found to be main-sequence dwarfs, 16% (82 systems) are subwarfs and only 8% (43 systems) are white dwarfs. The remaining six systems are subgiants or giants.

Figure 4.2 compares spectral types for 28 MOTION stars obtained by our group that have also been observed by Hawley et al. (1996) (filled circles), and 4 additional stars that have been observed by Kirkpatrick et al. (1991) (open circles). Only 21 points are shown because the same spectral types are repeated in several cases. Seven systems have spectral subtypes offset by 1.0 or more from published types. Figure 4.2 also shows that our spectral types are systematically earlier than others because our standard star spectral types have been carefully examined to be earlier than previously determined. Overall, $\sim 68\%$ of these systems have spectral subtype differences within 0.5 of a subtype.

¹Among the 528 systems with spectral types, 63 systems do not yet have spectral subtype assignments, e.g. Mx.xV, Mx.xVI, or DAx.x (white dwarfs), and are only classified by their luminosity classes.



(a) Statistics of MOTION sample spectroscopic results after this work.



(b) Statistics of MOTION sample spectroscopic results for different luminosity classes

Figure 4.1: (a): Dark grey represents the 43 systems with new spectra acquired during this effort. (b): 528 systems with known luminosity class are illustrated. Six systems characterized as “others” are either subgiants or giants.

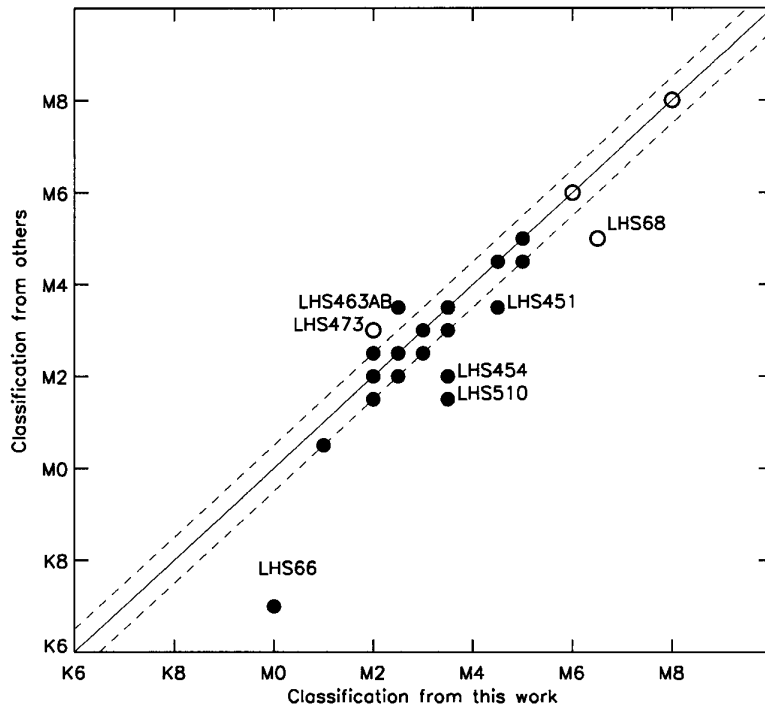


Figure 4.2: The solid line indicates that this work determines the same spectral type as in Hawley et al. (1996) (filled circles) or Kirkpatrick et al. (1991) (open circles). The two dashed lines indicate spectral types different by 0.5 subtypes. Stars with subtypes different by 1.0 or more are labeled.

Table 4.1: MOTION stars spectroscopy results

RA (J2000.0)	DEC	Name	nights	$\lambda(\text{\AA})$ coverage	Spectral Type this work	Others others	Others Ref.	Site
(1)	(2)	(3)	(4)	(5)	(6)	(7)	(8)	(9)
00 05 24.39	-37 21 26.7	LHS 1	1	5999-9478	M2.0 V	M1.5 V	Haw96	1.5
00 09 17.31	-19 42 31.6	LHS 105	1	6001-9482	M4.5 V			1.5
00 50 17.09	-39 30 08.3	LHS 125	1	5999-9478	K—VI			1.5
00 55 43.89	-21 13 07.1	LHS 127	1	5995-9480	K/M—VI			1.5
01 02 51.04	-37 37 43.7	LHS 132	1	6000-9481	M7.5 V			1.5
01 31 30.82	+10 01 29.8	LHS 1257	1	6001-9481	M—VI			1.5
01 38 49.04	+11 21 36.7	LHS 144	1	6000-9481	K/M—VI			1.5
01 43 01.02	-67 18 30.3	LHS 145	1	5998-9477	wd	DA7	McC99	1.5
01 53 08.99	-33 25 02.1	LHS 148	1	6001-9481	K/M—VI			1.5
02 02 52.16	+05 42 21.0	LHS 12	1	5999-9481	K/M—VI	M0.0 VI	Giz97	1.5
02 05 04.85	-17 36 52.7	LHS 149	2	5999-9479	M3.0 V	M2.5 V	Haw96	1.5
02 42 02.85	-44 30 58.7	LHS 158	1	6001-9481	K/M—VI			1.5
02 52 45.51	+01 55 50.5	LHS 161	1	5999-9478	K/M—VI	M2.0 VI	Giz97	1.5
02 56 13.21	-35 08 26.9	LHS 162	1	6001-9481	K/M—VI			1.5
03 06 28.67	-07 40 41.5	LHS 165	1	6001-9482	K—VI			1.5
03 13 22.92	+04 46 29.3	LHS 168	1	5999-9478	M5.0 V	M5.0 V	Haw96	1.5
03 35 38.61	-08 29 22.7	LHS 176	1	6001-9482	M5.0 V			1.5
03 50 44.29	-06 05 41.7	LHS 183	1	4997-9998	M3.5 V	M3.5 V	Haw96	4.0
04 03 38.44	-05 08 05.4	LHS 186	1	6001-9482	K/M—VI			1.5
04 10 28.15	-53 36 08.2	LHS 22	1	4999-9997	M4.5 V	M4.5 V	Haw96	4.0
04 25 38.35	-06 52 37.0	LHS 189AB	1	6001-9482	M—VI J			1.5

Table 4.1: continued

RA (J2000.0)	DEC (J2000.0)	Name	nights (4)	$\lambda(\text{\AA})$ coverage (5)	Spectral Type this work (6)	others (7)	Others Ref. (8)	Site (9)
04 31 43.99	-21 50 44.3	LHS 1676	1	6000-9481	M5.0 V			1.5
04 32 35.96	-39 02 14.6	LHS 193B	1	5999-9478	wd			1.5
04 32 36.55	-39 02 03.4	LHS 193A	1	5999-9478	K/M—VI			1.5
04 42 55.78	+18 57 29.4	LHS 196	1	5999-9478	M2.0 V	M2.0 V	Haw96	1.5
05 11 40.56	-45 01 06.4	LHS 29	1	5999-9478	K/M—VI	M1.0 VI	Giz97	1.5
05 13 05.36	-59 38 44.4	LHS 204	1	5999-9478	G—VI	— VI	Rya91	1.5
05 44 57.65	+26 02 60.0	LSR0544+2602	1	5999-9478	K5.0 V			1.5
06 57 46.58	-44 17 28.2	GJ 257AB	1	5999-9478	M3.5 V	M3.0 V	Haw96	1.5
07 04 45.84	-38 36 07.5	LHS 225AB	2	6002-9483	M2.5 V J			1.5
07 13 40.58	-13 27 57.1	LHS 227	1	5999-9478	K/M—VI			1.5
07 16 27.70	+23 42 10.4	LHS 228	1	5999-9478	M—VI			1.5
07 35 46.32	+03 29 36.0	LHS 232	1	5999-9478	K—VI			1.5
08 01 29.01	+10 43 04.2	LHS 1970	1	5999-9478	K/M—VI	K—VI	YPC	1.5
08 13 27.81	-09 27 56.6	LHS 244	1	5999-9478	K/M—VI			1.5
08 41 32.44	-32 56 32.9	LHS 253	1	4997-9998	wd	DA6.0	CNS	4.0
08 59 05.30	-31 13 26.6	LHS 258	1	4999-9999	M3.5 V	M3.0 V	Haw96	4.0
09 38 53.83	-33 48 45.4	CE89	1	5999-9478	M5.5 V			1.5
09 43 46.17	-17 47 06.2	LHS 272	1	4998-9998	M—VI	M3.0 VI	Giz97	4.0
10 36 03.10	-14 42 29.1	LHS 284	1	5999-9478	M4.5 V			1.5
10 43 02.81	-09 12 40.8	WT 1827	1	4999-9998	M5.0 V			4.0
10 44 21.28	-61 12 35.5	LHS 288	1	4999-9998	M5.0 V	M5.5 V	Bes91	4.0

Table 4.1: continued

RA (J2000.0)	DEC	Name	nights	$\lambda(\text{\AA})$ coverage	Spectral Type this work	others	Others Ref.	Site
(1)	(2)	(3)	(4)	(5)	(6)	(7)	(8)	(9)
10 48 12.62	-11 20 09.7	LHS 292	1	5999-9478	M7.0 V	M6.5 V	Hen94	1.5
10 48 14.58	-39 56 07.0	DENIS1048-3956	2	5997-9477	M8.5 V	M9.0 V	Del01	1.5,4.0
10 56 28.91	+07 00 53.2	LHS 36	1	5994-9479	M6.0 V	M6.0 V	Kir91	1.5
11 11 13.70	-41 05 32.7	LHS 300AB	2	4997-9999	K/M—VI J	K4.0 V J	Bid85	4.0
11 11 22.68	-06 31 56.4	LHS 299	1	5999-9478	K/M—VI			1.5
11 31 08.38	-14 57 21.3	LHS 306	1	4999-9997	M4.5 V	M4.5 V	Haw96	4.0
11 45 42.96	-64 50 29.7	LHS 43	1	4997-9998	wd	DQ6.0	CNS	4.0
12 23 56.21	-27 57 46.4	LHS 325a	1	5995-9480	M6.0 V	M6.5 V	Rey02	1.5
12 24 52.49	-18 14 32.2	LHS 45	1	4997-9998	M1.5 V			4.0
12 32 32.17	-26 10 14.3	LHS 2573	1	5999-9478	M3.0 V			1.5
12 37 52.27	-52 00 05.5	LHS 336	1	4998-9998	M2.5 V	M2.0 V	Haw96	4.0
12 38 49.11	-38 22 53.8	LHS 337	1	4998-9997	M4.5 V	M4.5 V	Haw96	4.0
12 40 24.19	-23 17 43.8	LHS 339	1	4998-9999	wd	DA	McC99	4.0
13 13 09.35	-41 30 39.7	ER 2	2	4997-9998	M4.0 V			4.0,1.5
13 39 15.35	+15 40 57.9	LHS 2774	1	5997-9478	M4.0 V			1.5
13 46 55.52	+05 42 56.4	LHS 360	1	4998-9999	K/M—VI			4.0
14 18 20.43	-52 24 12.6	LHS 367	1	4998-9997	K—VI			4.0
14 50 41.22	-16 56 30.8	LHS 382	1	5998-9479	M4.0 V			1.5
15 32 12.97	-41 16 32.2	LHS 397	1	4998-9999	M2.0 V	M2.5 V	Haw96	4.0
15 42 06.56	-19 28 18.4	LHS 54	1	4998-9999	M3.0 V	M3.0 V	Haw96	4.0
15 43 18.33	-20 15 32.9	LHS 406	1	4999-9999	M1.5 V	M1.0 V	Bid85	4.0

Table 4.1: continued

RA (J2000.0)	DEC	Name	nights	$\lambda(\text{\AA})$ coverage	Spectral Type this work	others	Others Ref.	Site
(1)	(2)	(3)	(4)	(5)	(6)	(7)	(8)	(9)
16 14 26.29	+02 14 49.1	LHS 414	1	5998-9479	M4.0 V			1.5
16 20 03.19	-37 31 48.1	LHS 416	1	5999-9481	M5.0 V			1.5
16 20 03.52	-37 31 44.5	LHS 415	1	5999-9481	M2.5 V	M2.5 V	Haw96	1.5
16 37 05.42	-01 32 00.5	LHS 424	1	5998-9479	K/M—VI			1.5
16 55 35.25	-08 23 40.8	LHS 429	1	6027-9548	M7.0 V			4.0
17 18 25.59	-43 26 37.6	LHS 440	1	4998-9997	M1.5 V	M1.0 V	Bid85	4.0
17 18 58.80	-34 59 48.6	LHS 443	1	5998-9479	M2.0 V	M1.5 V	Haw96	1.5
17 28 07.33	-62 27 14.2	LHS 3292	1	5999-9478	M3.5 V			1.5
17 28 39.93	-46 53 42.9	LHS 449	1	5999-9481	M2.5 V	M2.5 V	Haw96	1.5
17 37 03.66	-44 19 09.2	LHS 451	1	5998-9479	M4.5 V	M3.5 V	Haw96	1.5
17 46 34.25	-57 19 08.7	LHS 454	1	5998-9479	M3.5 V	M2.0 V	Haw96	1.5
18 20 57.18	-01 02 58.0	LHS 463AB	2	4997-9998	M2.5 V J	M3.5 V J	Haw96	4.0
19 16 55.25	+05 10 08.1	LHS 473	1	5997-9477	M2.0 V	M3.0 V	Kir91	1.5
19 16 57.61	+05 09 01.6	LHS 474	1	5998-9478	M8.0 V	M8.0 V	Kir91	1.5
19 20 47.97	-45 33 29.7	LHS 60	1	4998-9998	M4.5 V	M4.5 V	Haw96	4.0
19 21 38.70	+20 52 03.2	LHS 476	1	5999-9481	M4.5 V	M4.5 V	Haw96	1.5
19 56 57.61	-42 16 23.0	APMPMJ1957-4216	1	5996-9480	M5.5 V	M3.5 V	Rey02	1.5
20 11 12.05	-36 06 05.4	LHS 487	1	5997-9478	M2.5 V	M3.5 V	CNS3	1.5
20 40 33.86	+15 29 58.9	LHS 495	1	5999-9481	M4.5 V	M4.5 V	Haw96	1.5
21 01 04.80	+03 07 04.7	USNO2101+0307	1	6006-9481	M7.0 V			1.5
21 04 25.37	-27 52 46.8	LHS 3620	1	5999-9481	K/M—VI			1.5

Table 4.1: continued

RA (J2000.0)	DEC	Name	nights	$\lambda(\text{\AA})$ coverage	Spectral Type this work	others	Others Ref.	Site
(1)	(2)	(3)	(4)	(5)	(6)	(7)	(8)	(9)
21 05 14.03	-24 46 51.9	LHS 504	1	5996-9481	K/M—VI			1.5
21 11 57.86	-31 03 16.0	LHS 505	1	6000-9478	M3.5 V			1.5
21 17 15.27	-38 52 02.6	LHS 66	1	5999-9481	M0.0 V	K7.0 V	Haw96	1.5
21 30 47.66	-40 42 29.5	LHS 510	1	5999-9478	M3.5 V	M1.5 V	Haw96	1.5
21 55 47.95	-11 21 42.8	LHS 515	1	5999-9481	M—VI	M0/2 VI	Gia86	1.5
21 58 53.18	-57 56 03.5	LHS 3740	1	5999-9478	M3.0 V			1.5
22 09 40.34	-04 38 26.8	LHS 517	1	5998-9478	M3.5 V	M3.5 V	Haw96	1.5
22 13 42.88	-17 41 08.8	LHS 3776	1	5999-9478	M4.5 V	M4.0 V	YPC	1.5
22 20 26.97	-24 21 49.5	LHS 518	1	5997-9478	K/M—VI	M4.0 V	Bid85	1.5
22 27 59.21	-30 09 32.8	LHS 521	1	5999-9478	K—VI			1.5
22 38 33.59	-15 17 59.3	LHS 68	3	5998-9478	M6.5 V J	M5.0 V J	Kir91	1.5
22 41 41.00	-32 58 48.6	LHS 527	1	5999-9478	M5.5 V			1.5
22 55 45.37	-75 27 31.4	LHS 531	1	6000-9481	M2.5 V	M2.5 V	Haw96	1.5
22 56 24.66	-60 03 49.2	LHS 532	1	5995-9479	M5.0 V	M4.5 V	Haw96	1.5
23 05 51.92	-35 51 11.3	LHS 70	1	6001-9482	M1.0 V	M0.5 V	Haw96	1.5
23 15 51.60	-37 33 30.6	LHS 539	1	5999-9478	M3.5 V			1.5
23 17 06.03	-13 50 52.5	LHS 541	1	5999-9478	K/M—VI	M3.0 VI	Daw00	1.5
23 43 16.73	-24 11 16.4	LHS 73	1	5999-9478	K/M—VI	K7.0 V	YPC	1.5
23 49 12.52	+02 24 04.4	LHS 550	1	5999-9477	M1.5 V	M1.0 V	Hen94	1.5
giant stars								
00 14 09.61	-20 22 53.6	LHS 106	1	6002-9481	giant			1.5

Table 4.1: continued

RA	DEC	Name	nights	$\lambda(\text{\AA})$	Spectral Type	Others	Site
(J2000.0)	(2)	(3)	(4)	coverage	this work	others	Ref.
(1)	(2)	(3)	(4)	(5)	(6)	(7)	(8)
19 15 40.66	+16 09 41.7	LSR 1915+1609	1	5997-9478	giant		1.5

Notes.— Suffix J: joint spectral type; 1.5: CTIO 1.5-m; 4.0: CTIO 4.0-m. Ref.— Bes91: Bessell (1991), Bid85: Bidelman (1985), CNS: Gliese and Jahreiß (1991), Daw00: Dawson (1986), Del01: Delfosse et al. (2001), Gia86: Giampapa and Liebert (1986), Giz97: Gizis (1997), Haw96: Hawley et al. (1996), Hen94: Henry et al. (1994), Kir91: Kirkpatrick et al. (1991), McC99: McCook and Sion (1999), Rey02: Reyl   et al. (2002), Rya91: Ryan and Norris (1991), YPC: van Altena et al. (1995)

Table 4.2: Wavelength ranges for certain spectroscopic indices

Band	S1(Å)	W(Å)	S2(Å)
CaH1	6345-6355	6380-6390	6410-6420
CaH2	7042-7046	6814-6846	
CaH3	7042-7046	6960-6990	
TiO5	7042-7046	7126-7135	

4.3 Subdwarfs Confirmed by Spectroscopy

The MOTION sample is a highly kinematically biased sample; its name defines it as so. Because subdwarfs are old, metal poor, Galactic halo stars that have experienced significant disk heating over many billions of years, the MOTION sample will contain a certain fraction of subdwarfs. Halo stars have large heliocentric velocities because they have orbits that differ greatly from those of the disk stars, like the Sun. Consequently, halo stars tend to have large proper motions out to a greater distance than do disk stars. These low metallicity stars are fainter than their disk counterparts with similar temperatures, lying below the Population I main sequence on the HR Diagram. Hence, they are often called “subdwarfs”. Because of their low metallicity, they exhibit different spectral features than Galactic disk stars.

As shown in Figure 4.1(b), a significant subdwarf population, 82 (16%) out of 528 systems with spectral types, is found in the MOTION sample. We believe that this is the first time the subdwarf fraction has been quantified accurately for a sample defined as carefully as the MOTION sample. This group of 82 systems now provides a robust sample that can be targeted for future research, such as the determination of the mass-luminosity relation and duplicity frequency for low metallicity stars (discussed further in Chapter 6).

To characterize these subdwarfs using metallicity (generally, subdwarfs have $[\text{Fe}/\text{H}] < -1.2$), Gizis (1997) used the strength of molecular bands (CaH1, CaH2, CaH3 and TiO5) to separate M–K type subdwarfs from main sequence stars. A spectroscopic index is defined as

$$R_{\text{index}} = F_w / F_{\text{conti}} \quad (4.1)$$

where F_w is the mean molecular band flux within a wavelength range listed in Table 4.2, and F_{conti} is a pseudo-continuum flux — either the mean flux in a single sideband or estimated by the linear interpolation in the window, W, between two side bands, S1 and S2.

The molecular band strengths for 33 MOTION subdwarfs for which we have spectra are given in Table 4.3. The CaHn (where n is 1, 2, or 3) indices versus the TiO5 index for the sample are shown in Figure 4.3. Clearly, nearly all MOTION stars determined to be subdwarfs by this work fall in the plot regions outlined for subdwarfs or extreme subdwarfs. Differences between the so-called regular subdwarfs and the extreme subdwarfs are arbitrarily defined by CaHn and TiO5 bandstrengths, in the sense that the more extreme subdwarfs have smaller CaHn values for a given TiO5 bandstrength.

Two stars in Figure 4.3 are worthy of note. LHS504 has a noisy but almost identical continuum to LHS518, which is a subdwarf, but its location in the plots is somewhat uncertain. LHS1257 is a possible subdwarf based on its large photometric distance estimate (Table 3.3). At present, LHS1257 does not have a trigonometric parallax so it cannot be confirmed by placing it on an HR Diagram.

4.4 Subdwarfs Reconfirmed via the HR Diagram and the Reduced Proper Motion Diagram

The HR Diagram can also be used to confirm or refute the MOTION subdwarfs, if their trigonometric parallaxes are available. The results are shown in Figure 4.4. This figure has been created by choosing MOTION stars with published spectral types, V and K_s photometry, and trigonometric parallaxes which are the only truly reliable standard distance measurements (Stars with large parallax errors are included. For example, LHS466, shown as a circled point in Figure 4.4, has parallax $0''.0046 \pm 0''.0092$ van Altena et al. 1995). The 23 stars with “x”s in the HR column of Table 4.3 are shown with boxes, including the associated M_V errorbars². Twenty-two of the 23 stars fall below the main sequence stars (LHS204 is discussed below). LHS125 and LHS232 have very weak CaHn and TiO5 band absorption features, as illustrated in the plot inset. However, these two stars are still fainter than main sequence dwarfs with the same $(V - K_s)$ color even after considering the M_V error.

LHS204 has a strong $H\alpha$ (6563Å) absorption feature and is located on the lower edge of the main sequence band. Ryan and Norris (1991) have found that it has low metallicity, $[\text{Fe}/\text{H}] < -1.88$, which implies that it *is* a late G type subdwarf. Like LHS125 and LHS232, LHS204 has no CaHn or TiO5 features — it falls in the upper-

²The errorbars are computed from the trigonometric parallax errors and estimated errors of 0.03 magnitudes for the V photometry.

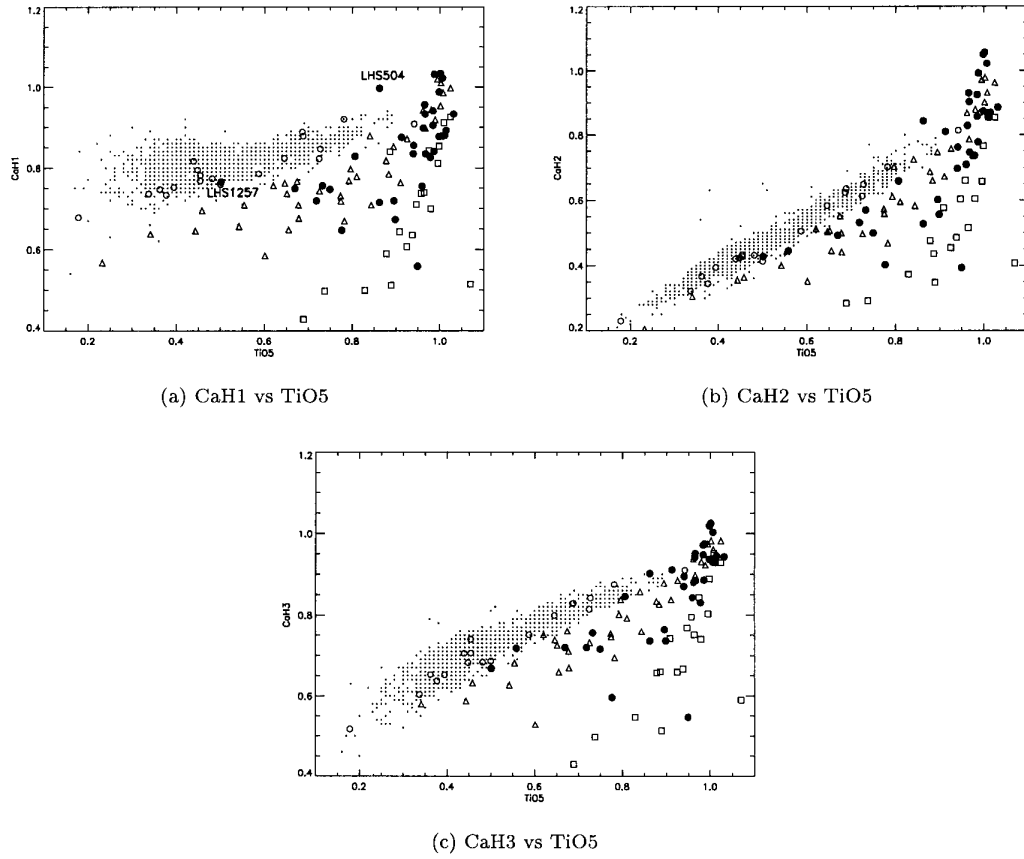


Figure 4.3: Stars classified as main sequence stars from Gizis (1997) appear as open circles, subdwarfs as open triangles, and extreme-subdwarfs as open boxes. Small dots represent main sequence stars from Hawley et al. (1996) using the same indices. Filled circles are MOTION stars classified as subdwarfs by this work. Late type stars have small TiO5 index values (left side of plots), while large CaHn index values are found for earlier type stars. The TiO5 values in the plots span spectral types of \sim M6 to \sim K5.

Name	TiO5	CaH1	CaH2	CaH3	HR	REPM
LHS12	0.912	0.875	0.810	0.911	x	
LHS29	0.939	0.834	0.697	0.870	x	
LHS73	1.014	0.892	0.870	0.945	x	
LHS125	0.987	1.032	0.992	0.975	x	
LHS127	0.718	0.719	0.531	0.720		x
LHS144	0.776	0.647	0.402	0.596	x	
LHS148	0.978	0.825	0.736	0.830		x
LHS158	0.806	0.828	0.658	0.846	x	
LHS161	0.959	0.755	0.709	0.843	x	
LHS162	0.895	0.719	0.601	0.764		x
LHS165	0.998	0.877	0.874	0.937	x	
LHS186	0.732	0.756	0.569	0.756	x	
LHS189AB	0.669	0.749	0.492	0.720		x
LHS193A	0.984	0.941	0.925	0.972	x	
LHS204	0.998	0.988	1.050	1.019	x	
LHS227	1.006	0.878	0.869	0.930	x	
LHS228	0.749	0.747	0.499	0.716	x	
LHS232	1.006	1.023	1.022	1.003	x	
LHS244	0.967	0.834	0.746	0.885	x	
LHS272	0.862	0.715	0.527	0.736	x	
LHS299	0.940	0.855	0.762	0.895	x	
LHS300AB	1.031	0.933	0.886	0.943	x	
LHS360	0.986	0.840	0.778	0.886		x
LHS367	1.011	0.880	0.854	0.929		x
LHS424	0.984	0.905	0.857	0.948	x	
LHS504	0.862	0.997	0.843	0.902		
LHS515	0.949	0.559	0.393	0.547	x	
LHS518	0.966	0.933	0.903	0.951		
LHS521	0.965	0.956	0.930	0.942	x	
LHS541	0.962	0.898	0.829	0.880	x	
LHS1257	0.501	0.765	0.427	0.668		x
LHS1970	1.142	0.683	0.718	0.780	x	
LHS3620	0.898	0.673	0.556	0.736		

Table 4.3: Spectroscopic indices for MOTION subdwarfs. The cross marks show stars appearing in Figure 4.4 (HR) and Figure 4.5 (REPM).

right corner of the spectroscopy indices plots in Figure 4.3. This implies that these indices cannot be used effectively to separate dwarfs and subdwarfs for stars with types earlier than LHS125 and LHS232.

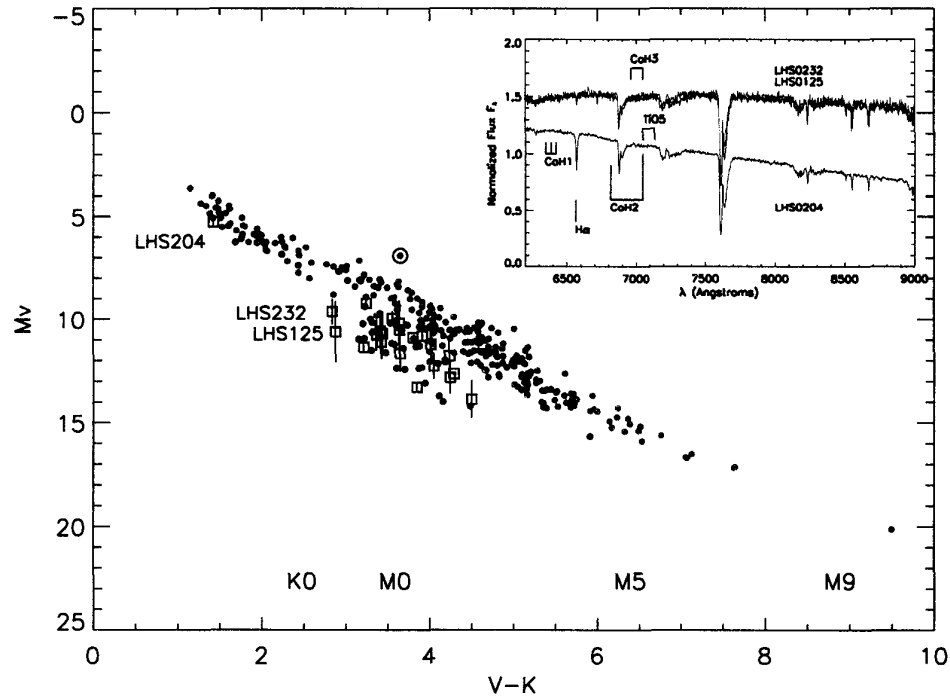


Figure 4.4: Red circles represent known dwarfs from the MOTION sample. Black circles are previously spectroscopically confirmed subdwarfs. Boxes represent 22 stars with new spectral types from this work that have $V - K_s$ and M_V . The spectra for LHS124, LHS204 and LHS232 are shown in the inset. The color of the object name corresponds to the color of its plotted spectrum. The black circle indicates LHS466 with high parallax error.

The seven stars with “x”s in the REPM column of Table 4.3 either do not have $(V - K_s)$ colors or parallaxes, but are confirmed to be subdwarfs by their locations in the reduced proper motion diagram shown in Figure 4.5. The three remaining stars without “x”s in either column are LHS504, LHS518, and LHS3620. Although these can not be confirmed to be subdwarfs by either the HR or reduced proper motion diagrams because of missing data, their CaHn and TiO5 indices do indicate that they are subdwarfs. We therefore conclude that all 33 stars listed in Table 4.3 are subdwarfs.

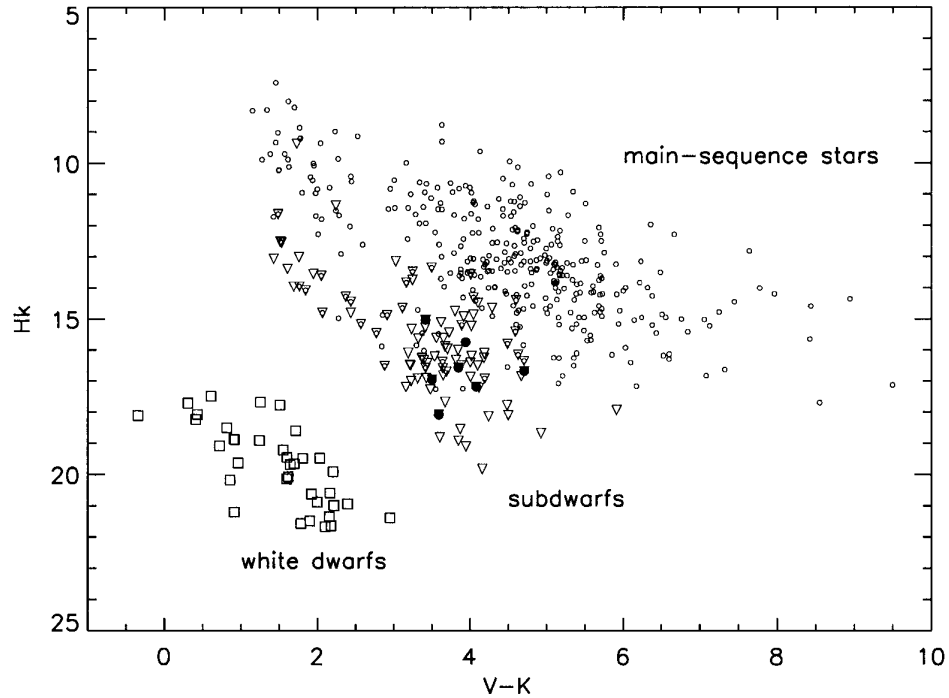


Figure 4.5: The open symbols have the same definitions as in Figure 3.4. Solid circles represent 7 MOTION subdwarfs in Table 4.3 marked with “x”s in the REPM column.

4.5 Subdwarf Spectroscopic Subtypes

As discussed above, the MOTION subdwarfs determined using the CTIO 4.0-m and 1.5-m data have not (yet) been assigned any subtypes, i.e. M0.0 VI or M0.5 VI, because we lack a set of reliable subdwarf standards. We do not use the linear fitted equations based on these TiO5 and CaHn indices discussed in Gizis (1997) to assign the numerical subtypes. We suspect that the available work is insufficient to assign reliable subtypes, and we discuss here two examples that address the numerical fitting problem.

Gizis (1997) has assigned Gl191 (LHS29) to have a spectral type of M1.0 VI and LHS272 to have a type of M3.0 VI. A comparison between these two stars and the RECONS spectral standard Gl203 (main sequence type M3.0 V) is shown in Figure 4.6. The figure shows that there is no significant difference between Gl191 and LHS272 at wavelengths longer than 7800Å; the main spectral differences lie between

6200Å and 7500Å. LHS272 is significantly different from our standard Gl203 M3.0 V spectrum, although it has been assigned the same subtype. It appears that the Gizis (1997) subtype was based only upon the strengths of TiO5 and CaHn bands, which is, of course, what separates the main sequence stars from the subdwarfs (and those from the extreme subdwarfs). In their effort, the pseudo-continuum point near 6500Å has been ignored, and the mismatch between Gl203 (M3.0 V) and LHS272 (M3.0 VI) is evident when properly compared. We conclude that the Gizis (1997) method is a poor one to use. Instead, portions of the spectra that are *not* affected by the CaHn bands (which define the subdwarfs as a class) should be compared to establish the subdwarf and extreme subdwarf sequences.

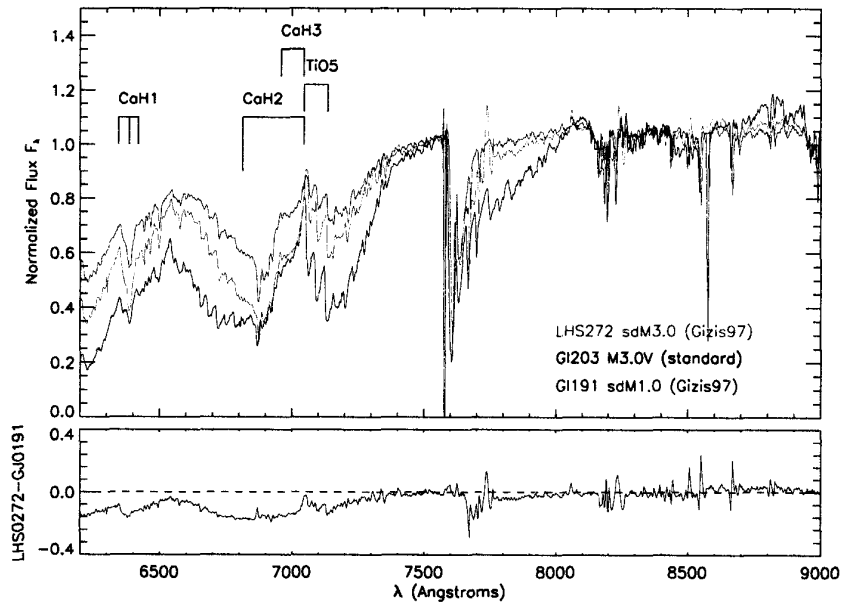


Figure 4.6: Comparison of spectra for LHS272, Gl203, and Gl191. The flux of each spectrum is normalized to 7500Å, a pseudo-continuum point for red dwarfs. The normalized flux difference between LHS272 and Gl191 is shown on the bottom of this figure. The CaII triplets (8498, 8542 and 8662Å) are shifted between LHS272 and Gl191 due to different radial velocities.

As a second example of the subdwarf subtype problem, LHS161 is listed as an extreme subdwarf with type M2.0 VI in Gizis (1997). Figure 4.7 shows its spectrum compared to five RECONS standard stars. The top portion of the figure compares LHS161 to Gl357 (M2.0 V) and Gl367 (M2.0 V), which have the same subtypes as assigned to LHS161. Clearly, the match is very poor. A better match is shown

in the middle of the figure, where LHS161 is compared to two RECONS standards with types of M0.0 V, G1784 and G1825. In these cases, the *only* differences between LHS161 and the standards are the strengths of the CaHn bands and the absorption wing slope from 6600Å to 6900Å. The pseudo-continuum near 6500Å matches well. When compared to G1879, a K7.0 V RECONS standard, LHS161 shows only a slight difference at wavelengths longer than 7500Å, but a poor match between 6200Å and 7500Å. (There are no reliable K8.0 V standards. The small differences between late K and early M types from 7500Å to 9000Å have long been the rationale for not using the K7.5 V to K9.5 V subtypes.

We conclude that Gizis (1997) has offered a good way to separate dwarfs, subdwarfs, and extreme subdwarfs spectroscopically using the CaHn and TiO indices. However, the subdwarf subtypes have not been assigned reliably. Questions that need to be addressed in the future include: Is the continuum of subdwarfs shortward of 7500Å less than that of dwarfs, more than that of dwarfs or the same as dwarfs? What spectral region is the best to use to assign subtypes? These questions will be addressed by future RECONS work.

Historically, the identification of a rather small number of K and M subdwarfs has prevented astronomers from developing a comprehensive picture of the subdwarf spectral sequence. Our identification of many more subdwarfs in the MOTION sample and development of a large database of spectra should allow us to construct a spectral sequence that can be subjected to matching with theoretical models for stars with various metallicities. Until such future work is carried out, we only distinguish whether the MOTION members are main sequence stars, or subdwarfs with spectral types K, K/M or M (see Table 4.1).

4.6 Estimated Spectral Types for Additional MOTION Stars

There are 10 MOTION stars without spectral types for which types can be estimated based on their M_V and $(V - K_s)$ values. The results are shown in Figure 4.8. The plot shows all previously known single dwarfs in the MOTION sample, excluding results from this work and MOTION stars without spectral types. The 10 MOTION stars without spectral types include three main sequence stars, six subdwarfs, and one giant (LHS202, $\pi = 0''.0039 \pm 0''.0133$ van Altena et al. 1995). LHS207's location above the main sequence indicates that it is a probable binary system. Nine additional stars

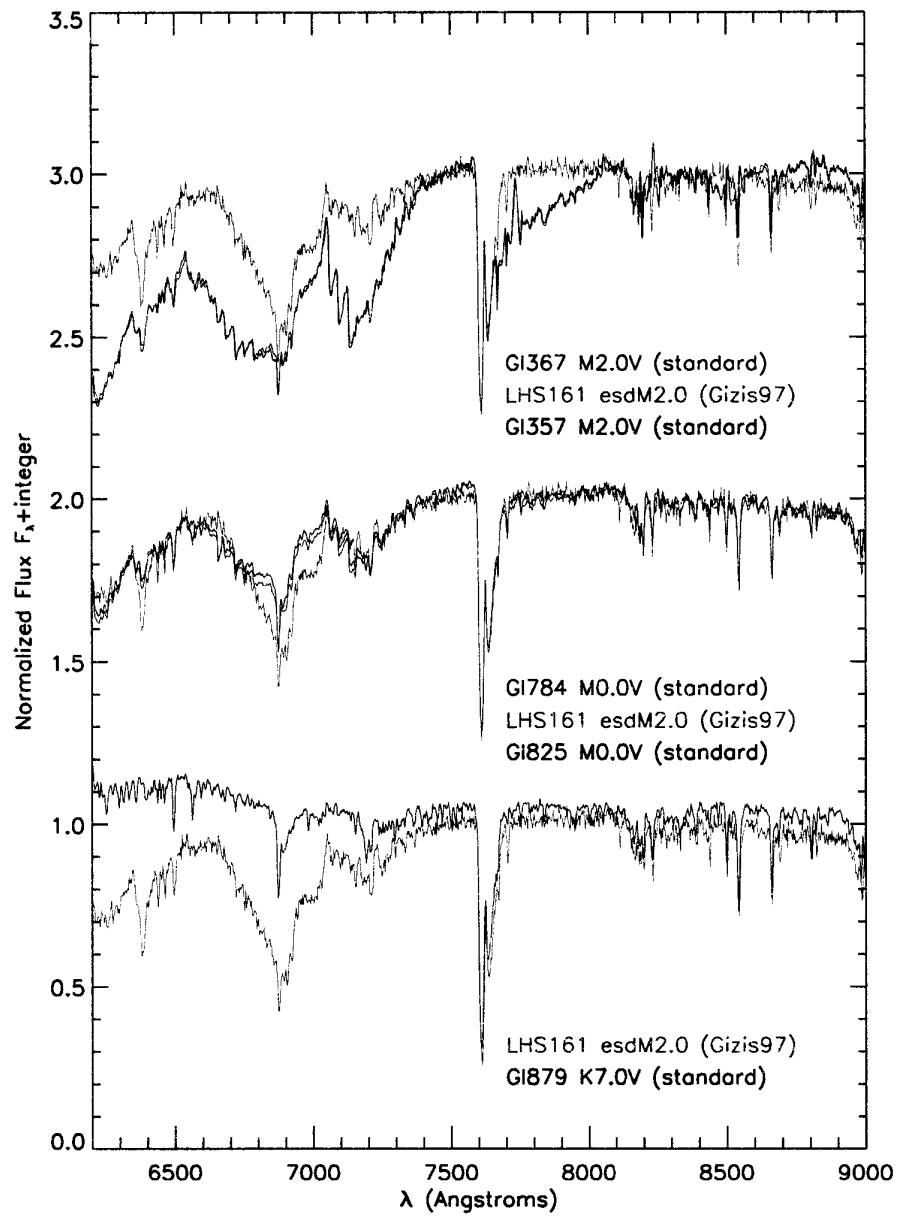


Figure 4.7: Comparison of the spectrum of LHS161 to several RECONS main sequence spectral standards. See text for details.

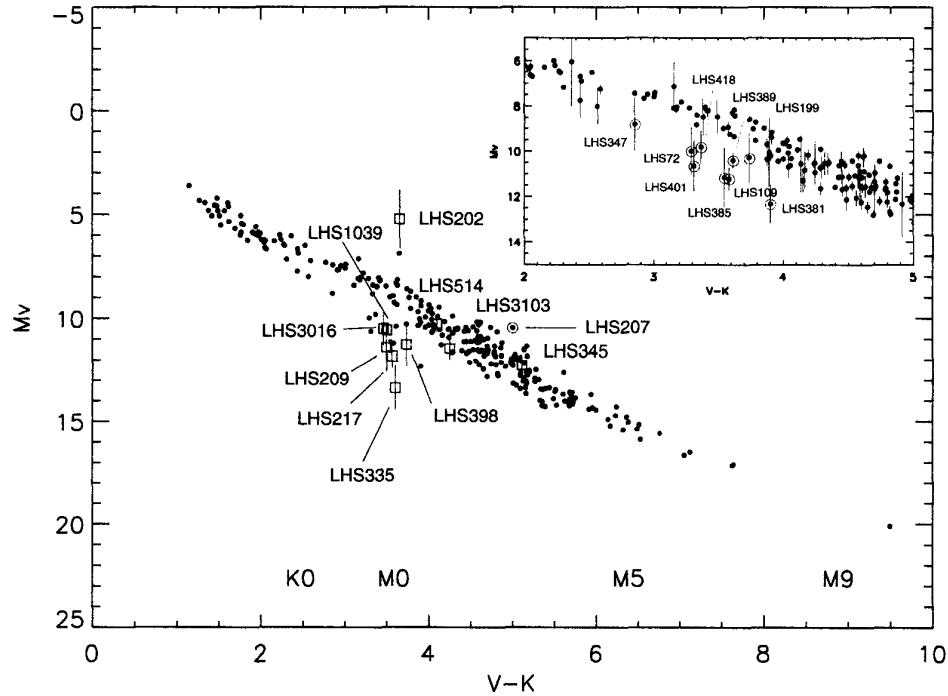


Figure 4.8: Black circles are main sequence stars in the MOTION sample known before including the results of this work. Red boxes represent stars without spectral types. The inset shows stars previously identified as dwarfs that are possible subdwarfs shown in red circles. Stars with M_V errors greater than 2.0 magnitudes are not plotted in the inset.

shown in the inset have been classified as dwarfs by others, but we believe they are possible subdwarfs.

4.7 Notes on Individual Objects

Notes relating to the spectroscopy of individual MOTION sample stars are presented here, ordered by RA.

LHS106 The star marked in the LHS Atlas could not be identified at the telescope. The coordinates for LHS106 listed in Bakos et al. (2002) are for a giant star.

LHS149 The spectral type is not listed in Hawley et al. (1996), but is available from the electronic version of that paper on the CDS/VizieR ftp site.

LHS189AB is a binary with a separation of $3''$ (Luyten 1979b). The composite spectrum indicates that the components form an M subdwarf binary. To our knowledge, this system is the first M subdwarf binary ever identified. The system was observed in the CTIOPI 1.5-m program and awaits reduction.

LHS193AB is a probable K/M subdwarf and white dwarf binary with a separation of $12''.59$ (Jao et al. 2003). A has $M_V = 9.2$ and $(V - K_s) = 3.24$; B has $M_V = 14.54$ and $(V - K_s) = 1.96$. To our knowledge, this is the first red subdwarf/white dwarf binary ever identified.

LHS204 The metallicity has been determined to be $[\text{Fe}/\text{H}] < -1.88$ by Ryan and Norris (1991).

LHS207 The location of LHS207 is above main sequence and indicates that it is a probable binary system.

LHS300AB is a binary with a separation $4''.28$ (Jao et al. 2003). The composite spectrum indicates that the components form a K/M subdwarf binary. For the combined system, $M_V = 10.71$ and $(V - K_s) = 3.37$.

DENIS1048-3956 The spectral type may be variable, possibly due to large spots in the stellar photosphere. RECONS spectra indicate changes in type between M8.0 V and M9.0 V during three observations in 2002-2003.

ER2 The spectral type is possibly variable, between M4.0 V and M5.0 V.

LHS54 The spectral type is not listed in Hawley et al. (1996), but is available from the electronic version of that paper on the CDS/VizieR ftp site.

LHS487 The spectrum is corrupted by the primary star, LHS486, a K3.0 V star at a separation of $7''.1$ (Poveda et al. 1994).

LHS540ABC Dawson and De Robertis (2000) report that LHS540AC is a joint G type subdwarf. Hartkopf et al. (2000) report that LHS540 is a close binary with separation $0''.7$. LHS541 (the “B” component) is a wide visual companion ($18''.8$ separation) to AC. Both this work and Dawson and De Robertis (2000) indicate that LHS541 is a subdwarf, making this a triple subdwarf system.

LSR1915+1609 It is a giant as explained in Section 1.2.1.

Chapter 5

New MOTION Star Companions¹

5.1 Companion Search

A comprehensive search for companions to 209 stars in 191 stellar systems was carried out using the CTIOPI astrometry images, many of which are MOTIONS stars. Images were examined for objects located within a 20'' radius of each target star using the contour capability in *IRAF/imexamine*. Typically, 1–10 sources were discovered per target. Most potential companions were quickly refuted by comparing first and second-epoch Digitized Sky Survey (hereafter, DSS) images and discovering proper motions inconsistent with the target stars. After culling the unrelated sources, eight potential new companions remained (listed in order of RA): GJ2022C, LHS193B, LHS1749B, LHS225B, LHS300B, RXJ1132–264B, GJ1226B and LTT7419B. Finder charts from CTIOPI frames for these systems are shown in Figure 5.1. Four of these systems — LHS193AB, LHS225AB, LHS300AB, and GJ1226AB — are members of the MOTION sample.

In order to characterize the search sensitivity, each frame was evaluated for image quality. Figure 5.2 shows a histogram of the full width half maximum (FWHM) values for the objects investigated, separated by the filters used for the observations. Most of the stars (90%) were examined using *V* or *R* images. The FWHM values were determined using a radial profile Moffat fit in *IRAF/imexamine*. When possible, frames were chosen that had FWHM better than 1''20 (3 pixels). For a modest fraction of the stars (12%), images with somewhat poorer FWHM were used because sharper images were not available. The mean FWHM value for the 209 targets

¹The first three sections are parts of the previously published paper by Jao et al. (2003)

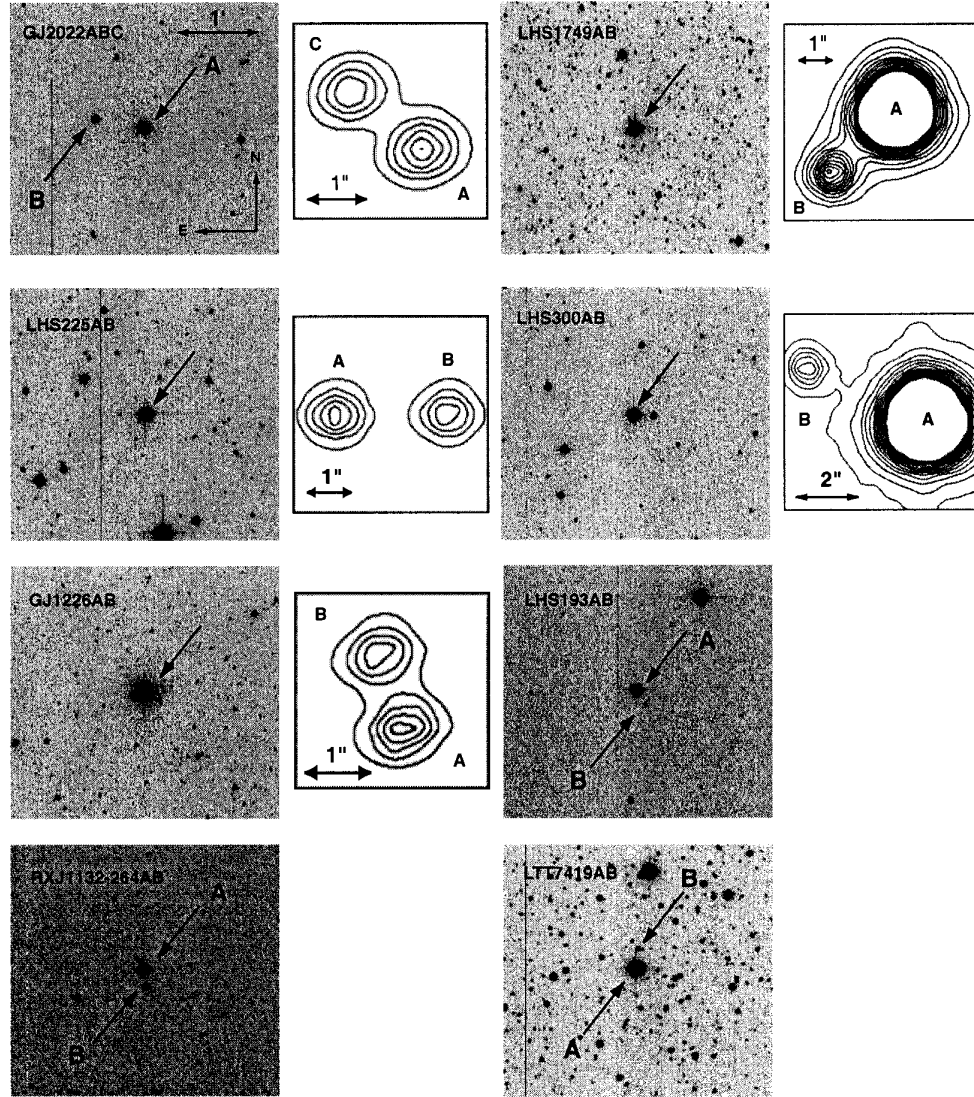


Figure 5.1: Eight new companions orbiting potential nearby stars found in CTIOPI images are shown. Each finder image is cut from a CTIOPI frame and is $3.3' \times 3.3'$ in size, with north up and east to the left. Insets show the contour maps from the *IRAF/imexamine* task. Companions to LHS193, RXJ1132–264 and LTT7419 are obvious in the CTIOPI frames.

searched is $1''.09$.

The CTIOPI program has resulted in at least a factor of five improvement in resolution over the plate scans of the DSS, thereby enabling the detection of closer and fainter companions. The DSS image plate scales are $1''.7/\text{pixel}$ for the first generation and $1''.0/\text{pixel}$ for the second generation, determined by using information in the FITS headers delivered from DSS. Examination of ~ 100 stellar sources in 20 POSS-II fields with CTIOPI targets reveals an average FWHM value of $5''.64$ for stars that were not saturated. For targets that were saturated, which includes most of the stars in CTIOPI, the average FWHM for the brightest non-saturated objects in the fields is $6''.65$ — this is a “best case” estimate for saturated stars, for which the resolution limit is typically much worse.

The detection limit of the CTIOPI frames is compared to that of DSS in Figure 5.3. Four CTIOPI objects were used as benchmarks for this illustration — two each with FWHM values matching the best ($0''.85$, solid triangles and circles) and worst seeing cases ($1''.20$, open triangles and circles) for the bulk of the sample, as shown in Figure 5.2. For these four targets, objects of varying magnitude differences were selected from the same frames searched for companions and artificially placed at increasing separations from the target stars in increments of $0''.401$ (one pixel). The points in Figure 5.3 represent the closest separation at which the simulated companion could be detected using the methodology described above. The same procedure was carried out on a DSS image (solid squares) for an unsaturated program star. Clearly, five of the eight new companion candidates (large starred points) were undetectable in DSS images, but are clearly resolved in CTIOPI images. We note that LHS193B, LTT7419B and RXJ1132–264B are at large separations from their primary stars and can be seen in DSS images. They were simply unnoticed before. This clearly illustrates that many companions to nearby star candidates can be (and are being) discovered, especially in the southern sky where historically less observational effort has been concentrated.

5.2 Astrometric Confirmation of New Doubles

A two-step process was used to confirm or refute the eight potential companions, as well as to check the validity of 16 previously cataloged companions also recovered during the search. First, the relative positions of the target stars and their potential companions were mapped using the series of astrometric frames in hand. This step was used to get the plate constants. Second, full astrometric analyses were carried out

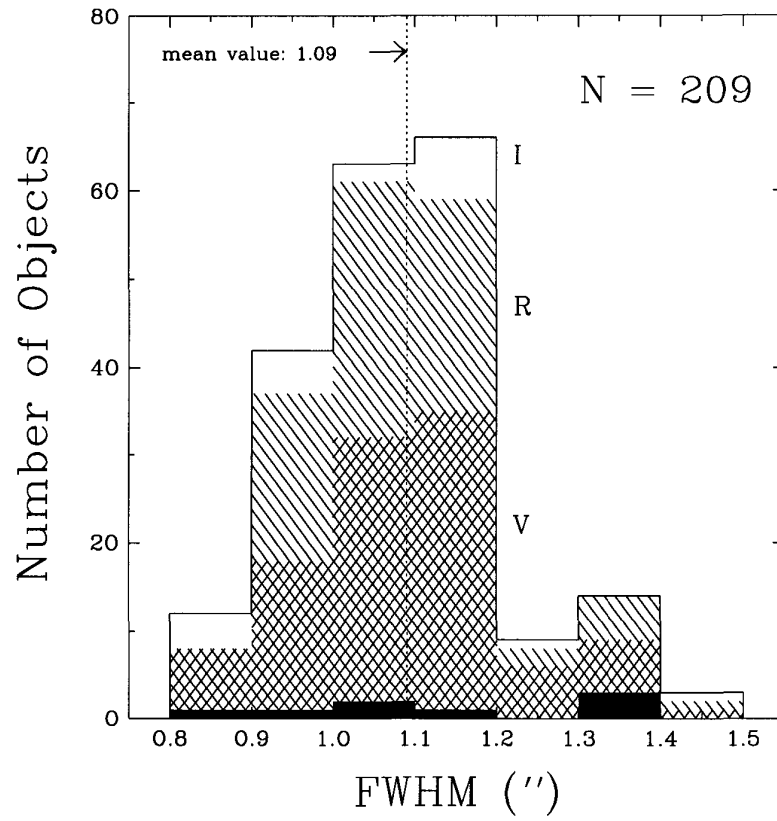


Figure 5.2: Histogram showing the FWHM of images used to search 209 stars during CTIOPI for new companions. The mean FWHM is $1''.09$, and 88% of the stars have $\text{FWHM} < 1''.20$. Stars searched using *V*, *R*, and *I* filters are drawn in crosshatched, slashed, and white space, respectively. The dark bars represent the eight new companions.

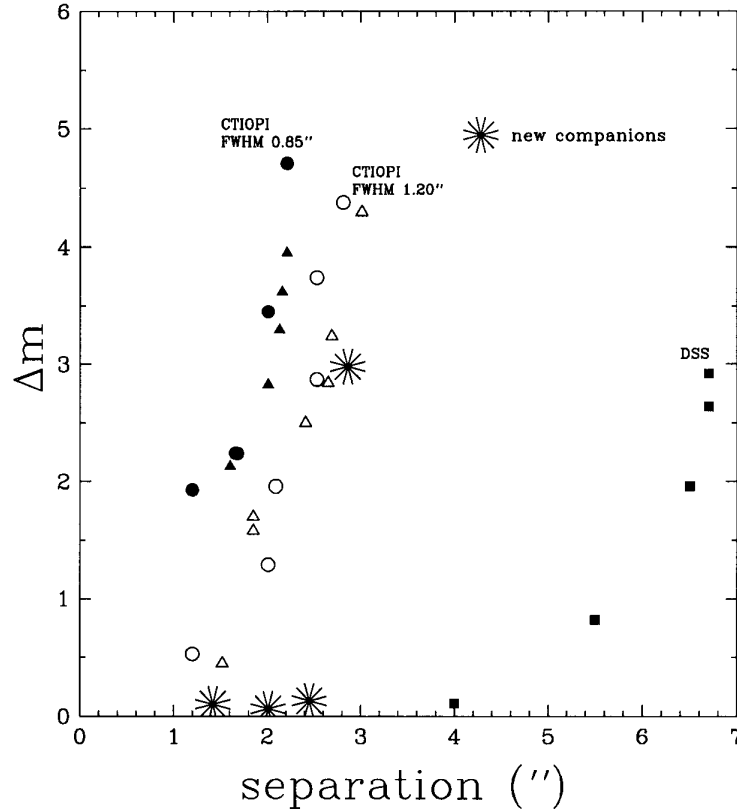


Figure 5.3: Schematic diagram illustrating the magnitude difference limits (in the primary astrometry filter for each star) reached between companions and targets at various separations. Circles and triangles represent the closest separations at which simulated companions could be detected in CTIOPI frames, using two frames with excellent seeing ($0''.85$, solid points) and two frames with poor seeing ($1''.20$, open points). Simulated companions to targets in DSS images are represented by solid squares. Five of the eight new companions discovered are plotted as starred points. Their positions on the plot demonstrate that increased resolution CTIOPI images were necessary for their discovery. The three additional discoveries were at separations larger than $7''$. These companions *could* be seen on the DSS images, but had not been identified as companions before.

to determine if multiple components had common proper motion. A series of astrometric frames were analyzed with SExtractor and a modified version of the University of Virginia parallax reduction pipeline² to determine precise relative separations and position angles, and ultimately, proper motion vectors.

To map the relative position of a potential companion over time, first a reference trail frame is selected from the parallax series. All other frames must be adjusted to match the trail frame in scale, rotation, and translation. The trail frame is chosen to have (1) correct orientation to the sky (i.e. north-south and east-west directions properly aligned on the CCD chip), (2) sufficient S/N in the target star and all reference stars to permit reliable centroids, and (3) a very short RA zenith distance (within 10' of the meridian) to reduce differential refraction effects.

A six constant plate model is then applied to each frame to provide sets of modified coordinates for the target star(s) and any potential companions, using the methodology outlined in Eichhorn and Jefferys (1971) and Jefferys (1979) and described by the following equations:

$$\alpha_1 = X' - aX + bY + c \quad (5.1)$$

$$\delta_1 = Y' - dX + eY + f \quad (5.2)$$

where X and Y are CCD coordinate sets extracted from SExtractor for science and reference stars, and X' and Y' are the corresponding coordinates on the reference trail frame. The plate constants a , b , c , d , e and f model the coordinate scales in X and Y , rotation, and translation. An iterative least squares method is carried out to reduce the differences between the trail plate and the plate examined, resulting in minimized values of α_1 and δ_1 .

The separation and position angle of the potential companion are then computed for each frame at multiple epochs, and plotted as in Figure 5.4 for LHS225AB. The heavy line indicates the best fit for the separation and position angle for LHS225AB at six epochs. If component B were a stationary field star that held its location at the first epoch of observation, its separation and position angle relative to the primary would change, as indicated by the dot-dashed line. Clearly, LHS225B maintains a constant separation and position angle throughout the 1.2 year baseline of our observations. All eight potential companions have been confirmed using this method

²This parallax pipeline is different from the one discussed in Chapter 2.

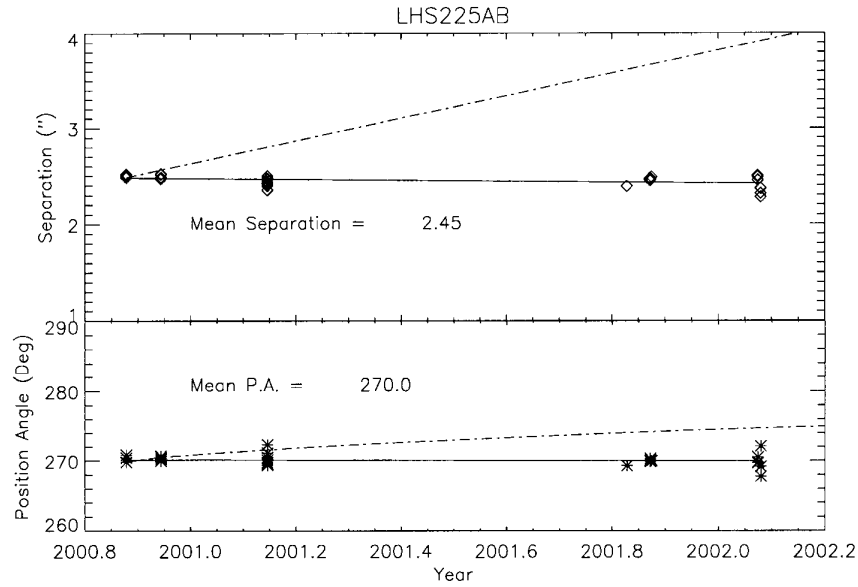


Figure 5.4: An example companion confirmation plot illustrating that the new component of LHS225B is physically associated with the primary star. The solid lines in the two panels mark the fits for position angle and separation. The dashed-dot line represents the relative motion of B to the primary star if it were a field star with zero proper motion.

(indicated with asterisks after the companion name in Table 5.1), as well as 16 previously known companions. Orbital motion of the companions would be detected if the best fit line varied from a constant value (either a tilted or curved line depending on orbital velocity). However, no orbital motion was detected for any of the new close companions, even for GJ1226AB, which has the smallest separation ($1.42''$).

Figure 5.5 illustrates the relative positions for the five new multiple systems with separations $< 5''$. Note that at smaller separations the centroid positions are more scattered, which results in relatively large errors in the four astrometric quantities derived — separation, position angle of the separation, system proper motion, and position angle of the system proper motion — which are given in Table 5.1. For each system the number of epochs and the timescale over which the frames were taken is also given in the final two columns.

After the relative positions were checked, the second step of the confirmation process was carried out by determining the proper motion vectors for the primaries and all companions. The model used to detect the change in relative positions in RA

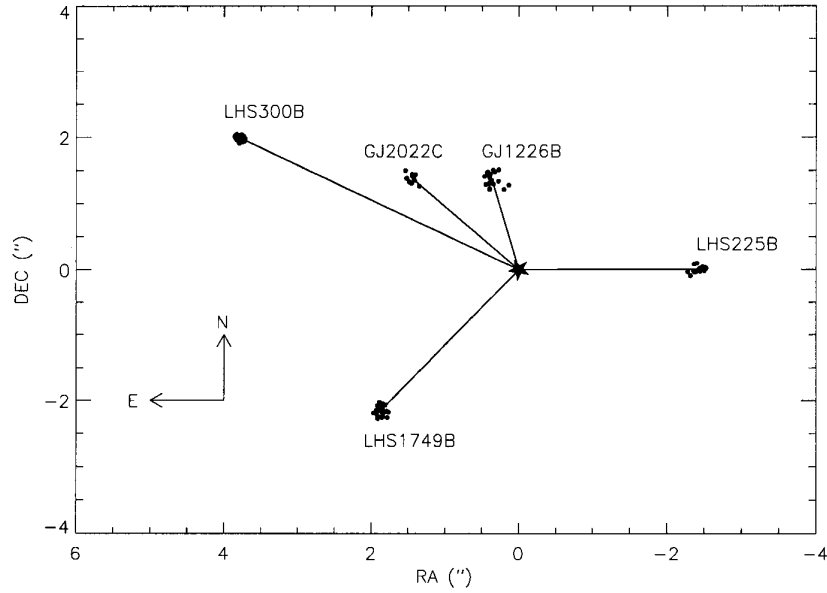


Figure 5.5: Five new companions with separations $< 5''$ are plotted. The star symbol marks the position of each system's primary. Note that with increasing separation, the centroid is more concentrated, indicating that centroiding accuracy increases at larger separations. The three widely separated new binary systems, LHS193AB, RXJ1132–262AB and LTT7419AB, are not shown in this figure. North is up and east is left.

and DEC, α_2 and δ_2 , respectively, is from van de Kamp (1967),

$$\alpha_2 = X' - (c_x + P_x \pi_x + \mu_x t) \quad (5.3)$$

$$\delta_2 = Y' - (c_y + P_y \pi_y + \mu_y t) \quad (5.4)$$

where X' and Y' are the modified coordinates in RA and DEC, c_x and c_y are constants, P_x and P_y are the parallax factors, π_x and π_y are the relative trigonometric parallaxes, μ_x and μ_y are relative proper motions, and t is the fractional year for each frame. Subscripts x and y are for quantities in RA and DEC, respectively. Parallax factors P_x and P_y for each frame are calculated from the Naval Observatory Vector Astrometry Subroutines (NOVAS), *solsys*.³ As before, a least squares method is

³available at <http://aa.usno.navy.mil/software/>

applied to produce the relative proper motions by minimizing the values of α_2 and δ_2 .

All of the eight new candidate companions have proper motions that are consistent in both magnitude and direction with their primaries, reconfirming that all companion candidates are true companions. Results of the astrometric solutions for proper motion and position angle are shown in Table 5.1 for 21 true multiple systems. The time series for BD-21°1074ABC and LTT9123AB are insufficient for reliable proper motion determinations, and one system has been refuted to be a true binary: HIP82724 and HIP82725 have the largest statistically different proper motions (4.0σ) of the systems observed, implying that they are not physically associated. The high errors in the proper motion position angles are the result of very small proper motions, which makes the direction of the motion difficult to determine. Based on our own spectroscopic observations taken at the CTIO 4-m telescope in April 2002, we confirm that the two stars are not a physical pair — HIP 82725 is a giant and HIP 82724 is a dwarf, yet they have similar magnitudes with $V = 11.72$ and 11.85, respectively.

Full analyses, including parallaxes, await acquisition of the final frames in the astrometric series. Typical errors are < 20 mas/year for the proper motions and $< 5^\circ$ for the position angles. Larger errors occur in cases where the system is a close multiple (LHS1749, LHS225, GJ1226) or the secondary is quite faint (LHS193).

Table 5.1: Astrometry data for CTIOPI resolved systems

Object Name	Separation (arcsec)	P.A. of Component (deg)	μ (" / yr)	P.A. of μ (deg)	No. of Epochs	Time Coverage (year)
(1)	(2)	(3)	(4)	(5)	(6)	(7)
MOTION stars						
G266-089A	1.383 ± 0.006	192.2 ± 0.4		
G266-089B	9.02 ± 0.01	321.08 ± 0.02	1.388 ± 0.007	192.0 ± 0.5	5	2000.87 ~ 2001.87
LHS193A	1.016 ± 0.007	45.2 ± 0.8		
LHS193B*	12.59 ± 0.05	210.67 ± 0.21	1.013 ± 0.031	41.3 ± 3.4	5	2000.87 ~ 2002.08
LHS225A	1.267 ± 0.023	102.5 ± 1.5		
LHS225B*	2.45 ± 0.06	270.06 ± 0.81	1.208 ± 0.020	102.4 ± 1.3	6	2000.88 ~ 2002.08
LHS300A	1.253 ± 0.003	264.0 ± 0.2		
LHS300B*	4.28 ± 0.04	62.27 ± 0.41	1.257 ± 0.016	264.3 ± 1.0	5	2001.15 ~ 2002.29
GJ1226A	1.146 ± 0.031	214.2 ± 3.0		
GJ1226B*	1.42 ± 0.09	14.99 ± 3.13	1.213 ± 0.046	211.1 ± 4.3	4	2000.57 ~ 2001.60
LHS501(A)	1.493 ± 0.002	107.9 ± 0.1		
LHS500(B) ^a	107.12 ± 0.02	185.18 ± 0.03	1.488 ± 0.002	108.3 ± 0.2	8	1999.71 ~ 2002.44
Non MOTION stars						
GJ2006A	0.117 ± 0.005	101.2 ± 4.4		
GJ2006B	17.87 ± 0.01	175.02 ± 0.08	0.100 ± 0.006	106.5 ± 4.5	5	2000.57 ~ 2001.83
GJ2022A	0.239 ± 0.048	126.9 ± 21.9		
GJ2022B	37.84 ± 0.05	78.53 ± 0.07	0.179 ± 0.016	129.2 ± 9.8		
GJ2022C*	2.01 ± 0.07	46.38 ± 1.31	0.303 ± 0.068	128.2 ± 23.8	5	1999.62 ~ 2000.87
G274-138A	0.344 ± 0.008	147.8 ± 2.5		
G274-138B	3.59 ± 0.01	60.40 ± 0.17	0.344 ± 0.009	146.5 ± 2.9	6	2000.57 ~ 2001.75

Table 5.1: continued

Object Name	Separation (arcsec)	P.A. of Component (deg)	μ (" / yr)	P.A. of μ (deg)	No. of Epochs	Time Coverage (year)
(1)	(2)	(3)	(4)	(5)	(6)	(7)
LP993-115(A)	0.386 ± 0.003	174.5 ± 0.7		
LP993-116(B) ^a	44.55 ± 0.02	61.09 ± 0.01	0.372 ± 0.003	172.8 ± 0.7	6	1999.62 ~ 2001.95
LP771-095(A)	0.475 ± 0.004	234.5 ± 1.0		
LP771-096(BC) ^a	7.22 ± 0.03	315.06 ± 0.05	0.484 ± 0.004	238.7 ± 1.0	3	1999.64 ~ 2001.75
LTT2043(A)	0.339 ± 0.005	238.4 ± 1.6		
LTT2044(B) ^a	49.58 ± 0.01	195.97 ± 0.01	0.333 ± 0.006	238.8 ± 2.1	5	2000.88 ~ 2002.08
BD-21°1074A		
BD-21°1074BC	8.22 ± 0.01	311.18 ± 0.16	2	
LHS1749A	0.811 ± 0.008	355.7 ± 0.7		
LHS1749B*	2.86 ± 0.06	139.02 ± 1.11	0.798 ± 0.038	355.8 ± 3.7	5	2000.88 ~ 2002.08
LHS2067(A)	0.632 ± 0.002	75.4 ± 0.3		
LHS2068(B) ^a	18.23 ± 0.02	89.28 ± 0.05	0.627 ± 0.006	77.1 ± 0.9	8	2000.14 ~ 2002.29
LTT3790(A)	0.213 ± 0.017	188.5 ± 2.7		
LTT3791(B) ^a	30.91 ± 0.01	119.82 ± 0.01	0.212 ± 0.017	188.7 ± 3.0	4	2000.14 ~ 2002.07
RXJ1132-264A	0.073 ± 0.002	255.4 ± 2.9		
RXJ1132-264B*	13.18 ± 0.01	185.49 ± 0.04	0.072 ± 0.003	255.1 ± 4.0	6	2000.14 ~ 2002.29
LHS2567(A)	0.599 ± 0.002	241.6 ± 0.4		
LHS2568(B) ^a	7.94 ± 0.01	60.96 ± 0.04	0.591 ± 0.002	242.1 ± 0.4	4	2000.07 ~ 2002.44
LHS3001(A)	0.972 ± 0.003	301.1 ± 0.4		
LHS3002(B) ^a	12.67 ± 0.02	45.46 ± 0.05	0.989 ± 0.005	300.7 ± 0.5	6	2000.58 ~ 2002.28
HIP82725	0.006 ± 0.003	62.2 ± 45.3		

Table 5.1: continued

Object Name	Separation (arcsec)	P.A. of Component (deg)	μ (" / yr)	P.A. of μ (deg)	No. of Epochs	Time Coverage (year)
(1)	(2)	(3)	(4)	(5)	(6)	(7)
HIP82724†	12.97 ± 0.01	109.09 ± 0.22	0.055 ± 0.012	63.7 ± 17.0	7	2000.23 ~ 2002.53
GJ2130AC	0.278 ± 0.002	195.6 ± 0.5		
GJ2130B	21.23 ± 0.01	88.22 ± 0.01	0.278 ± 0.002	196.2 ± 0.5	7	1999.64 ~ 2002.44
LTT7419A	0.387 ± 0.003	200.3 ± 0.7		
LTT7419B*	14.90 ± 0.02	353.83 ± 0.12	0.394 ± 0.006	204.1 ± 1.6	9	2000.57 ~ 2002.57
LHS3739(A)	0.535 ± 0.006	228.2 ± 1.2		
LHS3738(B) ^a	113.15 ± 0.03	353.30 ± 0.01	0.540 ± 0.005	226.7 ± 1.0	3	1999.64 ~ 2002.51
LTT9123(A)		
LTT9124(B) ^a	14.57 ± 0.01	136.24 ± 0.04	2	

a: Hereafter referred to as component(s) "B" (and "C") in the system, *: New companion, †: refuted companion

5.3 Differential Photometry

Differential photometry between the primary stars and the 23 true companions was measured using all available frames in the V , R and I filters. In addition to evaluating the colors of the components, the rich datasets available provide an opportunity to search for both long-term (a few years) and short-term (a few minutes) variability. Typically, a system is observed only once per observing run for astrometry, so the current datasets do not provide insight into variability on timescales of a few nights.

SExtractor was used to determine the fluxes for all resolvable components in each system. For components with separations less than $10''$, a $1''$ radius aperture was used to prevent the Moffat profile wings from overlapping, which would corrupt the relative counts and derived magnitude differences. A $5''$ radius aperture was used for systems with separations greater than $10''$, except in the case of LTT7419, for which a $1''$ aperture was used because of a faint background star near to component B.

Brightness ratios for each filter were derived using simple ratios of the total counts included in the apertures, i.e. psf fits were not done. Instrumental magnitude differences were determined using the usual conversion of brightness ratio to magnitude difference, and the results are listed in Table 5.2 (column 6). Because standard stars on the Johnson and Cousins systems were not observed, the magnitude differences listed are slightly different than what will be available when full photometric calibrations have been done. Of the 23 companions examined, six have a magnitude difference greater than 2.5 in the primary filter, making these companions more than 10 times fainter than their primaries. LTT7419AB has the largest magnitude difference observed, $\Delta V = 6.06$. The disparities between the number of frames and nights per filter for a given system (columns 4 and 5 of Table 5.2) arises because the bulk of frames taken are in a single filter for the astrometry program, while the other two filters are acquired only for relative or absolute photometry.

The errors on the magnitude differences were derived by taking the standard deviation of the nightly means, e.g. using six values for G266-089AB, not 30 values corresponding to the number of frames. A closer look at these errors provides a hint of the long-term variability in each system. The timescale over which long-term variability might be detected ranges from ~ 1.0 to 2.5 years, as listed in final column of Table 5.1. One exception to these timescales is the new close binary, GJ1226AB, for which fewer frames were available for astrometry than for variability. In many images the components were blended, making accurate centroid measurements impossible. However, flux ratios were obtainable from many of these blended frames, yielding a

variability baseline of 2000.57–2002.46.

Shown in Figure 5.6 are the magnitude difference errors in the primary filters plotted as a function of separation for the 23 companions (BD $-21^{\circ}1074$ ABC is not plotted because no reliable error can be deduced from only two nights of data). Companions more than 2.5 mag fainter than their primaries are circled points. Only four companions have $\sigma_{\Delta m} > 0.05$, which is selected as a rather conservative variability threshold. Of these, LHS1749AB has a small separation ($2''.86$) and a large $\Delta V = 2.98$, which conspire to cause a large measurement error unrelated to variability. LHS300AB also has a relatively small separation ($4''.28$) and large $\Delta R = 4.95$, again resulting in a large measurement error. RXJ1132–264AB is a wide binary ($13''.18$) and the series of $\Delta V = 2.98, 3.00, 2.55, 2.99, 3.10$, and 3.12 values are relatively consistent except for the third epoch (discussed below), hinting at some sort of variability. Finally, there is compelling evidence for long-term variability in GJ2006AB, which is widely separated ($17''.87$) and has a small $\Delta V = 0.27$, with measurements at four epochs of $\Delta V = 0.21, 0.17, 0.39$, and 0.29 . Comparison of both components to a field star indicates that both A and B may be variable. The errors for the remaining systems indicate that the typical measurement accuracy for magnitude differences during CTIOPI is a few hundredths of a magnitude.

A search for short-term variability, indicated by the error in a single night's measurements, is possible because several frames are usually taken on a system each night. The range of nightly errors for each system is given in the last column of Table 5.2. Examining the rich datasets taken in the primary parallax filters reveals five companions that have at least one night on which the error is greater than 0.05 mag. As before, in most cases (LHS193AB, LHS1749AB, LHS300AB, and GJ1226AB), the large errors can be attributed to small separations and/or large Δm . RXJ1132–264AB is the standout. The B component shows a flare event on 18 Apr 2000 that leads to a large error on that night, which is the single night with a very different ΔV value mentioned above. The series of four sequential frames yields $\Delta V = 2.31, 2.60, 2.63$, and 2.65 , revealing a significant spike in component B's luminosity at the beginning of the series, which is likely a flare caught near its peak.

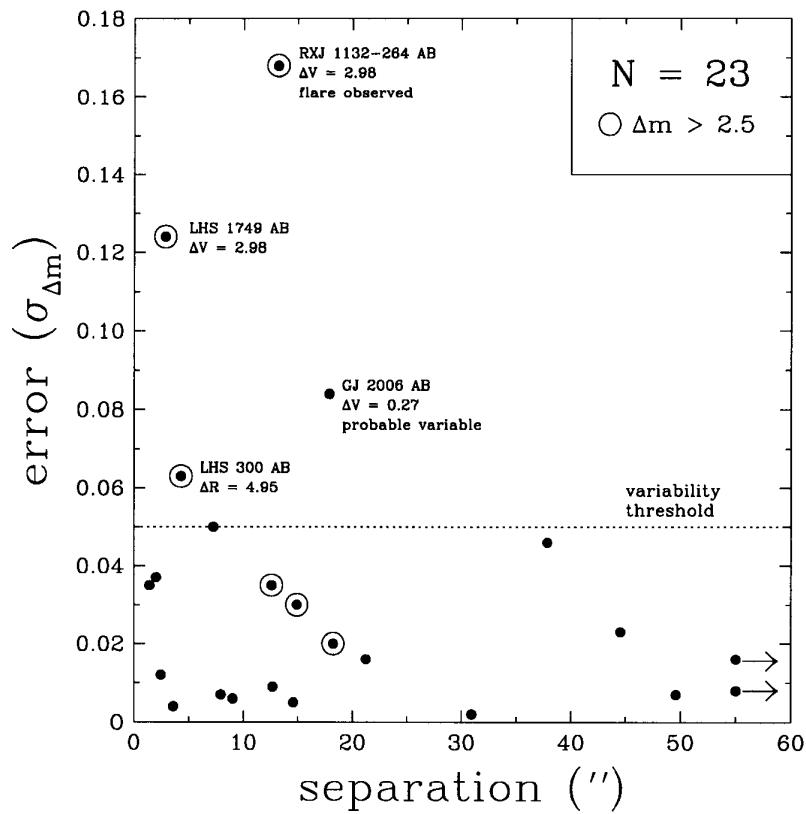


Figure 5.6: Errors in the magnitude differences between 23 companions and their primaries are plotted against separation. Open circles indicate a magnitude difference greater than 2.5. RXJ1132-264AB is a flare system and GJ2006AB is a likely variable system. Due to their large separations, LHS501AB and LHS3739AB are not plotted to scale, but are shown in the bottom right with arrows.

Table 5.2: Magnitude Difference for CTIOPI Resolved Systems

Object Name (1)	Aperture ^a (arcsec) (2)	Filter (3)	No. of Frames (4)	No. of Nights (5)	Δm (6)	Nightly Error ^b (7)
MOTION stars						
G266-089AB	1''	V	30	6	0.552±0.006	0.001–0.005
		R	6	2	0.512	0.001
		I	6	2	0.420	0.003
LHS193AB*	5''	V	34	6	5.933±0.035	0.017–0.123
LHS225AB*	1''	V	35	8	0.131±0.012	0.005–0.016
		R	6	5	0.126±0.013	0.003
		I	3	2	0.108	0.003
LHS300AB*	1''	V	1	1	4.667	...
		R	32	6	4.948±0.063	0.005–0.112
		I	1	1	4.972	...
GJ1226AB*	1''	V	8	2	0.157	0.027–0.197
		R	9	2	0.106	0.090–0.094
		I	33	6	0.103±0.035	0.032–0.070
LHS501AB	5''	V	83	14	2.129±0.017	0.001–0.008
		R	5	1	1.987	0.005
		I	5	1	1.780	0.005
Non MOTION stars						
GJ2006AB	5''	V	22	4	0.266±0.084	0.001–0.002
		R	5	2	0.304	0.000
		I	6	2	0.210	0.001
GJ2022AB	1''	V	8	3	1.315±0.039	0.012–0.026
		R	13	6	1.174±0.046	0.003–0.013
		I	5	2	1.063	0.019
GJ2022AC*	1''	V	8	2	0.064	0.042
		R	13	6	0.095±0.037	0.008–0.026
		I	5	2	0.076	0.003
G274-138AB	1''	I	41	7	0.117±0.004	0.003–0.010
LP993-115AB	5''	V	35	7	0.338±0.023	0.002–0.011
		R	1	1	0.224	...
		I	1	1	0.067	...
LP771-095A-BC	1''	V	28	5	0.304±0.050	0.007–0.041
		R	1	1	0.124	...
		I	4	1	−0.035	0.017
LTT2043AB	5''	V	38	6	0.285±0.007	0.001–0.002
		I	2	1	0.197	0.006
BD−211074A-BC	1''	V	15	2	0.722	0.007–0.014
		R	5	1	0.574	0.005

Table 5.2: continued

Object Name	Aperture ^a (arcsec)	Filter	No. of Frames	No. of Nights	δm	Nightly Error ^b
(1)	(2)	(3)	(4)	(5)	(6)	(7)
		I	8	2	0.220	0.004–0.006
LHS1749AB*	1''	V	30	7	2.979±0.124	0.026–0.161
LHS2067AB	5''	I	47	13	3.231±0.020	0.003–0.047
LTT3790AB	5''	V	37	5	1.533±0.002	0.001–0.004
		R	1	1	1.347	...
		I	1	1	0.969	...
RXJ1132-264AB*	5''	V	38	6	2.978±0.168	0.003–0.143
		R	5	1	2.613	0.003
		I	5	1	1.993	0.005
LHS2567AB	1''	V	5	1	1.149	0.002
		R	27	5	1.113±0.007	0.003–0.016
		I	5	1	1.054	0.009
LHS3001AB	5''	V	7	2	3.130	0.040–0.075
		R	5	2	2.460	0.006–0.011
		I	46	9	1.922±0.009	0.002–0.013
GJ2130AC-B	5''	V	47	8	0.997±0.016	0.001–0.005
		R	14	3	0.845±0.007	0.005–0.008
		I	14	3	0.531±0.006	0.001–0.008
LTT7419AB*	1''	V	60	9	6.065±0.036	0.008–0.021
		R	1	1	5.315	...
		I	1	1	4.393	...
LHS3739AB	5''	V	5	1	1.054	0.004
		R	21	4	0.850±0.008	0.001–0.004
		I	10	2	0.580	0.001–0.003
LTT9123AB	5''	V	15	3	1.717±0.005	0.001–0.003
		R	11	2	1.576	0.002–0.003
		I	10	2	1.319	0.002–0.003

a: Radius within which the flux was obtained for each component, *b*: Range of errors from individual nights, *: New companion.

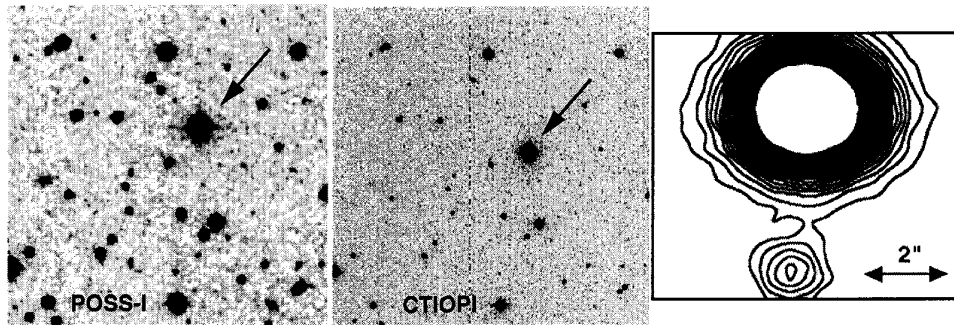


Figure 5.7: Same image scale and orientation as in Figure 5.1. The epochs for the POSS-I and CTIOPI frames are 1990.81 and 2003.60, respectively.

5.4 New Component for LHS206

Since the publication of Jao et al. (2003), we have discovered a companion to another MOTION sample star, LHS206. The companion was identified while making the MOTION finder chart and has been confirmed using follow up images taken during CTIOPI. As shown in Figure 5.7, the companion is not detectable in the POSS-I frame, but this 1990.81 frame shows that there is no source in the position that is $4''.5$ south of LHS206 at epoch 2003.60, thereby confirming that the companion is real. The basic astrometric and VRI photometric data are given in Table 5.3. The trigonometric parallax for the system is $0''.0523 \pm 0''.0022$ (van Altena et al. 1995). We estimate that LHS206A ($M_V = 11.39$, $(V - I) = 2.49$) is an early M dwarf, and that LHS206B ($M_V = 15.44$, $(V - I) = 3.30$) is a mid-M dwarf. This brings the number of new companions found during this thesis work to nine.

Table 5.3: Astrometry and photometry results for LHS206AB.

Name	V (mag)	R (mag)	I (mag)	Sep ($''$)	P.A. (deg)
LHS206A	12.80	11.71	10.31
LHS206B	16.85	15.25	13.55	4.52 ± 0.03	174.86 ± 0.4

Chapter 6

Discussion

This work has concentrated on an observationally defined sample of high proper motion stars, the MOTION sample of stars with $\mu \geq 1''0/\text{year}$. The primary goals of the work include an effort to discover new nearby stars, and the characterization of the complete sample to understand the astrometric, photometric, and spectroscopic nature of the sample members. During this work, we have also quantified the fraction of high proper motion objects that are subdwarfs (a much-neglected stellar population), found several new companions to MOTION sample members, and, of course, found several systems that are particularly noteworthy.

In this chapter we summarize the most important results of the MOTION sample investigation. These results include:

1. A probability table that estimates the odds that a star with proper motion of X is within the RECONS 10 pc sample or the CNS/NStars 25 pc sample.
2. The spatial distribution of MOTION sample members, divided into three primary populations — main sequence dwarfs, white dwarfs, and subdwarfs.
3. The tangential velocity distribution of MOTION sample members, including a discussion of the relevance of tangential velocity when attempting to define the subdwarf class.
4. The multiplicity of subdwarfs, and future work that can address the mass-luminosity relation for these metal poor stars.

6.1 Probabilities that MOTION Stars are Nearby

Table 6.1 presents a table of probabilities that describe how often a star of given proper motion will, in fact, turn out to be nearer than the RECONS sample horizon

of 10 pc, or nearer than the CNS/NStars sample horizon of 25 pc. These probabilities can be used to estimate how many new members of the two distance samples remain unidentified in the MOTION sample.

The MOTION sample members have been sorted into various proper motions bins. Fast moving systems with $\mu > 2''/yr$ have been split into bins $0''.5/yr$ in width, while those with $\mu < 2''/yr$ have been split into bins $0''.2/yr$ in width. At the conclusion of the present work, 73 MOTION systems do not have trigonometric parallaxes. Of these, 28 are main sequence stars with estimated photometric parallaxes given in Table 3.3. These have been excluded in the probability calculations because we have already estimated distances to these systems. None of these 28 systems are estimated to be within 10 pc, but 15 are likely to be between 10 and 25 pc.

The percentages have been computed for each proper motion bin first column based on the number of systems known to be nearer than 10 pc fourth column, those between 10 and 25 pc fifth column, and those beyond 25 pc sixth column, divided by the total number of systems in each proper motion bin with trigonometric parallaxes. The remaining number of systems statistically expected to be within 10 pc eleventh column is simply the product of the percentage of stars of given proper motion known to be within 10 pc seventh column and the number of stars that do not yet have any trigonometric or photometric distance determinations tenth column. The probable total number of stars within 10 pc that remain unidentified in the MOTION sample is the sum of the probable systems in all of the bins. We estimate that there are ~ 8 unidentified systems in the MOTION sample that are within the RECONS 10 pc horizon.

Table 6.1: Probability of MOTION stars within 10 pc

μ range "/yr	systems #	no D_{trig} (3)	Number of systems			percentage			no D_{trig} and no D_{phot} (10)	probable systems # <10pc (11)
			<10pc (4)	10~25pc (5)	>25pc (6)	<10pc (7)	10~25pc (8)	>25pc (9)		
(1)	(2)	(3)	(4)	(5)	(6)	(7)	(8)	(9)	(10)	(11)
>3.0	24	0	20	2	2	83.3	8.3	8.3	0	0.0
2.5~3.0	13	0	9	3	1	69.2	23.1	7.7	0	0.0
2.0~2.5	27	2(-1)	13	11(+1)	1	50.0	46.1	3.8	1	0.5
1.8~2.0	19	1(-1)	5	11(+1)	2	26.3	63.1	10.5	0	0.0
1.6~1.8	41	1	14	18	8	35.0	45.0	20.0	1	0.4
1.4~1.6	60	7(-3)	15	22(+2)	16(+1)	26.8	42.9	30.3	4	1.1
1.2~1.4	122	17(-8)	25	51(+6)	29(+2)	22.1	54.0	27.4	9	2.0
1.0~1.2	243	45(-15)	28	102(+5)	68(+10)	13.1	50.2	36.6	30	3.9
total	549	73(-28)	129	220(+15)	127(+13)				45	7.9

Note. – Numbers inside parentheses are the 28 systems with photometric parallaxes given in Table 3.3. Four possible subdwarfs listed in Table 3.3 are excluded. The percentages shown from columns (7) to (9) have included these 28 systems.

6.2 Space Distribution of MOTION Stars of Different Luminosity Classes

The MOTION sample mainly contains members of three different luminosity classes: main-sequence dwarfs, subdwarfs, and white dwarfs. Currently, 468 systems have trigonometric parallaxes and spectral types (systems with estimated spectral types by this work are included). The total distribution of systems for main sequence dwarfs : white dwarfs : subdwarfs is 354 : 33 : 81, indicating that 17% of the MOTION sample with trigonometric parallaxes is comprised of subdwarfs. The distance distributions for each class are given in Figure 6.1(a) and listed in Table 6.2. This breakdown indicates that 79% of main sequence dwarfs moving faster than $1''0/\text{yr}$ are within 20 pc, and a similar fraction, 82%, of white dwarfs are within 20 pc. The comparable fractions indicate that the white dwarfs are, as expected, products of the main sequence dwarf population. Beyond 20 pc, the number of main sequence dwarfs and white dwarfs in this sample drops dramatically.

The data also indicate that subdwarfs are, indeed, extremely rare — only two subdwarf systems, LHS29 (Gl191, M type) and Gl53AB (μ CasAB, G type), are known within 10 pc, which currently contains 248 stellar systems as of 2004 January 1 (Henry, private communication). In contrast to the other two samples, 75% of MOTION subdwarfs lie between 20 and 60 pc, where there is 26 times more volume sampled than in the 0 to 20 pc region. Note, however, that there are *not* 26 times as many subdwarfs found in the outer region. This is, of course, not surprising given the common observational bias that nearer objects are brighter and more easily detected than their more distant counterparts.

As discussed in Chapter 1, the current MOTION sample is deficient in objects that are moving very fast ($\mu > 2''0/\text{yr}$) and faint objects ($m_R > 19.5$). Thus, the space distributions for the three samples of objects discussed here are subject to these current survey limits. It is likely that additional systems, especially fast moving objects, faint white dwarfs, and faint subdwarfs, are missed at distances further than 20 pc. For example, two new MOTION subdwarfs found after 2003 January 1, LSR1610–0040 ($1''46/\text{yr}$) and 2MASS0532+8246 ($2''60/\text{yr}$), are likely to lie between 20 pc and 60 pc. In addition, the SuperCOSMOS RECONS search has found two new HPM stars with $\mu > 2''0/\text{yr}$: SCR1138–7721 with $\mu = 2''14/\text{yr}$ (photometric distance estimate is 9.4 pc) and SCR1845–6357 with $\mu = 2''56/\text{yr}$ (photometric distance estimate is 4.7 pc).

Using the data presented in Table 6.2, in Figure 6.1(b), we sort *only* the 354 main

class	distance bin (pc)							total
	0~10	10~20	20~30	30~40	40~50	50~60	>60	
dwarf	112	166	45	11	9	2	9	354
subdwarf	2	4	14	14	13	20	14	81
WD	13	14	2	1	0	0	3	33

Table 6.2: The distribution of MOTION sample systems broken into different luminosity classes.

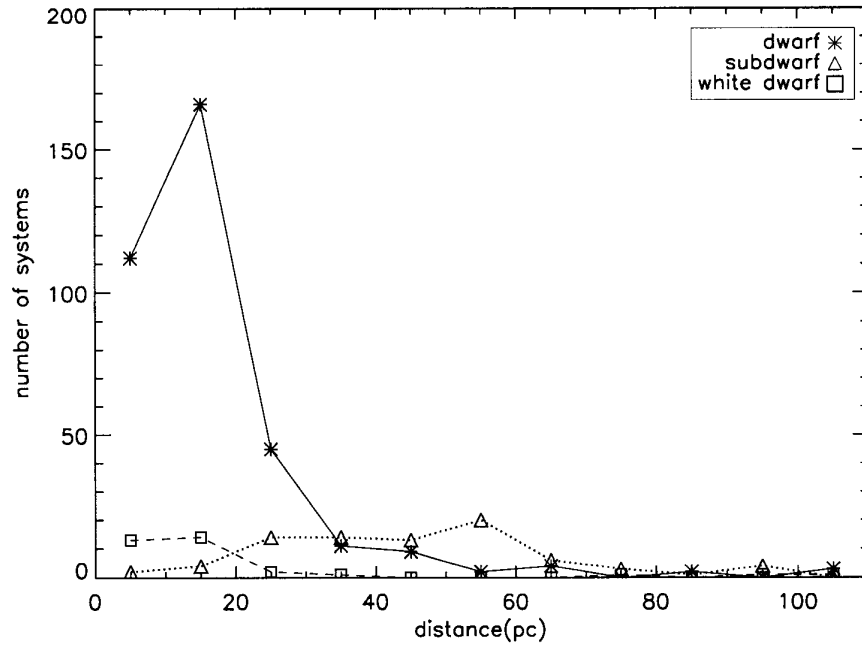
sequence MOTION systems by proper motion to illustrate graphically the probabilities that a star of given proper motion falls in the 10 pc, 10–25 pc, or beyond 25 pc, distance regime. It can be seen that MOTION main sequence dwarfs with $\mu > 2''0/\text{yr}$ are more likely to be within 10 pc than beyond 10 pc, while those with $\mu < 1''2/\text{yr}$ are most likely to be further than 25 pc.

6.3 Tangential Velocity Distribution of MOTION Stars

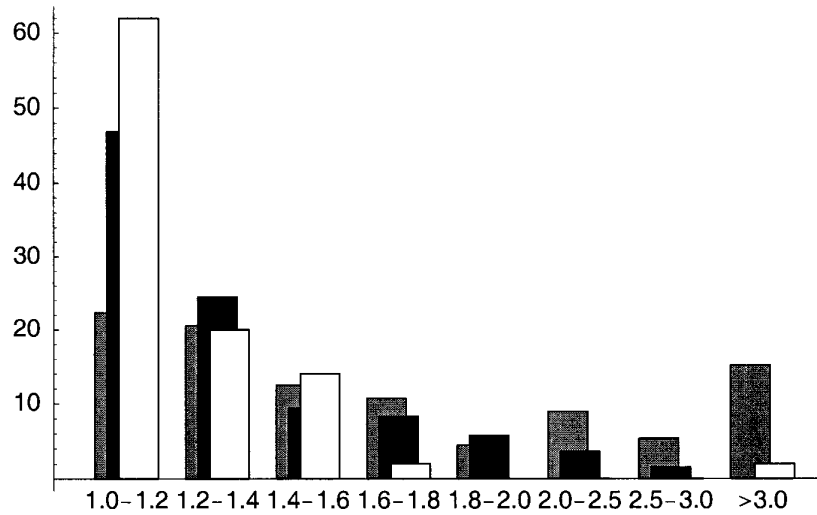
Tangential velocity is the most often used method to select a large sample of subdwarf candidates, which is then used to determine the subdwarf luminosity function based on a reduced proper motion diagram and photometric parallaxes. However, samples selected by velocity alone are not “cleaned” of high velocity stars that are not true subdwarfs, and therefore, our understanding of the subdwarf population is compromised.

The distributions of tangential velocities for the 468 systems discussed in the previous section (those with trigonometric parallaxes and spectral types) are plotted in Figure 6.2. The number of main sequence dwarfs drops with increasing velocity, while the opposite trend is seen for subdwarfs. The fraction of main sequence dwarfs with $V_{tan} > 200$ km/sec is only 8% (27/354, and the numbers of F, G, K and M dwarfs are 3, 4, 10, 10, respectively.)¹, while 78% (63/81) of the subdwarf sample exceeds this limit, a factor of 10 increase in the percentage of fast moving objects. As found before, the white dwarf population mimics that of the main sequence dwarfs, with

¹This fraction is very different from the percentage for all main sequence dwarfs. As a test, 17,355 dwarfs were selected from Hipparcos that have spectral types O~M V, $\pi > 2$ mas and $\pi > 2 \times \pi_{error}$. Only 31 entries (0.2%) have $V_{tan} > 200$ km/sec. These 31 stars include 1 B dwarf, 3 A dwarfs, 11 F dwarfs and 16 G dwarfs.



(a) The spatial distributions of the three different classes of stars found in the MOTION sample are shown. Main sequence dwarfs are represented by asterisks (solid line), white dwarfs are represented by boxes (dashed line), and subdwarfs are represented by triangles (dotted line). Actual values for each point are listed in Table 6.2. Note the very different distribution of subdwarfs from the other two samples.



(b) Gray bars indicate the percentage of MOTION dwarfs within 10 pc split into bins of different proper motion. The black and white bars represent the MOTION dwarfs with distances of $10\text{pc} < d < 25\text{pc}$ and $d > 25\text{pc}$, respectively.

Figure 6.1: The distance distributions of MOTION stars of various luminosity classes and proper motions.

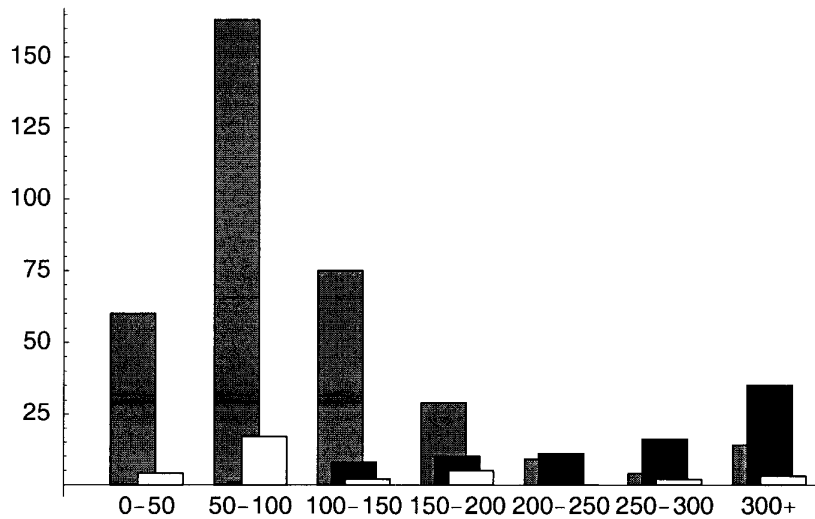


Figure 6.2: Histogram of tangential velocities for stars in the MOTION sample with trigonometric parallaxes and spectral types. The horizontal axis units are km/sec for each bin, and the vertical axis is the number of systems in each bin. Main sequence dwarfs, white dwarfs, and subdwarfs are plotted as gray, white, and black, respectively.

only 15% (5/33) having V_{tan} exceeding 200 km/sec.

Even when systems with trigonometric parallax errors greater than 10 mas are removed (in an effort to clean the sample), there remain 24 main sequence systems (Table 6.3) moving faster than 200 km/sec. These high velocity dwarfs might be thick disk stars that have low metallicity ($[Fe/H] < -0.4$), are older than 10 Gyrs, and have larger velocity dispersion than thin disk stars (Binney and Merrifield 1998). Nonetheless, spectroscopically these are not true subdwarfs of low metallicity and therefore they act as contaminants to any derived subdwarf sample. By adding these 24 systems to the sample of 63 true subdwarfs selected by $V_{tan} > 200$ km/sec, the sample would have 28% false subdwarf members, a rather unacceptable amount of contamination.

An extreme example of subdwarf sample contamination is the work of Schmidt (1975), who adopted thresholds in proper motion ($\mu > 1''.295/yr$) and V_{tan} (> 100 km/sec) to select possible high velocity halo stars and to determine the subdwarf mass and luminosity functions. We have discovered that all of his selected 57 stars are members of the MOTION sample. Two of these stars have incorrect proper motions, and 36 additional stars are not subdwarfs. Hence, this sample contains only

Type	distance (pc)						$\pi_{error} > 10\text{mas}$	total
	0~20	20~40	40~60	60~80	80~100	100+		
dwarfs	1	6	9	4	2	2	3	27
subdwarfs	1	14	34	9	5	0	0	63
WDs	1	1	0	1	1	1	0	5

Table 6.3: The number of MOTION systems with $V_{tan} > 200$ km/sec. The three dwarf systems with trigonometric parallax errors greater than 10 mas are LHS177, LHS328 and LHS466.

19 spectroscopically confirmed subdwarfs, or only 33% of the sample.

Gizis and Reid (1999) and Digby et al. (2003) both used a reduced proper motion diagram to select possible subdwarfs. Then, they each used photometric parallaxes to select candidates with $V_{tan} > 200$ km/sec. As a test, we used the same technique in the reverse direction to evaluate the expected contamination by main sequence dwarfs. We first selected the 26 main sequence dwarfs in the MOTION sample that have $V_{tan} > 200$ km/sec, using available trigonometric parallaxes (one system has no V magnitude so is not plotted). We then placed them on the reduced proper motion diagram shown in Figure 6.3. Although the stars fall in the subdwarf region and have $V_{tan} > 200$ km/sec, these stars are not subdwarfs. Thus, the subdwarf selection methods used by Gizis and Reid (1999) and Digby et al. (2003) will result in a contaminated sample. Digby et al. (2003) argues that a maximum of 0.04% (1 star in 2500) of the thick disk population will be included as contaminants in samples selected by $V_{tan} > 200$ km/sec. However, our work shows that the percentage must be significantly higher (28% computed above). We therefore conclude that the tangential velocity cutoff method used to separate subdwarfs from main sequence dwarfs can be used as a first step, but any output sample must be carefully evaluated for contamination.

Finally, the contamination from high tangential velocity white dwarfs can be eliminated by careful use of a reduced proper motion diagram, as shown in Figure 6.3. Note, however, that a long color baseline, $(V - K_s)$ on the x -axis, has been used to cleanly separate the white dwarf and subdwarf populations. Only long color baselines are reliable for separating the two populations.

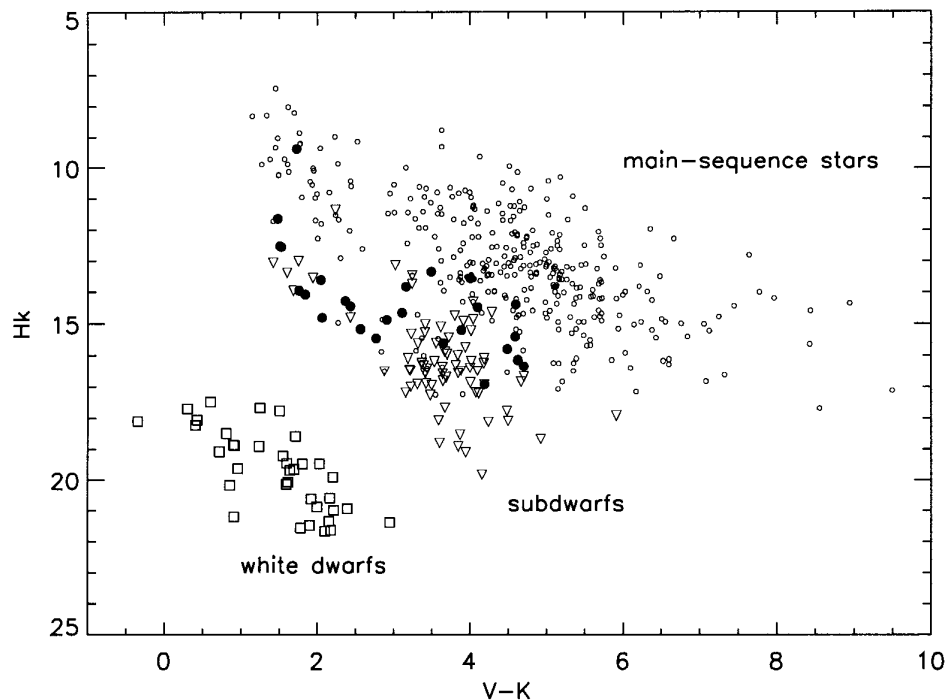


Figure 6.3: Filled circles show the 26 MOTION main sequence dwarfs with $V_{tan} > 200$ km/sec. Other symbols are the same as defined in Figure 3.4.

6.4 Subdwarf Multiplicity

The multiplicity of various types of main sequence dwarfs has been discussed in the last 15 years. Mason et al. (1998) found that more than 59% of O-type stars in clusters and associations have a visual, speckle, or spectroscopic companion. Duquennoy and Mayor (1991) found that 65% of solar-type primaries have companions with masses greater than $0.01 M_{\odot}$. Henry and McCarthy (1990) and Fischer and Marcy (1992) reported that the multiplicity fraction of M dwarfs drops to 34% and $\sim 42\%$, respectively.

Some data indicate that the binary fraction of metal-poor, high velocity subdwarfs is different from main sequence dwarfs. Oort (1926) pointed out that the binary fraction is two to three times lower among high velocity stars than typical disk stars. Stryker et al. (1985) found a lower limit of 20–30% for the binary frequency of a sample of AFG type subdwarfs. Carney et al. (1994) found that at least 15% of their sample

of halo F and G stars ($[m/H] \leq -1.2$) are spectroscopic binaries with periods shorter than 3000 days. Recently, Gizis and Reid (2000) carried out a small HST snapshot imaging program to search for companions around nine M subdwarfs. In their study, companions with $\Delta m = 0, 1, 3, 5$ mag were expected to be resolved at separations of $0''.09, 0''.14, 0''.23$ and $0''.32$, respectively. However, none of the nine subdwarf targets were found to have companions. Table 6.4 summarizes the multiplicity fractions of normal main sequence dwarfs and subdwarfs. Apparently, the AFG type subdwarfs have a significantly lower multiplicity fraction than the normal dwarfs.

	O-B type	A-G or G type	M type
dwarfs	59%	65%	34% \sim 42%
subdwarfs	unknown	15% \sim 30%	unknown

Table 6.4: Multiplicity comparison between main sequence dwarfs and subdwarfs

Available data indicate that the subdwarf multiplicity fraction *may* be lower than that of normal dwarfs, but the surveys done to date set lower limits (AFG stars) or are very limited in extent (KM stars). The MOTION sample is particularly well suited to a study of the multiplicity fraction of subdwarfs because we have established a robust sample of 82 spectroscopically confirmed subdwarfs that can be investigated. Given that the binary frequency of normal M dwarfs is roughly half that of their more massive AFG counterparts, and that AFG subdwarfs are binary 15-30% of the time, we might expect that the M subdwarfs would be binary $\sim 10\%$ of the time.

Determining the multiplicity rate of subdwarfs has important consequences for star formation. Binary formation is widely known to be due to the fragmentation process of a giant molecular cloud, from which many close binaries emerge. If the multiplicity fraction at the time of origin is the same for dwarfs and subdwarfs, and the subdwarf multiplicity fraction turns out to be much lower than that of dwarfs, then a subdwarf system must encounter objects in the disk much more frequently than is usually assumed (Stryker et al. 1985). If so, what hidden population causes these frequent collisions — white dwarfs, red dwarfs, brown dwarfs? An alternate explanation is that the star formation process is radically different for stars of low metallicity than for those of solar metallicity. Both the binary destruction scenario and the metallicity-dependent star formation scenario are possible hypotheses. Or, the answer might be much simpler. Perhaps the multiplicity rate is the same for subdwarfs and normal dwarfs, and neither scenario needs to be invoked. In order to know which to believe, we must know how many subdwarfs have companions.

Finally, we have identified that LHS189 and LHS190 form the first known M

subdwarf binary. This is only the first example of late type subdwarfs that might be found in the MOTION sample. For future work, we plan to use high resolution interferometers such as HST's Fine Guidance Sensors (FGS) and GSU's CHARA (The Center for High Angular Resolution Astronomy) Array to observe the MOTION sample of subdwarfs to reveal companions and map orbits, which will eventually result in the direct determination of subdwarf masses.

6.5 The Mass-Luminosity Relation for Subdwarfs

After the HR Diagram, the mass-luminosity relation (MLR) is arguably the most important map of stellar astronomy. Given a star's mass, one knows a great deal about its temperature, color, and structure, as well as its past and future evolution. Determining the MLR for massive stars is done using eclipsing binaries, but stars with small radii are rarely found in eclipsing systems. So, teams at Georgia State University (led by Todd Henry), the University of Texas, Austin (led by G. Fritz Benedict), and Lowell Observatory (led by Otto Franz) are using HST-FGS interferometry and radial velocity spectroscopy to determine the mass-luminosity relation for stars less massive than the Sun, concentrating in particular on the M dwarfs (Henry et al. 1999).

Figure 6.4 illustrates the MLR for the lowest mass stars (Henry 2004, private communication) and the models by Baraffe et al. (1998) for stars of solar metallicity and age. Masses have been derived from orbits determined using a combination of infrared speckle, HST-FGS interferometry, and radial velocity work. These recent results indicate that many M dwarfs lie at magnitudes much fainter than models indicate for a given mass.

Examination of the MLR yields two immediate questions: Are the M dwarfs falling below the models actually subdwarfs with low metallicity? Are the stars near the models preferentially young, and therefore the models, which are for stars of age 5 Gyr, wrong?

The best answers to these questions will come from an effort to determine the MLR for subdwarfs of all types, including M subdwarfs. This is a difficult, but important, endeavor because one of the consequences of the empirical MLR is that the most numerous components of the Galaxy, the M dwarfs, may be $\sim 20\%$ more massive than previously thought. This adds quite a bit of mass to the stellar component of the Galaxy's mass budget. We note that Jacob Bean (who worked at GSU and has moved to U. Texas) is attempting to determine accurate M dwarf metallicities for

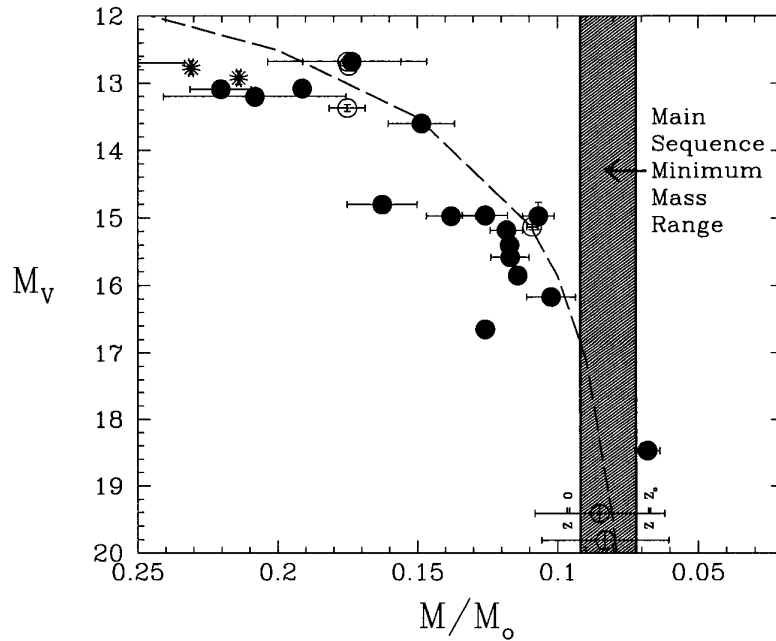


Figure 6.4: The Mass-Luminosity Relation for M dwarfs. Points shown in solid are from the Henry/Benedict team, two asterisks are from eclipsing binaries, and open points are from others. The shaded region indicates the range of masses for the substellar border, depending on metallicity.

the first time. The metallicity and MLR results can be combined to yield a complete picture of the MLR and its dependence on metallicity (and at some level, age).

Accurate masses for subdwarfs are rare. One of the few examples is μ Cas AB (Gl53AB, G VI, 7.54 pc, $\Delta K \sim 3.5$), which plays a pivotal role in determining the primordial helium abundance (Dennis 1965). A direct determination of the helium abundance requires accurate luminosities and masses for the two components, which are separated by at most $1''.5$. High resolution infrared speckle and image tracking efforts, combined with astrometric perturbation data, have yielded masses (McCarthy et al. 1993), but there remains significant room for improvement. Two different astrometric orbits, combined with the high resolution data, yield masses of 0.71 or $0.55 M_\odot$ and 0.16 or $0.14 M_\odot$ for the components.

However, μ Cas AB is only one system. Identifying promising subdwarf multiple systems that can be followed for orbit mapping and mass determination is crucial. Such systems can be used in combination to produce the first-ever MLR for subd-

warfs. The sample of subdwarfs found during this work — that now have astrometric, photometric, and spectroscopic coverage — is the ideal sample to use for mass determinations.

6.6 Summary

We summarize here details for several of the most noteworthy systems observed during this work.

This work has discovered five new members of the RECONS sample via trigonometric parallax work, each of which is among the nearest few hundred stellar systems. The five systems are: LHS22 (M4.5 V at 6.97 pc), LHS145 (white dwarf at 9.8 pc), LHS263 (M4.5 V at 8.20 pc), LHS337 (M4.5 V at 6.58 pc), and DEN1048-3956 (M8.5 V at 3.99 pc). An additional 25 systems have been found to lie within the 25 pc CNS/NStars horizon via trigonometric parallax, and 15 more systems probably also fall between 10 and 25 pc, as determined by their photometric parallaxes.

Only two systems, LHS29 (G1191, M VI) and G153AB (μ CasAB, G VI), are spectroscopically confirmed subdwarfs within 10 pc, indicating that the local density of subdwarfs is $\sim 1\%$. The LHS189 and LHS190 system comprises the first binary M subdwarf system ever identified. LHS193AB is the first subdwarf/white dwarf binary ever identified. LHS202 is probably a newly revealed giant member of the MOTION sample, bringing the total to 8 giants. LHS540AC and LHS541 comprise the first known triple subdwarf system.

Hence, this MOTION sample is one of the best samples for revealing hidden nearby stars and discovering new subdwarfs. This work has characterized all the properties of this sample so that we can understand where they are and what they are. These results can be used in studies of (1) the nearby stellar mass and luminosity functions, (2) the mass-luminosity relation for low mass stars, including subdwarfs, (3) the multiplicity fractions of the main sequence and subdwarf populations using high resolution interferometry, (4) searches for extrasolar planets, (5) the local Galactic kinematics and the construction of the 3-D movement of nearby stars (when the astrometry is combined with a radial velocity survey), and (6) the comprehensive evaluation of the rare Galactic halo relics known as K/M subdwarfs. Thus, the high proper motion stars of the MOTION sample will help us explore new territory in stellar astrophysics.

Appendix A

Complete List of MOTION Sample

Table A.1: MOTION Samples

RA	DEC (J2000.0)	P.M. Angle ($''/yr$)	Angle (deg)	Full Name	LHS	LOB	CNS3	YPC	HIP	HD	Ref.
(1)	(2)	(3)	(4)	(5)	(6)	(7)	(8)	(9)	(10)	(11)	(12)
00 02 10.21	+27 04 55.8	1.295	139.8	Gl 914 A	101	...	Gl 914 A	5807.00	171	224930	1
00 02 10.21	+27 04 55.8	1.295	139.8	Gl 914 B	Gl 914 B	1
00 02 10.21	+27 04 55.8	1.295	139.8	Gl 914 C C	1
00 02 10.73	-43 09 55.5	1.020	135.2	LHS 1005	1005	5808.00	3
00 04 34.86	-40 44 06.5	1.618	154.5	LHS 102 B B	1
00 04 36.45	-40 44 02.7	1.618	154.5	LHS 102 A	102	...	GJ 1001 A	5815.01	1
00 05 24.39	-37 21 26.7	6.108	112.5	LHS 1	1	267-025	Gl 1	5817.00	439	225213	1
00 06 43.19	-07 32 17.0	2.041	203.6	LHS 2	2	158-027	GJ 1002	9.01	1
00 07 26.68	+29 14 32.7	1.890	127.2	LHS 103	103	130-043	GJ 1003	9.11	1
00 09 16.46	+09 00 41.9	1.108	187.8	LHS 104	104	030-048	...	17.02	1
00 09 17.31	-19 42 31.6	1.148	59.5	LHS 105	105	1
00 11 31.82	+59 08 39.9	1.483	218.3	LSR0011+5908	2
00 12 46.97	+54 39 45.4	1.010	52.5	LHS 1039	1039	29.01	3
00 14 09.61	-20 22 53.6	1.277	262.8	LHS 106	106	1
00 15 33.49	-35 11 47.6	1.030	97.6	LHS 1048	1048	3
00 16 14.62	+19 51 37.6	1.037	137.5	LHS 107	107	032-006	GJ 1006 A	42.11 A	1295	...	1
00 16 16.14	+19 51 50.6	1.037	137.5	LHS 108	108	032-007	GJ 1006 B	42.11 B	1
00 17 40.01	-10 46 16.9	1.055	180.8	LHS 109	109	158-053	...	48.03	1
00 18 22.79	+44 01 22.7	2.899	82.2	LHS 3	3	171-047	Gl 15 A	49.00 A	1475	1326A	1
00 18 25.72	+44 01 38.1	2.899	82.2	LHS 4	4	171-048	Gl 15 B	49.00 B	...	1326B	1
00 19 36.59	-28 09 38.8	1.373	191.3	LHS 110	110	266-088	1
00 19 37.02	-28 09 45.7	1.373	191.3	LHS 111	111	266-089	1
00 20 04.38	-64 52 29.2	2.063	55.9	LHS 5	5	...	Gl 17	54.00	1599	1581	1
00 20 29.37	+33 05 06.4	1.362	129.2	LHS 112	112	54.01	1
00 25 44.37	-77 15 15.3	2.250	81.7	LHS 6	6	...	Gl 19	69.00	2021	2151	1
00 31 13.94	+53 04 45.4	1.000	49.0	LHS 1088	1088	217-055	...	83.01	L
00 31 35.42	-05 52 12.8	1.098	163.1	LHS 113	113	158-095	GJ 1013	87.01	1
00 32 29.62	+67 14 08.2	1.748	97.8	Gl 22 A	114	243-030	Gl 22 A	86.00 A	2552	...	1
00 32 29.62	+67 14 08.2	1.748	97.8	Gl 22 C	Gl 22 C	1
00 32 29.71	+67 14 04.6	1.748	97.8	Gl 22 B	115	...	Gl 22 B	86.00 B	1
00 35 02.87	-63 41 42.6	1.104	121.6	LHS 116	116	97.10	2743	3222	1
00 35 55.52	+10 28 35.5	1.186	110.5	LHS 117	117	032-035	GJ 1014	98.02	1
00 37 20.70	-24 46 02.4	1.369	90.4	Gl 25 A	118	...	Gl 25 A	104.00 A	2941	3443	1

Table A.1: continued

RA (1)	DEC (J2000.0) (2)	P.M. ("'/yr) (3)	Angle (deg) (4)	Full Name (5)	LHS (6)	LOB (7)	CNS3 (8)	YPC (9)	HIP (10)	HD (11)	Ref. (12)
00 37 20.70	-24 46 02.4	1.369	90.4	Gl 25 B	Gl 25 B	104.00 B	1
00 38 59.01	+30 36 58.5	1.561	88.3	LHS 119	119	069-010	Gl 26	107.00	1
00 43 26.01	-41 17 34.0	1.100	224.8	LHS 1134	1134	3
00 43 35.60	+28 26 41.4	1.062	187.0	LHS 120	120	132-019	GJ 1019	131.01	1
00 45 19.70	-33 29 29.5 ⁴	2.490	128.0	F351-50	4
00 48 23.01	+05 16 30.5	1.367	146.7	LHS 121	121	...	Gl 33	156.00	3765	4628	1
00 49 06.22	+57 48 54.6	1.219	115.6	LHS 123	123	...	Gl 34 A	155.00 A	3821	4614	1
00 49 05.17	+57 49 03.8	1.219	115.6	LHS 122	122	...	Gl 34 B	155.00 B	...	4614B	1
00 49 09.91	+05 23 19.1	2.980	155.7	LHS 7	7	001-027	Gl 35	160.00	3829	...	1
00 49 29.04	-61 02 32.7	1.119	94.0	LHS 124	124	...	GJ 1022	1
00 50 17.09	-39 30 08.3	1.025	165.6	LHS 125	125	1
00 51 29.74	+58 18 07.5	1.549	75.9	LHS 126	126	218-017	Gl 38	169.00	4012	...	1
00 55 43.89	-21 13 07.1	1.227	98.3	LHS 127	127	268-077	1
00 57 19.73	-62 14 44.4	1.076	81.3	LHS 128	128	...	Gl 45	193.00	4473	5633	1
00 58 27.93	-27 51 25.3	1.305	102.7	LHS 129	129	269-063	Gl 46	194.10	4569	...	1
01 00 56.37	-04 26 56.5	1.326	70.5	LHS 130	130	070-028	GJ 1025	1
01 02 32.16	+71 40 47.5	1.783	101.2	LHS 131	131	242-076	Gl 48	202.00	4856	...	1
01 02 51.04	-37 37 43.7	1.519	80.3	LHS 132	132	1
01 03 38.83	-45 47 31.4	1.713	187.6	LHS 133	133	212.00	4964	...	1
01 04 53.80	-18 07 28.7	1.342	71.5	LHS 134	134	268-110	GJ 1028	215.03	1
01 05 37.60	+28 29 33.6	1.906	95.0	LHS 135	135	069-047	GJ 1029	216.01	1
01 07 08.04	+63 56 28.8	1.556	76.5	LHS 136	136	243-060	Gl 52	217.00	5247	...	1
01 07 47.82	+34 12 30.5	1.464	69.9	LHS 137	137	132-057	Gl 52.2	222.00	1
01 08 16.21	+54 55 13.2	3.762	114.9	Gl 53 A	8	...	Gl 53 A	219.00 A	5336	6582	1
01 08 16.21	+54 55 13.2	3.762	114.9	Gl 53 B	Gl 53 B	1
01 08 27.09	+63 30 56.4	1.060	94.5	LHS 1198	1198	243-062	...	221.00	5353	...	3
01 09 21.85	+29 49 26.3	1.072	71.1	2MASSWJ0109216+294925	6
01 12 30.64	-16 59 56.1	1.345	62.3	LHS 138	138	268-135	Gl 54.1	248.01	5643	...	1
01 16 29.18	+24 19 26.8	1.841	112.2	LHS 139	139	034-015	GJ 1034	257.01	1
01 19 52.26	+84 09 32.9	1.081	295.1	LHS 140	140	265-008	GJ 1035	250.01	1
01 21 34.57	-41 39 23.2	1.345	109.4	LHS 141	141	...	Gl 57	282.00	6351	...	1
01 31 30.82	+10 01 29.8	1.000	158.8	LHS 1257	1257	3
01 32 26.21	-21 54 18.5	1.062	210.7	LHS 142	142	272-036	...	319.10	7170	...	1

Table A.1: continued

RA (1)	DEC (J2000.0) (2)	P.M. (""/yr) (3)	Angle (deg) (4)	Full Name (5)	LHS (6)	LOB (7)	CNS3 (8)	YPC (9)	HIP (10)	HD (11)	Ref. (12)
01 38 49.04	+11 21 36.7	1.623	144.9	LHS 144	144	341.01	1
01 39 47.83	-56 11 36.0	3.368	80.4	LHS 9	9	272-061	GI 65 A	343.10 A	1
01 39 47.60	-56 11 47.0	3.368	80.4	LHS 10	10	272-061	GI 65 B	343.10 B	1
01 43 01.02	-67 18 30.3	1.048	197.8	LHS 145	145	1
01 44 04.09	-15 56 14.7	1.922	296.8	LHS 146	146	...	GI 71	365.00 A	8102	10700	1
01 48 07.83	-17 11 03.1	1.186	187.6	LHS 147	147	376.01	1
01 53 08.99	-33 25 02.1	1.119	84.4	LHS 148	148	1
02 00 12.96	+13 03 07.2	2.097	147.8	LHS 11	11	003-033	GI 83.1	412.02	1
02 02 52.16	+05 42 21.0	2.432	106.3	LHS 12	12	003-036	...	422.00	9560	...	1
02 05 04.85	-17 36 52.7	1.299	96.8	LHS 149	149	272-148	GI 84	431.00	9724	...	1
02 05 11.62	-05 17 54.2	1.051	67.6	WD0205-053	4
02 07 23.38	-66 34 11.7	1.798	77.7	LHS 150	150	...	GI 85	441.00	1
02 10 25.90	-50 49 25.8	2.206	73.1	LHS 13	13	...	GI 86 A	445.00	10138	13445	1
02 10 35.44	+46 42 04.8	1.030	176.2	LHS 1349	1349	3
02 11 20.83	+39 55 21.5	1.144	115.7	LHS 151	151	074-007	GJ 1042	442.02	1
02 12 20.98	+03 34 32.3	2.598	223.5	LHS 14	14	159-045	GI 87	450.00	10279	...	1
02 13 49.99	+15 59 11.1	1.020	104.1	LHS 152	152	004-007	...	457.00	1
02 14 40.29	-01 12 05.1	1.000	94.6	LHS 1365	1365	159-050	...	460.00	10449	...	3
02 16 56.51	+42 58 10.4	1.009	125.2	LHS 153	153	134-022	GI 91.3	463.01	1
02 17 03.19	+34 13 27.3	1.180	101.9	LHS 154 B B	1
02 17 03.19	+34 13 27.3	1.180	101.9	LHS 154 A	154	...	GI 92 A	464.00 A	10644	13974	1
02 19 10.08	-36 46 41.1	1.497	68.5	LHS 154a	154a	...	GJ 1046	...	10812	...	1
02 31 27.66	+57 22 43.3	1.042	88.5	LHS 155	155	174-001	GI 101	504.00	1
02 34 12.45	+17 45 50.5	1.193	145.0	LHS 156	156	004-029	...	515.01	1
02 36 04.89	+06 53 12.9	2.322	51.4	LHS 15 A	15	073-070	GI 105 A	520.00 A	12114	16160	1
02 36 15.26	+06 52 18.0	2.322	51.4	LHS 16	16	073-071	GI 105 B	520.00 B	...	16160B	1
02 36 04.89	+06 53 12.9	2.322	51.4	LHS 15 C C	1
02 39 50.71	-34 07 57.5	1.721	161.7	LHS 157	157	...	GJ 1050	1
02 42 02.85	-44 30 58.7	1.095	89.1	LHS 158	158	1
02 46 14.92	-04 59 20.6	2.524	138.1	LHS 17	17	563.01	1
02 46 34.74	+16 25 10.2	1.020	233.5	LHS 1443	1443	562.01	3
02 52 07.10	+34 23 21.7	1.342	136.1	LHS 159	159	037-008	GI 116	588.00	13375	...	1
02 52 22.15	-63 40 47.5	1.149	58.4	LHS 160	160	...	GI 118	604.10	13389	...	1

Table A.1: continued

RA (1)	DEC (J2000.0) (2)	P.M. (""/yr) (3)	Angle (deg) (4)	Full Name (5)	LHS (6)	LOB (7)	CNS3 (8)	YPC (9)	HIP (10)	HD (11)	Ref. (12)
02 52 45.51	+01 55 50.5	1.455	110.0	LHS 161	161	075-047	...	598.01	1
02 56 13.21	-35 08 26.9	1.011	138.8	LHS 162	162	1
02 57 31.04	+10 47 24.5	1.821	102.9	LHS 163	163	005-007	GI 120	613.00	1
03 01 40.57	-34 57 56.5	1.320	158.9	LHS 164	164	1
03 04 09.63	+61 42 21.2	1.000	133.9	LHS 1492	1492	627.00 A	14286	18757	3
03 04 43.40	+61 44 09.0	1.040	133.8	LHS 1494	1494	246- 22	3
03 06 26.75	+01 57 54.5	1.010	157.2	LHS 1496	1496	077-023	GI 123	642.00	14445	19305	3
03 06 28.67	-07 40 41.5	1.511	125.2	LHS 165	165	645.01	1
03 08 25.56	+26 19 51.1	1.040	198.0	LHS 1501	1501	037-026	...	648.00	14594	19445	L
03 09 03.96	+49 36 47.8	1.269	94.0	LHS 166	166	...	GI 124	647.00 A	14632	19373	1
03 10 58.53	+73 46 19.7	2.104	120.0	LHS 18	18	221-005	GJ 1053	639.01	1
03 12 29.76	-38 05 20.1	1.434	59.7	LHS 167	167	...	GI 130	667.00	1
03 13 22.92	+04 46 29.3	1.706	86.4	LHS 168	168	077-031	GJ 1057	665.01	1
03 13 24.23	+18 49 37.7	1.654	131.1	LHS 169	169	005-022	GI 129	662.00	1
03 16 26.79	+38 05 55.8	1.286	146.0	LHS 170	170	038-001	...	674.00	15234	...	1
03 17 46.17	-62 34 31.3	1.482	64.1	LHS 171	171	...	GI 136	701.00	15330	20766	1
03 18 12.82	-62 30 23.0	1.482	64.1	LHS 172	172	...	GI 138	705.00 A	15371	20807	1
03 19 55.64	-43 04 11.3	3.147	76.5	LHS 19	19	...	GI 139	703.00	15510	20794	1
03 28 53.11	+37 22 56.7	1.550	133.3	LHS 173	173	078-038	...	721.00	16209	...	1
03 30 44.81	+34 01 07.2	1.560	161.6	LHS 174	174	037-040	...	729.00	1
03 31 17.27	+66 43 49.1	1.591	132.8	LHS 175	175	246-038	...	717.00	16404	...	1
03 35 38.61	-08 29 22.7	1.582	102.4	LHS 176	176	1
03 35 51.98	+41 42 18.1	1.012	83.5	LHS 177	177	078-042	...	745.00	1
03 38 15.69	-11 29 13.5	3.033	152.1	LHS 20	20	160-005	GJ 1062	757.00	1
03 42 29.45	+12 31 33.8	1.572	151.5	LHS 178	178	079-059	...	768.01	1
03 44 34.86	+18 26 09.8	1.204	159.4	LHS 179	179	006-030	GI 151	791.00	1
03 46 46.50	+24 56 02.8 ²	1.260	155.2	WD0346+246	2
03 47 02.09	+41 25 38.2	1.370	154.6	LHS 180	180	095-057	A GJ 1064 A	805.00 A	17666	23439A	1
03 47 02.62	+41 25 42.4	1.370	154.6	LHS 181	181	...	GJ 1064 B	805.00 B	...	23439B	1
03 50 13.89	+43 25 40.5	1.439	161.0	LHS 182	182	095-059	...	835.01	1
03 50 44.29	-06 05 41.7	1.428	196.8	LHS 183	183	160-028	GJ 1065	845.01	1
03 51 09.40	-56 27 07.1 ⁴	1.085	165.8	WD0351-564	4
03 53 19.71	-37 03 59.1	1.144	199.4	LHS 184	184	...	GI 155.3	864.10	18180	...	1

Table A.1: continued

RA	DEC	P.M.	Angle	Full Name	LHS	LOB	CNS3	YPC	HIP	HD	Ref.
(1)	(2)	($^{\circ}/\mu^{\circ}$)	(deg)	(5)	(6)	(7)	(8)	(9)	(10)	(11)	(12)
04 01 36.59	+18 43 39.8	1.174	166.8	LHS 185	185	007-017	GJ 157.2	886.01	1
04 03 15.02	+35 16 23.8	2.204	128.0	LHS 21	21	...	GJ 158	887.00	18915	25329	1
04 03 38.44	-05 08 05.4	1.166	167.9	LHS 186	186	160-042	...	896.02	1
04 06 11.77	+32 57 02.9	1.093	140.8	LHS 187	187	038-025	...	905.00	19143	281540	1
04 09 15.69	-53 22 25.4	1.211	60.4	LHS 188	188	...	GJ 163	924.00	19394	...	1
04 10 28.15	-53 36 08.2	2.521	198.1	LHS 22	22	...	GJ 1068	1
04 15 21.80	-07 39 29.3	4.079	213.3	LHS 24	24	160-060	GJ 166 B	945.00 B	...	26976	1
04 15 16.34	-07 39 10.7	4.079	213.3	LHS 23	23	...	GJ 166 A	945.00 A	19849	26965	1
04 15 21.56	-07 39 21.2	4.079	213.3	LHS 25	25	...	GJ 166 C	945.00 C	1
04 19 52.13	+42 33 30.5	1.535	159.4	LSR0419+4233	2
04 25 38.35	-06 52 37.0	1.223	148.0	LHS 190	190	1
04 25 38.35	-06 52 37.0	1.223	148.0	LHS 189	189	1
04 26 19.92	+03 36 36.0	1.033	186.4	LHS 191	191	981.01	1
04 30 52.53	+28 11 58.4	1.038	143.3	LHS 192	192	995.01	1
04 31 11.48	+58 58 37.6	2.383	144.8	LHS 26	26	175-034	GJ 169.1 A	986.01 A	21088	...	1
04 31 11.48	+58 58 37.6	2.383	144.8	LHS 27	27	...	GJ 169.1 B	986.01 B	1
04 31 43.99	-21 50 44.3	1.000	147.3	LHS 1676	1676	3
04 32 35.96	-39 02 14.6	1.013	41.3	LHS 193 B	5
04 32 36.55	-39 02 03.4	1.023	44.5	LHS 193 A	193	1
04 32 42.63	-39 47 12.4	1.100	167.4	LHS 1678	1678	3
04 37 47.41	-08 49 10.6	1.520	171.2	LHS 194	194	1026.01	1
04 38 22.32	-65 24 57.4	1.486	29.2	LHS 195	195	1050.00	21609	29907	1
04 42 55.78	+18 57 29.4	1.286	146.7	LHS 196	196	083-032	GJ 176	1046.00	21932	285968	1
04 46 18.50	+48 44 51.9	1.204	122.5	LHS 197	197	1052.01	1
04 52 34.58	+40 42 24.2	1.633	133.2	LHS 198	198	081-039	GJ 1073	1083.01	1
04 55 57.67	-61 09 46.6	1.102	123.0	LHS 199	199	...	GJ 181.1	1121.00	1
05 00 49.01	-05 45 13.2	1.223	153.1	LHS 200	200	...	GJ 183	1129.00	23311	32147	1
05 03 23.95	+53 07 42.4	2.008	140.5	LHS 28	28	191-019	GJ 184	1123.00	23518	...	1
05 05 11.75	+30 43 32.1	1.097	148.5	LSR0505+3043	2
05 08 10.95	-53 00 36.0	1.174	27.5	LHS 202	202	1172.00	1
05 08 35.05	-18 10 19.2	1.376	156.6	LHS 203	203	...	GJ 190	1168.00 A	23932	...	1
05 11 40.56	-45 01 06.4	8.688	131.3	LHS 29	29	...	GJ 191	1181.00	24186	33793	1
05 13 05.36	-59 38 44.4	1.030	60.3	LHS 204	204	1197.00	24316	34328	1

Table A.1: continued

RA	DEC	P.M.	Angle	Full Name	LHS	LOB	CNS3	YPC	HIP	HD	Ref.
(1)	(2)	(3)	(4)	(5)	(6)	(7)	(8)	(9)	(10)	(11)	(12)
05 15 30.95	+59 11 17.5	1.015	173.3	LSR0515+5911	2
05 16 59.67	-78 17 20.2	1.108	176.1	LHS 205	205	...	GJ 1077	1236.01	1
05 19 13.63	+42 13 49.0	1.181	119.3	LSR0519+4213	2
05 19 56.70	+20 10 52.6	1.024	153.2	LHS 205a	205a	1208.01	1
05 22 05.30	+38 14 14.6	1.703	164.1	LP251-035	1215.03	2
05 28 14.60	+02 58 14.3	1.186	198.1	LHS 206 A	206	099-010	GJ 1080	1239.02	1
05 28 14.60	+02 58 14.3	1.186	198.1	LHS 206 B	1
05 31 27.41	-03 40 38.2	2.235	160.2	LHS 30	30	099-015	GJ 205	1255.00 A	25878	36395	1
05 37 09.89	-80 28 08.9	1.100	16.9	LHS 208	208	1340.00	26394	39091	1
05 38 12.62	+79 31 19.4	1.192	141.2	LHS 207	207	1231.01	1
05 39 24.79	+40 38 42.8	1.057	141.8	LSR0539+4038	2
05 42 09.27	+12 29 21.7	2.571	128.4	LHS 31	31	102-022	GJ 213	1305.00	26857	...	1
05 44 03.42	+40 56 49.4	1.229	147.2	LHS 209	209	096-050	...	1307.01	1
05 44 31.98	-70 08 36.8	1.321	346.6	LHS 210	210	...	GJ 217.2	1341.00	27080	39194	1
05 44 57.65	+26 02 60.0	1.702	144.3	LSR0544+2602	2
05 48 00.20	+08 22 14.0	1.218	135.4	LHS 211	211	099-033	...	1326.01	1
05 49 35.44	+23 29 52.8	1.379	131.4	LSR0549+2329	2
05 55 09.53	-04 10 07.1	2.377	166.6	LHS 32	32	099-044	GJ 223.2	1363.02	1
05 56 25.47	+05 21 48.4	1.056	207.0	LHS 212	212	099-047	GJ 1087	1366.01	1
06 00 46.53	+68 08 29.0	1.174	161.4	LHS 213	213	249-027	...	1363.01 B	1
06 00 49.44	+68 09 22.8	1.174	161.4	LHS 214	214	249-028	...	1363.01 A	1
06 09 52.42	+23 19 12.8	1.104	130.7	LSR0609+2319	2
06 10 19.78	+82 06 24.6	1.337	180.7	LHS 215	215	222-011	GJ 226	1358.00	29277	...	1
06 14 01.56	+15 09 54.3	1.399	152.8	LHS 216	216	105-023	...	1438.01	1
06 21 14.85	+65 58 16.2	1.148	156.8	LHS 217	217	249-046	...	1460.01	1
06 27 33.30	+06 16 58.9	1.019	178.5	LSR0627+0616	2
06 37 58.09	+34 30 19.2	1.264	176.7	LHS 218	218	103-046	...	1537.02	1
06 45 08.88	-16 42 56.7	1.323	204.0	GJ 244 B	GJ 244 B	1577.00 B	...	18915B	1
06 45 08.88	-16 42 56.7	1.323	204.0	GJ 244 A	219	...	GJ 244 A	1577.00 A	32349	48915	1
06 47 38.00	+37 30 57.0	1.040	195.0	LHS 1870	1870	103-061	GJ 246	1579.00	32560	...	L
06 49 05.45	+37 06 50.6	1.618	172.3	LHS 220	220	087-008	GJ 1092	1588.03	1
06 54 04.23	+60 52 18.1	1.147	152.3	LHS 221 B	1
06 54 04.23	+60 52 18.1	1.147	152.3	LHS 221 A	221	250-029	...	1596.01	33142	...	1

Table A.1: continued

RA (1)	DEC (J2000.0) (2)	P.M. ("'/yr) (3)	Angle (deg) (4)	Full Name (5)	LHS (6)	LOB (7)	CNS3 (8)	YPC (9)	HIP (10)	HD (11)	Ref. (12)
06 57 46.58	-44 17 28.2	1.134	265.0	G1 257 B	G1 257 B	1641.01 B	1
06 57 46.58	-44 17 28.2	1.134	265.0	G1 257 A	222	...	G1 257 A	1641.01 A	33499	...	1
06 59 28.81	+19 20 55.9	1.225	137.3	LHS 223	223	109-035	GJ 1093	1635.01	1
07 03 55.71	+52 42 06.6	1.166	141.7	LHS 224	224	193-027	...	1642.01	1
07 04 45.84	-38 36 07.5	1.208	102.4	LHS 225 B	5
07 04 45.84	-38 36 07.5	1.206	100.9	LHS 225 A	225	1
07 10 01.81	+38 31 46.0	1.052	207.9	LHS 226 B	1
07 10 01.81	+38 31 46.0	1.052	207.9	LHS 226	226	087-026	G1 268 A	1668.00	34603	...	1
07 13 40.58	-13 27 57.1	1.277	153.3	LHS 227	227	1690.01	1
07 16 27.70	+23 42 10.4	1.123	122.0	LHS 228	228	1698.01	1
07 27 24.50	+05 13 32.7	3.761	171.2	LHS 33	33	089-019	G1 273	1755.00	36208	...	1
07 30 42.79	+48 11 58.6	1.295	189.8	LHS 229 C	1
07 30 42.79	+48 11 58.6	1.295	189.8	LHS 229 A	229	107-069	G1 275.2 A	1766.01 A	1
07 30 47.34	+48 10 26.3	1.295	189.8	LHS 230	230	107-070	G1 275.2 B	1766.01 B	1
07 30 47.34	+48 10 26.3	1.295	189.8	LHS 230 D	1
07 32 01.74	+57 55 44.0	1.000	177.8	LHS 1923	1923	3
07 33 52.87	+22 23 33.3	1.104	122.8	LHS 231	231	1783.01	1
07 35 46.32	+03 29 36.0	1.022	170.2	LHS 232	232	112-028	...	1791.02	1
07 39 18.05	+05 13 29.8	1.251	214.7	G1 280 B	G1 280 B	1805.00 B	1
07 39 18.05	+05 13 29.8	1.251	214.7	G1 280 A	233	...	G1 280 A	1805.00 A	37279	61421	1
07 40 19.36	-17 24 46.0	1.252	116.6	LHS 234	234	...	G1 283 B	1813.00 B	1
07 40 20.78	-17 24 49.2	1.252	116.6	LHS 235	235	...	G1 283 A	1813.00 A	1
07 43 24.36	+72 48 48.9	1.246	170.2	LHS 236	236	251-044	...	1795.01	1
07 45 34.99	-34 10 21.1	1.688	350.3	LHS 237	237	...	G1 288 A	1841.00 A	37853	63077	1
07 45 38.43	-33 55 51.3	1.688	350.3	LHS 237a	237a	...	G1 288 B	1841.00 B	1
07 48 16.37	+20 22 05.3	1.728	124.2	LHS 238	238	091-011	G1 289	1844.00	38082	12069	1
07 50 14.58	+07 11 48.8	1.778	173.2	LHS 239	239	...	GJ 1102 B	1850.01 B	1
07 50 15.35	+07 11 37.1	1.778	173.2	LHS 240	240	...	GJ 1102 A	1850.01 A	1
07 53 08.15	-67 47 31.5	2.041	135.6	LHS 34	34	...	G1 293	1882.00	1
07 53 33.10	+30 36 18.3	1.973	158.8	LHS 241	241	090-025	GJ 1104	1857.00 A	38541	64090	1
08 00 02.15	-40 02 22.0	1.070	139.1	LHS 1968	1968	1905.00	...	66020	3
08 00 32.13	+29 12 44.3	1.177	187.4	LHS 242	242	...	G1 295	1889.00	39157	65583	1
08 01 29.01	+10 43 04.2	1.020	161.5	LHS 1970	1970	1903.01	3

Table A.1: continued

RA	DEC	P.M.	Angle	Full Name	LHS	LOB	CNS3	YPC	HIP	HD	Ref.
(1)	(2)	(3)	(4)	(5)	(6)	(7)	(8)	(9)	(10)	(11)	(12)
08 03 06.12	+34 56 54.8	1.571	198.3	LHS 243	243	1
08 11 57.56	+08 46 22.9	5.211	167.1	LHS 35	35	050-022	GI 299	1942.00	1
08 13 27.81	-09 27 56.6	1.480	141.5	LHS 244	244	1954.01	1
08 18 23.92	-12 37 55.9	1.017	164.8	LHS 245	245	...	GI 302	1977.00	40693	69830	1
08 25 52.82	+69 02 00.6	1.377	205.4	LHS 246	246	1984.01	1
08 28 22.13	+35 00 59.1	1.102	251.5	GI 308 B	GI 308 B	2010.10 B	1
08 28 22.13	+35 00 59.1	1.102	251.5	GI 308 A	247	051-013	GI 308 A	2010.10 A	41554	...	1
08 29 40.73	-01 44 48.1	1.000	157.0	LHS 2017	2017	113-040	GI 308.2	2019.00	41661	...	L
08 29 49.35	+26 46 33.7	1.290	242.2	LHS 248	248	051-015	GJ 1111	2016.01	1
08 32 51.49	-31 30 03.2	1.350	304.3	LHS 249	249	...	GI 309	2042.00	41926	72673	1
08 35 49.11	+68 04 09.1	1.010	233.1	LHS 250	250	234-037	...	2028.01	1
08 36 25.55	+67 17 42.1	1.030	273.5	LHS 251	251	234-038	GI 310	2037.00 A	42220	...	1
08 41 20.13	+59 29 50.6	1.310	191.2	LHS 252	252	234-045	...	2057.11	1
08 41 32.44	-32 56 32.9	1.709	322.0	LHS 253	253	...	GI 318	2080.10	1
08 54 12.34	-08 05 00.2	1.240	130.8	LHS 254	254	1
08 55 07.62	+01 32 47.4	1.066	176.7	LHS 255	255	046-009	GI 328	2132.00	43790	...	1
08 55 24.82	+70 47 39.0	1.394	255.2	LHS 256	256	252-024	GI 325 A	2113.00 A	43820	76532	1
08 55 24.82	+70 47 39.0	1.394	255.2	LHS 257	257	...	GI 325 B	2113.00 B	1
08 59 05.30	-31 13 26.6	1.005	136.6	LHS 258	258	...	GJ 1118	1
09 00 52.09	+48 25 24.7	1.130	193.3	LHS 259	259	194-050	...	2149.11	1
09 14 24.74	+52 41 11.2	1.690	248.1	LHS 260	260	195-017	GI 338 A	2198.00 A	45343	79210	1
09 14 22.87	+52 41 11.9	1.690	248.1	LHS 261	261	195-018	GI 338 B	2198.00 B	120005	79211	1
09 15 56.15	+53 25 23.7	1.550	223.5	LHS 262	262	195-019	GI 339.1	2199.02	1
09 17 05.33	-77 49 23.4	1.023	139.3	LHS 263	263	...	GJ 1123	1
09 17 30.67	+77 14 40.5	1.050	269.7	GI 338.1B	GI 338.1 B	1
09 17 30.67	+77 14 40.5	1.050	269.7	GI 338.1A	264	252-030	GI 338.1 A	2191.00 A	45593	...	1
09 17 46.00	+58 25 21.5	1.134	180.0	LHS 265	265	195-022	...	2200.22	1
09 20 21.93	+26 43 43.0	1.007	120.8	LHS 266	266	2222.01	1
09 20 57.94	+03 22 06.5	1.178	163.2	LHS 267	267	046-034	...	2228.01	1
09 24 20.97	-80 31 21.3	1.253	8.5	LHS 268	268	...	GI 345	2272.00	46120	...	1
09 29 11.09	+25 58 09.3	1.086	254.8	LHS 269	269	1
09 32 51.47	+51 40 38.0	1.093	240.1	GI 354 B	GI 354 B	1
09 32 51.47	+51 40 38.0	1.093	240.1	GI 354 A	270	...	GI 354 A	2266.00 A	46853	82328	1

Table A.1: continued

RA (1)	DEC (2)	P.M. Angle (3)	Full Name (4)	LHS (5)	LOB (6)	CNS3 (7)	YPC (8)	HIP (9)	HD (10)	Ref. (11)
09 36 01.63	-21 39 38.8	1.000	LHS 2157	2157	2281.10	47103	...	3
09 38 53.83	-33 48 45.4	1.330	CE89	10
09 42 46.36	-68 53 06.1	1.120	LHS 271	271	...	GJ 1128	1
09 43 46.17	-17 47 06.2	1.426	LHS 272	272	1
09 44 47.34	-18 12 48.9	1.633	LHS 273	273	...	GJ 1129	1
09 46 48.45	+76 02 38.2	1.000	LHS 2188	2188	252-044	GJ 366	2302.00	47981	...	3
09 51 09.63	-12 19 47.6	1.807	LHS 274	274	161-080	GJ 369	2334.00	48336	...	1
10 00 44.31	+32 18 33.8	1.197	LHS 276	276	117-061	...	2365.00	49066	...	1
10 01 10.75	-30 23 24.5	1.297	LHS 277	277	...	GJ 377	2372.00	49091	...	1
10 02 21.80	+48 05 19.5	1.571	LHS 278	278	146-006	GJ 378	2370.10	49189	...	1
10 05 54.93	-67 21 31.2	1.197	WT0248	13
10 09 16.90	+35 14 52.2	1.277	LHS 279	279	1
10 11 22.18	+49 27 15.3	1.455	LHS 280	280	196-009	GJ 380	2390.00 A	49908	88230	1
10 14 51.79	-47 09 24.1	1.137	LHS 281	281	...	GJ 1132	1
10 25 23.93	+00 43 02.0 ³	1.101	LHS 282	282	2443.01	1
10 35 27.16	+69 26 58.9	1.752	LHS 283	283	236-034	...	2470.01	1
10 36 03.10	-14 42 29.1	1.120	LHS 284	284	1
10 37 02.71	+71 10 58.8	1.997	LHS 285	285	1
10 37 28.89	+30 11 10.7	1.011	LHS 286	286	1
10 41 37.93	+37 36 39.1	1.505	LHS 287	287	146-058	GJ 1134	2501.01	1
10 43 02.81	-09 12 40.8	1.971	WT1827	13
10 44 21.28	-61 12 35.5	1.657	LHS 288	288	2511.01	1
10 45 39.05	-19 06 52.9 ³	1.980	LHS 290	290	2512.01	1
10 45 39.10	-19 06 52.0	1.980	LHS 289	289	...	GJ 401	2512.00 A	52621	...	1
10 45 59.69	+59 04 50.5 ³	1.770	LHS 291	291	2509.02	1
10 48 12.62	-11 20 09.7	1.644	LHS 292	292	2516.02	1
10 48 14.58	-39 56 07.0	1.516	DENIS-PJ104814.7-395606	9
10 49 45.56	+35 32 50.5	1.231	LHS 293	293	044-040	GJ 1138	2517.11	1
10 50 52.02	+06 48 29.4	1.150	LHS 294	294	058-026	GJ 402	2524.00	53020	...	1
10 52 04.25	+13 59 51.4	1.126	LHS 295	295	044-042	GJ 403	2526.00	1
10 56 28.91	+07 00 53.2	4.696	LHS 36	36	045-020	GJ 406	2553.00	1
11 01 19.65	+03 00 17.2	1.103	LHS 296	296	045-027	...	2568.01	1
11 03 20.21	+35 58 11.9	4.778	LHS 37	37	119-052	GJ 411	2576.00	54035	95735	1

Table A.1: continued

RA (1)	DEC (J2000.0) (2)	P.M. ("'/yr) (3)	Angle (deg) (4)	Full Name (5)	LHS (6)	LOB (7)	CNS3 (8)	YPC (9)	HIP (10)	HD (11)	Ref. (12)
11 05 28.72	+43 31 36.7	4.531	281.9	LHS 38	38	176-011	GI 412 A	2582.00 A	54211	...	1
11 05 31.02	+43 31 18.0	4.531	281.9	LHS 39	39	176-012	GI 412 B	2582.00 B	1
11 10 08.38	+28 56 50.8	1.035	242.8	LHS 297	297	119-057	...	2596.21	1
11 11 10.71	-10 57 03.3	1.067	302.4	LHS 298	298	...	GI 415	2603.00	54651	97214	1
11 11 13.70	-41 05 32.7	1.257	264.3	LHS 300 B	5
11 11 13.70	-41 05 32.7	1.277	264.5	LHS 300 A	300	1
11 11 22.68	-06 31 56.4	1.107	202.5	LHS 299	299	163-059	...	2603.01	1
11 16 00.19	-57 32 51.5	2.733	294.9	LHS 40	40	...	GI 422	2621.00	55042	304043	1
11 20 05.09	+65 50 47.2	2.950	273.0	LHS 41	41	236-065	GI 424	2631.00	55360	...	1
11 21 38.48	+06 08 26.0	1.749	206.0	LHS 301	301	010-017	GJ 1146	2633.01	1
11 23 07.96	+25 53 36.8	1.059	252.0	LHS 302	302	2636.01	1
11 23 44.58	+08 33 48.3	1.036	278.4	LHS 303	303	010-019	GJ 2085	2641.00	55625	...	1
11 24 12.98	+21 21 35.6	1.050	270.2	LHS 304	304	120-045	GI 427	2642.00	1
11 28 00.49	-09 10 56.6	1.010	147.8	LHS 2412	2412	...	GI 429.2	2651.00	55955	...	3
11 28 27.73	+07 31 02.2	1.189	192.6	LHS 305	305	010-025	...	2654.00	55988	...	1
11 31 08.38	-14 57 21.3	1.393	164.0	LHS 306	306	1
11 32 45.31	+43 59 42.6	1.146	167.0	LHS 307	307	176-040	...	2669.01	1
11 34 29.50	-32 49 52.7	1.063	320.3	LHS 308	308	...	GI 432 A	2678.00 A	56452	100623	1
11 34 29.50	-32 49 52.7	1.063	320.3	LHS 309	309	...	GI 432 B	1
11 40 20.27	+67 15 32.4	3.209	175.2	LHS 42	42	236-080	...	2697.00	56936	...	1
11 42 11.05	+26 42 23.7	1.080	135.5	LHS 310	310	121-007	GI 436	2704.10	57087	...	1
11 45 42.96	-64 50 29.7	2.667	97.2	LHS 43	43	...	GI 440	2716.00	57367	...	1
11 46 31.08	-40 30 01.3	1.592	284.4	LHS 311	311	...	GI 442 A	2725.00 A	57443	102365	1
11 46 31.08	-40 30 01.3	1.592	284.4	LHS 313	313	...	GI 442 B	1
11 46 35.15	+50 52 54.8	1.036	238.1	LHS 312	312	176-053	...	2723.00	57450	...	1
11 46 42.91	-14 00 51.7	1.035	132.6	LHS 314	314	...	GI 443	2724.10	57459	...	1
11 47 44.40	+00 48 16.6	1.348	152.0	LHS 315	315	010-050	GI 447	2730.00	57548	...	1
11 50 57.78	+48 22 38.6	1.821	237.5	LHS 316	316	122-049	GJ 1151	2739.01	1
11 52 32.09	+27 30 51.3	1.000	249.0	LHS 2467	2467	121-027	...	2745.02	57901	...	L
11 52 58.75	+37 43 07.3	7.042	145.5	LHS 44	44	122-051	GI 451 A	2745.00	57939	103095	1
11 53 12.43	-31 23 56.1	1.140	263.1	LHS 317	317	1
11 56 54.87	+26 39 56.3	1.380	154.6	LHS 318	318	1
11 57 56.21	-27 42 25.0	1.246	239.5	LHS 319	319	...	GI 453	2762.00	58345	103932	1

Table A.1: continued

RA (1)	DEC (J2000.0) (2)	P.M. Angle ($''/yr$) (3)	Full Name (4)	LHS (5)	LOB (6)	CNS3 (7)	YPC (8)	HIP (9)	HD (10)	Ref. (11) (12)
12 02 33.66	+08 25 50.7	1.116	LHS 320	320	011-035	...	2777.01	1
12 02 40.13	+36 36 06.8	1.053	LHS 321	321	122-067	1
12 15 10.55	-10 18 44.9	1.024	LHS 322	322	2820.00 A	59750	106516	1
12 17 30.18	-29 02 20.7	1.145	LHS 323	323	1
12 18 59.41	+11 07 33.9	1.301	LHS 324	324	012-030	GJ 1156	2835.01	1
12 21 32.83	+28 54 22.6	1.042	LHS 325	325	1
12 23 56.21	-27 57 46.4	1.293	LHS 325a	325a	1
12 24 26.81	-04 43 36.7	1.311	LHS 326	326	1
12 24 52.49	-18 14 32.2	2.532	LHS 45	45	...	GJ 465	2857.00	60559	...	1
12 25 50.74	-24 33 17.8	1.013	LHS 327	327	1
12 28 39.92	-71 27 51.5	1.170	LHS 328	328	...	GJ 467 A	2873.00 A	1
12 28 42.98	-71 27 56.5	1.170	LHS 329	329	...	GJ 467 B	2873.00 B	1
12 29 14.20	+53 33 06.2	1.232	LHS 330	330	...	GJ 1159 B	2878.02 B	1
12 29 14.46	+53 32 44.9	1.232	LHS 331	331	199-017	GJ 1159 A	2878.02 A	1
12 29 34.54	-55 59 37.1	1.250	LHS 332	332	...	GJ 1158	1
12 31 15.80	+08 48 38.2	1.020	LHS 2570	2570	012-039	GJ 471	2885.00	61094	...	L
12 32 32.17	-26 10 14.3	1.080	LHS 2573	2573	3
12 33 17.41	+09 01 15.7	1.811	GJ 473 B	GJ 473 B	2890.00 B	1
12 33 17.41	+09 01 15.7	1.811	GJ 473 A	333	012-043	GJ 473 A	2890.00 A	1
12 34 15.78	+20 37 05.7	1.338	LHS 334	334	...	GJ 2093	1
12 34 53.18	+05 03 54.1	1.163	LHS 335	335	2900.01	1
12 37 52.27	-52 00 05.5	1.035	LHS 336	336	...	GJ 479	2910.00	61629	...	1
12 38 49.11	-38 22 53.8	1.487	LHS 337	337	1
12 38 52.43	+11 41 46.2	1.163	LHS 338	338	060-024	GJ 480	2915.00	61706	...	1
12 40 24.19	-23 17 43.8	1.102	LHS 339	339	1
12 40 46.30	-43 33 59.1	1.047	LHS 340	340	...	GJ 480.1	2919.00	61874	...	1
12 47 56.66	+09 45 05.1	1.077	LHS 341	341	060-032	GJ 486	2943.00	62452	...	1
12 50 07.76	+54 47 06.1	1.286	LHS 342	342	2951.01	1
12 56 23.74	+15 41 44.5	1.440	LHS 343	343	061-021	...	2669.02	1
13 00 09.07	+03 28 41.1	1.000	LHS 2661	2661	060-054	GJ 492	2976.00	L
13 00 33.52	+05 41 08.1	1.100	LHS 2664	2664	060-055	GJ 493.1	2981.02	L
13 00 42.51	+19 12 34.5	1.468	2MASSWJ1300425+191235	6
13 04 57.47	-52 26 34.7	1.151	LHS 344	344	...	GJ 496.1	2991.00	63833	113538	1

Table A.1: continued

RA	DEC	P.M.	Angle	Full Name	LHS	LOB	CNS3	YPC	HIP	HD	Ref.
(1)	(2)	(3)	(4)	(5)	(6)	(7)	(8)	(9)	(10)	(11)	(12)
13 08 39.57	+08 04 21.9	1.026	281.0	LHS 345	345	062-015	...	3001.01	1
13 09 20.41	-40 09 27.0	1.196	142.4	LHS 346	346	1
13 10 01.80	+22 30 05.3	1.140	229.5	LHS 347	347	061-035	1
13 11 52.39	+27 52 41.2	1.186	317.5	LHS 348	348	...	GI 502	3015.00 A	64394	114710	1
13 13 09.35	-41 30 39.7	1.040	272.0	Name ER 2	11
13 12 59.70	-47 28 06.6 ^S	2.128	268.0	Name ER 8	3016.01	12
13 18 24.31	-18 18 40.6	1.521	225.0	LHS 349	349	...	GI 506	3039.00 A	64924	115617	1
13 22 56.74	+24 28 03.4	1.080	215.6	LHS 350	350	149-081	...	3056.01	1
13 29 21.31	+11 26 26.7	1.228	165.0	LHS 351	351	063-032	GI 513	3076.04	1
13 29 59.77	+10 22 37.9	1.525	134.2	LHS 352	352	063-034	GI 514	3079.00	65859	...	1
13 30 02.79	-08 42 25.6	1.202	246.2	LHS 353	353	014-057	GI 514.1	3080.00	1
13 30 13.64	-08 34 29.4	1.188	247.7	LHS 354	354	014-058	GI 515	3081.00 A	65877	...	1
13 30 31.06	+19 09 34.1	1.397	200.5	LHS 355	355	149-094	GJ 1171	3084.01	1
13 36 31.85	+03 40 46.1	3.870	253.6	LHS 46	46	062-053	GI 518	3112.00	1
13 37 17.37	+35 01 01.5	1.232	252.9	LHS 356	356	1
13 39 15.35	+15 40 57.9	1.050	142.4	LHS 2774	2774	063-045	...	3119.01	3
13 40 08.87	+43 46 38.2	1.144	285.2	LHS 357	357	177-051	GJ 1174	3123.01	1
13 41 11.49	+30 01 26.1	1.599	273.7	LHS 358	358	3126.01	1
13 45 05.08	+17 47 07.5	1.898	166.7	LHS 359	359	063-052	GI 525	3133.00 A	67090	...	1
13 45 43.74	+14 53 29.4	2.298	129.3	LHS 47	47	063-053	GI 526	3135.00	67155	119850	1
13 46 55.52	+05 42 56.4	1.142	222.2	LHS 360	360	1
13 48 03.02	+23 34 46.3	1.484	275.6	LHS 361	361	...	GJ 1179 B	3146.11 B	1
13 48 13.42	+23 36 48.6	1.484	275.6	LHS 362	362	...	GJ 1179 A	3146.11 A	1
13 49 44.82	-22 06 40.0	1.805	254.4	LHS 363	363	...	GI 529	3154.00	67487	120467	1
14 01 03.19	-02 39 17.6	1.050	304.7	LHS 2842	2842	064-035	GI 536	3195.00	68469	122303	3
14 06 55.58	+38 36 56.1	1.046	159.7	LHS 364	364	165-047	...	3210.11	1
14 15 16.04	+47 47 26.2	1.436	237.5	LHS 365	365	1
14 15 32.55	+04 39 31.4	1.060	225.3	LHS 366	366	065-039	GJ 1182	3240.02	1
14 15 39.68	+19 10 55.9	2.284	208.4	LHS 48	48	...	GI 541	3242.00	69673	124897	1
14 18 20.43	-52 24 12.6	1.118	248.4	LHS 367	367	1
14 19 11.01	-07 18 12.0	1.355	235.5	LHS 368	368	124-023	GI 543	3252.00	1
14 20 07.36	-09 37 13.4	1.062	215.2	LHS 369	369	124-025	GI 545	3256.10	1
14 20 52.95	+36 57 17.2	1.363	279.6	LHS 370	370	1

Table A.1: continued

RA (J2000.0)	DEC (J2000.0)	P.M. ($^{\circ}$ / $^{\circ}$ / $^{\circ}$)	Angle (deg)	Full Name	LHS	LOB	CNS3	YPC	HIP	HD	Ref.
(1)	(2)	(3)	(4)	(5)	(6)	(7)	(8)	(9)	(10)	(11)	(12)
14 25 43.48	+23 37 01.4	1.376	144.9	LHS 371	371	166-027	GI 548 A	3273.00 A	70529	...	1
14 25 46.65	+23 37 13.7	1.376	144.9	LHS 372	372	166-028	GI 548 B	3273.00 B	70536	...	1
14 29 29.72	+15 31 57.8	1.711	321.8	LHS 373	373	135-056	GI 552	3283.00	70865	...	1
14 29 42.96	-62 40 46.7	3.809	281.7	LHS 49	49	...	GI 551	3278.00	70890	...	1
14 30 47.73	-08 38 46.7	1.269	260.0	LHS 374	374	124-047	GI 553	3285.00	70956	127339	1
14 31 38.25	-25 25 32.9	1.386	268.6	LHS 375	375	3289.01	1
14 35 08.89	+16 53 54.4	1.555	255.5	LHS 376	376	135-067	...	3300.02	1
14 39 00.31	+18 39 38.8	1.230	180.3	LHS 377	377	3312.01	1
14 39 28.16	+19 29 14.0	1.305	252.5	2MASSWJ1439283+192915	6
14 39 36.49	-60 50 02.3 H	3.664	280.9	LHS 50	50	...	GI 559 A	3309.00 A	71683	128620	1
14 39 35.08	-60 50 13.8 H	3.664	280.9	LHS 51	51	...	GI 559 B	3309.00 B	71681	128621	1
14 47 25.35	-17 42 15.8	1.177	252.6	LHS 378	378	3343.01 A	1
14 49 31.48	-26 06 32.5	1.217	260.7	LHS 379	379	...	GI 563.2 B	3346.00 B	72509	...	1
14 49 33.27	-26 06 20.8	1.217	260.7	LHS 380	380	...	GI 563.2 A	3346.00 A	72511	...	1
14 50 28.87	-08 38 36.8	1.589	190.1	LHS 381	381	3347.02	1
14 50 41.22	-16 56 30.8	1.451	242.7	LHS 382	382	1
14 51 40.48	-24 18 14.9	1.020	245.0	LHS 383	383	...	GI 565	3354.00	72688	130992	1
14 55 11.11	+53 40 49.2	1.083	295.3	LHS 384	384	200-062	GI 569.1	3378.00	73005	132142	1
14 55 35.83	-15 33 44.0	1.736	209.6	LHS 385	385	3372.01	1
14 57 15.07	-21 21 50.5	1.994	149.2	LHS 387 D D	1
14 57 26.55	-21 24 41.2	1.994	149.2	LHS 387 C C	1
14 57 26.55	-21 24 41.2	1.994	149.2	LHS 386	386	...	GI 570 B	3375.00 B	73182	131976	1
14 57 27.99	-21 24 55.4	1.994	149.2	LHS 387	387	...	GI 570 A	3375.00 A	73184	131977	1
14 57 32.29	+31 23 44.9	1.374	211.1	LHS 388	388	166-057	GI 570.2	3383.00	73192	...	1
15 03 14.29	+35 12 45.8	1.010	175.0	LHS 3016	3016	3402.01	3
15 03 24.59	+03 46 57.3	1.136	308.3	LHS 389	389	015-004	GI 1188	3400.01	1
15 06 14.27	-37 25 20.2	1.114	201.9	LHS 390	390	3404.00	73903	...	1
15 06 54.35	+13 21 06.1	1.092	269.9	2MASSWJ1506544+132106	6
15 07 23.59	+24 56 07.9	1.004	299.3	LHS 391	391	167-019	GI 579	3419.00	1
15 10 13.08	-16 22 46.0	3.681	195.9	LHS 53	53	...	GI 579.2 A	3425.00 A	74235	134439	1
15 10 12.96	-16 27 46.6	3.681	195.9	LHS 52	52	...	GI 579.2 B	3425.00 B	74234	134440	1
15 11 50.61	-10 14 18.0	1.005	257.6	LHS 392	392	151-034	...	3428.01	1
15 13 50.89	-01 21 05.1	1.375	248.8	GI 580 B	GI 580 B	1

Table A.1: continued

RA (J2000.0)	DEC (J2000.0)	P.M. ($''/yr$)	Angle (deg)	Full Name	LHS	LOB	CNS3	YPC	HIP	HD	Ref.
(1)	(2)	(3)	(4)	(5)	(6)	(7)	(8)	(9)	(10)	(11)	(12)
15 13 50.89	-01 21 05.1	1.375	248.8	Gl 580 A	393	...	Gl 580 A	3438.00 A	74537	135204	1
15 14 54.41	-31 50 13.8	1.010	212.1	LHS 3045	3045	3
15 19 26.83	-07 43 20.3	1.224	256.3	LHS 394	394	151-046	Gl 581	3458.00	74995	...	1
15 21 48.19	-48 19 03.4	1.645	260.1	LHS 395	395	...	Gl 582	3462.00	75181	136352	1
15 23 51.14	+17 27 57.3	1.302	196.8	LHS 396	396	136-103	Gl 585	3481.00	1
15 28 13.99	+16 43 10.8	1.020	263.0	LHS 3073	3073	137-008	...	3496.00	L
15 32 12.97	-41 16 32.2	1.539	228.5	LHS 397	397	...	Gl 588	3501.00	76074	...	1
15 34 27.75	+02 16 47.5	1.196	262.7	LHS 398	398	3513.01	1
15 35 20.34	+17 43 04.5	1.219	263.0	LHS 400	400	137-025	Gl 589 B	3520.00 B	1
15 35 20.53	+17 42 47.0	1.219	263.0	LHS 399	399	137-026	Gl 589 A	3520.00 A	1
15 39 39.06	-55 09 10.0	1.152	190.3	LHS 401	401	3530.00	1
15 40 03.59	+43 29 39.4	1.225	106.3	LHS 402	402	179-043	Gl 1194 A	3547.01 A	1
15 40 03.81	+43 29 35.3	1.225	106.3	LHS 403	403	...	Gl 1194 B	1
15 41 16.47	+75 59 34.3	1.141	133.8	LHS 404	404	257-020	Gl 597	3575.00	76832	...	1
15 41 28.86	+68 25 10.0	1.050	297.0	LHS 3103	3103	239-058	...	3567.01	L
15 42 06.56	-19 28 18.4	2.254	243.2	LHS 54	54	...	Gl 595	3547.00 A	76901	...	1
15 43 03.10	-10 56 00.8	1.187	254.2	LHS 405	405	...	Gl 1195	3552.00	76976	140283	1
15 43 18.33	-20 15 32.9	1.143	194.4	LHS 406	406	...	Gl 2116	1
15 45 40.21	-20 36 16.7	1.375	243.5	LHS 407	407	3564.01	1
15 56 27.19	+15 39 41.7	1.328	166.4	LHS 408	408	...	Gl 603	3604.00 A	78072	142860	1
15 57 13.10	+05 05 59.6	1.398	177.3	LHS 409	409	016-017	...	3606.00	1
15 57 14.71	+05 07 02.6	1.398	177.3	LHS 410	410	016-018	...	3607.00 A	1
16 02 50.95	+20 35 21.1	1.571	217.6	LHS 411	411	137-078	Gl 609	3633.00	1
16 08 14.96	-10 26 14.4	1.354	195.1	LHS 412	412	153-027	Gl 1198	3652.03	1
16 13 48.62	-57 34 13.8	1.635	209.4	LHS 413	413	...	Gl 615	3669.00	79537	145417	1
16 14 26.29	+02 14 49.1	1.570	247.3	LHS 414	414	3685.01	1
16 14 32.64	+19 06 10.8	2.033	280.0	LHS 55	55	...	Gl 1200	3687.01	1
16 20 03.52	-37 31 44.5	1.222	324.5	LHS 415	415	...	Gl 618 A	3701.00 A	80018	...	1
16 20 03.19	-37 31 48.1	1.222	324.5	LHS 416	416	...	Gl 618 B	3701.00 B	1
16 24 09.25	+48 21 10.6	1.231	111.6	LHS 417 B B	1
16 24 09.25	+48 21 10.6	1.231	111.6	LHS 417 A	417	202-045	Gl 623 A	3733.00 A	80346	...	1
16 25 13.95	+15 40 54.2	1.196	173.5	LHS 418	418	138-025	...	3731.01	1
16 30 18.08	-12 39 45.4	1.175	183.4	LHS 419	419	153-058	Gl 628	3746.00	80824	...	1

Table A.1: continued

RA	DEC	P.M.	Angle	Full Name	LHS	LOB	CNS3	YPC	HIP	HD	Ref.
(1)	(2)	(3)	(4)	(5)	(6)	(7)	(8)	(9)	(10)	(11)	(12)
16 30 28.45	+04 10 41.7	1.467	197.3	LHS 420	420	017-021	...	3753.00	80837	148816	1
16 34 20.36	+57 09 44.7	1.620	316.0	LHS 421	421	225-067	Gl 630.1 A	3775.03 A	1
16 34 21.59	+57 10 09.0	1.620	316.0	LHS 422	422	225-068	Gl 630.1 B	3775.03 B	1
16 35 40.40	-30 51 20.2	1.189	225.3	LHS 423	423	1
16 37 05.42	-01 32 00.5	1.227	227.0	LHS 424	424	017-028	...	3775.02	1
16 42 04.33	+10 25 58.7	1.252	202.1	LHS 425	425	138-059	...	3798.01	1
16 52 58.79	+00 01 35.0	1.673	205.3	LHS 426	426	019-004	Gl 641	3837.00	82588	152391	1
16 55 25.23	-08 19 21.4	1.190	222.5	LHS 427	427	...	Gl 643	3844.00	82809	...	1
16 55 28.77	-08 20 10.9	1.190	222.5	Gl 644 B	Gl 644 B	1
16 55 28.77	-08 20 10.9	1.190	222.5	Gl 644 D	Gl 644 D	1
16 55 28.77	-08 20 10.9	1.190	222.5	Gl 644 A	428	...	Gl 644 A	3845.00 A	82817	152751	1
16 55 35.25	-08 23 40.8	1.190	222.5	Gl 644 C	429	...	Gl 644 C	3845.00 D	1
17 04 22.34	+16 55 55.6	1.136	174.5	LHS 430	430	170-012	GJ 1209	3879.00	1
17 05 03.41	-05 03 59.4	1.461	219.2	LHS 431	431	019-013	Gl 653	3878.00 A	83591	154363	1
17 05 13.79	-05 05 39.4	1.461	219.2	LHS 432	432	019-014	Gl 654	3880.00	83599	154363B	1
17 12 07.81	+45 39 58.0	1.572	170.8	LHS 433	433	...	Gl 661 A	3907.00 A	84140	...	1
17 12 07.81	+45 39 58.0	1.572	170.8	LHS 434	434	...	Gl 661 B	3907.00 B	1
17 12 55.10	+42 19 54.4	1.083	250.1	LHS 435	435	203-052	GJ 1213	3911.00 A	84223	...	1
17 14 08.78	+60 47 30.0	1.007	238.4	LHS 436	436	1
17 15 20.91	-26 36 08.1	1.232	203.0	LHS 437	437	...	Gl 663 A	3908.00 A	...	155886	1
17 15 20.91	-26 36 08.1	1.232	203.0	LHS 438	438	...	Gl 663 B	3908.00 B	84405	155885	1
17 16 13.36	-26 32 46.1	1.232	203.0	LHS 439	439	...	Gl 664	3913.00	84478	156026	1
17 18 25.59	-43 26 37.6	1.056	225.3	LHS 440	440	1
17 20 39.56	+32 28 03.9	1.055	173.8	LHS 441	441	...	Gl 672	3946.00 A	84862	157214	1
17 18 57.09	-34 59 23.9	1.180	98.3	Gl 667 B	Gl 667 B	3924.00 B	1
17 18 57.09	-34 59 23.9	1.180	98.3	Gl 667 A	442	...	Gl 667 A	3924.00 A	84709	156384	1
17 18 58.80	-34 59 48.6	1.180	98.3	Gl 667 C	443	...	Gl 667 C	3924.00 C	1
17 19 02.96	-46 38 13.3	1.000	77.3	LHS 445	445	...	Gl 666 B	3919.00 B	1
17 19 03.76	-46 38 10.9	1.000	77.3	LHS 444	444	...	Gl 666 A	3919.00 A	84720	156274	1
17 20 46.27	+49 15 20.4	1.304	155.5	LHS 446	446	203-063	GJ 1216	3949.01	1
17 25 45.24	+02 06 41.2	1.334	205.8	LHS 447	447	019-024	Gl 673	3955.00	85295	157881	1
17 27 39.89	+14 29 02.0	1.142	254.4	LHS 448	448	139-039	Gl 1219	3964.01	1
17 28 07.33	-62 27 14.2	1.030	188.6	LHS 3292	3292	3

Table A.1: continued

RA	DEC	P.M.	Angle	Full Name	LHS	LOB	CNS3	YPC	HIP	HD	Ref.
(1)	(2)	(3)	(4)	(5)	(6)	(7)	(8)	(9)	(10)	(11)	(12)
(J2000.0)		($^{\circ}$ / $^{\circ}$)	(deg)								
17 28 39.93	-46 53 42.9	1.044	147.0	LHS 449	449	...	GI 674	3958.00	85523	...	1
17 36 25.93	+68 20 21.2	1.311	195.2	LHS 450	450	240-063	GI 687	4029.00 A	86162	...	1
17 37 03.66	-44 19 09.2	1.155	216.3	LHS 451	451	...	GI 682	3992.00	86214	...	1
17 37 53.34	+18 35 30.1	1.381	42.8	LHS 452	452	170-055	GI 686	4009.00	86287	...	1
17 38 51.39	+51 27 17.5	1.011	301.4	LHS 453	453	4037.01	1
17 42 10.75	-08 49 00.2	1.020	243.0	LHS 3315	3315	020-009	...	4028.02	L
17 46 34.25	-57 19 08.7	1.739	219.2	LHS 454	454	...	GI 693	4040.00	86990	...	1
17 48 08.12	+70 52 36.0	1.651	311.0	LHS 455	455	240-072	GI 1221	4085.11	1
17 49 50.54	+82 46 26.1	3.587	337.3	LHS 56	56	259-021	GI 699.1	4149.01	1
17 50 58.97	-56 36 07.0	1.256	237.6	LHS 456	456	4059.03	1
17 57 48.51	+04 41 36.4	10.310	355.8	LHS 57	57	140-024	GI 699	4098.00 A	87937	...	1
17 58 22.91	+14 17 37.8	1.014	235.4	LSR1758+1417	2
18 02 46.27	+37 31 03.0	1.158	171.9	LHS 457	457	192-036	GI 1223	4130.01	1
18 05 27.35	+02 29 58.8	1.127	166.6	LHS 458	458	...	GI 702 A	4137.00 A	1
18 05 27.35	+02 29 58.8	1.127	166.6	LHS 459	459	...	GI 702 B	4137.00 B	1
18 09 50.14	-02 47 43.2	1.005	214.9	LSR1809-0247	2
18 17 06.49	+13 28 25.0	1.207	201.5	LSR1817+1328	2
18 17 15.07	+68 33 19.0	1.740	203.5	LHS 460	460	260-001	GI 1225	4226.01	1
18 18 03.42	+38 46 34.3	1.091	197.8	LHS 461	461	204-057	...	4205.00 B	1
18 18 04.24	+38 46 32.6	1.091	197.8	LHS 462	462	204-058	...	4205.00 A	1
18 20 57.18	-01 02 58.1	1.213	211.1	LHS 463 B B	5
18 20 57.18	-01 02 58.0	1.082	207.9	LHS 463 A	463	021-010	GI 1226 A	1
18 22 06.68	+06 20 37.7	1.158	272.7	LHS 464	464	141-004	GI 712	4221.00	1
18 22 27.15	+62 03 01.8	1.544	217.1	LHS 465	465	227-029	GI 1227	4238.01	1
18 26 11.06	+30 14 18.9	2.380	253.3	LSR1826+3014	2
18 35 43.20	-08 16 06.2	1.251	229.8	LHS 466	466	155-027	...	4275.01	1
18 41 36.37	+00 55 13.8	1.990	178.6	LHS 467	467	021-023	...	4308.00	91668	...	1
18 42 46.69	+59 37 49.4	2.273	323.3	LHS 58	58	227-046	GI 725 A	4330.00 A	91768	173739	1
18 42 46.91	+59 37 36.9	2.273	323.3	LHS 59	59	227-047	GI 725 B	4330.00 B	91772	173740	1
18 48 44.87	-02 33 45.7	1.116	234.9	LHS 468	468	022-001	...	4337.02	1
18 53 39.92	-38 36 44.5	1.011	161.1	LHS 469	469	...	GI 732 A	4355.00 A	1
18 58 00.14	+05 54 29.2	1.239	189.5	LHS 470	470	022-010	GI 740	4398.00	93101	176029	1
19 07 42.97	+32 32 41.5	1.635	48.9	GI 747 B	GI 747 B	4459.00 B	1

Table A.1: continued

RA	DEC	P.M.	Angle	Full Name	LHS	LOB	CNS3	YPC	HIP	HD	Ref.
(1)	(2)	(3)	(4)	(5)	(6)	(7)	(8)	(9)	(10)	(11)	(12)
19 07 42.97	+32 32 41.5	1.635	48.9	Gl 747 A	471	207-016	Gl 747 A	4459.00 A	1
19 12 14.60	+02 53 11.0	1.853	106.8	LHS 472 B	1
19 12 14.60	+02 53 11.0	1.853	106.8	LHS 472 A	472	022-018	Gl 748 A	4472.00	94349	...	1
19 16 55.25	+05 10 08.1	1.461	203.1	LHS 473	473	022-022A	Gl 752 A	4494.00 A	94761	180617	1
19 16 57.61	+05 09 01.6	1.461	203.1	LHS 474	474	022-022B	Gl 752 B	4494.00 B	1
19 20 47.97	-45 33 29.7	2.945	167.3	LHS 60	60	...	Gl 754	4505.00	1
19 20 54.37	-82 33 16.1	1.261	165.0	LHS 475	475	1
19 21 38.70	+20 52 03.2	1.751	212.6	LHS 476	476	185-018	GJ 1235	4531.03	1
19 32 21.56	+69 39 40.4	1.838	161.2	LHS 477	477	...	Gl 764	4607.00 A	96100	185144	1
19 45 45.49	+27 07 31.7	1.226	181.5	Gl 766 B	Gl 766 B	1
19 45 45.49	+27 07 31.7	1.226	181.5	Gl 766 A	478	185-037	Gl 766 A	4646.00 A	97237	...	1
19 46 48.61	+12 04 59.3	1.482	205.1	LHS 479	479	142-052	...	4649.01	1
19 54 00.13	-47 48 37.3	1.072	186.2	LHS 480	480	...	Gl 769	4674.00	1
19 56 57.61	-42 16 23.0	1.026	173.8	APMPMJ1957-4216	15
20 00 05.70	+30 57 32.2	1.339	16.7	LSR2000+3057	2
20 03 52.12	+23 20 26.6	1.368	227.6	LHS 481	481	186-011	Gl 778	4762.00	98792	190404	1
20 04 01.95	-65 35 58.3	1.010	164.8	LHS 3512	3512	...	Gl 774 B	4734.00 B	3
20 04 04.74	-65 36 01.2	1.020	163.8	LHS 3513	3513	...	Gl 774 A	4734.00 A	98811	...	3
20 05 02.23	+54 26 03.2	1.455	232.7	LHS 482	482	230-026	Gl 781	4775.00	98906	...	1
20 05 32.83	-67 19 15.3	1.097	129.1	LHS 484	484	...	Gl 776	4738.00	98959	189567	1
20 05 34.88	-10 56 54.6	1.081	94.9	LHS 483	483	4763.01	1
20 08 43.70	-66 10 55.5	1.651	133.2	LHS 485	485	...	Gl 780	4754.00	99240	190248	1
20 11 12.05	-36 06 05.4	1.632	163.8	LHS 486	486	...	Gl 783 A	4782.00 A	99461	191408	1
20 11 12.05	-36 06 05.4	1.632	163.8	LHS 487	487	...	Gl 783 B	1
20 15 17.38	-27 01 58.7	1.251	98.0	LHS 488	488	...	Gl 785	4804.00	99825	192310	1
20 19 04.57	+12 35 04.1	1.213	184.7	LHS 489	489	4838.01	1
20 23 35.85	-21 22 14.1	1.205	152.8	LHS 490	490	4852.00	100568	193901	1
20 27 29.08	+35 59 24.8	1.328	228.9	LHS 491	491	201-019	...	4869.02	1
20 27 42.08	-56 27 25.2	1.283	161.4	LHS 492	492	...	GJ 1252	1
20 28 03.81	-76 40 15.9	1.430	152.9	LHS 493	493	...	GJ 1251	1
20 33 40.31	+61 45 13.7	1.052	30.5	LHS 494	494	230-042	GJ 1254	4901.02	1
20 36 21.62	+51 00 05.3	1.054	100.8	LSR2036+5059	2
20 40 33.86	+15 29 58.9	1.487	63.3	LHS 495	495	144-025	GJ 1256	4929.11	1

Table A.1: continued

RA	DEC	P.M.	Angle	Full Name	LHS	LOB	CNS3	YPC	HIP	HD	Ref.
(1)	(2)	($''/yr$) (3)	(deg) (4)	(5)	(6)	(7)	(8)	(9)	(10)	(11)	(12)
20 42 18.78	−52 41 57.5	1.069	176.4	LHS 496	496	...	GI 798	4924.00	102186	...	1
20 42 57.14	−18 55 06.2	1.016	150.3	GI 800 B	GI 800 B	1
20 42 57.14	−18 55 06.2	1.016	150.3	GI 800 A	497	...	GI 800 A	4934.00 A	102235	...	1
20 43 19.24	+55 20 53.0	1.915	27.6	LHS 498	498	231-013	GI 802	4949.00	1
20 51 41.73	−79 18 39.9	1.216	144.6	LHS 499	499	...	GI 808	4934.10	1
20 55 37.11	−14 03 54.8	1.486	107.5	LHS 500	500	...	GI 810 B	4999.00 B	1
20 55 37.76	−14 02 08.1	1.486	107.5	LHS 501	501	...	GI 810 A	4999.00 A	1
20 56 46.59	−10 26 54.8	1.155	182.8	LHS 502	502	...	GI 811.1	5015.00	103388	...	1
20 57 40.08	−44 07 45.8	1.098	208.5	LHS 503	503	...	GI 812.1	5009.00	103458	199288	1
21 01 04.80	+03 07 04.7	1.040	92.0	USNO2101+0307	14
21 04 25.37	−27 52 46.8	1.040	180.5	LHS 3620	3620	3
21 04 53.38	−16 57 32.2	2.251	206.3	LHS 61	61	...	GI 817	5065.00	104059	...	1
21 05 14.03	−24 46 51.9	1.091	198.4	LHS 504	504	1
21 06 53.84	+38 44 57.9	5.204	52.2	LHS 62	62	...	GI 820 A	5077.00 A	104214	201091	1
21 06 55.16	+38 44 31.5	5.204	52.2	LHS 63	63	...	GI 820 B	5077.00 B	104217	201092	1
21 07 55.41	+59 43 19.4	2.098	208.7	LHS 64	64	231-001	...	5092.00	1
21 09 17.43	−13 18 09.1	2.096	160.1	LHS 65	65	...	GI 821	5084.00	104432	...	1
21 11 57.86	−31 03 16.0	1.060	125.0	LHS 505	505	1
21 13 34.09	−19 19 46.3	1.112	192.2	LHS 506	506	5100.00	104777	...	1
21 17 15.27	−38 52 02.6	3.453	250.5	LHS 66	66	...	GI 825	5117.00	105090	202560	1
21 21 34.80	−19 03 38.6	1.064	213.4	LHS 507	507	5137.01	1
21 29 36.80	+17 38 35.9	1.058	69.8	LHS 508 B	...	126-004	... B	1
21 29 36.80	+17 38 35.9	1.058	69.8	LHS 508 A	508	126-004	GI 829 A	5177.00	106106	...	1
21 30 02.76	−12 30 36.3	1.056	104.4	LHS 509	509	...	GI 830	5174.00	106147	204587	1
21 30 47.66	−40 42 29.5	1.730	143.7	LHS 510	510	1
21 31 18.64	−09 47 26.4	1.194	90.8	GI 831 B	GI 831 B	5184.00 B	1
21 31 18.64	−09 47 26.4	1.194	90.8	GI 831 C C	1
21 31 18.64	−09 47 26.4	1.194	90.8	GI 831 A	511	026-007	GI 831 A	5184.00 A	106255	...	1
21 38 43.65	−33 39 55.3	1.190	116.5	LHS 512	512	1
21 39 00.91	−24 09 29.0	1.208	124.4	LHS 513	513	...	GI 836	5213.00	1
21 40 53.05	+78 49 21.4	1.147	63.0	LHS 514	514	261-046	...	5257.01	1
21 55 47.95	−11 21 42.8	1.088	120.1	LHS 515	515	5293.01	1
21 55 57.11	−45 39 34.3	1.040	155.2	LHS 3732	3732	3

Table A.1: continued

RA (1)	DEC (J2000.0) (2)	P.M. Angle ($''/yr$) (3)	Full Name (4)	LHS (5)	LOB (6)	CNS3 (7)	YPC (8)	HIP (9)	HD (10)	Ref. (11) (12)
21 56 55.25	-01 54 09.3	1.426	LHS 516	516	5301.01	1
21 58 53.18	-57 56 03.5	1.000	LHS 3740	3740	3
22 03 21.60	-56 47 09.7	4.695	LHS 67	67	...	GI 845	5314.00	108870	209100	1
22 04 10.56	-56 46 58.1	4.822	LHS 67 Ba	8
22 04 10.56	-56 46 58.1	4.822	LHS 67 Bb	8
22 04 40.92	-19 46 42.0	1.030	LHS 3754	3754	3
22 09 40.34	-04 38 26.8	1.037	LHS 517	517	027-016	GI 849	5358.00	109388	...	1
22 13 42.88	-17 41 08.8	1.010	LHS 3776	3776	...	GI 1265	5375.01	3
22 14 34.73	-38 59 07.3	1.056	WD2214-390	4
22 20 26.97	-24 21 49.5	1.055	LHS 518	518	1
22 22 35.85	-50 48 26.9	1.080	LHS 519	519	5406.00	110468	212038	1
22 24 36.89	-72 15 19.4	1.470	GI 855.1B	GI 855.1 B	1
22 24 36.89	-72 15 19.4	1.470	GI 855.1A	520	...	GI 855.1 A	5404.00 A	110618	...	1
22 27 59.21	-30 09 32.8	1.012	LHS 521	521	1
22 28 49.03	+05 48 13.8	1.638	LHS 522	522	018-051	GI 861	5434.00	1
22 28 54.37	-13 25 19.4	1.083	LHS 523	523	5431.01	1
22 29 48.96	+41 28 48.6	1.293	LHS 524	524	215-050	GI 1270	5441.01	1
22 30 33.55	-75 15 24.2	2.421	SSPMJ2231-7515	7
22 30 40.00	-75 13 55.3	2.415	SSPMJ2231-7514	7
22 32 56.74	+53 47 40.5	1.318	GI 863.1B	GI 863.1 B	1
22 32 56.74	+53 47 40.5	1.318	GI 863.1A	525	233-017	GI 863.1 A	5455.00 A	1
22 34 53.68	-01 04 58.0	1.135	LHS 526	526	5458.01	1
22 38 33.59	-15 17 59.3	3.254	GI 866 A	68	156-031	GI 866 A	5475.00	1
22 38 33.59	-15 17 59.3	3.254	GI 866 B	GI 866 B	1
22 38 33.59	-15 17 59.3	3.254	GI 866 C	1
22 41 41.00	-32 58 48.6	1.124	LHS 527	527	5490.01	1
22 42 38.74	+17 40 09.2	1.240	LHS 528	528	067-015	GI 1271	5499.01	112120	...	1
22 51 23.01	+29 39 44.3	1.269	LHS 529	529	128-007	GI 1275	5534.01	1
22 53 16.75	-14 15 49.2	1.143	LHS 530	530	156-057	GI 876 A	5546.00	113020	...	1
22 53 53.35	-06 46 54.5	2.570	LHS 69	69	...	GI 1276	5548.01	1
22 55 45.37	-75 27 31.4	1.420	LHS 531	531	...	GI 877	5547.00	113229	...	1
22 56 24.66	-60 03 49.2	1.060	LHS 532	532	...	GI 1277	1
22 56 34.82	+16 33 12.3	1.051	LHS 533	533	067-037	GI 880	5563.00	113296	216899	1

Table A.1: continued

RA	DEC	P.M.	Angle	Full Name	LHS	LOB	CNS3	YPC	HIP	HD	Ref.
(1)	(2)	(3)	(4)	(5)	(6)	(7)	(8)	(9)	(10)	(11)	(12)
($J2000.0$)		($^{\circ}/yr$)	(deg)								
23 05 51.92	-35 51 11.3	6.907	78.9	LHS 70	70	...	GI 887	5584.00	114046	217987	1
23 06 35.80	+71 43 25.5	1.320	71.5	LHS 534	534	241-044	1
23 07 30.00	+68 40 05.1	1.125	88.5	LHS 535	535	241-045	...	5600.03	1
23 08 26.05	+31 40 23.9	1.390	77.2	LHS 536	536	128-034	...	5600.02	1
23 09 32.95	+00 42 39.5	1.301	192.2	LHS 537	537	028-043	...	5603.20 A	1
23 10 42.16	-19 13 34.9	1.421	178.4	LHS 538	538	...	GI 1281	1
23 13 16.94	+57 10 06.0	2.095	81.7	LHS 71	71	...	GI 892	5616.00 A	114622	219134	1
23 15 51.60	-37 33 30.6	1.306	78.2	LHS 539	539	1
23 17 05.03	-13 51 03.9	1.282	204.2	LHS 540 C	5631.00 C	1
23 17 05.03	-13 51 03.9	1.282	204.2	LHS 540	540	273-001	...	5631.00 A	114962	219617	1
23 17 06.03	-13 50 52.5	1.282	204.2	LHS 541	541	5631.00 E	1
23 19 09.52	-06 12 50.0	1.728	201.7	LHS 542	542	1
23 21 37.44	+17 17 25.3	1.483	201.0	LHS 543	543	068-008	...	5652.01	115332	...	1
23 25 40.24	+53 08 06.0	1.071	71.2	LHS 543a	543a	5675.01	1
23 31 22.20	+59 09 55.9	1.104	84.3	LHS 544	544	217-011	GI 895.4	5693.00	116085	221354	1
23 34 03.33	+00 10 45.9	1.388	227.8	LHS 545	545	029-043	GI 899	5699.00	116317	...	1
23 35 10.47	-02 23 20.8	1.157	137.4	LHS 546	546	157-077	GI 1286	5703.11	1
23 36 51.77	+01 09 52.6	1.205	94.9	LHS 548	548	157-086	GI 901	5712.00	1
23 36 52.30	-36 28 51.8	1.155	87.9	LHS 547	547	1
23 41 55.00	+44 10 38.9	1.617	177.0	LHS 549	549	171-010	GI 905	5736.00	1
23 43 13.64	-24 09 52.1	2.557	150.1	LHS 72	72	029-053	...	5741.10 A	1
23 43 16.73	-24 11 16.4	2.557	150.1	LHS 73	73	275-092	...	5741.10 B	1
23 49 12.52	+02 24 04.4	1.374	134.5	LHS 550	550	029-068	GI 908	5763.00	117473	...	1
23 57 44.11	+23 18 16.8	1.460	135.0	LHS 551	551	129-047	GI 1292	5786.01 A	1
23 59 27.88	-16 56 41.1	1.162	98.0	LHS 552	552	266-020	...	5796.00	...	224618	1
23 59 51.38	-34 06 42.5	1.050	126.0	LHS 4058	4058	3

Note.- The name for LHS and LOB catalogs should have “LHS” and “G”, respectively as prefixes to their ID when using SIMBAD. The full name for all primary stars can be retrieved by SIMBAD. However, the full name for the components may not be retrieved by SIMBAD.

The last column indicates the sources of the proper motions. Notes on individual objects can be found in section 1.2.1, 2.7.1 and 4.7.

Ref.- (L) Gidas et al. (1971, 1978). (1) Luyten (1979a). (2) Lépine et al. (2002b). (3) Bakos et al. (2002) (4) Oppenheimer et al. (2001a). (5) Jao et al. (2003). (6) Gizis et al. (2000). (7) Scholz et al. (2002). (8) Scholz et al. (2003) McCaughrean et al. (2004). (9) Delfosse et al. (2001). (10) Ruiz et al. (2001). (11) Ruiz and Maza (1987). (12) Ruiz et al. (1986). (13) WT catalogs. (14) Monet et al. (2000). (15) Reyé et al. (2002).

Most the coordinates are from 2MASS and has been transformed to epoch and equinox J2000.0, except some objects with superscripts besides DEC. H): European Space Agency (1997), S): SIMBAD. The coordinate superscripts on the DEC shown as numbers have the same references code as proper motion references.

Appendix B

MOTION Stars Parallax, Photometry and Spectroscopy

The first and second columns are the coordinates at equinox and epoch 2000.0. The third column is the object name. The fourth column is the weighted mean parallax from the references listed in the twelfth column. If the same parallax code is shown twice, it means that there are two different observations. The optical and near-infrared photometry is given from the fifth to the tenth column. All the JHK_s photometry is from 2MASS except for LHS282, LHS290 and ER8. Various photometry references are given in thirteenth column. The spectral types and references are given in the eleventh and fourteenth column, respectively. All of the codes used in this table can be found at the end of this table.

Table B.1: MOTION stars Parallax, Photometry and Spectroscopy

RA (J2000.0)	DEC	Name	Parallax (mas)	V	R	I	J	H	K	Type	π	Ref. phot (13)	spect (14)
(1)	(2)	(3)	(4)	(5)	(6)	(7)	(8)	(9)	(10)	(11)	(12)	(13)	(14)
00 02 10.21	+27 04 55.8	GI 914 A	82.25 \pm 0.76	5.34	4.78	4.38	4.702J	4.179J	4.068J	G5.0 V	YSH	5	Gra01
00 02 10.21	+27 04 55.8	GI 914 B	82.25 \pm 0.76	8.42J	7.48J	6.73J	---	---	---	K7.0 V	YSH	5	Chr69
00 02 10.21	+27 04 55.8	GI 914 C	82.25 \pm 0.76	---	---	---	---	---	---	---	YSH	5	---
00 02 10.73	-43 09 55.5	LHS 1005	127.40 \pm 6.80	13.05	---	---	12.597	12.425	12.445	DA5.0	Y	33	McC99
00 04 34.86	-40 44 06.5	LHS 102 B	104.70 \pm 11.40	---	---	---	13.109	12.055	11.396	L4.0 V	Y	---	Mar99
00 04 36.45	-40 44 02.7	LHS 102	104.70 \pm 11.40	12.87	11.66	10.11	8.601	8.043	7.737	M3.5 V	Y	T	Haw96
00 05 24.39	-37 21 26.7	LHS 1	229.20 \pm 1.07	8.54	7.57	6.41	5.328	4.828	4.523	M2.0 V	YH	4	TB.R
00 06 43.19	-07 32 17.0	LHS 2	213.00 \pm 3.60	13.76	12.17	10.16	8.323	7.792	7.439	M5.5 V	Y	35	Hen94
00 07 26.68	+29 14 32.7	LHS 103	53.50 \pm 2.50	14.16	13.01	11.54	10.153	9.719	9.465	M3.5 V	Y	35	Haw96
00 09 16.46	+09 00 41.9	LHS 104	19.30 \pm 3.00	13.73	12.87	10.32	11.091	10.566	10.412	K7.0 VI	Y	T	Giz97
00 09 17.31	-19 42 31.6	LHS 105	...	15.56	14.36	12.68	10.883	10.327	10.074	M4.5 V	---	T	TB
00 11 31.82	+59 08 39.9	LSR0011+5908	...	15.65	13.89	11.85	9.945	9.393	9.093	M5.5 V	Y	T	Lep03
00 12 46.97	+54 39 45.4	LHS 1039	28.30 \pm 2.40	13.29	12.39	11.52	10.499	9.972	9.787	VI	---	35	HRDIA
00 14 09.61	-20 22 53.6	LHS 106	...	---	---	---	---	---	---	m	---	---	LUYTN
00 15 33.49	-35 11 47.6	LHS 1048	...	---	---	---	10.801	10.260	10.058	M4.0 V	---	---	Bid85
00 16 14.62	+19 51 37.6	LHS 107	66.01 \pm 1.60	12.26	11.05	9.46	7.875	7.322	7.087	M4.0 V	YH	35	Haw96
00 16 16.14	+19 51 50.6	LHS 108	66.01 \pm 1.60	13.21	12.00	10.41	8.893	8.339	8.097	M4.0 V	YH	35	Haw96
00 17 40.01	-10 46 16.9	LHS 109	28.40 \pm 3.50	13.95	---	---	11.046	10.563	10.366	K5.0 V	Y	13	Bid85
00 18 22.79	+44 01 22.7	LHS 3	280.59 \pm 0.95	8.08	---	5.94	5.252	4.476	4.018	M1.0 V	YH	20	Haw96
00 18 25.72	+44 01 38.1	LHS 4	280.59 \pm 0.95	11.06	9.83	8.24	6.789	6.191	5.948	M3.5 V	YH	35	Haw96
00 19 36.59	-28 09 38.8	LHS 110	28.59 \pm 1.94	---	---	---	10.630	10.117	9.876	M4.0 V	C	---	Bid85
00 19 37.02	-28 09 45.7	LHS 111	29.90 \pm 2.00	---	---	---	10.249	9.734	9.475	M3.5 V	C	---	Bid85
00 20 04.38	-64 52 29.2	LHS 5	116.47 \pm 0.64	4.22	3.89	3.57	3.068	2.738	2.769	G0.0 V	YH	8	Hou88
00 20 29.37	+33 05 06.4	LHS 112	79.30 \pm 3.70	16.09	14.40	12.34	10.284	9.691	9.330	M5.5 V	Y	35	Haw96
00 25 44.37	-77 15 15.3	LHS 6	133.86 \pm 0.51	2.80	2.45	2.12	1.676	1.434	1.372	G1.0 IV	YH	8	Hou88
00 31 13.94	+53 04 45.4	LHS 1088	20.30 \pm 3.90	15.00	13.91	12.48	11.158	10.621	10.409	M3.5 V	Y	35	Giz97
00 31 35.42	-05 52 12.8	LHS 113	62.30 \pm 4.20	12.73	11.59	10.14	8.762	8.217	7.945	M3.5 V	Y	35	Haw96
00 32 29.62	+67 14 08.2	GI 22 A	98.21 \pm 1.42	10.28J	9.24J	7.97J	6.844JD	6.268JD	6.037JD	M2.0 V J	YSH	35	McC91
00 32 29.62	+67 14 08.2	GI 22 C	98.21 \pm 1.42	13.64	---	---	---	---	---	---	---	24	---
00 32 29.71	+67 14 04.6	GI 22 B	98.21 \pm 1.42	12.13	---	---	7.172C	6.538C	6.377C	M3.0 V	YSH	24	McC91
00 35 02.87	-53 41 42.6	LHS 116	34.06 \pm 0.86	8.55	---	---	6.910	6.436	6.312	K2.0 V	YH	17	Hou88
00 35 55.52	+10 28 35.5	LHS 117	63.60 \pm 4.50	15.32	13.88	12.00	10.222	9.656	9.367	M5.0 V	Y	35	Haw96
00 37 20.70	-24 46 02.4	GI 25 A	64.88 \pm 0.81	5.57J	5.17J	4.80J	4.437JD	3.976J	4.027J	G5.0 V	YSH	8	Bid85
00 37 20.70	-24 46 02.4	GI 25 B	64.88 \pm 0.81	---	---	---	---	---	---	---	YSH	8	Hou88
00 38 59.01	+30 36 58.5	LHS 119	80.10 \pm 3.90	11.08	10.03	8.75	7.453	6.864	6.606	K1.0 V	Y	35	Haw96
00 43 26.01	-41 17 34.0	LHS 1134	...	---	---	---	8.572	8.026	7.710	M3.0 V	Y	35	Haw96
00 43 35.60	+28 26 41.4	LHS 120	51.80 \pm 4.00	14.51	13.33	11.81	10.403E	9.654E	9.654E	M4.0 V	Y	35	Haw96
00 45 19.70	-33 29 29.5	F351-50	...	---	---	---	FFF	FFF	FFF	WD	---	---	Opp01
00 48 23.01	+05 16 50.5	LHS 121	134.36 \pm 0.79	5.72	5.21	4.76	4.367	3.722	3.683	K1.0 V	YH	8	Hou88
00 49 06.22	+57 48 54.6	LHS 123	168.38 \pm 0.59	3.44	3.11	2.78	2.109	2.086	1.988	G3.0 V	YH	7	CNS91
00 49 05.17	+57 49 03.8	LHS 122	168.38 \pm 0.59	7.51	---	---	7.167	4.147	3.881	K7.0 V	YH	7	Hen94
00 49 09.91	+05 23 19.1	LHS 7	231.88 \pm 1.79	12.40	12.14	11.91	11.688	11.572	11.498	DZ8.0	YH	4	Gre84
00 49 29.04	-61 02 32.7	LHS 124	47.12 \pm 5.54	12.18	11.19	9.93	8.627	8.089	7.837	M2.5 V	C	T	Haw96
00 50 17.09	-39 30 08.3	LHS 125	18.01 \pm 5.63	14.33	13.59	12.92	12.047	11.575	11.452	K--- VI?	C	T	TB
00 51 29.74	+58 18 07.5	LHS 126	54.36 \pm 1.80	10.67	9.80	8.89	7.831	7.235	7.047	K7.0 V	YH	35	Haw96
00 55 43.89	-21 13 07.1	LHS 127	...	15.81	14.87	13.73	12.458	11.920	11.733	K/M--- VI	---	T	TB

Table B.1: continued

RA (J2000.0)	DEC	Name	Parallax (mas)	V	R	I	J	H	K	Spect. Type	π	Ref. phot (13)	spect (14)
(1)	(2)	(3)	(4)	(5)	(6)	(7)	(8)	(9)	(10)	(11)	(12)	(13)	(14)
00 57 19.73	-62 14 44.4	LHS 128	51.75 \pm 1.06	9.47	8.68	7.98	7.081	6.486	6.284	K5.0 V	YH	4	Har96
00 58 27.93	-27 51 25.3	LHS 129	76.34 \pm 2.82	11.77	10.65	9.17	7.763	7.203	6.892	M3.5 V	YH	4	Har96
01 00 56.37	-04 26 56.5	LHS 130	87.18 \pm 2.46	13.35	12.08	10.52	9.042	8.485	8.224	M3.5 V	Y	T	Har96
01 02 32.16	+71 40 47.5	LHS 131	122.33 \pm 1.18	9.98	8.92	7.57	6.301	5.699	5.449	M3.0 V	YH	35	Har96
01 02 51.04	-37 37 43.7	LHS 132	11.130	10.479	10.069	M7.5 V	YH		TB
01 03 38.83	-45 47 31.4	LHS 133	16.31 \pm 8.76	11.62	9.429	8.873	8.709	K3.0 V	YH	16	YPC95
01 04 53.80	-18 07 28.7	LHS 134	99.80 \pm 5.00	14.45	12.99	11.11	9.387	8.753	8.453	M5.0 V	Y	35	Har96
01 05 37.60	+28 29 33.6	LHS 135	79.30 \pm 3.00	14.79	13.29	11.35	9.486	8.881	8.550	M5.0 V	Y	35	Har96
01 07 08.04	+63 56 28.8	LHS 136	66.47 \pm 1.21	8.97	8.18	7.44	6.468	5.824	5.688	K5.0 V	YH	35	Har96
01 07 47.82	+34 12 30.5	LHS 137	45.10 \pm 3.20	13.37	12.33	11.06	9.843	9.310	9.082	M2.5 V	Y	35	Har96
01 08 16.21	+54 55 13.2	G1 53 A	132.57 \pm 0.57	5.17d	4.031J	3.597J	3.505J	G5.0 VI J	YH	24	Gr01
01 08 16.21	+54 55 13.2	G1 53 B	132.57 \pm 0.57	11.00d	YH	24	
01 08 27.09	+63 30 56.4	LHS 1198	8.04 \pm 3.17	11.52	10.99	10.51	9.756	9.281	9.153	K2.0 V	YH	35	Bid85
01 09 21.85	+29 49 26.3	2MA0109+2949	12.912	12.158	11.681	M9.5 V	YH		Gl200
01 12 30.64	-16 59 56.1	LHS 138	268.84 \pm 2.95	12.10	10.73	8.96	7.258	6.749	6.420	M4.5 V	YH	4	Hen94
01 16 29.18	+24 19 26.8	LHS 139	48.10 \pm 4.50	15.00	13.78	12.16	10.705	10.166	9.909	M4.0 V	Y	35	Har96
01 19 52.26	+84 09 32.9	LHS 140	71.60 \pm 2.70	14.75	13.38	11.38	9.855	9.314	9.025	M5.0 V	Y	35	Har96
01 21 34.57	-41 39 23.2	LHS 141	59.33 \pm 1.58	10.12	9.25	8.38	7.356	6.758	6.581	K7.0 V	YH	4	Har96
01 31 30.82	+10 01 29.8	LHS 1257	...	16.38	15.21	13.77	12.401	11.931	11.675	M---VI?	YH	T	TB
01 32 26.21	-21 54 18.5	LHS 142	55.43 \pm 2.08	11.21	10.18	9.11	7.977	7.346	7.100	M1.0 V	YH	7	Har96
01 38 49.04	+11 21 36.7	LHS 144	19.90 \pm 3.60	15.21	13.98	12.767	12.767	12.289	12.080	K/M---VI	Y	T	TB
01 39 47.83	-56 11 36.0	LHS 9	373.70 \pm 2.70	12.06J	10.40J	8.34J	3.573a	6.684a	3.558	M5.5 V	Y	4	Kir91
01 39 47.60	-56 11 47.0	LHS 10	373.70 \pm 2.70	---	---	---	4.043	6.742a	3.510	M6.0 V	Y	4	Kir91
01 43 01.02	-67 18 30.3	LHS 145	102.07 \pm 1.64	13.83	13.55	13.23	12.867	12.659	12.579	DAT.0	YH	T	TB.R
01 44 04.09	-15 56 14.7	LHS 146	274.39 \pm 0.76	3.49	3.06	2.68	2.149	1.800	1.794	G8.0 V	YH	8	How88
01 48 07.83	-17 11 03.1	LHS 147	14.00 \pm 9.20	17.62	17.38	17.16	16.097	15.563	15.200	DC7.0	Y	21	McC99
01 53 08.99	-33 26 02.1	LHS 148	...	16.42	15.49	14.57	13.519	13.012	12.832	M0.0 VI	Y	28	TB
02 00 12.96	+13 03 07.2	LHS 11	224.80 \pm 2.90	12.31	10.95	9.21	7.514	6.970	6.648	M4.5 V	Y	4	Kir91
02 02 52.16	+05 42 21.0	LHS 12	34.91 \pm 3.00	12.24	11.34	10.44	9.474	8.900	8.684	K/M---VI	YH	20	TB.R
02 05 04.85	-17 36 52.7	LHS 149	106.37 \pm 1.98	10.19	9.14	7.84	6.542	5.898	5.662	M3.0 V	YH	4	TB.R
02 05 11.62	-05 17 54.2	WDO205-053	...	---	---	---	16.682	16.137	15.792	WD	YH		Op901
02 07 23.38	-66 34 11.7	LHS 150	64.60 \pm 17.80	11.50	10.49	9.32	8.132	7.613	7.364	M1.5 V	Y	4	Har96
02 10 25.90	-50 49 25.8	LHS 13	91.62 \pm 0.61	6.12	5.66	5.24	4.785	4.245	4.125	K1.0 V	YH	8	How88
02 10 35.44	+46 42 04.8	LHS 1349	...	15.71	14.34	12.55	10.916	10.392	10.101	V	YH	35	How88
02 11 20.83	+39 55 21.5	LHS 151	59.80 \pm 3.50	14.51	14.26	14.04	13.832	13.670	13.595	DAZ7.0	Y	3	McP99
02 12 20.98	+03 34 32.3	LHS 14	96.08 \pm 1.46	10.04	9.10	7.99	6.830	6.321	6.077	M1.5 V	YH	4	Har96
02 13 49.99	+15 59 11.1	LHS 162	6.70 \pm 3.80	13.19	12.54	11.94	11.091	10.546	10.420	K3.0 V	Y	35	Bid85
02 14 04.29	-01 12 05.1	LHS 1365	16.17 \pm 1.33	9.03	8.68	8.34	7.899	7.589	7.520	G0.0 V	YH	31	Bid85
02 16 56.51	+42 58 10.4	LHS 153	50.20 \pm 4.10	16.22	15.77	15.37	14.645	13.725	13.184C	DA9.0	Y	3	Gr684
02 17 03.19	+34 13 27.3	LHS 154 B	92.41 \pm 0.82	5.03J	---	---	---	---	---	---	YH	7	---
02 19 10.08	-36 46 41.1	LHS 154a	71.56 \pm 2.99	11.62	10.56	9.27	7.924	7.317	7.031	M2.5 V	YH	7	Gr01
02 31 27.66	+57 22 43.3	LHS 155	52.60 \pm 2.30	13.22	12.07	10.59	9.218	8.637	8.418	M3.5 V	Y	35	Har96
02 34 12.45	+17 45 50.5	LHS 156	27.30 \pm 4.10	14.90	---	---	11.431	10.957	10.716	M3.0 VI	Y	36	Gi997
02 36 04.89	+06 53 12.9	LHS 15	136.98 \pm 0.88	5.81d	5.24	4.74	4.1521	3.6571	3.481J	K3.0 V	YH2	24.8	CNS01
02 36 15.26	+06 52 18.0	LHS 16	136.98 \pm 0.88	11.66	10.46	8.88	7.333	6.793	6.574	M3.5 V	YH2	35	Hen94

Table B.1.: continued

RA	DEC	Name	Parallax (mas)	V	R	I	J	H	K	Spect.	π	Ref.	
(1)	(2)	(3)	(4)	(5)	(6)	(7)	(8)	(9)	(10)	Type	(12)	phot (13)	spect (14)
02 36 04.89	+06 53 12.9	LHS 15 C	136.98± 0.88	16.90d	—	—	—	—	—	—	YH2	24	—
02 39 50.71	−34 07 57.5	LHS 157	92.10± 4.43	11.79	10.68	9.35	8.060	7.540	7.305	M2.5 V	C	T	Haw96
02 42 02.85	−44 30 58.7	LHS 158	27.12± 1.95	13.54	12.66	11.60	10.433	9.937	9.726	M1.5 V	C	T	HB
02 46 14.92	−04 59 20.6	LHS 17	60.30± 8.20	16.32	14.67	12.68	10.970	10.499	10.152	M6.0 V	Y	T	Haw96
02 46 34.74	+16 25 10.2	LHS 1443	68.50± 3.50	17.31	15.17	12.88	10.971	10.519	10.185	M6.0 V	Y	T	Haw96
02 52 07.10	+34 23 21.7	LHS 159	69.08± 1.59	9.63	8.83	8.06	7.053	6.462	6.298	K5.0 V	YH	35	Haw96
02 52 22.15	−63 40 47.5	LHS 160	86.82± 1.88	11.38	10.32	8.99	7.671	7.115	6.829	M2.5 V	YH	4	Haw96
02 52 45.51	+01 55 50.5	LHS 161	25.30± 5.00	14.64	13.70	12.78	11.714	11.198	10.995	K/M— VI	Y	T	TB.R
02 56 13.21	−35 08 26.9	LHS 162	...	15.38	14.44	13.43	12.280	11.725	11.536	K/M— VI	Y	T	TB
02 57 31.04	+10 47 24.5	LHS 163	50.00± 5.80	13.06	11.95	10.52	9.162	8.663	8.428	M3.0 V	Y	4	Haw96
03 01 40.57	−34 57 56.5	LHS 164	32.48± 6.84	—	—	—	11.381	10.768	10.641	—	YH	—	—
03 04 09.63	+61 42 21.2	LHS 1492	37.79± 4.03	6.67	—	—	5.391	5.115	5.027	—	YH	33	—
03 04 43.40	+61 44 09.0	LHS 1494	37.79± 4.03	12.55	11.49	10.15	8.877	8.328	8.103	G4.0 V	YH	35	YP035
03 06 26.75	+01 57 54.5	LHS 1496	66.91± 1.64	9.07	8.23	7.44	6.492	5.843	5.646	K5.0 V	YH	4	Haw96
03 06 28.67	−07 40 41.5	LHS 165	21.50± 4.10	14.43	13.60	12.76	11.758	11.200	11.006	K— VI	Y	35	TB
03 08 25.56	+26 19 51.1	LHS 1501	25.34± 1.11	8.06	—	—	6.948	6.696	6.640	F5.0 V	YH	1	Bld55
03 09 03.96	+49 36 47.8	LHS 166	94.86± 0.66	4.04	3.74	3.45	3.143	2.875	2.723	G0.0 IV— V	YH	7	Gr01
03 10 58.53	+73 46 19.7	LHS 18	83.30± 3.40	14.61	13.27	11.46	9.850	9.409	9.083	M5.0 V	Y	35	Haw96
03 12 29.76	−38 05 20.1	LHS 167	79.60± 9.70	11.43	10.40	9.18	8.028	7.423	7.185	M1.5 V	Y	4	HB
03 13 22.92	+04 46 29.3	LHS 168	117.10± 3.50	13.66	12.44	10.58	8.775	8.208	7.833	M5.0 V	Y	35	TB.R
03 13 24.23	+18 49 37.7	LHS 169	30.00± 2.30	14.16	13.28	12.45	11.486	11.012	10.819	K7.0 VI	Y	35	Gr07
03 16 26.79	+38 05 55.8	LHS 170	31.53± 2.11	10.62	9.87	9.25	8.352	7.768	7.597	K0.0 VI	YH	T	Gr07
03 17 46.17	−62 34 31.3	LHS 171	82.90± 0.53	5.33	5.17	4.82	4.462	4.041D	3.994D	G3/5 V	YH	8	Hou88
03 18 12.82	−62 30 23.0	LHS 172	82.63± 0.54	5.24	4.89	4.56	4.271	3.874	3.860	G2.0 V	YH	8	CNS91
03 19 55.64	−43 04 11.3	LHS 19	165.01± 0.55	4.26	3.85	3.47	3.032	2.709	2.636	G5.0 V	YH	8	CNS91
03 28 53.11	+37 22 56.7	LHS 173	37.98± 2.25	11.03	10.22	9.48	8.606	7.972	7.788	K7.0 VI	YH	T	Gr07
03 30 44.81	+34 01 07.2	LHS 174	22.60± 7.40	12.76	11.86	10.90	9.844	9.350	9.143	G3/97	Y	35	Gr07
03 31 17.27	+66 43 49.1	LHS 175	18.51± 1.38	9.91	9.30	8.87	8.535	8.165	8.069	G4.0 V	YH	6	Bld55
03 35 38.61	−08 29 22.7	LHS 176	...	15.89	14.29	12.32	10.377	9.801	9.456	M5.0 V	Y	T	TB
03 35 51.98	+41 42 18.1	LHS 177	23.10±15.00	12.54	11.57	10.45	9.284	8.739	8.534	M2.0 V	Y	35	Bld55
03 38 15.69	−11 29 13.5	LHS 20	62.40± 3.30	13.01	11.98	10.79	9.631	9.112	8.831	M2.5 VI	Y	35	R05
03 42 29.45	+12 31 33.8	LHS 178	45.10±12.00	12.92	11.96	10.87	9.599	9.113	8.878	M1.5 VI	Y	7	Gr07
03 44 34.86	+18 26 09.8	LHS 179	52.60± 3.00	15.19	14.91	14.65	14.590	14.350	14.230	DQ8.0	Y	3	Gr04
03 46 46.50	+24 56 02.8	WD0346+246	WD	YH	26	Haw97
03 47 02.09	+41 25 38.2	LHS 180	41.37± 1.82	8.17	7.73	7.29	6.618	6.192	6.120	K1.0 V	YH	7	Bld55
03 47 02.62	+41 25 42.4	LHS 181	41.37± 1.82	8.77	8.25	7.75	6.949	6.481	6.347	K2.0 V	YH	7	Bld55
03 50 13.89	+43 25 40.5	LHS 182	23.10± 2.80	13.91	13.00	12.12	11.097	10.669	10.519	M0.0 VI	Y	35	Gr07
03 50 44.29	−06 05 41.7	LHS 183	105.40± 3.20	12.80	11.59	10.04	8.570	7.998	7.751	M3.5 V	Y	35	TB.R
03 51 09.40	−56 27 07.1	WD0351-564	WD	YH	4	Op01
03 53 19.71	−37 03 59.1	LHS 184	40.19± 2.62	12.14	11.17	9.97	8.743	8.211	7.948	M2.0 V	YH	4	Haw96
04 01 36.59	+18 43 39.8	LHS 185	16.20± 4.70	15.52	14.32	13.47	12.356	11.738	11.517	M0.5 VI	Y	33	Gr07
04 03 15.02	+35 16 23.8	LHS 21	54.20± 0.86	8.50	8.02	7.56	6.768	6.297	6.195	K0.0 V	YH	7	Bld55
04 03 38.44	−05 08 05.4	LHS 186	18.70± 3.04	14.87	13.85	12.73	11.566	11.101	10.854	K/M— VI	YU	T	TB
04 06 11.77	+32 57 02.9	LHS 187	27.96± 1.75	10.01	9.40	8.87	8.080	7.507	7.420	K4.0 V	YH	35	Bld55
04 09 15.69	−53 22 25.4	LHS 188	66.69± 1.97	11.84	10.76	9.34	7.948	7.428	7.135	M3.5 V	YH	4	Haw96
04 10 28.15	−53 36 08.2	LHS 22	143.42± 1.92	13.62	12.21	10.44	8.747	8.213	7.900	M4.5 V	C	T	TB.R

Table B.1: continued

RA (J2000.0)	DEC	Name	Parallax (mas)	V	R	I	J	H	K	Spect. Type	π	Ref. phot (13)	spect (14)
(1)	(2)	(3)	(4)	(5)	(6)	(7)	(8)	(9)	(10)	(11)	(12)	(13)	(14)
04 15 21.80	-07 39 29.3	LHS 24	199.00±0.77	9.52	9.14	—	9.849C	9.986C	9.861C	DA4.0	YH	36.7	CNS91
04 15 16.34	-07 39 10.7	LHS 23	199.00±0.77	4.43	3.97	3.55	3.013	2.594	2.498	K1.0 Ve	YH	8	CNS91
04 15 21.56	-07 39 21.2	LHS 25	199.00±0.77	11.19	9.95	8.32	6.747	6.278	5.962	M4.5 V	YH	20	Haw96
04 19 32.13	+42 33 30.5	LSR0419+4233	11.094	10.383	9.900	M8.5 Ve	—J	35	Lep03
04 25 38.35	-06 52 37.0	LHS 190	35	TB
04 25 38.35	-06 52 37.0	LHS 189	...	14.251	13.191	11.931	11.1421	10.658J	10.311J	M—VI J	—J	35	TB
04 26 19.92	+03 36 36.0	LHS 191	58.40±1.80	18.32	—	13.95	11.623	11.072	10.693	M6.5 V	Y	20	Haw96
04 30 52.53	+28 11 58.4	LHS 192	10.20±0.80	17.33	—	15.35	14.245	13.721	13.461	M1.0 VI	Y	20	Giz97
04 31 11.48	+58 58 37.6	LHS 26	180.63±0.78	11.07J	9.86J	8.26J	6.622	6.012	5.717	M4.0 V	YH	20	Haw96
04 31 11.48	+58 58 37.6	LHS 27	180.63±0.78	DC5.0	YH	20	CNS91
04 31 43.99	-21 50 44.3	LHS 1676	...	16.01	14.57	12.71	11.021	10.550	10.280	M5.0 V	—J	T	TB
04 32 35.96	-39 02 14.6	LHS 193 B	28.81±3.42	17.25	16.45	15.30	15.980C	15.786C	15.291C	WD	C	T	TB
04 32 36.55	-39 02 03.4	LHS 193	32.20±1.71	11.67	10.84	10.09	9.177	8.551	8.427	M—VI	C	T	TB
04 32 42.63	-39 47 12.4	LHS 1678	...	12.49	11.46	10.26	13.006	12.906	12.763C	DQ7.0	Y	T	Bid85
04 37 47.41	-08 49 10.6	LHS 194	105.20±2.60	13.75	13.43	13.17	8.512	8.192	8.090	F8.0 V	YH	16	Hou88
04 38 22.32	-65 24 57.4	LHS 195	16.94±0.98	9.85	6.462	5.824	5.607	M2.0 V	YH	35	TB.R
04 42 55.78	+18 57 29.4	LHS 196	108.81±1.87	9.98	8.96	7.73	11.559	11.056	10.764	M6.0 V	Y	23	Haw96
04 46 18.50	+48 44 51.9	LHS 197	52.10±0.90	17.29	9.071	8.551	8.306	M4.0 V	Y	35	Haw96
04 52 34.58	+40 42 24.2	LHS 198	77.40±2.40	13.44	12.21	10.58	9.042	8.507	8.312	K7.0 V	Y	4	Haw96
04 55 57.67	-61 09 46.6	LHS 199	44.40±10.80	12.05	11.14	10.15	4.389	3.797	3.706	K3.0 V	YH	8	CNS91
05 00 49.01	-05 45 13.2	LHS 200	113.59±0.73	6.23	5.61	5.12	7.001D	6.414D	6.172D	M0.5 V	YH	35	Haw96
05 03 23.95	+53 07 42.4	LHS 28	71.09±1.62	9.98	9.08	8.11	13.368	12.866	12.695	M3.5 VI	Y	T	HRDIA
05 05 11.75	+30 43 32.1	LSR0505+3043	10.45	9.388	8.612	IV	YH	4	Hen02
05 08 10.95	-53 00 53.1	LHS 202	3.90±13.30	12.27	11.36	10.45	6.175	5.591	5.314	M3.5 V	YH	8	TB.R
05 08 35.05	-18 10 19.2	LHS 203	107.05±1.99	10.32	9.17	7.67	5.821	5.316	5.049	K/M—VI	YH	T	TB.R
05 11 40.56	-45 01 06.4	LHS 29	255.27±0.86	8.85	7.90	6.90	8.316	8.046	7.998	G—VI	YH	20	Lep03
05 13 05.36	-59 38 44.4	LHS 204	14.70±1.00	9.42	9.10	8.77	11.320	10.661	10.319	M7.0 V	Y	20	Haw96
05 15 30.95	+59 11 17.5	LSR0515+5911	8.066	7.441	7.199	M2.0 V	Y	23	Giz97
05 16 59.67	-78 17 20.2	LHS 205	77.50±11.00	11.90	10.87	9.49	13.614	13.112	12.930	M3.5 VI	Y	23	Lep03
05 19 13.63	+42 13 49.0	LSR0519+4213	15.359	14.933	14.772	M4.5 VI	Y	23	Lep03
05 19 56.70	+20 10 52.6	LHS 205a	10.30±1.30	18.33	13.179	12.749	12.648	M3.0 VI	Y	35	Haw96
05 22 05.30	+38 14 14.6	LP251-035	16.70±1.90	16.25	8.979J	8.496J	8.224CJ	M3.0 V J	—J	Y	—
05 28 14.60	+02 58 14.3	LHS 206 A	52.30±2.20	12.81J	11.70J	10.28J	M1.5 V	YH	20	Kir91
05 28 14.60	+02 58 14.3	LHS 206 B	52.30±2.20	4.999	4.149D	4.039	G1.0 V	YH	7	Hou88
05 31 27.41	-03 40 38.2	LHS 30	175.17±1.05	7.95	6.98	5.88	4.869	4.424	4.241D	M6.0 VI	Y	23	Haw96
05 37 09.89	-80 28 08.9	LHS 208	54.91±0.45	5.65	5.34	5.05	12.137	11.638	11.330	M8.0 Ve	Y	4	Haw96
05 38 12.62	+79 31 19.4	LHS 207	45.10±1.40	18.40	11.109	10.446	10.044	M4.0 V	YH	13	HRDIA
05 39 24.79	+40 38 42.8	LSR0539+4038	6.598	6.212	6.094	G8.0 V	YH	8	Hou88
05 42 09.27	+12 29 21.7	LHS 31	170.37±3.09	11.57	10.34	8.74	7.124	6.627	6.389	M4.0 V	YH	4	Haw96
05 44 03.42	+40 56 49.4	LHS 209	18.00±4.60	15.12	12.335	11.816	11.622	VI	Y	13	HRDIA
05 44 31.98	-70 08 36.8	LHS 210	39.14±0.75	8.07	7.65	7.23	15.822C	15.293	15.141	K5.0 V	Y	8	Hou88
05 44 57.65	+26 02 60.0	LSR0544+2602	10.693	10.460	10.460	M0.0 VI	Y	T	Giz97
05 48 00.20	+08 22 14.0	LHS 211	19.30±3.10	14.13	13.20	12.25	16.603	16.333	15.794	DC8.0	Y	3	CNS91
05 49 35.44	+23 29 52.8	LSR0549+2329	13.047	12.860	12.777	DZ9.0	Y	3	CNS91
05 55 09.53	-04 10 07.1	LHS 32	155.00±2.10	14.47	13.97	13.49	12.930	12.720	12.653	DAP9.0	Y	3	CNS91
05 56 25.47	+05 21 48.4	LHS 212	125.00±3.60	14.16	13.78	13.41

Table B.1: continued

RA (J2000.0)	DEC (J2000.0)	Name	Parallax (mas)	V	R	I	J	H	K	Spect. Type	π (12)	Ref. phot (13)	spect (14)
(1)	(2)	(3)	(4)	(5)	(6)	(7)	(8)	(9)	(10)	(11)			
06 00 46.53	+68 08 29.0	LHS 213	49.80±1.50	13.32	12.16	10.65	9.178E	8.588E	8.334E	M4.0 V	Y	35	Haw96
06 00 49.44	+68 09 22.8	LHS 214	49.80±1.50	12.94	11.80	10.33	8.922	8.351	8.075	M3.5 V	Y	35	Haw96
06 09 52.42	+23 19 12.8	LSR0609+2319	13.156	12.645	12.407	M5.0 VI	Y		Lep03
06 10 19.78	+82 06 24.6	LHS 215	106.41±1.30	10.49	9.45	8.18	6.869	6.295	6.061	M2.5 V	YH	35	Kir91
06 14 01.56	+15 09 54.3	LHS 216	30.10±3.10	14.66	13.67	12.58	11.372	10.884	10.661	M2.0 VI	Y	20	Gi297
06 21 14.85	+65 58 16.2	LHS 217	22.60±3.10	15.04	12.143	11.671	11.472	VI	Y	14	HRDIA
06 27 33.30	+06 16 58.9	LSR0627+0616	...	16.30	15.32	14.37	13.287	12.826	12.629	M1.5 VI	Y	T	Lep03
06 37 58.09	+34 30 19.2	LHS 218	29.40±3.50	14.78	13.71	12.37	11.052	10.536	10.293	M3.5 V	Y	35	Gi297
06 45 08.88	-16 42 56.7	GI 244 B	380.02±1.28	DA2.0	YH	4	CNS91
06 45 08.88	-16 42 56.7	GI 244 A	380.02±1.28	-1.43J	-1.42J	-1.41J	-1.391J	-1.391J	-1.390J	A1.0 V	YH	4	CNS91
06 47 38.00	+37 30 57.0	LHS 1870	65.84±1.78	13.07	12.657	12.662C	12.755	DA2.0	YH	7	Gre84
06 49 05.45	+37 06 50.6	LHS 220	75.00±2.20	13.78	12.58	11.00	9.561	9.053	8.773	M4.0 V	Y	35	Haw96
06 54 04.23	+60 52 18.1	LHS 221 B	94.83±1.41	YSH	35	...
06 54 04.23	+60 52 18.1	LHS 221	94.83±1.41	10.95J	9.86J	8.48J	7.128J	6.604J	6.345J	M3.0 V J	YSH	35	Haw96
06 57 46.58	-44 17 28.2	GI 257 B	124.21±2.55	YH	20	TB R
06 59 28.81	+19 20 55.9	LHS 223	124.21±2.55	10.76J	9.68J	8.26J	6.883J	6.365J	6.056J	M3.5 V J	YH	20	TB R
07 03 55.71	+52 42 06.6	LHS 224	128.80±3.10	14.52	13.09	11.19	9.160	8.547	8.230D	M5.0 V	Y	35	Haw96
07 04 45.84	-38 36 07.5	LHS 225 B	44.09±4.52	13.02	11.99	10.63	Y	35	Haw96
07 04 45.84	-38 36 07.5	LHS 225	59.89±3.10	12.87	11.85	10.51	8.950JC	8.159JC	7.952JC	M2.5 V J	C	T	TB
07 10 01.81	+38 31 46.0	LHS 226 B	162.93±1.77	YH	35	Kir91
07 10 01.81	+38 31 46.0	LHS 226	162.93±1.77	11.48J	10.16J	8.44J	6.731J	6.152J	5.846J	M4.5 V J	YH	35	Kir91
07 13 40.58	-13 27 57.1	LHS 227	16.70±3.30	14.45	13.59	12.78	11.749	11.257	11.036	K/M—VI	Y	T	TB
07 16 27.70	+23 42 10.4	LHS 228	17.70±3.00	15.53	14.56	13.34	12.023	11.520	11.298	M—VI	Y	T	TB
07 27 24.50	+05 13 32.7	LHS 33	263.76±1.25	9.85	8.71	7.16	5.714	5.219	4.857	M3.5 V	YH	4	Kir91
07 30 42.79	+48 11 58.6	LHS 229 C	90.00±1.00	Y	4	...
07 30 42.79	+48 11 58.6	LHS 229	90.00±1.00	13.52J	12.24J	10.62J	9.141J	8.618J	8.340J	M4.0 V J	Y	4	Haw96
07 30 47.34	+48 10 26.3	LHS 230	90.00±1.00	14.65J	14.12J	13.63J	13.083J	12.838J	12.756J	DC9.0	Y	21	Gre84
07 30 47.34	+48 10 26.3	LHS 230 D	90.00±1.00	Y	21	Ber01
07 32 01.74	+57 55 44.0	LHS 1923	Y	23,12	Haw96
07 33 52.87	+22 23 33.3	LHS 231	40.20±1.00	16.37	15.00	13.18	11.606	11.119	10.880	M4.5 V	Y	23,12	Haw96
07 35 46.32	+03 29 36.0	LHS 232	15.46±2.25	13.68	13.00	12.38	11.506	11.012	10.841	K—VI?	YU	T	TB
07 39 18.05	+05 13 29.8	GI 280 B	286.05±0.81	YH	8	CNS91
07 39 18.05	+05 13 29.8	GI 280 A	286.05±0.81	0.37J	0.13J	-0.12J	-0.498	-0.666	-0.658	F5.0 IV—V	YH	8	CNS91
07 40 19.36	-17 24 46.0	LHS 234	112.40±2.70	16.54	14.68	12.43	10.155	9.628	9.291	M6.0 V	Y	4	Hen94
07 40 20.78	-17 24 49.2	LHS 235	112.40±2.70	13.01	12.86	12.71	12.653	12.611	12.583	DZQ5.0	Y	4	YPC95
07 43 24.36	+72 48 48.9	LHS 236	18.20±2.80	13.08	12.30	11.55	10.582	10.000	9.850	K7.0 VI	Y	35	Gi297
07 45 34.99	-34 10 21.1	LHS 237	65.78±0.56	5.36	5.02	4.66	4.478	3.908	3.750	G0.0 V	YH	8	Hou88
07 45 38.43	-33 55 51.3	LHS 237a	65.78±0.56	16.60	15.96	15.39	14.780C	14.548C	14.399C	DC9.0	YH	3	Kun84
07 48 16.37	+20 22 05.3	LHS 238	68.49±1.74	11.45	10.47	9.33	8.120	7.396	7.160	M1.0 V	YH	35	Haw96
07 50 14.58	+07 11 48.8	LHS 239	54.70±0.70	16.96	16.31	15.70	15.031	14.898	14.746	DC9.0	Y	3	Gre84
07 50 15.35	+07 11 37.1	LHS 240	54.70±0.70	16.63	16.05	15.55	14.996	14.719	14.634	DC9.0	Y	3	Gre84
07 53 08.15	-67 47 31.5	LHS 341	141.20±8.40	13.60	13.21	12.85	12.726	12.476	12.362	DQ9.0	Y	4	CNS91
07 53 33.10	+30 36 18.3	LHS 34	36.19±0.92	8.29	8.02	7.65	6.956	6.611	6.537	G2.0 VI	YH	7	SIMBA
08 00 02.15	-40 02 22.0	LHS 1968	58.20±11.00	9.65	8.83	8.06	7.045	6.459	6.266	K7.0 V	Y	4	YPC95
08 00 32.13	+29 12 44.3	LHS 242	59.32±0.76	7.00	6.60	6.24	5.539	5.170	5.095	G4.0 V	YH	7	Bid85

Table B.1: continued

RA (J2000.0)	DEC (2)	Name	Parallax (mas)	V	R	I	J	H	K	Spect. Type	π (12)	Ref. phot (13)	spect (14)
08 01 29.01	+10 43 04.2	LHS 1970	12.90 \pm 0.70	17.72	16.72	15.66	14.580	13.999	13.875	K—VI	Y	T	TB.R
08 03 06.12	+34 56 54.8	LHS 243	...	16.09	14.80	13.12	11.512	11.040	10.741	V?		12	REPM
08 11 57.56	+08 46 22.9	LHS 35	146.30 \pm 3.10	12.82	11.56	9.90	8.424	7.927	7.660	M4.5 V	Y	35	Haw96
08 13 27.81	−09 27 56.6	LHS 244	17.00 \pm 2.90	14.37	13.45	12.50	11.450	10.934	10.729	K/M—VI	Y	35	TB
08 18 23.92	−12 37 55.9	LHS 245	79.48 \pm 0.77	5.94	5.52	5.15	4.953	4.364	4.165	K0.0 V	YH	8	Hou88
08 25 52.82	+69 02 00.6	LHS 246	79.23 \pm 3.11	15.67	—	—	10.078	9.496	9.161	M5.5 V	Y U	11	Haw96
08 28 22.13	+35 00 59.1	Gl 308 B	53.65 \pm 5.18	—	—	—	—	—	—	—	YH	35	—
08 28 22.13	+35 00 59.1	Gl 308 A	53.65 \pm 5.18	10.731	9.791	8.791	7.6331	7.0473	6.8283	M0.0 V J	YH	35	Haw96
08 29 40.73	−01 44 48.1	LHS 2017	14.87 \pm 2.64	11.88	11.34	10.84	10.081	9.585	9.446	K3.0 V	YH	4	Bi885
08 29 49.35	+26 46 33.7	LHS 248	275.80 \pm 3.00	14.90	12.90	10.64	8.235	7.617	7.260	M6.5 V	Y	4	Hen94
08 32 51.49	−31 30 03.2	LHS 249	82.16 \pm 0.66	6.39	5.96	5.55	5.333	4.763	4.438	G9.0 V	YH	8	Bi885
08 35 49.11	+68 04 09.1	LHS 250	77.60 \pm 4.50	11.64	10.57	9.20	7.861	7.287	7.053	M2.5 V	Y	4	Haw96
08 36 25.55	+67 17 42.1	LHS 251	71.46 \pm 1.20	9.32	8.42	7.49	6.425	5.782	5.580	K7.0 V	YH	35	Haw96
08 41 20.13	+59 29 50.6	LHS 252	99.80 \pm 3.40	15.05	13.48	11.47	9.615	8.996	8.668	M5.5 V	Y	35	Haw96
08 41 32.44	−32 56 32.9	LHS 253	112.70 \pm 9.70	11.85	11.75	11.63	11.578	11.539	11.547	DA6.0	Y	4	TB.R
08 54 12.34	−08 05 00.2	LHS 254	...	17.41	15.51	13.44	11.560	11.083	10.810	M6.5 V		20	Gi697
08 55 07.62	+01 32 47.4	LHS 255	48.86 \pm 1.95	9.98	9.09	8.22	7.191	6.523	6.352	K7.0 V	YH	4	Haw96
08 55 24.82	+70 47 39.0	LHS 256	89.50 \pm 3.50	8.70	7.891	7.101	5.4311	4.7501D	4.5593	K5.0 V	Y	24	Bi885
08 59 05.30	−31 13 26.6	LHS 258	54.52 \pm 1.84	13.79	12.56	10.95	9.408	8.862	8.586	M3.5 V	C	T	TB.R
09 00 52.09	+48 25 24.7	LHS 259	50.70 \pm 3.30	14.14	12.99	11.50	10.080	9.551	9.320	M3.5 V	Y	35	Haw96
09 14 22.74	+52.41 11.2	LHS 260	162.13 \pm 2.37	7.55	6.81	5.94	4.779D	4.043D	4.136D	M0.0 V	YHH	7	Ki91
09 14 22.87	+52.41 11.9	LHS 261	162.13 \pm 2.37	7.71	6.87	5.99	4.889D	3.987D	3.988D	K7.0 V	YHH	7	Ki91
09 15 56.15	+53 25 23.7	LHS 262	97.30 \pm 1.90	13.85	13.63	13.51	13.308	13.211	13.133	DXP7.0	Y	4	Gr684
09 17 05.33	−77 49 23.4	LHS 263	122.02 \pm 2.55	13.16	11.86	10.16	8.329	7.768	7.448	M4.5 V	C	T	Hen02
09 17 30.67	+77 14 40.5	Gl 338.1B	42.80 \pm 4.40	—	—	—	—	—	—	—	Y	35	—
09 17 30.67	+77 14 40.5	Gl 338.1A	39.00 \pm 2.69	10.083	9.243	8.413	7.3981	6.7531	6.6023	K5.0 V J	YH	35	Haw96
09 17 46.00	+58 25 21.5	LHS 265	64.40 \pm 4.00	15.12	13.75	11.95	10.261	9.698	9.402	M4.5 V	Y	35	Haw96
09 20 21.93	+26 43 43.0	LHS 266	47.20 \pm 3.25	15.62	14.19	12.51	11.073	10.571	10.290	M4.5 V	Y U	T	Haw96
09 20 57.94	+03 22 06.5	LHS 267	60.80 \pm 4.10	13.52	12.17	10.70	9.363	8.798	8.520	M3.5 V	Y	T	Haw96
09 24 20.97	−80 31 21.3	LHS 268	16.53 \pm 0.98	10.15	9.80	9.43	8.886	8.526	8.464	— VI	YH	4	Rya91
09 29 11.09	+25 58 09.3	LHS 269	...	16.41	14.78	12.81	10.906	10.310	9.958	V		T	REPM
09 32 51.47	+51 40 38.0	Gl 354 B	74.06 \pm 0.73	13.80	—	—	—	—	—	—	YH	24.7	Gr885
09 32 51.47	+51 40 38.0	Gl 354 A	74.06 \pm 0.73	3.17	2.923	2.653	2.2803	2.0793	1.9703	F6.0 IV J	YH	7	YPC95
09 36 01.63	−21 39 38.8	LHS 2157	111.31 \pm 1.96	10.90	9.86	8.57	7.337	6.740	6.475	M3.0 V	YH	39	YPC95
09 38 53.83	−33 48 45.4	CE89	...	16.87	15.34	13.38	11.512	11.053	10.776	M5.5 V	3	T	TB
09 42 46.36	−68 53 06.1	LHS 271	156.80 \pm 1.70	12.74	11.39	9.65	7.953	7.385	7.037	M4.5 V	T	T	Hen02
09 43 46.17	−17 47 06.2	LHS 272	78.35 \pm 1.93	13.16	12.10	10.89	9.118	8.874	8.674	M—VI	C	T	TB.R
09 44 47.34	−18 12 48.9	LHS 273	90.19 \pm 2.97	12.39	11.20	9.64	8.122	7.536	7.257	M3.5 V	C	T	Hen02
09 46 48.45	+76 02 38.2	LHS 2188	63.61 \pm 1.32	10.64	9.69	8.59	7.437	6.841	6.629	M1.5 V	YH	35	Haw96
09 51 09.63	−12 19 47.6	LHS 274	73.57 \pm 5.70	10.06	9.13	8.11	6.988	6.400	6.150	M0.5 V	YH	4	Haw96
10 00 44.31	+32 18 33.8	LHS 276	36.46 \pm 2.14	11.88	10.96	9.92	8.780	8.207	8.005	M1.0 V	YH	35	Gi697
10 01 10.75	−30 23 24.5	LHS 277	62.99 \pm 2.28	11.44	10.36	8.97	7.598	6.994	6.700	M3.0 V	YH	19	Haw96
10 02 21.80	+48 05 19.5	LHS 278	67.22 \pm 1.58	10.10	9.17	8.13	6.948D	6.355D	6.160D	M1.0 V	YH	35	Haw96
10 05 54.93	−67 21 31.2	WT0248	38.55 \pm 2.47	14.52	13.40	11.95	10.556	10.099	9.870	M3.0 V	C	T	Hen02
10 09 16.90	+35 14 52.2	LHS 279	...	16.46	14.66	12.84	11.333	10.842	10.609	M5.5 V		12	Be91

Table B.1: continued

RA (J2000.0)	DEC (J2000.0)	Name	Parallax (mas)	V	R	I	J	H	K	Spect. Type	π	Ref. phot (13)	spect (14)
(1)	(2)	(3)	(4)	(5)	(6)	(7)	(8)	(9)	(10)	(11)	(12)	(13)	(14)
10 11 22.18	+49 27 15.3	LHS 280	205.81 \pm 0.67	6.59	5.74	4.97	3.894	3.298	2.962	K7.0 V	YH	20	Ki91
10 14 51.79	-47 09 24.1	LHS 281	85.99 \pm 2.05	13.49	12.26	10.69	9.245	8.666	8.322	M3.5 V	C	T	Haw96
10 25 23.93	00 43 02.0	LHS 282	7.70 \pm 8.40	18.14	17.71	17.26	16.810	16.480	16.360	DQ8.0	Y	T	McC99
10 35 27.16	+69 26 58.9	LHS 283	75.90 \pm 3.80	11.95	10.83	9.33	7.898	7.389	7.161	M3.5 V	Y	4	Haw96
10 36 03.10	-14 42 29.1	LHS 284	...	16.79	15.49	13.81	12.283	11.793	11.583	M4.5 V	Y	T	TB
10 37 02.71	+71 10 58.8	LHS 285	...	16.88	16.33	15.80	15.194	14.839	14.980	DK--	Y	21	McC99
10 37 28.89	+30 11 10.7	LHS 286	...	---	---	---	11.790	11.286	10.966	M6.0 V	Y	35	SIMBA
10 41 37.93	+37 36 39.1	LHS 287	96.70 \pm 2.30	12.98	11.72	10.07	8.493	8.005	7.714	M4.5 V	Y	35	Haw96
10 43 02.81	-09 12 40.8	WT1827	79.71 \pm 2.45	15.11	13.57	11.59	9.667	9.097	8.728	M5.0 V	C	T	TB
10 44 21.28	-61 12 35.5	LHS 288	206.66 \pm 3.21	13.94	12.31	10.27	8.492	8.054	7.728	M5.0 V	YC	T	TB.R
10 45 39.05	-19 06 52.9	LHS 289	56.90 \pm 12.00	15.52	15.03	---	14.620	14.410	14.360	DQ9.0	Y	3,4	McC99
10 45 39.10	-19 06 52.0	LHS 289	56.90 \pm 6.50	11.031	10.121	9.151	8.069	7.496	7.252	M0.5 V	Y	4	Haw96
10 45 59.69	+59 04 50.5	LHS 291	10.60 \pm 5.40	17.80	17.53	17.40	FFPF	FFPF	FFPF	DQ8.0	Y	21	Gre84
10 48 12.62	-11 20 09.7	LHS 292	220.30 \pm 3.60	15.70	13.62	11.21	8.857	8.263	7.926	M7.0 V	Y	27	TB.R
10 48 14.58	---	DEN1048-3956	250.46 \pm 1.74	17.39	15.06	12.57	9.538	8.905	8.447	M8.5 V	C	T	TB.R
10 49 45.56	+35 32 50.5	LHS 293	102.90 \pm 3.20	13.01	11.77	10.12	8.537	8.042	7.743	M4.5 V	Y	35	Haw96
10 50 52.02	+06 48 29.4	LHS 294	147.01 \pm 5.44	11.65	10.43	8.85	7.319	6.707	6.371	M4.0 V	YH	4	Ki91
10 52 04.25	+13 59 51.4	LHS 295	83.90 \pm 25.70	12.71	11.54	10.05	8.607	8.064	7.795	M3.5 V	Y	T	Haw96
10 56 28.91	+07 00 53.2	LHS 36	419.10 \pm 2.10	13.53	11.67	9.50	7.085	6.482	6.084	M6.0 V	Y	4	TB.R
11 01 19.65	+03 00 17.2	LHS 296	71.80 \pm 3.10	14.06	12.82	11.21	9.708	9.230	8.907	M4.0 V	Y	35	Haw96
11 03 20.21	+35 58 11.9	LHS 37	393.42 \pm 0.70	7.47	6.46	5.32	4.320ED	3.722ED	3.501ED	M2.0 V	YH	20	Ki91
11 05 28.72	+43 31 36.7	LHS 38	206.02 \pm 1.08	8.77	7.79	6.70	5.538	5.002	4.769	M1.0 V	YH	35	Hen94
11 05 31.02	+43 31 18.0	LHS 39	206.02 \pm 1.08	14.44	12.77	10.68	8.742	8.177	7.839	M5.5 V	YH	4	Hen94
11 10 08.38	+28 56 50.8	LHS 297	28.70 \pm 3.70	13.23	12.23	10.93	9.640	9.151	8.911	M3.5 V	Y	T	Bi85
11 11 10.71	-10 57 03.3	LHS 298	47.87 \pm 1.26	9.26	8.58	7.99	7.106	6.499	6.334	K3/4 V	YH	4	Hou88
11 11 13.70	-41 05 32.7	LHS 300	32.26 \pm 2.31	---	---	---	---	---	---	M4.0 V	C	T	TB.R
11 11 13.70	-41 05 32.7	LHS 300	32.26 \pm 2.31	13.171	12.251	11.471	10.4831	10.0131	9.8021	K/M-- VI J	C	T	TB.R
11 11 22.68	-06 31 56.4	LHS 299	12.00 \pm 2.90	14.78	13.85	12.94	11.924	11.373	11.143	K/M-- VI	Y	T	TB
11 16 00.19	-57 32 51.5	LHS 40	79.53 \pm 2.67	11.64	10.57	9.17	7.811	7.304	7.035	M3.5 V	YH	4	Haw96
11 20 05.09	+65 50 47.2	LHS 41	110.09 \pm 1.07	9.32	8.41	7.43	6.306	5.730	5.534	M0.0 V	YH	35	Haw96
11 21 38.48	+06 08 26.0	LHS 301	54.20 \pm 4.20	13.57	12.49	11.11	9.766	9.264	8.969	M3.5 V	Y	35	Gi97
11 23 07.96	+25 53 36.8	LHS 302	57.20 \pm 3.70	15.14	13.77	11.97	10.294	9.745	9.459	M5.0 V	Y	35	Haw96
11 23 44.58	+08 33 48.3	LHS 303	46.51 \pm 2.25	11.19	10.22	9.14	7.994	7.395	7.161	M0.5 V	YH	19	Haw96
11 24 12.98	+21 21 35.6	LHS 304	74.40 \pm 2.80	14.21	14.01	13.76	13.574	13.420	13.399	D47.0	Y	21	Gre84
11 28 00.49	-09 10 56.6	LHS 2412	39.64 \pm 2.94	12.37	11.43	10.38	9.289	8.739	8.494	M1.0 V	YH	T	Haw96
11 28 27.73	+07 31 02.2	LHS 305	38.22 \pm 1.71	10.24	9.49	8.82	7.818	7.228	7.061	K5.0 V	YH	7	Bi85
11 31 08.38	-14 57 21.3	LHS 306	88.66 \pm 1.72	14.19	12.80	11.05	9.359	8.764	8.497	M4.5 V	C	T	TB.R
11 32 45.31	+43 59 42.6	LHS 307	16.21 \pm 3.30	15.32	14.37	13.49	12.249	11.759	11.542	M0.5 VI	Y	4	Gi97
11 34 29.50	-32 49 52.7	LHS 308	104.84 \pm 0.81	5.971	5.521	5.101	4.784	4.138	4.022	K0.0 V	YH	8	Hou88
11 34 29.50	-32 49 52.7	LHS 309	104.84 \pm 0.81	---	---	---	---	---	---	DC--	YH	8	Hen02
11 40 20.27	+67 15 32.4	LHS 42	39.64 \pm 1.97	12.20	---	---	9.409	8.901	8.667	M0.0 VI	YHU	18	Gi97
11 42 11.05	+26 42 23.7	LHS 310	98.23 \pm 2.03	10.65	9.58	8.24	6.900	6.319	6.073	M3.0 V	YH	35	Ki91
11 45 42.96	-64 50 29.7	LHS 43	215.83 \pm 1.43	11.51	11.34	11.20	11.188	11.130	11.104	DQ6.0	YHC	T	TB.R
11 46 31.08	-40 30 01.3	LHS 311	108.18 \pm 0.70	4.891	4.521	4.161	3.931	3.490	3.489	G5.0 V	YH	8	CNS91
11 46 31.08	-40 30 01.3	LHS 313	108.18 \pm 0.70	---	---	---	---	---	---	M4.0 V	YH	8	Hen02
11 46 35.15	+50 52 54.8	LHS 312	12.82 \pm 1.49	9.91	9.55	9.20	8.678	8.375	8.306	G0.0 VI	YH	35	Gay97

Table B.1: continued

RA (J2000.0)	DEC	Name	Parallax (mas)	V	R	I	J	H	K	Spect. Type	π	Ref. phot (13)	spect (14)
11 46 42.91	-14 00 51.7	LHS 314	50.22± 2.94	11.69	10.64	9.28	7.965	7.275	7.069	M3.0 V	YH	4	Haw96
11 47 44.40	+00 48 16.6	LHS 315	298.72± 1.35	11.16	9.85	8.17	6.505	5.945	5.654	M4.0 V	YH	4	Hen94
11 50 57.78	+48 22 38.6	LHS 316	122.10± 2.90	13.24	11.91	10.17	8.488	7.952	7.637	M4.5 V	Y	35	Haw96
11 52 32.09	+27 30 51.3	LHS 2467	10.63± 1.88	12.24	11.70	11.18	10.445	9.916	9.806	— VI	YH	T	Rya91
11 52 58.75	+37 43 07.3	LHS 44	109.78± 0.70	6.42	6.01	5.60	4.937	4.500	4.373	G8.0 Vp	YH	18	YPC95
11 53 12.43	-31 23 56.1	LHS 317	63.40± 1.40	13.65	12.42	10.81	9.308	8.776	8.555	M4.0 V	1	T	Haw96
11 56 54.87	+26 39 56.3	LHS 318	...	15.45	14.49	13.56	12.503	11.983	11.797	VI	YH	T	REPM
11 57 56.21	-27 42 25.0	LHS 319	98.19± 0.88	6.99	6.32	5.78	4.992D	4.617D	4.325D	K4.0 V	YH	8	Bid85
12 02 33.66	+08 25 50.7	LHS 320	25.80± 3.60	14.00	13.03	11.87	10.740	10.184	9.986	M2.0 VI	Y	T	Giz97
12 02 40.13	+36 36 06.8	LHS 321	...	12.35	11.43	10.38	9.230	8.687	8.493	M0.5 V	YH	4	Bid85
12 15 10.55	-10 18 44.9	LHS 322	44.16± 1.00	6.11	5.89	5.63	5.132	5.004	4.839	F5.0 V	YH	7	Bid85
12 17 30.18	-29 02 20.7	LHS 323	...	16.93	15.66	14.00	12.544	12.050	11.778	M3.0 V?	Y	T	Rey02
12 18 59.41	+11 07 33.9	LHS 324	152.90± 3.00	13.80	12.31	10.34	8.525	7.880	7.570	M5.0 V	Y	35	Haw96
12 21 32.83	+28 54 22.6	LHS 325	13.572	13.201	13.116	M6.0 Ve	...	T	Bes91
12 23 56.21	-27 57 46.4	LHS 325a	...	18.39	16.42	14.20	11.977	11.401	11.069	M6.0 V	...	T	TB.R
12 24 26.81	-04 43 36.7	LHS 326	...	14.90	13.97	13.03	11.927	11.430	11.234	VI	...	T	REPM
12 24 52.49	-18 14 32.2	LHS 45	111.46± 1.68	11.27	10.23	8.92	7.734	7.247	6.950	M1.5 V	YHC	T	TB
12 25 50.74	-24 33 17.8	LHS 327	11.48± 2.10	12.71	12.15	11.60	10.813	10.306	10.144	K0.0 V	C	T	Bid85
12 28 39.92	-71 27 51.5	LHS 328	21.50±19.10	13.65	12.55	11.15	9.811	9.304	9.051	M3.0 V	Y	4	YPC95
12 28 42.98	-71 27 56.5	LHS 329	21.50±19.10	15.75	14.38	12.66	10.977	10.498	10.181	M4.5 V	Y	4	YPC95
12 29 14.20	+53 33 06.2	LHS 330	39.90± 1.00	18.45	12.202	11.697	11.369	M6.0 V	Y	20	Haw96
12 29 14.46	+53 32 44.9	LHS 331	39.90± 1.00	14.21	13.05	11.47	9.983	9.499	9.223	M3.0 V	Y	4	Haw96
12 29 34.54	-55 59 37.1	LHS 332	75.19± 1.77	13.23	12.02	10.41	8.890	8.354	8.065	M3.0 V	C	T	Haw96
12 31 15.80	+08 48 38.2	LHS 2570	74.31± 1.44	9.66	8.76	7.85	6.782	6.091	5.892	K7.0 V	YH	4	Haw96
12 32 32.17	-26 10 14.3	LHS 2573	...	13.49	12.41	11.05	9.752	9.229	9.020	M3.0 V	...	7	TB
12 33 17.41	+09 01 15.7	Gl 473 B	227.90± 4.60	—J	Y	T	—
12 33 17.41	+09 01 15.7	Gl 473 A	227.90± 4.60	12.46J	10.88J	8.92J	6.995J	6.397J	6.042J	M5.5 V J	Y	T	Hen92
12 34 15.78	+20 37 05.7	LHS 334	...	17.97	16.76	15.12	13.746	13.252	13.044	M4.5 VI	...	T	Jah01
12 34 53.18	+05 03 54.1	LHS 335	22.30± 5.40	16.60	15.64	14.71	13.646	13.143	13.000	VI	Y	T	HRDIA
12 37 52.27	-52 00 05.5	LHS 336	104.37± 2.05	10.67	9.59	8.24	6.864	6.285	6.020	M2.5 V	YH	4	TB.R
12 38 49.11	-38 22 53.8	LHS 337	145.91± 1.46	12.73	11.42	9.73	8.174	7.756	7.386	M4.5 V	C1	T	TB.R
12 38 52.43	+11 41 46.2	LHS 338	67.53± 2.51	11.51	10.41	8.98	7.581	6.939	6.691	M3.0 V	YH	4	Haw96
12 40 24.19	-23 17 43.8	LHS 339	...	16.53	16.12	15.73	15.354	15.080	14.936	DA—	...	T	TB.R
12 40 46.30	-43 33 59.1	LHS 340	127.54± 3.80	12.24	11.07	9.62	8.217	7.703	7.413	M3.0 V	YH	4	Hen02
12 47 56.66	+09 45 05.1	LHS 341	121.82± 2.84	11.39	10.22	8.68	7.135	6.666	6.362	M3.5 V	YH	4	Haw96
12 50 07.76	+54 47 06.1	LHS 342	39.60± 0.70	17.79	17.03	16.34	15.795	15.659	15.396	DC9.0	Y	21	McC99
12 56 23.74	+15 41 44.5	LHS 343	18.60± 3.70	13.87	13.00	12.31	11.355	10.861	10.664	K0.0 VI	Y	20	Giz97
13 00 09.07	+03 28 41.1	LHS 2661	60.30± 3.80	15.77	15.38	15.01	14.655	14.316	14.220	DC—	Y	4	Bid85
13 00 33.52	+05 41 08.1	LHS 2664	123.10± 3.50	13.41	12.05	10.28	8.553	7.966	7.660	M4.5 V	Y	4	Haw96
13 00 42.51	+19 12 34.5	2MA1300+1912	12.717	12.080	11.624	L1.0 V	...	T	Giz00
13 04 57.47	-52 26 34.7	LHS 344	63.19± 1.32	9.04	8.20	7.42	6.438	5.835	5.637	K5.0 V	YH	4	Hou88
13 08 39.57	+08 04 21.9	LHS 345	27.10± 3.40	15.07	13.82	12.19	10.702	10.195	9.959	V	Y	T	HRDIA
13 09 20.41	-40 09 27.0	LHS 346	61.25± 1.11	12.86	11.73	10.24	8.793	8.242	7.989	M3.5 V	C	T	Haw96
13 10 01.80	+22 30 05.3	LHS 347	18.77± 4.90	12.44	11.76	11.14	10.261	9.709	9.588	K0.0 V	C	T	Bid85
13 11 52.39	+27 52 41.2	LHS 348	108.87± 0.69	4.26	3.94	3.63	3.232	2.992	2.923	G0.0 V	YH	7	Gra01
13 13 09.35	-41 30 39.7	ER2	83.58± 1.58	12.91	11.61	9.96	8.292	7.684	7.412	M5.0 V	C	T	TB

Table B.1: continued

RA (J2000.0)	DEC (J2000.0)	Name	Parallax (mas)	V	R	I	J	H	K	Spect. Type	π	Ref. phot (13)	spect (14)
(1)	(2)	(3)	(4)	(5)	(6)	(7)	(8)	(9)	(10)	(11)	(12)	(13)	(14)
13 12 59.70	-47 28 06.6	ER8	66.50±2.40	17.13	16.41	15.72	15.210	15.110	15.030	DC9.0	Y	3	McC99
13 18 24.31	-18 18 40.6	LHS 349	117.35±0.69	4.72	4.33	3.97	3.334	2.974	2.956	G5.0 V	YH	8	Hou88
13 22 56.74	+24 28 03.4	LHS 350	73.10±2.70	12.96	11.77	10.21	8.728	8.162	7.957	M4.0 V	Y	35	Haw96
13 29 21.31	+11 26 26.7	LHS 351	62.90±6.70	12.11	11.05	9.64	8.368	7.820	7.535	M3.5 V	Y	4	Haw96
13 29 59.77	+10 22 37.9	LHS 352	132.57±1.18	9.05	8.07	7.01	5.902	5.300	5.036	M1.0 V	YH	4	Hen94
13 30 02.79	-08 42 25.6	LHS 353	67.30±4.90	14.33	13.01	11.29	9.599	9.047	8.749	M4.0 V	Y	4	Haw96
13 30 13.64	-08 34 29.4	LHS 354	59.56±2.25	12.39	12.40	12.40	12.621	12.677	12.736	DA5.0	YH	4	Gre84
13 30 31.06	+19 09 34.1	LHS 355	68.70±4.40	14.71	13.39	11.67	10.065	9.543	9.221	M4.5 V	Y	35	Haw96
13 36 31.85	+03 40 46.1	LHS 46	121.40±3.40	14.61	14.09	13.63	13.064	12.819	12.690	DZ9.0	Y	4	CNS91
13 37 17.37	+35 01 01.5	LHS 356	13.307	12.877	12.621	m	Y	4	LUYTN
13 39 15.35	+15 40 57.9	LHS 2774	34.40±5.00	14.27	13.13	11.70	10.333	9.815	9.574	M4.0 V	Y	T	TB
13 40 08.87	+43 46 38.2	LHS 357	62.70±3.80	12.78	11.61	10.07	8.544	8.017	7.745	M3.5 V	Y	4	Haw96
13 41 11.49	+30 01 26.1	LHS 358	48.10±1.90	15.83	...	12.80	11.184	10.742	10.478	M4.5 V	Y	23	Haw96
13 45 05.08	+17 47 07.5	LHS 359	77.11±1.38	9.81	8.92	8.04	6.997	6.401	6.220	K5.0 V	YH	35	Haw96
13 45 43.74	+14 53 29.4	LHS 47	184.21±1.16	8.46	7.50	6.39	5.181	4.775	4.415	M1.5 V	YH	35	Hen94
13 46 55.52	+05 42 56.4	LHS 360	...	15.16	14.27	13.41	12.390	11.849	11.662	K/M—VI	Y	T	TB
13 48 03.02	+23 34 46.3	LHS 361	82.90±2.20	15.65	13.07	14.53	13.921	13.669	13.621	DC9.0	Y	35	McC99
13 48 13.42	+23 36 48.6	LHS 362	82.90±2.20	15.32	13.83	11.87	10.082	9.506	9.179	M5.5 V	Y	35	Haw96
13 49 44.82	-22 06 40.0	LHS 363	70.57±1.00	8.17	7.42	6.78	5.919	5.323	5.160	K4/5 V	YH	8	Hou88
14 01 03.19	-02 39 17.6	LHS 2842	98.39±1.54	9.68	8.73	7.65	6.516	5.935	5.683	M1.0 V	YH	4	Haw96
14 06 55.58	+38 36 56.1	LHS 364	37.40±4.30	14.56	13.56	12.62	11.466	11.015	10.860	M1.5 VI	Y	4	Giz97
14 15 16.04	+47 47 26.2	LHS 365	...	16.41	15.41	14.32	13.121	12.662	12.448	VI	Y	7	REPM
14 15 32.55	+04 39 31.4	LHS 366	71.70±3.40	14.30	12.95	11.10	9.433	8.936	8.618	M5.0 V	Y	35	Haw96
14 15 39.68	+19 10 55.9	LHS 48	88.78±0.68	-0.12	-0.76	-1.34	-2.252	-2.810	-2.911	K1.5 III	YH	4	Kee89
14 18 20.43	-52 24 12.6	LHS 367	...	13.20	12.34	11.51	10.500	9.981	9.786	K—VI	Y	T	TB
14 19 11.01	-07 18 12.0	LHS 368	51.90±4.40	13.48	12.39	10.99	9.665	9.233	8.917	M3.0 V	Y	4	Haw96
14 20 07.36	-09 37 13.4	LHS 369	71.68±1.37	12.84	11.69	10.15	8.740	8.191	7.976	M3.5 V	Y C	T	Haw96
14 20 52.95	+36 57 17.2	LHS 370	...	16.28	14.73	12.84	11.054	10.553	10.254	M5.0 V	Y	T	Bes91
14 25 43.48	+23 37 01.4	LHS 371	61.89±1.22	9.76	8.86	7.91	6.769	6.162	5.973	M0.0 V	YHH	35	Haw96
14 25 46.65	+23 37 13.7	LHS 372	61.89±1.22	10.01	9.08	8.07	6.889	6.302	6.091	M0.5 V	YHH	35	Haw96
14 29 29.72	+15 31 57.8	LHS 373	69.80±2.00	10.68	9.67	8.46	7.229	6.605	6.393	M2.0 V	YH	35	Haw96
14 29 42.96	-62 40 46.7	LHS 49	770.37±0.43	11.05	9.43	7.43	5.357	4.835	4.384	M5.5 V	YHC4	4	Hen97
14 30 47.73	-08 38 46.7	LHS 374	61.06±1.50	9.38	8.51	7.66	6.616	6.007	5.769	K7.0 V	YH	4	Haw96
14 31 38.25	-25 25 32.9	LHS 375	41.70±1.00	15.62	14.57	13.35	12.150	11.674	11.507	M4.0 VI	Y	27	Giz97
14 35 08.89	+16 53 54.4	LHS 376	20.80±5.00	15.08	13.96	12.49	11.132	10.630	10.377	M3.5 V	Y	T	Giz97
14 39 00.31	+18 39 38.8	LHS 377	28.40±0.70	18.39	...	14.91	13.194	12.733	12.479	M7.0 VI	Y	23	Giz97
14 39 28.16	+19 29 14.0	2MA1439+1929	64.80±3.30	21.04	18.32	16.12	12.759	12.041	11.546	L1.0 V	U	9	Giz00
14 39 36.49	-60 50 02.3	LHS 50	745.13±0.90	0.01	-0.35	-0.68	-1.4547	-1.886J	-2.008J	G2.0 V	YSH	4	CNS91
14 39 35.08	-60 50 13.8	LHS 51	745.13±0.90	1.34	0.87	0.46	K0.0 V	YSH	4	CNS91
14 47 25.35	-17 42 15.8	LHS 378	69.00±4.00	16.34	15.89	15.44	14.948	14.640	14.724	DC9.0	Y	T	CNS91
14 49 31.48	-26 06 32.5	LHS 379	63.48±7.57	12.07	11.08	9.92	8.661	8.132	7.893	M1.5 V	YHH	4	Haw96
14 49 33.27	-26 06 20.8	LHS 380	63.48±7.57	11.68	10.70	9.62	8.438	7.864	7.640	M1.0 V	YHH	4	Haw96
14 50 28.87	-08 38 36.8	LHS 381	27.40±5.40	15.14	14.17	13.12	11.970	11.460	11.237	K7.0 V	Y	35	YPC95
14 50 41.22	-16 56 30.8	LHS 382	21.41±2.58	15.30	14.61	13.17	11.848	11.377	11.111	M4.0 V	C	T	TB
14 51 40.48	-24 18 14.9	LHS 383	59.14±1.04	7.82	7.23	6.74	5.990	5.493	5.385	K3.0 V	YH	8	Hou88
14 55 11.11	+53 40 49.2	LHS 384	41.84±0.63	7.77	7.32	6.90	6.268	5.893	5.798	K1.0 V	YH	4	Bid85

Table B.1: continued

RA (J2000.0)	DEC (J2000.0)	Name	Parallax (mas)	V	R	I	J	H	K	Spect. Type	π (12)	Ref. phot (13)	spect (14)
14 55 35.83	-15 33 44.0	LHS 385	20.40± 5.80	14.61	16.67	12.78	11.738	11.277	11.062	M0.0 V	Y	T	YPC95
14 57 15.07	-21 21 50.5	LHS 387 D	169.85± 0.82	—	—	20.94s	15.324	15.268	15.242	T8.0 V	YHS	9	Bur02
14 57 26.55	-21 24 41.2	LHS 387 C	169.85± 0.82	—	—	—	—	—	—	—	YHS	8	Hen94
14 57 26.55	-21 24 41.2	LHS 386	169.85± 0.82	—	—	—	4.550J	3.910J	3.802J	M1.0 V J	YHS	8	Hen94
14 57 27.99	-21 24 55.4	LHS 387	169.85± 0.82	5.64J	4.94J	4.30J	3.663	3.085	3.048	K4.0 V J	YHS	8	Hou88
14 57 32.29	+31 23 44.9	LHS 388	29.09± 4.95	11.15	10.31	9.48	8.444	7.818	7.657	K7.0 V	YH	35	Haw96
15 03 14.29	+35 12 45.8	LHS 3016	18.10± 3.40	14.19	13.28	12.65	11.484	10.927	10.726	VI	Y	35	HRDIA
15 03 24.59	+03 46 57.3	LHS 389	47.00± 4.10	12.04	11.14	10.22	9.225	8.669	8.426	K7.0 V	Y	T	Haw96
15 06 14.27	-37 25 20.2	LHS 390	15.00± 8.70	12.53	11.73	11.01	10.133	9.597	9.420	K5.0 V	Y	T	Bid85
15 06 54.35	+13 21 06.1	2MA1506+1321	...	—	—	—	13.365	12.380	11.741	L3.0 V	Y	—	Giz00
15 07 23.59	+24 56 07.9	LHS 391	59.80± 3.60	10.05	9.19	8.32	7.296	6.647	6.474	K7.0 V	Y	35	Haw96
15 10 13.08	-16 22 46.0	LHS 53	33.83± 0.90	9.04	8.60	8.15	7.526	7.176	6.978	K0.5 V	YHH	4	Hou88
15 10 12.96	-16 27 46.6	LHS 52	33.83± 0.90	9.42	8.92	8.45	7.761	7.275	7.147	K0.0 V	YHH	4	Bid85
15 11 50.61	-10 14 18.0	LHS 387	67.40± 3.10	14.26	12.95	11.26	9.651	9.127	8.867	M4.5 V	Y	35	Haw96
15 13 50.89	-01 21 05.1	G1 580 B	57.79± 0.83	—	—	—	—	—	—	—	YH	8	—
15 13 50.89	-01 21 05.1	G1 580 A	57.79± 0.83	6.59J	6.17J	5.79J	5.286J	4.986J	4.766J	K0.0 V J	YH	8	Bid85
15 14 54.41	-31 50 13.8	LHS 3045	...	14.39	13.53	12.74	11.764	11.232	10.997	K5.0 V?	Y	T	Bid85
15 19 26.83	-07 43 20.3	LHS 394	157.48± 1.64	10.55	9.44	8.04	6.706	6.095	5.837	M2.5 V	YHC	T	Hen94
15 21 48.19	-48 19 03.4	LHS 395	68.67± 0.79	5.65	5.29	4.94	4.308	3.898	4.159	G3/5 V	YH	8	Hou88
15 23 51.14	+17 27 57.3	LHS 396	85.10± 2.90	13.72	12.43	10.72	9.105	8.620	8.279	M4.5 V	Y	4	Haw96
15 28 13.99	+16 43 10.8	LHS 3073	17.00± 3.80	14.12	12.96	12.79	11.138	10.586	10.397	K7.0 V I	Y	T	Giz97
15 32 12.97	-41 16 32.2	LHS 397	168.36± 1.38	9.31	8.25	6.92	5.647D	5.025	4.759D	M2.0 V	YH	4	TB.R
15 34 27.75	+02 16 47.5	LHS 398	16.00± 3.80	15.24	14.27	13.28	12.201	11.711	11.502	VI	Y	35	HRDIA
15 35 20.34	+17 43 04.5	LHS 400	70.30± 2.10	14.94	13.56	11.82	10.282	9.800	9.519	M4.5 V	Y	4	Haw96
15 35 20.53	+17 42 47.0	LHS 399	70.30± 2.10	12.34	11.26	9.95	8.694	8.149	7.940	M2.5 V	Y	4	Haw96
15 39 39.06	-55 09 10.0	LHS 401	38.40± 9.60	12.72	11.87	11.11	10.151	9.598	9.407	M0.0 V	Y	T	CNS91
15 40 03.59	+43 29 39.4	LHS 402	74.20± 4.80	12.24	11.12	9.77	8.312C	7.777C	7.563	M3.0 V	Y	T	Haw96
15 40 03.81	+43 29 35.3	LHS 403	74.20± 4.80	14.22	12.87	11.23	8.893C	9.999	8.202C	M3.5 V	Y	T	Haw96
15 41 16.47	+75 59 34.3	LHS 404	75.66± 1.90	12.23	11.11	9.68	8.260	7.716	7.442	M3.0 V	YH	4	Haw96
15 41 28.86	+68 25 10.0	LHS 3103	26.00± 3.30	14.36	—	—	10.827	10.316	10.105	V	Y	10	HRDIA
15 42 06.56	-19 28 18.4	LHS 54	101.80± 4.38	11.88	10.77	9.34	7.920	7.421	7.168	M3.0 V	YH	4	TB.R
15 43 03.10	-10 56 00.8	LHS 405	17.16± 0.83	7.21	6.85	6.53	6.014	5.696	5.588	A5.0 Ib	YH	7	Hou88
15 43 18.33	-20 15 32.9	LHS 406	47.47± 1.74	13.06	12.07	10.93	9.780	9.232	9.018	M1.5 V	C	T	TB.R
15 45 40.21	-20 36 16.7	LHS 407	33.50± 2.00	16.57	15.51	14.18	12.820	12.336	12.087	M5.0 VI	Y	30	Giz97
15 56 27.19	+15 39 41.7	LHS 408	89.85± 0.71	3.85	3.53	3.29	3.149	2.875	2.703	F6.0 V	YH	7	Gra01
15 57 13.10	+05 05 59.6	LHS 409	24.81± 3.08	15.30	14.20	12.83	11.539	11.079	10.814	M3.5 V	YY	35	Bid85
15 57 14.71	+05 07 02.6	LHS 410	24.81± 3.08	13.36	12.42	11.35	10.225	9.735	9.472	M1.0 V	YY	35	Giz97
16 02 50.95	+20 35 21.1	LHS 411	100.30± 3.10	12.57	11.33	9.73	8.132	7.648	7.369	M4.0 V	Y	4	Haw96
16 08 14.96	-10 26 14.4	LHS 412	47.10± 2.70	14.69	13.43	11.78	10.257	9.749	9.529	M4.5 V	Y	T	Haw96
16 13 48.62	-57 34 13.8	LHS 413	72.68± 0.82	7.53	7.05	6.59	5.888	5.395	5.293	— VI	YH	8	Rya91
16 14 26.29	+02 14 49.1	LHS 414	35.30± 2.90	14.79	13.70	12.27	10.928	10.458	10.164	M4.0 V	Y	35	TB
16 14 32.64	+19 06 10.8	LHS 55	55.90± 3.30	12.87	11.77	10.32	8.990	8.478	8.262	M3.5 V	Y	T	Giz97
16 20 03.52	-37 31 44.5	LHS 415	118.69± 2.22	10.60	9.52	8.16	6.793	6.223	5.950	M2.5 V	YH	4	TB.R
16 20 03.19	-37 31 48.1	LHS 416	118.69± 2.22	14.15	12.74	10.92	8.339C	7.765C	7.650C	M5.0 V	YH	4	Haw96
16 24 09.25	+48 21 10.6	LHS 417 B	124.72± 1.13	15.57	—	—	—	—	—	—	YH	2	Hen94
16 24 09.25	+48 21 10.6	LHS 417	124.72± 1.13	10.28	9.25J	7.95J	6.635J	6.141J	5.915J	M2.5 V J	YH	35	Hen94

Table B.1: continued

RA (J2000.0)	DEC (J2000.0)	Name	Parallax (mas)	V	R	I	J	H	K	Spect. Type	π	Ref. phot (13)	spect (14)
(1)	(2)	(3)	(4)	(5)	(6)	(7)	(8)	(9)	(10)	(11)	(12)	(13)	(14)
16 25 13.95	+15 40 54.2	LHS 418	18.80 \pm 3.20	13.44	12.59	11.81	10.805	10.246	10.072	K7.0 V	Y	T	Gi297
16 30 18.08	-12 39 45.4	LHS 419	26.01 \pm 1.67	10.10	8.94	7.42	5.950	5.373	5.075	M3.0 V	YH	4	Hen94
16 30 28.45	+04 10 41.7	LHS 420	24.44 \pm 0.89	7.29	---	---	6.159	5.862	5.809	F8.0 V	YH	32	Bid85
16 34 20.36	+57 09 44.7	LHS 421	69.20 \pm 2.50	12.91	11.67	9.99	8.501	8.039	7.796	M4.5 V	Y	20	Haw96
16 34 21.59	+57 10 09.0	LHS 422	50.49 \pm 3.29	14.99	14.68	14.38	14.110	14.077	14.135	DQ8.0	Y	21	Gr684
16 35 40.40	-30 51 20.2	LHS 423	50.49 \pm 3.29	12.66	11.58	10.16	8.887	8.359	8.075	M3.0 V	C	T	Haw96
16 37 05.42	-01 32 00.5	LHS 424	20.80 \pm 3.60	14.17	13.31	12.50	11.518	11.057	10.803	K/M---VI	Y	T	TB
16 42 04.33	+10 25 58.7	LHS 425	25.80 \pm 5.00	15.10	14.10	12.94	11.741	11.251	11.003	M2.0 VI	Y	T	Gi297
16 52 58.79	+00 01 35.0	LHS 426	59.10 \pm 0.86	6.63	6.22	5.84	5.235	4.942	4.835	G5.0 V	YH	8	Bid85
16 55 25.23	-08 19 21.4	LHS 427	154.97 \pm 0.56	11.80	10.59	9.05	7.535	7.056	6.724	M3.5 V	YSYH	4	Kir91
16 55 28.77	-08 20 10.9	GI 644 B	154.97 \pm 0.56	---	---	---	---	---	---	---	---	4	Hen94
16 55 28.77	-08 20 10.9	GI 644 D	154.97 \pm 0.56	---	---	---	---	---	---	---	---	4	Hen94
16 55 35.35	-08 23 40.8	GI 644 A	154.97 \pm 0.56	9.03J	7.94J	6.56J	5.270JD	4.775J	4.403J	M2.5 V J	YSYH	4	Hen94
17 04 22.34	+16 55 55.6	LHS 430	58.20 \pm 3.20	16.78	14.60	12.18	9.776	9.201	8.816	M7.0 V	YSYH	4	TB
17 05 03.41	-05 03 59.4	LHS 431	93.88 \pm 0.98	7.73	11.22	9.89	8.571	8.073	7.795	M2.5 V	Y	35	Haw96
17 05 13.79	-05 08 39.4	LHS 432	93.89 \pm 0.98	10.08	7.01	6.38	5.522	4.942	4.726	K5.0 V	YHYH	8	Bid85
17 12 07.81	+45 39 58.0	LHS 433	156.57 \pm 1.19	9.37J	9.11	7.96	6.780	6.193	5.975	M2.0 V	YHYH	4	Haw96
17 12 07.81	+45 39 58.0	LHS 434	40.01 \pm 2.72	10.18	---	---	---	---	---	M3.5 V J	YSH	35	Haw96
17 14 08.78	+60 47 30.0	LHS 435	---	---	---	8.59	7.550	6.918	6.763	K5.0 V	YH	35	Bid85
17 15 20.91	-26 36 08.1	LHS 437	167.51 \pm 0.75	4.32J	3.84J	3.40J	2.518J	2.013J	1.840J	m	YHYH	8	LiUYTN
17 16 13.36	-26 32 46.1	LHS 439	167.51 \pm 0.75	6.32	5.62	5.04	4.155	99999	---	K1.0 Ve	YHYH	8	CNS91
17 18 25.59	-43 26 37.6	LHS 440	36.90 \pm 2.20	12.98	11.98	10.86	9.704	9.134	8.948	K5.0 Ve	YHYH	8	CNS91
17 20 39.56	+32 28 03.9	LHS 441	69.53 \pm 0.56	5.39	5.04	4.71	4.160	3.905	3.911	G0.0 V	YH	7	Gr601
17 18 57.09	-34 59 23.9	GI 667 B	138.22 \pm 0.70	---	---	---	---	---	---	K5.0 V	YSH	8	CNS91
17 18 58.80	-34 59 48.6	GI 667 C	138.22 \pm 0.70	5.90J	5.26J	4.71J	3.903J	3.230J	3.123J	K3.0 V	YSH	8	CNS91
17 19 02.96	-46 38 13.3	LHS 445	114.17 \pm 1.34	---	---	---	---	---	---	M2.0 V	YSH	20	TB.R
17 19 03.76	-46 38 10.9	LHS 444	114.17 \pm 1.34	5.47J	5.00J	4.54J	4.077u	5.112	4.856D	K7.0 V	YH	8	Haw96
17 20 46.27	+49 15 20.4	LHS 446	58.60 \pm 4.90	14.53	13.29	11.70	10.124	9.641	9.376	G8.0 V	Y	4	Haw96
17 23 45.24	+02 06 41.2	LHS 447	129.57 \pm 0.91	7.53	6.69	5.93	4.934	4.341	4.370	K7.0 V	YH	8	Hen94
17 27 39.89	+14 29 02.0	LHS 448	50.10 \pm 2.60	13.70	---	---	9.693	9.218	8.958	M3.5 V	Y	13	Hen94
17 28 07.33	-62 27 14.2	LHS 3292	61.11 \pm 1.50	12.74	11.54	9.95	8.422D	7.847D	7.567D	M3.5 V	C	T	TB
17 28 39.93	-46 53 42.9	LHS 449	220.25 \pm 1.59	9.37	8.30	6.97	5.711	5.154	4.855	M2.5 V	YH	8	TB.R
17 36 25.93	+68 20 21.2	LHS 450	220.49 \pm 0.82	9.17	8.08	6.68	5.335	4.766	4.548	M3.0 V	YH	35	Haw96
17 37 03.66	-44 19 09.2	LHS 451	199.65 \pm 2.30	10.95	9.71	8.12	6.544	5.917	5.606	M4.5 V	YH	4	TB.R
17 37 53.34	+18 35 30.1	LHS 452	123.66 \pm 1.49	9.61	8.63	7.55	6.360	5.790	5.572	M0.0 V	YH	35	Hen94
17 39 51.75	+51 27 17.5	LHS 453	10.30 \pm 0.90	18.02	---	---	14.633	14.126	14.076	M3.5 VI	Y	23	Gi297
17 42 10.75	-08 49 00.5	LHS 3315	42.90 \pm 3.20	13.52	12.45	11.08	9.812	9.324	9.065	M3.0 V	Y	13	Haw96
17 46 34.25	-57 19 08.7	LHS 454	171.69 \pm 2.14	10.76	9.60	8.18	6.855	6.297	6.016	M3.5 V	YH	4	TB.R
17 48 08.12	+70 52 36.0	LHS 455	164.70 \pm 2.40	14.22	13.68	13.14	12.709	12.528	12.507	DXPe.0	Y	4	Gr684
17 49 50.54	+82 46 26.1	LHS 56	63.90 \pm 2.90	14.34	14.12	13.87	13.634	13.472	13.431	DAY.0	Y	3	Gr684
17 50 58.97	-56 36 07.0	LHS 456	39.20 \pm 12.60	12.08	11.13	10.08	8.994	8.422	8.187	M2.0 V	Y	28	YPC95
17 57 48.51	+04 41 36.4	LHS 57	54.42 \pm 0.67	9.57	8.35	6.79	5.244	4.834	4.524	M4.0 V	YH4	4	Kir91

Table B.1: continued

RA (J2000.0)	DEC	Name	Parallax (mas)	V	R	I	J	H	K	Spect. Type	π	Ref. phot	spect
(1)	(2)	(3)	(4)	(5)	(6)	(7)	(8)	(9)	(10)	(11)	(12)	(13)	(14)
17 58 22.91	+14 17 37.8	LSR1758+1417	...	16.30	16.12	16.69	14.931	14.659	14.659	DA10.		T	Lep03
18 02 46.27	+37 31 03.0	LHS 487	83.50 \pm 3.90	14.80	13.40	11.55	9.720	8.887	8.887	M5.0 V	Y	35	Haw96
18 05 27.35	+02 29 58.8	LHS 458	199.70 \pm 3.40	4.02J	3.51J	3.06J	2.343J	1.876J	1.791JD	K0.0 Ve	Y	8	CNS91
18 05 27.35	+02 29 58.8	LHS 459	49.00 \pm 3.40	---	---	---	---	---	---	K5.0 Ve	Y	8	CNS91
18 09 50.14	-02 47 43.2	LSR1809-0247	...	16.25	14.87	13.04	11.426	10.924	10.675	M5.0 V		T	Lep03
18 17 06.49	+13 28 25.0	LSR1817+1328	...	15.88	15.37	14.88	14.377	14.100	14.075	DA10.		T	Lep03
18 17 15.07	+68 33 19.0	LHS 460	53.70 \pm 3.30	15.39	14.06	12.35	10.783	10.283	10.036	M5.0 V	Y	35	Gi297
18 18 03.42	+38 46 34.3	LHS 461	88.40 \pm 3.60	13.54	12.29	10.71	9.197D	8.629D	8.370D	M4.0 V	Y	35	Haw96
18 18 04.24	+38 46 32.6	LHS 462	88.40 \pm 3.60	11.88	10.78	9.42	8.040D	7.487D	7.222D	M3.0 V	Y	35	Haw96
18 20 57.18	-01 02 58.1	LHS 463 B	31.39 \pm 6.14	---	---	---	---	---	---	M3.0 V	C	27	TB.R
18 20 57.18	-01 02 58.0	LHS 463	42.43 \pm 5.27	12.63J	11.49J	10.04J	8.754J	8.186J	7.949J	M2.5 V J		T	TB.R
18 22 06.68	+06 20 37.7	LHS 464	68.90 \pm 2.20	12.60	11.48	10.63	8.671	8.132	7.935	M3.5 V	Y	4	Haw96
18 22 27.15	+62 03 01.8	LHS 465	121.50 \pm 2.20	13.46	12.12	10.35	8.640	8.047	7.743	M4.5 V	Y	4	Haw96
18 26 11.06	+30 14 18.9	LSR1826+3014	...	13.36	17.40	14.35	11.659	11.175	10.811	M8.5 V		22	Lep02
18 35 43.20	-08 16 06.2	LHS 466	4.20 \pm 9.20	13.78	12.93	12.14	11.091C	10.413	10.132	K5.0 V	Y	T	Bid85
18 41 36.37	+00 55 13.8	LHS 467	32.00 \pm 2.17	12.19	11.33	10.52	9.523	8.995	8.781	K7.0 VI		T	Gi297
18 42 46.69	+59 37 49.4	LHS 58	283.00 \pm 1.69	9.69	7.83	6.48	5.189D	4.741D	4.432D	M3.0 V	YH H	35	Ki191
18 42 46.91	+59 37 36.9	LHS 59	283.00 \pm 1.69	8.57	7.33	7.13	5.721D	5.197D	5.000D	M3.5 V	YH H	35	Ki191
18 48 44.87	-02 33 45.7	LHS 468	35.00 \pm 4.40	13.57	12.57	11.39	10.164	9.654	9.417	M1.0 V	Y	T	Bid85
18 53 39.92	-38 36 44.5	LHS 469	74.70 \pm 11.80	12.65	11.46	9.87	8.396	7.818	7.589	M3.5 V	Y	T	Haw96
18 58 00.14	+05 54 29.2	LHS 470	90.14 \pm 1.43	9.21	8.28	7.81	6.239	5.587	5.357	M0.5 V	YH	4	Haw96
19 07 42.97	+32 32 41.5	Gi 747 B	122.30 \pm 2.50	---	---	---	---	---	---	M3.0 V	Y	35	-
19 07 42.97	+32 32 41.5	Gi 747 A	122.30 \pm 2.50	11.26J	10.10J	8.64J	7.242J	6.66J	6.416J	M3.0 V J	Y	35	Haw96
19 12 14.60	+02 53 11.0	LHS 472 B	99.24 \pm 1.78	---	---	---	---	---	---	M3.5 V	YH	4	-
19 12 14.60	+02 53 11.0	LHS 472	99.24 \pm 1.78	11.10J	9.99J	8.52J	7.087J	6.572J	6.294J	M3.5 V J	YH	4	Ki191
19 16 55.25	+05 10 08.1	LHS 473	171.01 \pm 0.62	9.10	8.07	6.78	5.583D	4.929	4.673	M2.0 V	YH	4	TB.R
19 16 57.61	+05 09 01.6	LHS 474	171.01 \pm 0.62	17.20	15.10	12.84	9.908	9.226	8.765	M8.0 V	YH	4	TB.R
19 20 47.97	-45 33 29.7	LHS 60	169.17 \pm 1.53	12.23	10.94	9.26	7.661	7.130	6.845	M4.5 V	Y C	4	TB.R
19 20 54.37	-82 33 16.1	LHS 475	77.62 \pm 2.27	12.68	11.50	10.00	8.555	8.004	7.686	M3.0 V	C	T	Haw96
19 21 38.70	+20 52 03.2	LHS 476	100.10 \pm 3.50	13.37	12.09	10.43	8.796	8.219	7.935	M4.5 V	Y	35	TB.R
19 32 21.56	+69 39 40.4	LHS 477	173.59 \pm 0.41	4.67	4.34	3.95	3.423	3.039	2.900	K0.0 V	YH	25.7	CNS91
19 45 45.49	+27 07 31.7	Gi 766 B	93.06 \pm 3.74	---	---	---	---	---	---	M4.0 V J	YS	35	Haw96
19 45 45.49	+27 07 31.7	Gi 766 A	93.06 \pm 3.74	12.37J	11.12J	9.52J	7.998J	7.410J	7.144J	M4.0 V J	YS	35	Gi297
19 46 48.61	+12 04 59.3	LHS 479	21.70 \pm 2.70	14.26	13.29	12.28	11.182	10.658	10.448	M1.0 VI	Y	T	Haw96
19 54 00.13	-47 48 37.3	LHS 480	39.60 \pm 8.50	12.53	11.52	10.27	9.076	8.536	8.286	M2.5 V	Y	4	TB.R
19 56 57.61	-42 16 23.0	APMPM1957	...	---	---	---	---	---	---	M5.5 V		T	Lep03
20 00 05.70	+30 57 32.2	LSR2000+3057	...	16.62	14.72	12.63	10.674	10.114	9.778	M6.0 Ve		T	Lep03
20 03 52.12	+23 20 26.6	LHS 481	63.68 \pm 0.69	7.27	6.84	6.42	5.671	5.172	5.113	K2.0 V	YH	7	Bid85
20 04 01.95	-65 35 58.3	LHS 3612	74.70 \pm 8.90	12.83	11.71	10.24	8.871	8.378	8.129	M3.5 V	Y	4	Haw96
20 04 04.74	-65 36 01.2	LHS 3613	74.70 \pm 8.90	11.35	10.34	9.06	7.796	7.284	7.057	M2.5 V	Y	4	Re95
20 05 02.23	+54 28 03.2	LHS 482	60.90 \pm 2.08	12.00	11.03	9.36	8.830	8.346	8.113C	M1.5 VI	YH	35	How88
20 05 32.83	-67 19 15.3	LHS 484	56.43 \pm 0.74	6.08	5.71	5.36	5.108	4.724	4.511	G3.0 V	YH	8	Gr684
20 05 34.88	-10 56 54.6	LHS 483	57.70 \pm 0.80	16.95	16.36	15.86	15.276	14.995	14.746	DC9.0	Y	3	CNS91
20 08 43.70	-66 10 55.5	LHS 485	153.78 \pm 0.65	3.55	3.14	2.79	2.299	2.041	1.933	G8.0 V	YH	8	CNS91
20 11 12.05	-36 06 05.4	LHS 486	165.33 \pm 0.90	5.31J	4.79J	4.31J	3.518	2.999	3.008	K3.0 V	YH	8	CNS91
20 11 12.05	-36 06 05.4	LHS 487	165.33 \pm 0.90	---	---	---	---	---	---	M2.5 V	YH	8	TB.R

Table B.1: continued

RA (J2000.0)	DEC (J2000.0)	Name	Parallax (mas)	V	R	I	J	H	K	Spect. Type	π	Ref. phot (13)	spect (14)
20 15 17.38	-27 01 58.7	LHS 488	113.35 \pm 0.89	5.73	5.23	4.81	4.112	3.582	3.501	K0.0 V	YH	8	CNS91
20 19 04.57	+12 35 04.1	LHS 489	18.10 \pm 4.20	15.33	14.43	13.60	12.531	12.057	11.852	M0.0 VI	Y	T	Giz97
20 23 35.85	-21 22 14.1	LHS 490	23.37 \pm 1.21	8.67	—	—	7.500	7.219	7.144	F7.0 V	YH	33	Hou88
20 27 29.08	+35 59 24.8	LHS 491	20.40 \pm 4.20	14.75	13.75	12.69	11.596	11.102	10.869	M1.5 VI	Y	35	Giz97
20 27 42.08	-56 27 25.2	LHS 492	50.53 \pm 2.14	12.20	11.19	9.93	8.697	8.161	7.915	M2.5 V	C	T	Haw96
20 28 03.81	-76 40 15.9	LHS 493	79.09 \pm 2.24	13.96	12.76	11.11	9.359	8.875	8.600	M4.5 V	C	T	Haw96
20 33 40.31	+61 45 13.7	LHS 494	63.00 \pm 2.70	12.54	11.35	9.80	8.287	7.657	7.397	M4.0 V	Y	35	Haw96
20 36 21.62	+51 00 05.3	LSR2036+5059	...	—	—	—	13.611	13.160	12.936	M7.5 VI	Y	35	Lep03
20 40 33.86	+15 29 58.9	LHS 495	102.00 \pm 2.20	13.45	12.10	10.36	8.641	8.075	7.749	M4.5 V	Y	35	TB.R
20 42 18.78	-52 41 57.5	LHS 496	82.57 \pm 1.25	8.81	7.98	7.23	6.274	5.665	5.474	M5.0 V	H	8	Haw96
20 42 57.14	-18 55 06.2	GI 800 B	62.50 \pm 6.96	—	—	—	—	—	—	—	YH	—	—
20 42 57.14	-18 55 06.2	GI 800 A	62.50 \pm 6.96	10.80J	9.86J	8.76J	7.557J	6.949J	6.739J	M1.5 V	YH	4	Haw96
20 43 19.24	+55 20 53.0	LHS 498	63.00 \pm 5.50	14.69	13.26	11.36	9.563	9.058	8.753	M5.0 V	Y	35	Haw96
20 51 41.73	-79 18 39.9	LHS 499	63.00 \pm 11.70	11.83	10.83	9.65	8.459	7.908	7.664	M1.5 V	Y	4	Haw96
20 55 37.11	-14 03 54.8	LHS 500	81.89 \pm 1.53	14.61	13.25	11.46	9.717	9.218	8.915	M5.0 V	Y C	4	Haw96
20 55 37.76	-14 02 08.1	LHS 501	77.57 \pm 1.48	12.46	11.34	9.62	8.117	7.638	7.365	M4.0 V	Y C	4	Haw96
20 56 46.59	-10 26 54.8	LHS 502	55.81 \pm 6.27	11.50	10.44	9.11	7.766	7.142	6.884	M2.5 V	YH	4	Haw96
20 57 40.08	-44 07 45.8	LHS 503	46.30 \pm 0.81	6.51	6.17	5.83	5.446	5.153	5.018	G0.0 V	YH	8	Bid85
21 01 04.80	+03 07 04.7	USNO2101+0307	...	18.99	16.72	14.37	11.704	10.961	10.567	M7.0 V	T	T	TB
21 04 25.37	-27 52 46.8	LHS 3620	...	—	—	—	13.410	12.891	12.696	K/M— VI	YH	4	Haw96
21 04 53.38	-16 57 32.2	LHS 61	56.14 \pm 2.62	11.45	10.50	9.42	8.285	7.744	7.545	M1.0 V	YH	4	Haw96
21 05 14.03	-24 46 51.9	LHS 504	...	—	—	—	13.355	12.889	12.630	K/M— VI	YH	18	Kir91
21 06 53.84	+38 44 57.9	LHS 62	286.04 \pm 0.56	5.20	4.54	3.93	3.114	2.540	2.248	K5.0 V	YH	20	Kir91
21 06 55.16	+38 44 31.5	LHS 63	286.04 \pm 0.56	6.03	—	4.41	3.546	2.895	2.544	K7.0 V	Y	35	Rei95
21 07 55.41	+59 43 19.4	LHS 64	41.80 \pm 2.70	13.23	12.26	11.20	10.122	9.583	9.390	M1.5 VI	YH	4	Haw96
21 09 17.43	-13 18 09.1	LHS 65	82.08 \pm 2.04	10.87	9.91	8.83	7.688	7.121	6.909	M1.0 V	YH	4	Haw96
21 11 57.86	-31 03 16.0	LHS 505	...	—	—	—	11.622	11.101	10.844	M3.5 V	YH	33	Bid85
21 13 34.09	-19 19 46.3	LHS 506	11.91 \pm 2.85	11.76	—	—	9.390	8.749	8.598	K4.0 V	YH	14	YPC95
21 17 15.27	-38 52 02.6	LHS 66	253.43 \pm 1.12	6.87	5.77	4.91	4.046	3.256	3.100D	M0.0 V	YH	20	Hen94
21 21 34.80	-19 03 38.6	LHS 507	14.20 \pm 4.00	15.21	—	—	12.659	12.242	12.053	M— VI	YH	4	Hen94
21 29 36.80	+17 38 35.9	LHS 508 B	148.25 \pm 1.73	—	—	—	—	—	—	—	YH	20	Hen94
21 29 36.80	+17 38 35.9	LHS 508	148.25 \pm 1.73	10.31J	9.20J	7.73J	6.249J	5.737J	5.453J	M3.5 V J	YH	20	Hen94
21 30 02.76	-12 30 36.3	LHS 509	55.52 \pm 1.40	9.10	8.32	7.60	6.656	5.990	5.881	K5.0 V	YH	4	Haw96
21 30 47.66	-40 42 29.5	LHS 510	83.60 \pm 2.52	13.12	11.92	10.34	8.870	8.419	8.134	M3.5 V	C	T	TB.R
21 31 18.64	-09 47 26.4	GI 831 B	125.79 \pm 2.29	—	—	—	—	—	—	—	YH	4	—
21 31 18.64	-09 47 26.4	GI 831 C	125.79 \pm 2.29	—	—	—	—	—	—	—	YH	4	—
21 31 18.64	-09 47 26.4	GI 831 A	125.79 \pm 2.29	12.04J	10.74J	9.04J	7.316J	6.701J	6.379J	M4.5 V J	YH	4	Hen94
21 38 43.65	-33 39 55.3	LHS 512	82.02 \pm 2.10	12.55	11.36	9.87	8.437	7.843	7.574	M3.5 V	C	27	Haw96
21 39 00.91	-24 09 29.0	LHS 513	73.30 \pm 12.00	13.45	12.27	10.70	9.185	8.609	8.359	M4.0 V	Y	4	Haw96
21 40 53.05	+78 49 21.4	LHS 514	24.80 \pm 2.40	13.28	12.30	11.11	9.940	9.391	9.180	V	Y	35	HRDIA
21 55 47.95	-11 21 42.8	LHS 515	19.50 \pm 4.00	17.41	—	—	13.639	13.186	12.912	M— VI	Y	15	TB.R
21 55 57.11	-45 39 34.3	LHS 3732	...	14.19	—	—	11.716	11.137	11.003	K3.0 VI	Y	33	IBa97
21 56 55.25	-01 54 09.3	LHS 516	74.80 \pm 3.20	14.65	13.29	11.50	9.880	9.315	9.026	M5.0 V	Y	35	Haw96
21 58 53.18	-57 56 03.5	LHS 3740	...	14.11	—	—	9.853	9.271	8.997	M3.0 V	YH	33	TB
22 03 21.60	-56 47 09.7	LHS 67	275.84 \pm 0.69	4.68	4.06	3.54	2.894	2.349	2.237	K5.0 Ve	YH	8	CNS91
22 04 10.56	-56 46 58.1	LHS 67 Ba	275.84 \pm 0.69	—	—	—	11.908J	11.306J	11.208J	T1.0 V	YH	—	McC04

Table B.1: continued

RA (1)	DEC (2)	Name (3)	Parallax (mas) (4)	V (5)	R (6)	I (7)	J (8)	H (9)	K (10)	Spect. Type (11)	π (12)	Ref. phot (13)	spect (14)
22 04 10.56	-56 46 58.1	LHS 67 Bb	275.84± 0.69	---	---	---	---	---	---	T6.0 V	YH	-	McC04
22 04 40.92	-19 46 42.0	LHS 3754	...	---	---	---	10.541	10.151	9.853	---	---	---	---
22 09 40.34	-04 38 26.8	LHS 517	114.35± 1.77	10.39	9.30	7.88	6.510	5.899	5.594	M3.5 V	YH	4	TB.R
22 13 42.88	-17 41 08.8	LHS 3776	96.00± 3.90	13.57	12.27	10.57	8.955	8.422	8.115	M4.5 V	Y	35	TB.R
22 14 34.73	-38 59 07.3	WD2214-390	...	---	---	---	14.892	14.644	14.557	WD	---	---	Opp01
22 20 26.97	-24 21 49.5	LHS 518	21.68± 5.38	---	---	---	11.038	10.594	10.393	K/M-- VI	C	---	TB.R
22 22 35.85	-50 48 26.9	LHS 519	35.07± 1.30	8.79	---	---	7.080	6.621	6.510	K2.0 V	YH	33	Hou88
22 24 36.89	-72 15 19.4	GI 855.1B	34.58± 0.60	---	---	---	---	---	---	---	---	---	CNS91
22 24 36.89	-72 15 19.4	GI 855.1A	34.58± 0.60	5.27J	4.87J	4.46J	4.146J	3.586J	3.543JD	G0.0 V J	YH	8	CNS91
22 27 59.21	-30 09 32.8	LHS 521	21.60± 1.59	14.68	13.84	13.11	12.129	11.656	11.463	K-- VI	C	27	TB
22 28 49.03	+05 48 13.8	LHS 522	22.80± 2.60	14.15	13.31	12.53	11.584	11.104	10.927	K7.0 VI	Y	4	Giz97
22 28 54.37	-13 25 19.4	LHS 523	88.80± 4.90	16.90	14.90	12.56	10.768	10.217	9.843	M6.5 V	Y	4	Haw96
22 29 48.96	+41 28 48.6	LHS 524	72.50± 2.90	13.24	12.01	10.40	8.849	8.326	8.039	M4.0 V	Y	35	Haw96
22 30 33.55	-75 15 24.2	J2231-7515	65.53± 5.16	16.90	16.19	15.56	14.858	14.824	14.723	WD	C	T	Sch02
22 30 40.00	-75 13 55.3	J2231-7514	69.77± 4.78	16.59	15.95	15.36	14.662	14.658	14.436	WD	C	T	Sch02
22 32 56.74	+53 47 40.5	GI 863.1B	43.10± 4.30	13.50	---	---	---	---	---	---	---	---	---
22 32 56.74	+53 47 40.5	GI 863.1A	43.10± 4.30	10.10J	9.27J	8.47J	7.458J	6.915J	6.686J	K5.0 V	Y	35	Haw96
22 34 53.68	-01 04 58.0	LHS 526	42.50± 3.70	14.83	13.56	11.91	10.388	9.775	9.518	M4.5 V	Y	35	Haw96
22 38 33.59	-15 17 59.3	GI 866 A	289.50± 4.40	12.37J	10.70J	8.64J	6.553J	5.954J	5.537J	M6.5 V J	Y	4	TB.R
22 38 33.59	-15 17 59.3	GI 866 B	289.50± 4.40	---	---	---	---	---	---	---	---	---	TB.R
22 38 33.59	-15 17 59.3	GI 866 C	289.50± 4.40	---	---	---	---	---	---	---	---	---	TB
22 41 41.00	-32 58 48.6	LHS 527	37.10± 2.50	---	---	---	12.019	11.522	11.205	M5.5 V	Y	---	TB
22 42 38.74	+17 40 09.2	LHS 528	48.20± 2.65	11.76	10.71	9.39	8.062	7.378	7.182	M2.5 V	YH	35	Haw96
22 51 23.01	+29 39 44.3	LHS 529	47.80± 4.20	15.54	15.14	14.75	14.316	13.983	13.941	DA9.0	Y	21	Gre84
22 53 16.75	-14 15 49.2	LHS 530	212.59± 1.96	10.19	8.98	7.39	5.934	5.349	5.010	M3.5 V	YH	T	Hen94
22 53 53.35	-06 46 54.5	LHS 531	123.70± 4.30	15.71	15.10	14.56	14.013	13.685	13.546	DZ9.0	Y	21	CNS91
22 55 45.37	-75 27 31.4	LHS 532	116.10± 1.32	10.38	9.31	7.95	6.616	6.084	5.811	M2.5 V	YH	4	TB.R
22 56 24.66	-60 03 49.2	LHS 532	75.45± 0.98	14.01	12.60	10.81	8.984	8.360	8.108	M5.0 V	C3	28	TB.R
22 56 34.82	+16 33 12.3	LHS 533	145.79± 1.13	8.65	7.67	6.55	5.360	4.800	4.523	M1.3 V	YH	4	Hen94
23 05 51.92	-35 51 11.3	LHS 70	303.64± 0.87	7.84	6.37	5.32	4.338	3.608	3.465	M1.0 V	YH	8	TB.R
23 06 35.80	+71 43 25.5	LHS 534	...	11.78	10.77	9.56	8.336	7.805	7.564	M2.5 V	Y	35	Haw96
23 07 30.00	+68 40 05.1	LHS 535	65.50± 3.60	12.45	11.36	9.97	8.624	8.095	7.919	M3.5 V	Y	35	Haw96
23 08 26.05	+31 40 23.9	LHS 536	22.40± 3.00	14.67	13.74	12.78	11.714	11.182	10.982	M0.5 VI	Y	35	Giz97
23 09 32.95	+00 42 39.5	LHS 537	18.60± 4.60	9.92	9.49	9.06	8.465	8.054	7.977	G0.0 VI	Y	T	Giz97
23 10 42.16	-19 13 34.9	LHS 538	41.14± 2.31	12.47	11.48	10.26	8.976	8.461	8.232	M2.0 V	C	33	Haw96
23 13 16.94	+57 10 06.0	LHS 71	153.41± 0.54	5.53	5.01	4.53	3.981	3.469	3.261	K3.0 V	YH	15	CNS91
23 15 51.60	-37 33 30.6	LHS 539	52.85± 2.01	14.98	13.66	11.96	10.403	9.872	9.592	M3.5 V	C	T	TB
23 17 05.03	-13 51 03.9	LHS 540 C	14.47± 2.13	---	---	---	---	---	---	---	---	---	---
23 17 05.03	-13 51 03.9	LHS 540	14.47± 2.13	8.18J	7.88J	7.54J	7.082J	6.860J	6.771J	G-- VI J	YH	4	Daw00
23 17 06.03	-13 50 52.5	LHS 541	14.47± 2.13	16.46	15.49	14.37	13.032C	12.559C	12.414C	K/M-- VI	YH	4	TB.R
23 19 09.52	-06 12 50.0	LHS 542	32.00± 3.70	18.15	17.53	16.99	16.306	15.837	15.200	DC9.0	U	3	Gre84
23 21 37.44	+17 17 25.3	LHS 543	93.41± 2.61	11.55	10.46	8.89	7.391	6.771	6.507	M4.0 V	YH	35	Haw96
23 25 40.24	+53 08 06.0	LHS 543a	40.40± 3.10	14.59	---	---	---	9.878	9.284	M4.5 V	Y	13	Haw96
23 31 22.20	+59 09 55.9	LHS 544	59.18± 0.66	6.74	6.30	5.91	5.346	4.975	4.797	G8.0 V	YH	7	Bin85
23 34 03.33	+00 10 45.9	LHS 545	72.60± 3.42	11.18	10.15	8.89	7.664	7.070	6.828	M2.5 V	YH	4	Haw96
23 35 10.47	-02 23 20.8	LHS 546	138.30± 3.50	14.67	13.07	11.03	9.148	8.505	8.183	M5.5 V	Y	35	Hen94

Table B.1: continued

RA (J2000.0)	DEC (J2000.0)	Name	Parallax (mas)	V	R	I	J	H	K	Spect. Type	π (12)	Ref. phot (13)	spect (14)
(1)	(2)	(3)	(4)	(5)	(6)	(7)	(8)	(9)	(10)	(11)	(12)	(13)	(14)
23 36 51.77	+01 09 52.6	LHS 548	28.60±15.20	13.08	12.07	10.91	9.759	9.255	9.012	M1.5 V	Y	4	Haw96
23 36 52.30	-36 28 51.8	LHS 547	86.23± 2.03	13.76	12.46	10.79	9.191	8.666	8.422	M4.5 V	C	T	Haw96
23 41 55.00	+44 10 38.9	LHS 549	316.00± 1.10	12.29	10.77	8.82	6.884	6.247	5.929	M4.5 V	Y	35	Hen94
23 43 13.64	-24 09 52.1	LHS 72	37.60± 8.90	12.11	11.31	10.54	9.605	9.041	8.817	K4.0 V	Y	35	Bid85
23 43 16.73	-24 11 16.4	LHS 73	37.60± 8.90	12.81	11.97	11.14	10.112	9.586	9.373	K/M— V1	Y	35	TB.R
23 49 12.52	+02 24 04.4	LHS 550	168.51± 1.40	8.98	8.03	6.95	5.827	5.282	5.043	M1.5 V	YH	4	TB.R
23 57 44.11	+23 18 16.8	LHS 551	72.80± 2.70	11.72	10.60	9.16	7.800	7.321	7.060	M3.5 V	Y	35	Haw96
23 59 27.88	-16 56 41.1	LHS 552	28.40±10.10	8.96	—	—	7.471	7.069	6.955	K0.0 V	Y	33	Hou88
23 59 51.38	-34 06 42.5	LHS 4058	60.80± 4.47	12.20	—	—	8.590	7.979	7.748	M3.0 V	C	33	Haw96

Note.—99999: null is shown in 2MASS JHK data. C: affected by confusion with another nearby source, d: deconvolved magnitudes, D: affected by a nearby diffraction spike, E: two data was shown for one star. One close to the centroid is choosen, F: too faint to be shown in 2MASS, J: joint magnitude, P: affected by a nearby persistence artifact, u: not to be believed, Ref.— Parallax references. C: CTIOPI, H: European Space Agency (1997), S: Soderhjelm (1999), U: USNO, Y: van Altena et al. (1995), IAI: Ianna et al. (1994), IAI2: Ianna et al. (1996), IAN: Ianna, P. A. (unpublished), BEN: Benedict et al. (1999).
 Photometry references. 1: Alonso et al. (1994), 2: Barbieri et al. (1996), 3: Bergeron et al. (2001), 4: Bessell (1990), 5: ten Brummelaar et al. (2000), 6: Carney (1983), 7: CNS3-website (2004), 8: various Cousin's photometry references noted from Bessell (1990), 9: Dahn et al. (2002), 10: Dahn et al. (1982), 11: Dahn et al. (1988), 12: Dawson and Forbes (1989), 13: Harrington and Dahn (1980), 14: Harrington et al. (1985), 15: Harrington et al. (1993), 16-18: European Space Agency (1997), 19: Koen et al. (2002), 20: Leggett (1992), 21: Leggett et al. (1998), 22: Lepine et al. (2002a), 23: Monet et al. (1992), 24: Nstar-website (2004), 25: Oja (1985), 26: Oppenheimer et al. (2001b), 27: Patterson, R. J. (unpublished), 28: Patterson et al. (1998), 29: Reid et al. (2002), 30: Ruiz and Anguita (1993), 31: Ryan (1989), 32: Sandage and Kowal (1986), 33: SIMBAD, 34: this work, 35: Weis (1996), 36: van Altena et al. (1995)
 Spectroscopy references. Bert01: Bergeron et al. (2001), Bes91: Bessell (1991), Bid85: Bidelman (1985), Bur02: Burgasser et al. (2002), CNS91: Giese and Jahnke (1991), Chrt99: Christy and Walker (1969), Daw00: Dawson and De Robertis (2000), Giz00: Gizis et al. (2000), Giz97: Gizis (1997), Gre84: Greenstein (1984), Gra01: Gray et al. (2001), Gra85: Gray and Nagar (1985), Ham97: Hambly et al. (1997), Haw96: Hawley et al. (1996), Hen92: Henry et al. (1992), Hen94: Henry et al. (1994), Hen97: Henry et al. (1997), Hen02: Henry et al. (2002), Hou88: Houk (1988), HRDI: from the H-R diagram in Fig 4.8, IBa97: Iba and Irwin (1997), Jah01: Jahnke et al. (2001), Kun84: Kunkel et al. (1984), Kee89: Keenan and McNeil (1989), Kir91: Kirkpatrick et al. (1991), Lep03: Lepine et al. (2003b), Lep02: Lepine et al. (2002a), LUYTN: Luyten (1979a), Mar99: Martin et al. (1999), McC99: McCook and Stion (1999), McC04: McCaughrean et al. (2004), Opp01: Oppenheimer et al. (2001a), Rei95: Reid et al. (1995), Rey02: Reyé et al. (2002), REPM: from the reduced proper motion diagram Fig 3.4, Rya91: Ryan and Norris (1991), SIMBA: SIMBAD, Sch02: Scholz et al. (2002), Cay97: Cayrel de Strobel et al. (1997), TB.R: revised spectroscopy by this work, TB: this work, YPC95: van Altena et al. (1995)

Appendix C

Least Squares Method for DCR

The least squares method is applied to solving for the mean refraction R_m as a third order polynomial function of $(V - I)$. Hereafter, R_m is re-defined as y_{ij} where i is plate number and j is the star number ID; x_{ij} is the color for each star.

We have n different fields, and each plate has m_i stars ($i = 1 \sim n$). Because the mean $(V - I)$ for each plate is different, the zero order coefficient for each plate will be different from a_1 to a_n . However, the higher order coefficients, b , c and d , will remain the same for all the plates.

$$\begin{aligned} y_{ij} &\approx a_i + bx_{ij} + cx_{ij}^2 + dx_{ij}^3, i = 1 \sim n, \\ f(x_{ij}) &= a_i + bx_{ij} + cx_{ij}^2 + dx_{ij}^3 - y_{ij}. \end{aligned} \quad (C.1)$$

Therefore,

$$\frac{\partial f^2}{\partial a_i} = 2(a_i + bx_{ij} + cx_{ij}^2 + dx_{ij}^3 - y_{ij}) = 0, \quad (C.2)$$

$$\frac{\partial f^2}{\partial b} = 2(ax_{ij} + bx_{ij}^2 + cx_{ij}^3 + dx_{ij}^4 - y_{ij}x_{ij}) = 0, \quad (C.3)$$

$$\frac{\partial f^2}{\partial c} = 2(ax_{ij}^2 + bx_{ij}^3 + cx_{ij}^4 + dx_{ij}^5 - y_{ij}x_{ij}^2) = 0, \quad (C.4)$$

$$\frac{\partial f^2}{\partial d} = 2(ax_{ij}^3 + bx_{ij}^4 + cx_{ij}^5 + dx_{ij}^6 - y_{ij}x_{ij}^3) = 0. \quad (C.5)$$

From equation (C.2), the coefficient a_1 can be presented as

$$\begin{aligned}
a_1 + bx_{11} + cx_{11}^2 + dx_{11}^3 - y_{11} &= 0, \\
a_1 + bx_{12} + cx_{12}^2 + dx_{12}^3 - y_{12} &= 0, \\
&\dots\dots\dots \\
a_1 + bx_{1m_1} + cx_{1m_1}^2 + dx_{1m_1}^3 - y_{1m_1} &= 0.
\end{aligned} \tag{C.6}$$

The conventional least squares method requires the zero order coefficient be the same for all the plates. In order to apply regular least squares method, the zero order coefficient can be calculated by summing all the derivatives in equation (C.6),

$$a_1 = \frac{\sum_{j=1}^{m_1} y_{1j}}{m_1} - \left(b \frac{\sum_{j=1}^{m_1} x_{1j}}{m_1} + c \frac{\sum_{j=1}^{m_1} x_{1j}^2}{m_1} + d \frac{\sum_{j=1}^{m_1} x_{1j}^3}{m_1} \right) \tag{C.7}$$

and from equation (C.3) to (C.5),

$$\begin{aligned}
a_1 \sum_{j=1}^{m_1} x_{1j} + b \sum_{j=1}^{m_1} x_{1j}^2 + c \sum_{j=1}^{m_1} x_{1j}^3 + d \sum_{j=1}^{m_1} x_{1j}^4 &= \sum_{j=1}^{m_1} y_{1j} x_{1j}, \\
a_1 \sum_{j=1}^{m_1} x_{1j}^2 + b \sum_{j=1}^{m_1} x_{1j}^3 + c \sum_{j=1}^{m_1} x_{1j}^4 + d \sum_{j=1}^{m_1} x_{1j}^5 &= \sum_{j=1}^{m_1} y_{1j} x_{1j}^2, \\
a_1 \sum_{j=1}^{m_1} x_{1j}^3 + b \sum_{j=1}^{m_1} x_{1j}^4 + c \sum_{j=1}^{m_1} x_{1j}^5 + d \sum_{j=1}^{m_1} x_{1j}^6 &= \sum_{j=1}^{m_1} y_{1j} x_{1j}^3,
\end{aligned} \tag{C.8}$$

By substituting equation (C.7) into equation (C.8), the zero order coefficient can be removed and this linear equation can be solved for coefficients b, c, and d after we sum over the i for all the plates.

Therefore,

$$\begin{bmatrix} s_{11} & s_{12} & s_{13} \\ s_{21} & s_{22} & s_{23} \\ s_{31} & s_{32} & s_{33} \end{bmatrix} \begin{bmatrix} b \\ c \\ d \end{bmatrix} = \begin{bmatrix} t_{11} \\ t_{21} \\ t_{31} \end{bmatrix} \tag{C.9}$$

where,

$$\begin{aligned}
s_{11} &= \sum_i^n \sum_j^{m_i} x_{ij}^2 - \sum_i^n \left(\frac{\sum_j^{m_i} x_{ij} \sum_j^{m_i} x_{ij}}{m_i} \right), \\
s_{12} &= \sum_i^n \sum_j^{m_i} x_{ij}^3 - \sum_i^n \left(\frac{\sum_j^{m_i} x_{ij} \sum_j^{m_i} x_{ij}^2}{m_i} \right), \\
s_{13} &= \sum_i^n \sum_j^{m_i} x_{ij}^4 - \sum_i^n \left(\frac{\sum_j^{m_i} x_{ij} \sum_j^{m_i} x_{ij}^3}{m_i} \right), \\
s_{22} &= \sum_i^n \sum_j^{m_i} x_{ij}^4 - \sum_i^n \left(\frac{\sum_j^{m_i} x_{ij}^2 \sum_j^{m_i} x_{ij}^2}{m_i} \right), \\
s_{23} &= \sum_i^n \sum_j^{m_1} x_{ij}^5 - \sum_i^n \left(\frac{\sum_j^{m_i} x_{ij}^2 \sum_j^{m_i} x_{ij}^3}{m_i} \right), \\
s_{33} &= \sum_i^n \sum_j^{m_1} x_{ij}^6 - \sum_i^n \left(\frac{\sum_j^{m_i} x_{ij}^3 \sum_j^{m_i} x_{ij}^3}{m_i} \right),
\end{aligned} \tag{C.10}$$

with $s_{21} = s_{12}$, $s_{31} = s_{13}$, and $s_{32} = s_{23}$.

$$\begin{aligned}
t_{11} &= \sum_i^n \sum_j^{m_i} y_{ij} x_{ij} - \sum_i^n \frac{\sum_j^{m_i} x_{ij} \sum_j^{m_i} y_{ij}}{m_i}, \\
t_{21} &= \sum_i^n \sum_j^{m_i} y_{ij} x_{ij}^2 - \sum_i^n \frac{\sum_j^{m_i} x_{ij}^2 \sum_j^{m_i} y_{ij}}{m_i}, \\
t_{31} &= \sum_i^n \sum_j^{m_i} y_{ij} x_{ij}^3 - \sum_i^n \frac{\sum_j^{m_i} x_{ij}^3 \sum_j^{m_i} y_{ij}}{m_i}
\end{aligned} \tag{C.11}$$

After b, c and d are obtained from equation (C.9), a_i can be solved for each plate from equation (C.7).

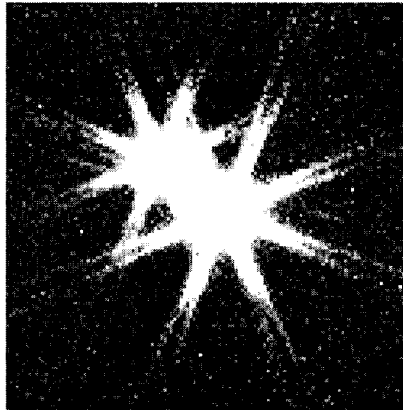
Appendix D

CTIOPI Photometry Reduction Manual

Revision History

1. 04/20/03 by Wei-Chun Jao. Add remark section.
2. 08/05/03 by Wei-Chun Jao. New evalfit.pl script released for matching CTIOPI/SMARTS photometry catalogue.
3. 08/07/03 by John Subasavage. Add cosmicray section.
4. 08/28/03 by Wei-Chun Jao. New standard.pl script released for matching CTIOPI/SMARTS photometry catalogue.

CTIOPI Photometry Reduction Manual



Wei-Chun Jao
Georgia State University

08/28/2003

D.1 Before It Starts

Before starting to reduce photometry, you need to know a little background of photometry (i.e., extinction, airmass, transformation equation etc.). **Astronomical Photometry** written by Henden and Kaitchuck is a good introductory book for those who are getting a first look at photometry. Users also have to be familiar with IRAF. User guides can be found in IRAF's website – <http://iraf.noao.edu/docs/photom.html>, especially:

1. **A User's Guide to Stellar CCD Photometry with IRAF;**
2. **A User's Guide to CCD Reductions with IRAF.**

This manual will skip these introductory parts and start with processed data. Please read the **Parallax Reduction Guide** (Appendix E) to learn how to process the raw data for CTIO.

Have all the finder charts, observing log (if available) and airmass table (a bird's eye view of all the objects observed in that night) ready.

D.2 Organize Your Processed Data

Load packages **daophot**, **photcal**, **redpi** before you begin anything¹. After processing raw data, you will need to fix the image header immediately. Load the **astutil/setairmass** task. See Figure D.1. Edit **setairmass** parameters for the correct observatory site. Run this task to calculate airmass at the middle exposure. A new header keyword, **utmiddle**, will be added in the header. If any of the following headers are missing, *date-obs*, *RA*, *ST*, *epoch* or *airmass*, then **setairmass** won't work. You need add those header-keywords back to the header by using **hedit** task.

Sort these data into two directories, **standard** and **science**.

Run **files *.o.fits >> listfile** in IRAF for both standard and science images. Then, run the **displayexam** task to select the images without saturated stars. This step is important for the data reduction, since photometry for saturated stars can't be determined. Furthermore, IRAF won't generate annoying "INDEF"s in the data file. In the meantime, you can determine the average seeing (FWHM) for this night's data. This average FWHM will be entered in the **phot** task. If the observing log is

¹Patterson, R. J. *et al* (1998) show that no significant difference was found between IRAF/APPHOT and IRAF/DAOPHOT, although **APPHOT** is used for aperture photometry.

available, you may select those good frames and the average seeing based on those recorded in log book. For example, if a field is observed in V, R and I, choose the best one in I band in order to reduce some output problems from IRAF. Otherwise, the same V and R images will need to be used twice to make two sets of VRI. If a field is observed in V, V, R, R, I and I, two sets of VRI can be chosen so that you will have two sets of photometry results calculated from IRAF. One additional step is to determine which star frames will need an aperture correction. This is a good time to make a note whether each frame can use the standard 7'' radius aperture and if not, what the maximum aperture without contamination is. Standards rarely need an aperture correction; however, science stars are often in crowded fields and require the correction.

D.3 Standard Stars

The basic steps for reducing uncrowded standard stars fields are as follows.

1. Determine the aperture size you wish to use. This aperture size will be applied to all the standard stars from all the nights for all the filters. Edit the **datapars**, **centerpars**, **fitsskypars** and **photpars** tasks parameters in the **phot** task.
2. Use the **redpi/apercorr** task to tag the standard stars so instrumental magnitudes can be calculated.
3. Organize the standard star configuration file and collect your standard stars' VRI instrumental magnitudes.
4. Apply transformation equations to get apparent magnitudes for standard stars.

An aperture size is key to aperture photometry reductions. You need to select a "suitable" aperture size to cover the brightness profile. Most of the standard stars we choose in CTIO are Landolt (1992) standard stars which are now included in the Astronomical Almanac in 2003. The aperture size he uses is 7'' in radius and 14'' in diameter. Therefore, the aperture size we choose should not be less than 7'' in radius. However, it highly depends on the FWHM of your images. Usually, if a image with $\text{FWHM} < 4$ pixels in radius, the aperture size will be 12 to 15 pixels in radius according to IRAF manuals.

The main IRAF task used to finish this aperture photometry is **phot**. This task has been included in **redpi/apercorr option 3** task; **phot** is a task which invokes other tasks inside including **datapars**, **centerpars**, **fitskypars** and **photpars**.

D.3.1 Modify Parameters in *PHOT* Task

When you load the **redpi/apercorr** task, there will be 4 options. You need to select option 4 for standard stars because standard stars are usually in uncrowded fields, so no aperture correction will be applied. After choosing option 4, you will need to modify the following parameters in each of these tasks by scrolling down to each and typing *:e*.

photpars

This task specifies the size of the aperture. It is 7" in radius in Figure D.1. If *mkapert* sets to be "yes", it will indicate the aperture size on the radial plot while you tag the stars. This is helpful to see whether any contamination will fall within the aperture.

datapar

Figure D.2 shows the parameters examples for this task. The key parameters are *fwhmpsf* because it will be different from night to night. This FWHM will be the average for all the images. If we specify the scale to be 0.401" for CTIO 0.9m data (i.e., the plate scale), the unit of FWHM will be in arcseconds. Other parameters are a one-time setup.

centerpar

This task will determine the centering algorithm while we tag the stars. Therefore, the *calgorithm* will be "centroid" as shown in Figure D.2. The other parameter needing modification from image to image is *cbox*. Usually it is two times of the *fwhmpsf*. The unit here is still in arcseconds.

fitskypars

The background noise will affect the quality of aperture photometry. You will need to select the size of the sky and sky annulus to calculate the background noise. Currently, we choose the radius as 20" and use a 3" annulus width as shown in Figure D.2. If *mksky* is set to be "yes", it will indicate sky annulus on the radial plot.

After you modify all these parameters, this **apercorr** task will automatically display every image within the **listfile** so you can move the cursor on the images to tag the stars you need. A radial plot will be shown and will mark the aperture and sky annulus size. A new file ***.mag.1** will be generated after you click *q* to quit the

tagging sequence. Please make sure that the tagging order on the images is consistent in each filter. It will be easy for us to find which stars have problem.

D.3.2 Make Observation Files

The instrumental magnitude for each standard star has been calculated and listed within each ***.mag.1** file. Before assembling them into a master file, you need to use the **mkimsets** task to sort these images. See Figure D.3. The output file should be named “standard.imsets”, which stands for “standard fields image sets”. The first column indicates the ID of each standard field, the second, third and forth columns are V, R, and I filters, respectively. You can see that the standard field 1 is observed one time in the V and R filters, but two times in the I filter (1004 and 1005) in Figure D.3. Standard field 2 is observed two times each.

D.3.3 Make a Master List of Instrumental Magnitudes

The next step will be to extract all the instrumental magnitudes in ***.mag.1** into a master file. The task will be used is **mknoobsfile** as shown in Figure D.3. The output named “standard.obs” is a master list. If there are three stars in standard field 1, this “standard.obs” file will label these stars in sequential order, 1, 2 and 3. After it finishes, please open this output file to check the filter orders, because this task sometimes will have problems. If an aperture correction was applied, be sure to include that filename (usually **aperture.corr**) under the **apercors** parameter.

D.3.4 Make Configure File and Standard *VRI* Magnitude Table

An example configure file is shown in Figure D.4; it defines the transformation equation for the photometry. More details of this equation is given in section D.5. All of the “.cfg” files for standard and science stars are found in the directory named “default” in the top directory on the photometry disk. The standard stars magnitude table needs to be created and an example is shown in Figure D.3. All standard stars you use need to be included in “landvri.dat” file. **The stars ID in “landvri.dat” should be identical with those in “standard.obs”.**

```

-----
-setairmass-
-----
    images = "@listfile"      Input images
    (observatory = "CTIO")    Observatory for images
    (intype = "beginning")    Input keyword time stamp
    (outtype = "effective")   Output airmass time stamp\n
    (date = "date-obs")      Observation date keyword
    (exposure = "exptime")    Exposure time keyword (seconds)
    (airmass = "airmass")     Airmass keyword (output)
    (utmiddle = "utmiddle")   Mid-observation UT keyword (output)\n
    (show = yes)             Print the airmasses and mid-UT?
    (update = yes)           Update the image header?
    (override = yes)         Override previous assignments?
    (mode = "ql")

-----
-task=phot-
-----
    image = ""               Input image(s)
    coords = ""              Input coordinate list(s) (default: image.coo.?)
    output = ""              " Output photometry file(s) (default: image
    skyfile = ""             Input sky value file(s)
    (plotfile = "")          Output plot metacode file
    (datapars = "")          Data dependent parameters
    (centerpars = "")        Centering parameters
    (fitskypars = "")        Sky fitting parameters
    (photpars = "")          Photometry parameters
    (interactive = yes)       Interactive mode ?
    (radplots = yes)         Plot the radial profiles?
    (verify = )_.verify)     Verify critical phot parameters ?
    (update = )_.update)     Update critical phot parameters ?
    (verbose = )_.verbose)   Print phot messages ?
    (graphics = )_.graphics) Graphics device
    (display = )_.display)   Display device
    (icommands = "")         Image cursor: [x y wcs] key [cmd]
    (gcommands = "")         Graphics cursor: [x y wcs] key [cmd]
    (mode = "ql")

-----
-photpars-
-----
    (weighting = "constant") Photometric weighting scheme
    (apertures = "7")        List of aperture radii in scale units
    (zmag = 25.)             Zero point of magnitude scale
    (mkapert = yes)          Draw apertures on the display
    (mode = "ql")

```

Figure D.1: parameters examples for **setairmass**, **phot** and **photpars**.

```

-----
-datapars-
-----
      (scale = 0.401)           Image scale in units per pixel
      (fwhmpsf = 1.3)          FWHM of the PSF in scale units
      (emission = yes)         Features are positive ?
      (sigma = 5.)             Standard deviation of background in counts
      (datamin = -4.)          Minimum good data value
      (datamax = 65535.)       Maximum good data value
      (noise = "poisson")      Noise model
      (ccdread = "gttron21")    CCD readout noise image header keyword
      (gain = "gtgain21")      CCD gain image header keyword
      (readnoise = 4.7)        CCD readout noise in electrons
      (epadu = 3.1)            Gain in electrons per count
      (exposure = "exptime")    Exposure time image header keyword
      (airmass = "airmass")     Airmass image header keyword
      (filter = "filter2")      Filter image header keyword
      (obstime = "utmiddle")    Time of observation image header keyword
      (itime = 20.)             Exposure time
      (xairmass = 1.2660490274429) Airmass
      (ifilter = "diar")        Filter
      (otime = "4:50:29.7")     Time of observation
      (mode = "ql")

-----
-centerpars-
-----
      (calgorithm = "centroid") Centering algorithm
      (cbox = 2.6)              Centering box width in scale units
      (cthreshold = 0.)         Centering threshold in sigma above background
      (minsnratio = 1.)         Minimum signal-to-noise ratio for centering alg
      (cmaxiter = 10)           Maximum iterations for centering algorithm
      (maxshift = 4.)           Maximum center shift in scale units
      (clean = no)              Symmetry clean before centering
      (rclean = 1.)             Cleaning radius in scale units
      (rclip = 2.)              Clipping radius in scale units
      (kclean = 3.)             K-sigma rejection criterion in skysigma
      (mkcenter = no)           Mark the computed center
      (mode = "ql")

-----
-fitskypars-
-----
      (salgorithm = "mode")     Sky fitting algorithm
      (annulus = 20.)           Inner radius of sky annulus in scale units
      (dannulus = 3.)           Width of sky annulus in scale units
      (skyvalue = 0.)           User sky value
      (smaxiter = 10)           Maximum number of sky fitting iterations
      (slclip = 0.)             Lower clipping factor in percent
      (shiclip = 0.)            Upper clipping factor in percent
      (snreject = 50)           Maximum number of sky fitting rejection iterati
      (sloreject = 3.)          Lower K-sigma rejection limit in sky sigma
      (shireject = 3.)          Upper K-sigma rejection limit in sky sigma
      (khist = 3.)              Half width of histogram in sky sigma
      (binsize = 0.10000000149012) Binsize of histogram in sky sigma
      (smooth = no)             Boxcar smooth the histogram
      (rgrow = 0.)              Region growing radius in scale units
      (mksky = yes)             Mark sky annuli on the display
      (mode = "ql")

```

Figure D.2: parameters examples for **datapars**, **centerpars** and **fitskypars**.

D.3.5 Final Steps for Standard Stars

The last task to use in this standard stars data processing is **fitparams**, shown in Figure D.5. Basically, the task will apply a least-squares method on the transformation equation to calculate apparent magnitudes for standard stars and also determine transformation equation coefficients (**standard.coeff**) so that we can apply those coefficients on our science stars.

This task will plot a residual and also tells you if the solution converges or not. If it does not converge in one filter, you may need to delete a couple of high residual stars then fit again (shown in Figure D.7). Please read the help manual of the **fitparam** task for more detail. You may quit this task after these three fittings converge. If the solution converges the first time, there will be three main blocks in **standard.coeff** file. If not, some extra blocks with “diverge” will be noted in this file. The last three blocks in this file indicates the final coefficient results for this transformation.

In order to generate a master photometry list for CTIOPI, a perl script has to be run, **perl ~/bin/standard.pl**. The input files are “standard.imsets” and “standard.obs”. Please modify the “standard.imsets” file. First, remove the first two blank lines. Second, make one line for each object. A file “standard.catalog” as shown in Figure D.6 is generated after running this script. **This script will not calculate extinction curves and it generates a catalogue only.**

Furthermore, please manually add those useless images (ex: bad images, saturated images) back to this catalogue file.

Now you have finished processing the standard stars and get the transformation coefficients. Next, continue to work on science stars.

D.4 Science Stars

Science star fields are usually more crowded than the standard star fields. However, our CTIO images are far less crowded than those in globular culsters. The necessity of aperture correction strongly depends on the fields. Determining aperture size is

```

-----
-mkimsets-
-----
imlist = "*.o.mag.1"      The input image list
idfilters = "v,r,i"      The list of filter ids
imsets = "standard.imsets" The output image set file
(imobsparams = "")      The output image observing parameters file
  (input = "photfiles")  The source of the input image list
  (filter = )           The filter keyword
  (fields = "")         Additional image list fields
  (sort = "")           The image list field to be sorted on
  (edit = yes)          Edit the input image list before grouping
  (rename = yes)        Prompt the user for image set names
  (review = yes)        Review the image set file with the editor
  (list = "")
  (mode = "ql")

-----
standard.imsets example:
-----
field1 : dec02s.1001.o dec02s.1003.o dec02s.1004.o
field1 : dec02s.1001.o dec02s.1003.o dec02s.1005.o
field2 : dec02s.1009.o dec02s.1011.o dec02s.1010.o
field2 : dec02s.1012.o dec02s.1013.o dec02s.1014.o

-----
-mknobsfile-
-----
photfiles = "*.o.mag.1"      The input list of APPHOT/DAOPHOT databases
idfilters = "v,r,i"          The list of filter ids
imsets = "standard.imsets"   The input image set file
observations = "standard.obs" The output observations file
(obsparams = "")            The input observing parameters file
(obscolumns = " ")          The format of obsparams
(minmagerr = 0.001)         The minimum error magnitude
(shifts = "")               The input x and y coordinate shifts file
(apercors = "")            The input aperture corrections file
(aperture = 1)              The aperture number of the extracted magnitude
(tolerance = 5.)            The tolerance in pixels for position matching
(allfilters = no)           Output only objects matched in all filters
(verify = yes)              Verify interactive user input ?
(verbose = yes)             Print status, warning and error messages ?
(mode = "ql")

-----
standard.obs example:
-----
field1-1      v      5:59:25.5  1.512  607.395  749.645  16.147  0.001
*             r      6:01:47.8  1.526  607.467  748.719  14.937  0.001
*             i      6:03:35.7  1.537  609.185  748.972  14.170  0.001
field1-2      v      5:59:25.5  1.512  543.660  558.728  17.673  0.003
*             r      6:01:47.8  1.526  543.682  557.738  17.036  0.003
*             i      6:03:35.7  1.537  545.469  558.193  17.288  0.005
field1-3      v      5:59:25.5  1.512  967.006  226.776  16.597  0.001
*             r      6:01:47.8  1.526  967.282  225.602  16.247  0.002
*             i      6:03:35.7  1.537  968.751  226.254  16.706  0.003

-----
example file of landvri.dat
-----
field1-1      10:54:05.0 -00:50:15.0      8.754      8.240      7.756
field1-2      10:53:52.0 -00:50:40.0      9.246      8.698      8.201
field1-3      10:48:13.0 -11:20:12.0     15.600     13.400     11.180
field2-1      04:02:40.9 -44:45:09.0     13.097     12.658     12.274
field2-2      04:02:31.8 -44:47:08.0     14.090     13.778     13.452
field2-3      04:02:44.0 -44:47:00.0     15.751     15.239     14.793

```

Figure D.3: parameters for **mkimsets**, and the output file format.


```

# Declare the standards catalog variables
catalog
v      4          # the V magnitude
r      5          # the R magnitude
i      6          # the I magnitude

# Declare the observations file variables
observations

Tv      3          # time of observation in filter V
Xv      4          # airmass in filter V
xv      5          # x coordinate in filter V
yv      6          # y coordinate in filter V
mv      7          # instrumental magnitude in filter V
error(mv) 8          # magnitude error in filter V

Tr      10         # time of observation in filter R
Xr      11         # airmass in filter R
xr      12         # x coordinate in filter R
yr      13         # y coordinate in filter R
mr      14         # instrumental magnitude in filter R
error(mr) 15        # magnitude error in filter R

Ti      17         # time of observation in filter I
Xi      18         # airmass in filter I
xi      19         # x coordinate in filter I
yi      20         # y coordinate in filter I
mi      21         # instrumental magnitude in filter I
error(mi) 22        # magnitude error in filter I

# Sample transformation section for the Landolt UBVRI system
transformation

set rv = v-mv
set rr = r-mr
set ri = i-mi
set vr = mv-mr
set vi = mv-mi
set dri = mr-mi

fit v1=0.0, v2=0.0, v3=0.0, v4=0.0
VFIT: v = mv + v1 +v2*Xv + v3*(mv-mi) + v4*(mv-mi)*Xv

fit r1=0.0, r2=0.0, r3=0.0,r4=0.0
RFIT: r = mr + r1 +r2*Xr + r3*(mr-mi) + r4*(mr-mi)*Xr

fit i1=0.03, i2=0.02, i3=0.04, i4=0.03
IFIT: i = mi + i1 +i2*Xi + i3*(mr-mi) + i4*(mr-mi)*Xi

```

Figure D.4: standard star configuration example.

```

-----
-fitparam-
-----

observations = "standard.obs"      List of observations files
catalogs = "landvri.dat"          List of standard catalog files
config = "standard.cfg"           Configuration file
parameters = "standard.coeff"      Output parameters file
(weighting = "photometric")        Weighting type (uniform,photometric,equations)
(addscatter = yes)                 Add a scatter term to the weights ?
(tolerance = 1.00000000000000E-7) Fit convergence tolerance
(maxiter = 30)                    Maximum number of fit iterations
(nreject = 3)                     Number of rejection iterations
(low_reject = 3.)                 Low sigma rejection factor
(high_reject = 3.)               High sigma rejection factor
(grow = 0.)                      Rejection growing radius
(interactive = yes)              Solve fit interactively ?
(logfile = "logfile")            Output log file
(log_unmatche = yes)             Log any unmatched stars ?
(log_fit = yes)                  Log the fit parameters and statistics ?
(log_results = yes)              Log the results ?
(catdir = " ")                  The standard star catalog directory
(graphics = "stdgraph")          Output graphics device
(cursor = " ")                  Graphics cursor input
(mode = "ql")

-----
-mkapfile-
-----

photfiles = "*.aper.1"           The input list of APPHOT/DAOPHOT databases
naperts = 14                     The number of apertures to extract
apercors = "aperture.corr"        The output aperture corrections file
(smallap = 5)                    The first aperture for the correction
(largeap = 9)                    The last aperture for the correction
(magfile = " ")                  The optional output best magnitudes file
(logfile = " ")                  The optional output log file
(plotfile = " ")                 The optional output plot file
(obsparams = " ")                The observing parameters file
(obscolumns = "2 3 4 5")          The observing parameters file format
(append = no)                    Open log and plot files in append mode
(maglim = 0.1)                   The maximum permitted magnitude error
(nparams = 5)                    Number of cog model parameters to fit
(swings = 1.2)                   The power law slope of the stellar wings
(pwings = 0.1)                   The fraction of the total power in the stellar
(pgauss = 0.5)                   The fraction of the core power in the gaussian
(xgescale = 0.9)                 The exponential / gaussian radial scales
(xwings = 0.)                    The extinction coefficient
(interactive = yes)              Do the fit interactively ?
(verify = no)                    Verify interactive user input ?
(gcommands = " ")               The graphics cursor
(graphics = "stdgraph")          The graphics device
(mode = "ql")

-----
-evalfit-
-----

observations = "science.obs"      List of observations files
config = "science.cfg"           Configuration file
parameters = "standard.coeff"     Fitted parameters file
calib = "evalfit.out"            Output calibrated standard indices file
(catalogs = " ")                List of standard catalog files
(errors = "oberrors")           Error computation type (undefined,oberrors,equ)
(objects = "program")            Objects to be fit (all,program,standards)
(print = " ")                   Optional list of variables to print
(format = " ")                  Optional output format string
(append = no)                   Append output to an existing file ?
(catdir = )_.catdir             The standard star catalog directory
(mode = "al")

```

Figure D.5: parameters examples for **fitparam**, **mkapfile** and **evalfit**.

Name	FILTER	FITS	AM	APER	MAG	SNerr	Sterr	DATEreduce	WHO
LHS2621	V	20030329.09.096.o	1.587	---	16.187	0.006	0.013	2003-08-11	Subasavage
LHS2621	X	20030329.09.097.o	1.584	---	15.783	0.006	0.018	2003-08-11	Subasavage
LHS2621	I	20030329.09.098.o	1.581	---	15.445	0.010	0.017	2003-08-11	Subasavage
LHS2734A	V	20030329.09.104.o	1.094	---	16.126	0.006	0.013	2003-08-11	Subasavage
LHS2734A	I	20030329.09.103.o	1.103	---	15.322	0.004	0.018	2003-08-11	Subasavage
LHS2734A	I	20030329.09.102.o	1.112	---	14.593	0.004	0.017	2003-08-11	Subasavage
LHS2734B	V	20030329.09.104.o	1.094	---	18.827	0.057	0.013	2003-08-11	Subasavage
LHS2734B	I	20030329.09.103.o	1.103	---	17.893	0.031	0.018	2003-08-11	Subasavage
LHS2734B	I	20030329.09.102.o	1.112	---	16.743	0.025	0.017	2003-08-11	Subasavage
LHS2734B	V	20030329.09.131.o	1.538	---	14.767	0.004	0.013	2003-08-11	Subasavage
SCR1138-7721	I	20030329.09.132.o	1.542	---	13.201	0.001	0.018	2003-08-11	Subasavage
SCR1138-7721	I	20030329.09.133.o	1.547	---	11.250	0.001	0.017	2003-08-11	Subasavage
SCR1322-7254	V	20030329.09.144.o	1.387	---	15.322	0.002	0.013	2003-08-11	Subasavage
SCR1322-7254	I	20030329.09.145.o	1.390	---	14.122	0.002	0.018	2003-08-11	Subasavage
SCR1322-7254	I	20030329.09.146.o	1.392	---	12.594	0.002	0.017	2003-08-11	Subasavage
SCR1328-7253	V	20030329.09.149.o	1.399	---	16.895	0.006	0.013	2003-08-11	Subasavage
SCR1328-7253	I	20030329.09.148.o	1.396	---	15.645	0.004	0.018	2003-08-11	Subasavage
SCR1328-7253	I	20030329.09.147.o	1.393	---	13.994	0.003	0.017	2003-08-11	Subasavage
SCR1726-8433	V	20030329.09.150.o	1.757	---	14.254	0.002	0.013	2003-08-11	Subasavage
SCR1726-8433	I	20030329.09.151.o	1.755	---	13.004	0.001	0.018	2003-08-11	Subasavage
SCR1726-8433	I	20030329.09.152.o	1.753	---	11.415	0.001	0.017	2003-08-11	Subasavage
SCR1735-7020	V	20030329.09.170.o	1.333	---	99.999	0.005	0.013	2003-08-11	Subasavage
SCR1735-7020	I	20030329.09.169.o	1.337	---	99.999	0.004	0.018	2003-08-11	Subasavage
SCR1735-7020	I	20INDEF	0.000	---	99.999	0.000	0.017	2003-08-11	Subasavage
SCR2012-5956	V	20030329.09.191.o	1.287	---	16.063	0.011	0.013	2003-08-11	Subasavage
SCR2012-5956	I	20030329.09.192.o	1.280	---	15.484	0.008	0.018	2003-08-11	Subasavage
SCR2012-5956	I	20030329.09.193.o	1.275	---	15.035	0.012	0.017	2003-08-11	Subasavage
SCR2012-5956	I	20030329.09.194.o	xxxxx	xxx	xxxxxx	xxxxx	xxxxx	2003-08-11	Subasavage << bad image
E2_M	V	20030127.09.071.o	1.050	---	---	---	---	2003-08-28	Jao
E2_M	I	20030127.09.072.o	1.055	---	---	---	---	2003-08-28	Jao
E2_M	I	20030127.09.073.o	1.061	---	---	---	---	2003-08-28	Jao
E2_O	V	20030127.09.071.o	1.050	---	---	---	---	2003-08-28	Jao
E2_O	I	20030127.09.072.o	1.055	---	---	---	---	2003-08-28	Jao
E2_O	I	20030127.09.073.o	1.061	---	---	---	---	2003-08-28	Jao
E2_S	V	20030127.09.071.o	1.050	---	---	---	---	2003-08-28	Jao
E2_S	I	20030127.09.072.o	1.055	---	---	---	---	2003-08-28	Jao
E2_I	V	20030127.09.071.o	1.061	---	---	---	---	2003-08-28	Jao
E2_I	I	20030127.09.072.o	1.050	---	---	---	---	2003-08-28	Jao
E2_T	V	20030127.09.073.o	1.061	---	---	---	---	2003-08-28	Jao
E2_T	I	20030127.09.071.o	1.050	---	---	---	---	2003-08-28	Jao
E2_T	I	20030127.09.072.o	1.055	---	---	---	---	2003-08-28	Jao
E2_T	I	20030127.09.073.o	1.061	---	---	---	---	2003-08-28	Jao
E2_T	I	20030127.09.074.o	xxxxx	---	---	---	---	2003-08-28	Jao
98_575	V	20030127.09.124.o	1.412	---	---	---	---	2003-08-28	Jao
98_575	I	20030127.09.123.o	1.402	---	---	---	---	2003-08-28	Jao
98_575	I	20030127.09.122.o	1.398	---	---	---	---	2003-08-28	Jao
98_576	V	20030127.09.124.o	1.412	---	---	---	---	2003-08-28	Jao
98_576	I	20030127.09.123.o	1.396	---	---	---	---	2003-08-28	Jao
98_582	V	20030127.09.122.o	1.402	---	---	---	---	2003-08-28	Jao
98_582	I	20030127.09.121.o	1.412	---	---	---	---	2003-08-28	Jao
98_582	I	20030127.09.120.o	1.398	---	---	---	---	2003-08-28	Jao
98_585	V	20030127.09.123.o	1.402	---	---	---	---	2003-08-28	Jao
98_585	I	20030127.09.122.o	1.398	---	---	---	---	2003-08-28	Jao

Figure D.6: example output file from **evalfit.pl** and **standard.pl** (bottom one) script

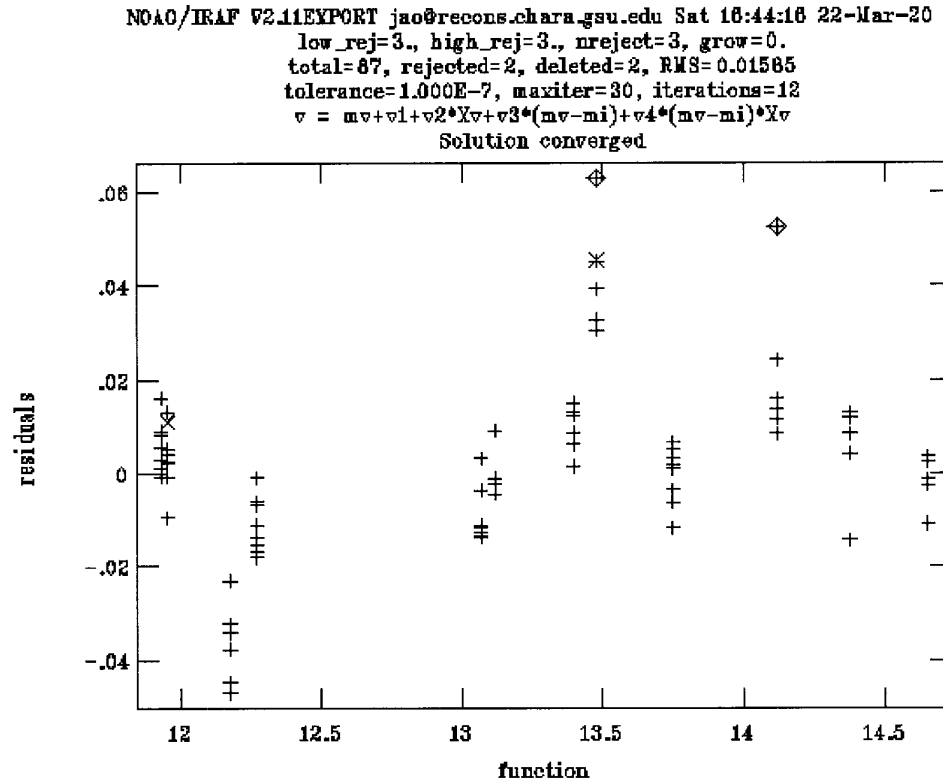


Figure D.7: **fitparam** fitting plot example, and it shows that this solution is converged. Two diamond indicates this task deletes data automatically and two cross mark indicates they are deleted by users.

a more of an art than a science. The larger the aperture, the larger the error from the sky subtraction and more cosmic rays will be included. Therefore, a correct “aperture size” is the one which is large enough to include most of the flux from a star. Theoretically, a star flux will not increase after a critical aperture size. An aperture correction is a magnitude correction from a small size to a larger critical aperture size. Basically, if there are no other objects within the $7''$ radius, the regular aperture photometry without aperture correction should work. If not, an aperture correction is necessary. The goal is that if you can apply a $7''$ or larger radius aperture on an object, do not apply a small aperture size on it. No correction is better than correction.

The basic steps of the processing procedure for science stars are listed below.

1. Run **imexam** on every science image, to determine the average FWHM and also determine which images require an aperture correction. Remove cosmic rays if necessary.
2. Edit all parameters in **phot**.
3. If an image needs to have an aperture correction applied, tag 3 or 4 field stars which are reasonably isolated.
4. Calculate the amount of correction based on these isolated stars.
5. Tag your science stars with selected aperture size.
6. Generate the science star configure file and collect your science stars VRI instrumental magnitudes.
7. Based on the transformation equation coefficients from standard stars, calculate apparent magnitudes.

D.4.1 Examine Science Images

Understanding the quality of your science images is important, because you need to apply the right method to process precious data. Run the **redpi/displayexam** to examine all the science images. Meanwhile, record the FWHM of each image and also determine the necessity of aperture correction for science stars. In addition, make a note which of images have cosmic rays within the $7''$ radius of the science star.

D.4.2 Remove Cosmic Rays

It is always better to remove a cosmic ray rather than to apply an aperture correction to avoid it. This is done with the `iraf` command **cosmicrays** in package **noao.imred.ccdred**. A bad pixel map which is located in the top level of CTIOPI photometry “default” directory is needed to run this task. Using default parameter values first is fine to see if it does the job. Often, this command will have to be run a few times to remove the cosmic ray of concern. If you choose to review parameters interactively, you can delete specific points by placing the cursor over the point and pressing *d*. Repeat this process until the cosmic ray is completely removed or its peak flux is no more than 1% of that of the science star. See the help page by typing *help cosmicrays* for information on parameter tweaking.

D.4.3 Tag Isolated Stars in a Crowd Field

Load the **redpi/apercorr** task and choose option 1. It will allow you to edit the parameters of the **phot** task. Section D.3.1 has explained these parameters. The most important task is **photpars**. You need to choose a large variety of aperture sizes, 3", 3.5", 4", 4.5", 5", 5.5", 6", 6.5", 7", 7.5", 8", 8.5" and 9" in radius. Then you tag 3 or more “isolated” stars with reasonable counts in the same field. The new generated file is called ***.aper.1**.

D.4.4 Apply Aperture Correction

Option 2 in **redpi/apercorr** will do this work. An actual task behind the curtain is **mkapfile** shown in FigD.5. A curve of growth, which is a plot of magnitude within a given aperture versus aperture size, will be shown for each image with ***.aper.1**.

index	1	2	3	4	5	6	7	8	9	10	11	12	13	14
radius size	3	3.5	4	4.5	5	5.5	6	6.5	7	7.5	8	8.5	9	9.5

The parameter **naperts** is the total number of apertures you want to extract. In the example above, there are fourteen different sizes. **smallap** indicates the small aperture index you would like to apply on the science stars. **largeap** indicates the large aperture size index to which you would like to correct. The example shown in Figure D.5 is that **smallap** ID is 5 (5" radius) and **largeap** ID is 9 (7" radius). The output file for this **mkapfile** is called **aperture.corr**.

This file is a simple text file containing the image name in column 1, the aperture correction computed from **smallap** to **largeap** in column 2, and the estimated error

in the aperture correction in column 3. If multiple aperture sizes were used on one night, create a 4th column and enter the aperture radius in arcseconds for each image. A `#` needs to precede this column so that it does not affect the calculation to come later. For example:

```
20030101.09.101.o -0.01218093 8.684811E-4 #5"
20030101.09.112.o -0.08370557 0.004138806 #1"
```

D.4.5 Get Instrumental Magnitudes for Science Stars

This step is similar to the standard stars tagging procedure. A task you need to load is **redpi/apercorr** option 3. This option will let you to edit **phot** parameters. The only important parameter you need to notice is **apertures**. The correct aperture size is the same as **smallap** which you use in aperture correction. Again, when tagging science stars, **the tagging order should be the same for all filters**. The output file is called ***.mag.1**.

D.4.6 Make Science Star Observation Files and Master List Files

The **mkimsets** task is used for science stars just as for standard stars. The output file is "science.imsets". After this file is generated, please make sure the top two blank lines to be removed. **mknoobsfile** is also used for generating a master list of instrumental magnitudes. Make necessary changes for this task. **imsets="science.imsets"**, **observation="science.obs"** and **apercors="aperture.corr"**.

D.4.7 Calculate Apparent Magnitude

There are two ways to calculate the apparent magnitude. One is by **evalfit**, an IRAF standard task, and the other is **evalfit.pl** which is a perl script. The latter produces an output consistent with the CTIOPI photometry catalogue and is preferred.

Evalfit Task

Before using this task you need to copy the "standard.coeff" from the standard star directory. No modification for this file is necessary. The other two files you need to use in this task are "science.cfg" which is the same as "standard.cfg", and "science.obs". Therefore, science and standard stars will have the same definition of transformation equation. An example parameter for **evalfit** is shown in Figure D.5.

The output file is called “evalfit.out”. The S/N magnitude error is also printed in this file. More discussion about error can be found in section D.5.

Perl script

This perl scrip is called **evalfit.pl**. Have a copy of it under your bin directory, because the date/format perl module is called, logon **penston** and type **perl ~/bin/evalfit.pl** to excute it. This perl script is only applied for a second-order transformation equation as shown in section D.5. The “standard.coeff” and “science.obs” is also necessary for this script. However, you need to modify this file by leaving the last block of VRI converged fitting results in this file. No diverge result can exist in this file.

The default name for the file created by **mkimsets** needs to be science.imsets for this script. Also in the case where a series of frames were taken of a double star, you need to insert an extra line for the second star which has the same frame names as the first star. For example,

LHS300AB : 20030101.09.101.o 20030101.09.102.o 20030101.09.103.o

should be modified to look as follows:

LHS300A : 20030101.09.101.o 20030101.09.102.o 20030101.09.103.o

LHS300B : 20030101.09.101.o 20030101.09.102.o 20030101.09.103.o

The output file is called “science.ans” shown in Figure D.6. This file includes the standard star error as well as other important parameters such as airmass. More discussion about magnitude error can be found in section D.5. This file needs to be manually edited to include the diameter of the aperture size used. For example, if you used the standard 7" radius, you will enter 14" for that image.

As discussed in the standard stars section, **Please manually add those useless images (ex: bad images, saturated images) back to this catalogue file.**

D.5 Transformation Equations

The transformation equations for aparent magnitude $V(RI)_c$ are as follows,

$$V = m_V + a_1 + a_2X + a_3(m_V - m_I) + a_4(m_V - m_I)X, \quad (D.1)$$

$$R = m_R + b_1 + b_2X + b_3(m_R - m_I) + b_4(m_R - m_I)X, \quad (D.2)$$

$$I = m_I + c_1 + c_2X + c_3(m_R - m_I) + c_4(m_R - m_I)X \quad (D.3)$$

where, V, R and I are aparent magnitudes for a standard star, m_{VRI} is the instrut-mental magnitude from IRAF, a_1 to a_4 are transformation coefficients(same for b_i

and c_i), and X is airmass.

The least-squares method is performed by **fitparam** task to calculate those transformation coefficients based on the standard stars observation. This task not only calculates the transformation coefficients but calculates the so called “external error” or “standard stars error”. This standard deviation error can be found in the **fitparam** output “logfile”.

Another magnitude error is “internal error” or “night to night error”, which is the error from the repeated observations of the same object. The smallest error is called “photon error”. This error calculates the signal to noise ratio received by the detector. This error is printed in the output file of **evalfit IRAF** task. Because of the large signal to noise ratio, this error is usually very small.

D.6 Remark

This part discusses choosing the inner radius of the sky annulus and its width. This test uses the **noao.digiphot.daophot.phot** task and is applied for the standard star fields, SA98, observed on Nov01, night3 run. The seeing of that night is 1.4”. The key parameters in this test is “fitskypars” as shown in Figure D.2

The mean sky counts results are shown in the Table D.1 This table shows that even a nearby star within the sky annulus width, like, SA–676 and SA98–675, the mean sky counts does not be effected. The 20” radius sky annulus even has lower standard deviation than 10” radius sky. A mean sky counts with 10” radius may be blended by the weak wing of star’s profile.

star	10”(radius) 3”(width)	20”(radius) 3”(width)	note
SA98–650	58.33632	57.91608	
SA98–670	63.51149	58.55741	
SA98–676	60.38068	58.39950	mix with SA98–675
SA98–675	61.22947	58.12084	mix with SA98–676

Table D.1: The apparent magnitude for different aperture size

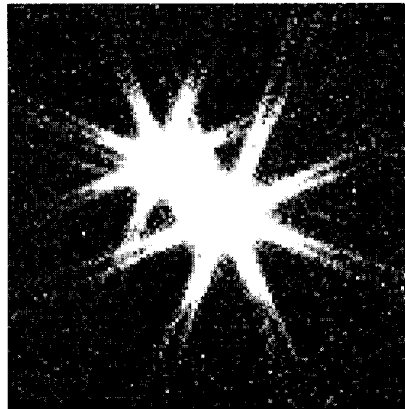
Appendix E

CTIOPI Parallax Reduction Manual

Revision History

1. 11/18/2001 The first version is finished and release to U. of Chile.
2. 03/01/2003 add JPL DE405 section.
3. 06/30/2003 modified the pipeline from U. of Virginia (FORTRAN) version to U. of Texas (Gaussfit) versions. Included the WCSTools, plate rotation task.
4. 07/15/2003 IDL routine is finished for plotting data.
5. 01/13/2004 release the current version to U. of Chile and add the quick references table.

CTIOPI Parallax Reduction Manual



Wei-Chun Jao
Georgia State University
01/20/2004

E.1 Introduction

This manual explains step by step how to reduce from the raw data which are taken in the CTIO to the final absolute parallax. The main programs are, IRAF/redpi package, SExtractor/sex, FORTRAN/genpif and Gaussfit. **A quick reference guide is available from Table E.2 to Table E.4**

E.2 Install *redpi* Package

For example, if your account is under /disk1/proxima/

- In your home directory, make a new directory called **iraf**. Go into that directory by typing **cd iraf** and make another directory called **redpi**. Move into that directory by typing **cd redpi**
- Unzip the package in the redpi directory by typing **tar xzf pack.tar.gz**
- Modify your **login.cl** and **loginuser.cl**.
 1. add the following command to your login.cl file by typing **emacs login.cl** and then enter:
 set redpidir = "/disk1/proxima/iraf/redpi/"
 2. modify **set imtype= "fits, imh"**
 3. edit a new file called loginuser.cl by typing **emacs loginuser.cl**. (If loginuser.cl already exists, edit it by typing the same thing, and add the following.) Enter the following two lines into loginuser.cl:
 task redpi.pkg = redpidir\$redpi.cl
 keep

E.2.1 *redpi* Package Usage Guide

This package subtracts the bias from the images and divides the images by the flat fields. First, log into IRAF by typing **cl** under your IRAF directory. If you are the first time user, you may type **mkdir iraf**, **cd iraf** and **mkiraf** to finish your installation of IRAF program. Then type **redpi** to load this package. Your window should then look like this:

```
cl>redpi
```

CTIOPI Data Reduce Package

fix99 fixname gof headmet proc displayexam wcsangle taglist

Each of the tasks in the redpi package listed above is described here.

1. **fixname** will ask you to enter the leading image file name characters. It will take any kind of format, for example, nov00s, nov00b, 030207.09, 030207.15, 20030911.09 or 20030911.15. It will rename the keywords in the image headers to the required format for IRAF processing.
 1. fixname will first rename *imagetyp* in the image header from capital letters to lower letters, which are required for IRAF (*imagetyp* must be “zero”, “flat” or “object”) in order for the **proc** task.
 2. fixname then sorts all images by different type into files for bias frames, flat field frames, and image frames. The files generated by fixname and other tasks are shown in Table E.1.
2. **gof** generates three master files that list the individual frames taken in the V, R, and I filters.
3. **proc** carries out the following steps:
 1. It asks you for the bias section, trim section, CCD readout noise and CCD gain which you need to enter. Answers for these values are different for the 0.9m and 1.5m, and the options are given on the screen.
 2. Combines bias frames and generates a single **superbias** frame. Overscan will be removed.
 3. Processes flat field images and generates three frames, one for each filter, **superflatv**, **superflatr**, **superflati**. Overscan will be removed.
 4. Processes raw science images and outputs the processed images as ***.o.fits**
4. **fix99** must be run **ONLY** for some data taken in 1999. It will change the format of *date-obs* in the header so that this format will be consistent with 2000 (and later) format.
5. **displayexam** will automatically display and examine the images which are in the listfile.

input files	output files
fixname	
*.fits	blist (bias list) flatfile (flat list) obfile (object file list) tfile (all the image file list) vflist (V band flat list), rflist, iflist vslist (V band object list), rslis, islist
gof	
vslist rslis,islist	vslisto (output file list, *.o.fits) rslis, islist
proc	
*.fits all the output file from fixname all the output file from gof	*.o.fits (reduced science frame) superbias superbflat(vri)
fix99	
listfile	N/A
headmet	
listfile	lhs1234.hinfo, lhs1234.met and listfile
displayexam	
listfile	N/A
wcsangle	
badpix.flip.pl wcs.sex and wcs.param	wcs.cat angle.out
taglist	
taglist	lhs1234.list.xxxxxxxxxx

Table E.1: The input and out files from redpi package. listfile contains all the science frames you want to examine.

6. **headmet** will grab information in the header that will be used to calculate the parallax factors for each frame.

headmet will ask you to enter the object's name **using 7 characters**.

ex: gj0555 —> gj00555, lhs1234 —> lhs1234.

Please open this *.hinfo output file, after you run this task. Check the format, because sometimes some images will not have coordinate, airmass or wrong format of observation date and time. Especially, the seconds, please leave it as **xx.x** format, (**F4.1**), because the images after 2001 also, will have the seconds accurate to the thousands. If RA and DEC is missed in some images, please copy the coordinate from the previous night. The key data we will use from this file is UT time and exposure time. The last column in the file is the filter. You may check whether all the images are in the parallax filter or not.

Currently, the output file *.met is not used for data reduction.

7. **wcsangle** is used to calculate the rotation angle of the trail plate relative to the Guide Star Catalog 2.2 (GSC2.2). Two external programs are called by this task, which are SExtractor/sex and WCSTools/imwcs. Users have to download the latest WCSTools from the website¹. The WCSTools version is 3.3.0 when this manual is written. This user guide will skip the detail of installing it and users can find more in the help page of WCSTools. SExtractor is the main centroid program we use in this parallax reduction and detail of it is discussed in the section E.3.

After you choose the trail plate, you may run this task under IRAF environment with your ds9 or ximtool launched. This task will need **badpix.flip.pl**², **wcs.param** and **wcs.sex**. You need to enter the coordinate of the last parallax star (if you have more than 1 science star). The coordinate should be the same as you run **genpif** which is discussed in the later section. This bad pixel map is for removing the bad columns in the images, so it can increase the SExtractor efficient to find stellar objects.

After the bad pixels are removed, an emacs program will open this file called **wcs.cat** output from SExtractor. This file contains, (x,y) coordinate, instru-

¹WCSTools is available at <http://tdc-www.harvard.edu/software/wcstools/>

²Please following the instruction in **A User's Guide to CCD Reductions with IRAF** to make a bad pixel mask. After you make it, please flip this image to match the sky with North-up and East-left in order to compare with GSC2.2 database. **users need to modify the command line in the wcsangle.cl to set the path of wcs.sex and wcs.param files.**

mental magnitude and FWHM in pixel. The coordinate has also been oriented in order to match the sky. You **have to** edit this file to keep objects with $1.5 < FWHM(0.9m) < 6.25$ and $2.5 < FWHM(1.5m) < 10.4$ pixel and magnitude brighter than 18.0. Save any changes then exit the emacs program. Then, this trail image will be displayed on the image displaying program with a red dot marked on every object in this `wcs.cat` file. You may examine these selected objects on the display program so that you can remove some very faint objects or possible cosmic rays later. After you finish this examining procedure, the emacs program will be launched once again to edit this `wcs.cat` file. After all, the **imwcs** program will be executed. You will see the rotation angle relative to the GSC2.2 is printed on the screen and an **angle.out** will also be generated. Because this **imwcs** program will run over the Internet to access the GSC2.2 in STScI, sometimes the server over there is down and you will need to run it later.

8. **taglist** is for tagging the images to get the preliminary coordinates. More details will be discussed in SExtractor section.

E.2.2 Reduce the Raw Data

fxname (and/or *fx99* if necessary), *gof*, and *proc* **must** be used in order. after reducing the raw data, make a directory for each individual parallax field, then sort these reduced images into each directory you just have created. We have not yet found a clever way to do this automatically so it is done one parallax field at a time. The current sorted images are located at `/recons/disk6/CTIOPI/regions/` in GSU.

E.3 SExtractor – Get the Centroid

E.3.1 Install SExtractor

Download the latest version of SExtractor³. Untar this zipped file by typing: **tar xzfv sex_2.x.x.tar.gz**. Then follow the installation guide (**INSTALL**) which is under a new generated directory called **sextractor2.x.x**. After you compile the source codes, there should be an executable file called *sex* under your *bin* directory.

³SExtractor is available at ftp://ftp.iap.fr/pub/from_users/bertin/sextractor/

E.3.2 Brief Introduction to SExtractor

SExtractor is a program designed mainly to resolve a crowded star field image. It will deblend overlapping extended objects. While using this program, you need to work under a directory which contains all the images of this particular object, **lhs1234**. (ie, I WILL USE *lhs1234* AS AN EXAMPLE THROUGHOUT THIS MANUAL). Every image accompanies an image configuration file called **lhs1234.sex.***, which is generated from a seed file called **lhs1234.sex**. This file sets the searching criterion for SExtractor, including searching radius, output file name, or saturation limit, etc. The other file which specifies what parameters need to be calculated is called **lhs1234.param**. Basically, all images under the same directory will share this same parameter file. For more detail of SExtractor, please refer to the SExtractor manual, which is under your **sextractor2.x.x** directory.

E.3.3 Configuration and Parameter File

Before you run SExtractor, please make sure:

- Your directory path is under lhs1234/.
- This directory must includes all images (***.o.fits**), one **lhs1234.sex** and one **lhs1234.param**.

Configuration File – lhs1234.sex

For the first time users, you may get a copy of this configuration file from **sextractor2.x.x/config/default.sex**. However, you need to modify this default file. The following are the items which need to be changed.

```
CATALOG_NAME  PARAMETERS_NAME  DETECT_THRESH
ANALYSIS_THRESH  SATUR_LEVEL  PIXEL_SCALE
FILTER=N
```

The example for this configuration is in Figure E.1. Please pay attention to the last block in this file. You need to enter those configurations, because it is **not** included in the *default.sex* file. The **ASSOC_RADIUS** parameter is 10 pixel for 0.9m and 20 for 1.5m.

We found that SExtractor can find centroid well based on these configurations. However, if this parallax star has a very close companion (separation<1.5"), we need to modified these terms.

- DETECT_MINAREA=2
- DEBLEND_NTHRESH=50
- DEBLEND_MINCONT=0.0001

Parameter File – lhs1234.param

This file will contain parameters which will be calculated and shown in *lhs1234.coord**. Please follow the order listed below and refer to SExtractor manual for more detail of these parameters.

X_IMAGE: Object position along x in pixel

Y_IMAGE: Object position along y in pixel

FLUX_MAX: Peak flux above background in counts

THETA_IMAGE: Position angle in degree

ELONGATION: semi-major axis length/semi-minor axis length

ELLIPTICITY: ellipticity of star or galaxy

FWHM_IMAGE: FWHM assuming the gaussian core in pixel

VECTOR_ASSOC(3): The preliminary coordinate for reference or parallax stars

E.3.4 Running SExtractor

Currently, we use bash scripts to run SExtractor program. One is **sss** for 0.9m, and the other is **bbb** for 1.5m. Put those two scripts under your *bin* directory. You may run this task under shell environment instead of IRAF environment. Please make sure all of your parallax frames are under LHS1234 directory.

Type **sss** or **bbb** to run this script under *lhs1234* directory. You will see these options on the screen.

please choose one of the following options

- 0) sort *.fits file by time sequential
- 1) sort *.list.*
- 2) generate *.sex.* for the first time
- 3) fix *.sex.* file

```

# Default configuration file for SExtractor V1.2b14 - > 2.0
# EB 23/07/98
# (*) indicates parameters which can be omitted from this config file.

#----- Catalog -----
CATALOG_NAME    lhs1234.coord1  # name of the output catalog
CATALOG_TYPE    ASCII_HEAD     # "NONE", "ASCII_HEAD", "ASCII", "FITS_1.0"
                                # or "FITS_LDAC"

PARAMETERS_NAME lhs1234.param  # name of the file containing catalog contents

#----- Extraction -----
DETECT_TYPE     CCD            # "CCD" or "PHOTO" (*)
FLAG_IMAGE      flag.fits     # filename for an input FLAG-image
DETECT_MINAREA  5              # minimum number of pixels above threshold
DETECT_THRESH   3              # <sigmas> or <threshold>, <ZP> in mag.arcsec-2
ANALYSIS_THRESH 3              # <sigmas> or <threshold>, <ZP> in mag.arcsec-2

FILTER          N              # apply filter for detection ("Y" or "N")?
FILTER_NAME     default.conv  # name of the file containing the filter

DEBLEND_NTHRESH 32             # Number of deblending sub-thresholds
DEBLEND_MINCONT 0.005          # Minimum contrast parameter for deblending

CLEAN           Y              # Clean spurious detections? (Y or N)?
CLEAN_PARAM     1.0            # Cleaning efficiency

MASK_TYPE       CORRECT        # type of detection MASKing: can be one of
                                # "NONE", "BLANK" or "CORRECT"

#----- Photometry -----
PHOT_APERTURES  5              # MAG_APER aperture diameter(s) in pixels
PHOT_AUTOPARAMS 2.5, 3.5      # MAG_AUTO parameters: <Kron_fact>, <min_radius>

SATUR_LEVEL     63000.0        # level (in ADUs) at which arises saturation

MAG_ZEROPOINT   0.0            # magnitude zero-point
MAG_GAMMA       4.0            # gamma of emulsion (for photographic scans)
GAIN            0.0            # detector gain in e-/ADU.
PIXEL_SCALE     0.4            # size of pixel in arcsec (0=use FITS WCS info).

#----- Star/Galaxy Separation -----
SEEING_FWHM     1.2            # stellar FWHM in arcsec
STARNNW_NAME    default.nnw   # Neural-Network_Weight table filename

#----- Background -----
BACK_SIZE       64             # Background mesh: <size> or <width>, <height>
BACK_FILTERSIZE 3              # Background filter: <size> or <width>, <height>

BACKPHOTO_TYPE  GLOBAL         # can be "GLOBAL" or "LOCAL" (*)
BACKPHOTO_THICK 24             # thickness of the background LOCAL annulus (*)

#----- Check Image -----
CHECKIMAGE_TYPE  NONE          # can be one of "NONE", "BACKGROUND",
                                # "MINIBACKGROUND", "-BACKGROUND", "OBJECTS",
                                # "-OBJECTS", "SEGMENTATION", "APERTURES",
                                # or "FILTERED" (*)
CHECKIMAGE_NAME  check.fits    # Filename for the check-image (*)

#----- Memory (change with caution!) -----
MEMORY_OBJSTACK 2000           # number of objects in stack
MEMORY_PIXSTACK 100000         # number of pixels in stack
MEMORY_BUFSIZE  1024           # number of lines in buffer

#----- Miscellaneous -----
VERBOSE_TYPE     NORMAL        # can be "QUIET", "NORMAL" or "FULL" (*)

#----- New Stuff -----
ASSOC_DATA       1,2,3         # Nos of columns in the ASSOC file copied to the output
ASSOC_NAME       lhs1234.list  # Name of the ASSOC ASCII file
ASSOC_PARAMS     1,2,3         # # of columns in the ASSOC file
ASSOC_RADIUS     10            # search radius (pixel) for ASSOC
ASSOC_TYPE       FIRST         # method for cross-matching in ASSOC
ASSOCSELEC_TYPE  MATCHED       # only matched detections

```

Figure E.1: The example of configuration file and enter the last block called “new stuff”.

- 4) run the SExtractor program
- 5) sort the output files
- 6) add more *.sex file

Option 0

Option 0 is to sort all images by time. This task will generate a new file called **listfile**, which contains all the images' file name and the first image will be the earliest one. If you add new frames, it will delete the existing *listfile* and generate a new one. It will also tell you total numbers of frames printed on the screen.

Option 1

Modify the *.list.* file which will be discussed more in the next session.

Option 2

Because every image will have its own configuration file, this option generates numbers of configuration files based on a seed file called **lhs1234.sex**. If there are 50 frames in this directory, 50 configuration files will be generated, from **lhs1234.sex.1** to **lhs1234.sex.50**⁴. Every generated file will be identical to that seed file, except **CATALOG_NAME**. The number of **CATALOG_NAME** should be correspond to the number of **lhs1234.sex.***.

Option 3

We will explain about selecting reference stars and science stars before discussing this option 3. The following are the general guidelines for choosing the preliminary reference stars for parallax reduction.

1. Ideally, you first crosscheck the parallax setup frame against the frame(s) on which you will do photometry. If any star near an edge has fallen off the VRI frames, you can't use it for a reference star because you won't have VRI for refraction and the correction to absolute parallax. If you don't have the VRI photometry frames, yet, keep the stars along the edge as reference stars.

⁴**rm lhs1234.sex.1[0-9]** to delete files from 10 to 19, if you need to delete them.

2. To select reference stars, choose a single frame in the parallax filter that has seeing better than 1.5" and has ellipticity less than about 0.2.
3. Each possible reference star should be checked to make sure that it is not a close double star or a galaxy.
4. You want a balanced reference field. So, choose a reference star configuration that surrounds the target star (if possible).
5. You should have at least 5 reference stars, but not more than 15. Tests have shown that more than 15 reference stars typically makes the residuals worse, not better.
6. If the peak count < 100 is a possible reference star, don't use that star. This does NOT mean that anything above 100 counts is useful. You really want to stay above about 1000 counts, but can try going lower if you don't have 5 reference stars.

These pre-selected stars will be under further examination after the first round of parallax reduction.

We found that parallax star offset of those images under **lhs1234** is not consistent from one night to the other or between different observation runs. Therefore, **tag the reference stars and science stars in each night/block is necessary**. You can use `redpi/displayexam` to examine the image first, to remove some bad images, like elongated frames or telescope wobbling frames, etc. Then copy the **listfile** to **taglist**.

For example, if we have images for *lhs1234* in the listfile:

```
(row 01):aug99s.1100.o.fits – 10 images,
(row 11):aug99s.2200.o.fits – 9 images,
(row 20):may00s.2100.o.fits – 11 images,
(row 31):jun00s.4220.o.fits – 12 images,
(row 43):sep01s.1230.o.fits – 8 images.
```

We assume the pi star offset is consistent within one night. You may choose one image for each night to display and tag it. Therefore, the **taglist** should only contain five rows.

```
(row 01):aug99s.1100.o.fits,
(row 02):aug99s.2200.o.fits,
(row 03):may00s.2100.o.fits,
(row 04):jun00s.4220.o.fits,
(row 05):sep01s.1230.o.fits.
```

After you edit the **taglist** file, you may start to use **redpi/taglist** task to tag the preliminary centroids.

1. launch ximtool or SAOimage (ds9).

2. `cl>taglist`

Then you need to enter the 7 characters object name. If there are 11 references, mark numbers besides reference star from 1 to 11 on this print out sheet (Table E.4). **The parallax star is ALWAYS the LAST one. If you have more than 1 parallax star, put your primary star in the last one.** Parallax star will be #12 in this example.

3. Move your cursor over a reference star, then hit space key as you move the cursor from #1 star to #12 star. **You have to follow this sequence. Ctrl_z** to exit this task.

4. *lhs1234.list.20000502* will be generated for 0.9m and *lhs1234.list.may00b.2100* for 1.5m data. The number of *.list.* will be the same as the line in **taglist** file. After you finish tagging all the images, this task will stop. This tagging series is time consuming, so please be patient.

5. Use **Option 1** to modify the last two columns of each *.list.* file to the following format

```
670.50 1422.50 1
1002.50 1110.50 2
846.50 1022.50 3
444.50 600.50 4
.....
555.50 444.50 125
```

⁵If there are two or more pi stars, it will have #13 or higher.

After you get the preliminary coordinate, you may run this *option 1*. This option will modify the **ASSOC_NAME** in *.sex.* files. Having an open *listfile* is essential while you choose this option.

For example, if we need to modify coordinate file at second night of May 2000. This option 3 will ask you these questions:

1. which *.sex.* needs to be changed (the first one)
enter 20. (the first image at that night is in 20th row in the listfile)
2. how many frames in that night
enter 11
3. the third block after the . field separator of *.list.*****
enter 20000502 or **may02b.2100**

The whole idea about this is that each *.list.* file name is unique and can not be the same.

Hint: It is strongly recommended to use the third or the forth image as the tagging file for each night in the taglist.

Option 4

This option will execute *sex* command and get the centroid. It generates 50 files from *lhs1234.coord1* to *lhs1234.coord50*. This option has two sub choices, one is for *reducing as first time* and the other is *reducing added frames*. For example, you have reduced all the frames under lhs1234, but new frames are added from later observation runs. You need to choose the second choice, so that it will not ruin the old data. Please check *option 6* to know how to add new *.sex files.

SExtractor sometimes finds 13 stars even though there are only 12 stars in *lhs1234.list.****** file. One way to check whether SExtractor finds them all or not is to note that as this program runs, the SExtractor will prompt the result on the screen. The other way is to run **wc -l *.coord*** to count how many lines are there in each *.coord* file. Any number shown on the screen needs to have 8 subtract from it, because there are 8 lines of header in each *.coord* file. If it lost some objects or it finds more objects than you selected, run this image individually and reset the coordinate list file by using iraf task **rimcursor**. For example, if SExtractor found 5 objects in the sep01s.1235.o.fits,

1. **cl>display sep01s.1235.o.fits 1 fl+**

2. **rimcursor >> lhs1234.list.sep01b.1235** or
rimcursor >> lhs1234.list.20010911.235

3. run **sss/option 1**

command for reduce image individually:

sex sep01s.1235.o.fits -c lhs1234.sex.33 (sep01s.1235.0.fits is the 33th frame in the *listfile* file.)

The new **lhs1234.list.20010911.235** is necessary for this particular image. Make sure to modify the **lhs1234.sex.33** after the new **lhs1234.list.20010911.235** is created.

If SExtractor finds more than you need, open the *.coord* file and delete those you don't need.

Again, this centroid is time consuming, especially for a resolvable binary system. Patience can guarantee your finding the right reference and science stars. If any star's (x,y) coordinate is not correct or missed, it will causes **gaussfit** program to diverge. 99% of **gaussfit** error is because of this issue.

Option 5

This option will gather and sort all the *lhs1234.coord** files and generate a file called *lhs1234.sexout*. This is a master list of *.coord* files. The earliest images will be in the first line.

Option 6

When you choose this option, **please run option 0 first**. Option 6 will append new frames to *listfile*. Then do option 3 to fix *.sex file and option 4 to execute SExtractor. Please make sure that there is NO *.sexout under this directory BEFORE YOU RUN OPTION 4. Then run option 5 to sort the output file file and generate a new *.sexout file.

E.4 VRI Photometry Stars

Please refer to the **CTIOPI photometry Reduction User Guide** to reduce the VRI photometry for all selected reference stars and science stars. The photometry will be named as **lhs1234.phot** and the input format has to be (*A10, 3(2x,F6.3)*). For example,

xgj01025-1	16.021	15.325	14.745		xlhs1234-1	16.021	15.325	14.745
xgj01025-2	16.680	16.273	15.841	or	xlhs1234-2	16.680	16.273	15.841
gjj01025-10	13.359	12.109	10.555		lhs1234-10	13.359	12.109	10.555

E.5 JPL DE405

Please visit <ftp://ssd.jpl.nasa.gov/pub/eph/export/> to download the DE405 package in FORTRAN version. The goal here is to generate a binary ephemerides file. The installation of this package is skipped here. Please follow the readme which is associated with the DE405 package to finish compiling and run a test program. You may compare your result with the astronomical almanac to make sure your program is correctly compiled. Please rename this generated binary file as **de405.1980.2020.eph** which means this binary file covers from 1980 to 2020.

E.6 Generate Lots of Files

Before continuing the parallax data reduction, please make sure **lhs1234.hinfo**, **lhs1234.phot**, **lhs1234.sexout** are generated. Make a symbolic link for **de405.1980.2020.eph** under this directory. For example,
 (unix prompt)> ln -s **/**/default/de405.1980.2020.eph de405.1980.2020.eph**.
 The ****** indicates the path where you put/save this binary file.

Have the coordinate and proper motion of this science star ready for **genpif** FORTRAN program. This program is compiled from three programs, which are *genpif.f*, *genpif.sub1.f* and *genpif.sub2.f*. The coordinate of this last tagged/science star has to be equinox J2000, but the epoch can be any time. A couple of questions prompted by **genpif** are as following,

1. **please choose telescope:0.9M=0, 1.5M=1**
2. **applied DCR refraction; NO=0, YES=1**
3. **ENTER RA AND DEC (HH MM SS DD MM SS) AND Epoch**
4. **mu("/YR), angle(degree)**
5. **total frame #**
6. **enter the object name,the same as *.hinfo:**

7. **how many total star are there:**
8. **include all the stars fainter than 100 peak count**
(Yes=1, No=0)
9. **which filter is used V=1, R=2, I=3** (if DCR is applied)

The most common errors while using **genpif** are,

1. user doesn't create the link file for de405.1980.2020.eph.
2. the format problem of lhs1234.phot.

There are two different kinds of files that will be generated after running this program. They are **coord.*** and **lhs1234.pifonly**. Also, this program will print frames ID which meets the trail plate requirement on the screen. The trail plate criterion are,

1. All the pre-selected reference stars and science stars are with peak counts less than 65500 and greater than 100.
2. All the pre-selected reference stars and science stars are with ellipticity less than 0.2.
3. All the pre-selected reference stars and science stars are with FWHM less than 2.5".

If you want to include all the faint objects less than 100 peak counts, the trail plate criterion will be,

1. All the pre-selected reference stars and sciences are with peak counts less than 65500.
2. All the pre-selected reference stars and sciences are with ellipticity less than 0.6.
3. All the pre-selected reference stars and sciences are with FWHM less than 2.5".

Furthermore, if the last parallax stars are not in the **coord.*** file due to various reasons, this frame ID will also be printed on the screen. For example, if the screen prints

star ID 12 is not in coord. 40

You need to remove this frame,

prompt>mv coord.40 40.coord to rename this file.

The data in the generated **coord.*** from left to right column are, frame ID, star ID, Julian Date, parallax factor in RA, parallax factor in DEC, centroid in X direction and centroid in Y direction. The centroid has been calculated in order to match the sky, North-up and East-right. Therefore, the (x,y) coordinate will be different from the output by SExtractor. Furthermore, if DCR is chosen, the coordinate (x,y) has DCR fixed.

The **lhs1234.pifonly** file contains all the information of the last parallax star (if you have more than 1 science star). They are frame ID, year fraction, parallax factor in RA, parallax factor in DEC, hour angle and FWHM in arcsec from left to right. If there are more than 1 image is listed on the screen as a trail plate. Please open this **lhs1234.pifonly** file to select the best one with good seeing among those frames which are printed on the screen after **genpif**. Record this frame ID on the parallax reduction sheet, which is shown in Figure E.4. At the mean time, you may swing back to the IRAF window to run **redpi/wcsangel** task. After you get the rotation angle, record it on the parallax reduction sheet and run a FORTRAN program, **pltrotate** to rotate the trail plate.

E.7 Running Gaussfit

Gaussfit is a program designed by the astrometry team in U. of Texas for solving least squares equations. The Gaussfit program needs to be compiled depending on the operation system and have **gaussfit** under your bin directory. The latest Gaussfit program will be attached with this user guide instead of the Gaussfit ftp site. As of September 2003, the released copy on the **ftp://clyde.as.utexas.edu/pub/gaussfit** can't handle more than 99 parallax frames. The current copy is kindly provided by B. E. McArthur in the U. of Texas. Users should keep track on the new updated version on this ftp site.

The detail of Gaussfit is skipped here. Users can find the Gaussfit user guide through **ftp://clyde.as.utexas.edu/pub/gaussfit/manual/**.

Before running the Gaussfit program, you need to remove some of the bad frames with very few stars left in the coord.* files. Type
(unix prompt)> wc -l coord.*

It will give you the available star counts in each coord.* files. The number shown on the screen should have 2 subtracted from it to get the true star counts because

there are two leading headers in every files. If a frame with line counts less than 8, including science stars, it should be removed. If there are two science stars, the limit will be 9. In other words, 5 reference stars are necessary. Then, for example, if coord.13 has only 4 star counts in that file,type

```
(unix prompt)> mv coord.13 13.coord
```

Cross out these bad frame ID numbers on the parallax reduction sheet. After it is finished, run a batch script called **gauss.uty** which is saved under your bin directory.

There are two options in the script,

option 1: This option mainly generates the necessity files for the Gaussfit program.

They are, **cataloge**, **env**, **setPar**, **piPar** and **muPar**. I called these files utility files. The most of important of all, this task will create a directory called **coordbak** which contains all the coord.*. Of course, the *.coord files, bad images with very few star counts or lost science stars will not copy to this directory.

option 2: This option will remove the data star with the ID you have entered.

Choose option 1, first. You need to enter the trail plate file, for example, **coord.20** in the prompt. You now can edit the model file, **ctio.model**. Three different modified is required, First, enter the trail plate number in the doconstraints() block,

```
exportconstraint(a[20]-1);
exportconstraint(b[20]);
exportconstraint(c[20]);
exportconstraint(d[20]);
exportconstraint(e[20]-1);
exportconstraint(f[20]);
```

Second, replace **xxxxxxx** in the model() block with the Julian data from the trail plate. Replace the **xxxxxxx** in the domusums() block with the science star ID. If there are more than 1 science star, ID=12 and ID=13, it is better to create a new directory called **B.component**. Copy coord.* under coordbak/ directory to this B.component directory or re-run **genpif** under B.component directory. Use **gauss.uty/option2** to remove 12 or 13, so that there is only one science star in each directory. Replace the **xxxxxxx** with appropriate star ID.

Type **gaussfit ctio.model env** under your shell window. When Gaussfit finishes, you will notice the “Chi-Square” and “DOF” will be printed on the screen.

Three more new files, *results*, *results.corr* and *results.cov* will be generated. The final relative parallax and proper motion can be found in **piPar** and **muPar**.

The next step is to calculate the photometric distance for the reference stars. Type

```
(unix prompt)> cp lhs1234.phot lhs1234.refphot
```

Delete the science stars in the *.refphot file. This lhs1234.refphot file is used by a FORTRAN program **refdist**. A new file, lhs1234.refdistance, is created.

E.8 Finalize the Parallax Reduction

We have finished the first round of parallax reduction. Based on this output, we need to further examine the quality of the reference stars. An IDL program, **parallax.stats.pro** is used to assist you to analysis the output data.

type idl under your shell window to launch your idl program.

```
IDL>.run parallax.stats.pro (run it twice)
```

```
IDL>piplot, 100,13
```

The first number after “piplot” is the last frame ID in the env file and the second number is the last star ID in the coord.* file. A couple of output files are created, **lhs1234.stats.residual.out**, **lhs1234.stats.pi.residual.out** and **lhs1234.stats.plot.ps**.

lhs1234.residual.out contains the star ID with the highest residual in both X and Y direction among every frame. **lhs1234.stats.pi.residual.out** contains the year fraction and X and Y residual in both direction. The only postscript file plots the year of fraction against hour angle, seeing, x-residual and y-residual in the upper-left, lower-left, upper-right and lower-right plots respectively. The insets inside the hour angle plot, is the parallax factor. The horizontal axis is the parallax factor in x and the vertical axis is parallax factor in y. Due to the size of this plot, no label is shown. However, the residual is only plotted for the last science star. The example plot is shown in Figure E.2.

There are a couple of ways to determine whether the reference stars are good or not. If any references meets any of the following criterion, you may consider it as a bad reference star.

1. If a star appears the most in the lhs1234.stats.residual.out
2. high parallax ($>0.005''$) in the piPar file.

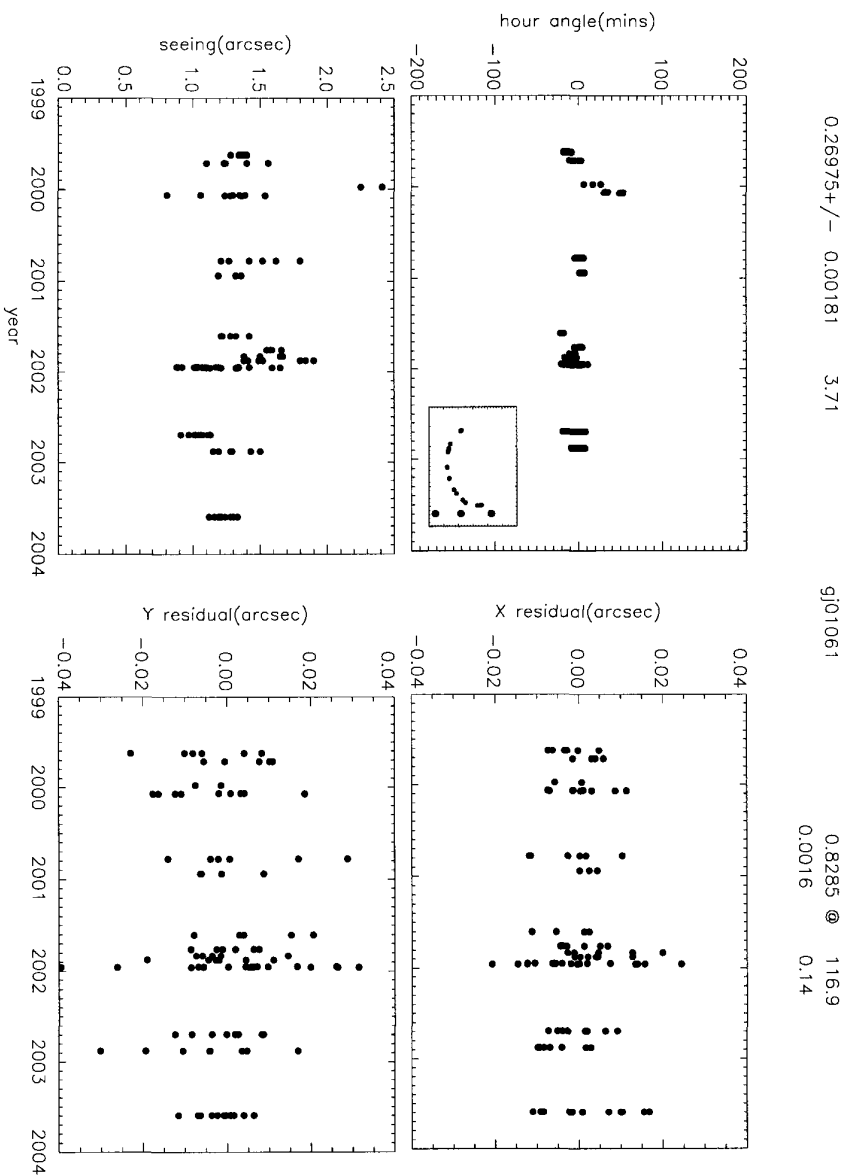


Figure E.2: The example plot from the parallax.stats.pro IDL program. The numbers shown on top of this plot are parallax, error, distance in pc, star name, proper motion and angle. The second line under the proper motion and angle are errors, respectively.

3. a reference with large photometric parallax ($>0.002''$)

Basically, this is just a general guideline. If the parallax error is less than 2 mas, these reference stars are very good. With the current setting in CTIOPI, it is impossible to lower the parallax error below 1 mas. The other problem is the total number of references. More reference stars DOESN'T mean a better result, but fewer reference stars (less than) 5 will possibly give bad results. For example, in the CTIOPI GJ1025 field, 7 initial reference stars are selected. After the first round of reduction, one star has been removed. We have to keep the other 6 stars even though star ID 6 and 7 with photometric distance greater than $0.002''$ and large parallax in piPar file. Removing star ID 4 can lower our parallax error. However, removing 6 and 7 from the current list will increase the error dramatically. The reason is if we remove too many "bad" stars, we will have lost the reference points to calculate the plate constants. The star ID 4 is removed because of high residual in the most of frames.

If you need to remove any star in the coord.* file, use **gauss.uty/option 2** bash script. Then re-run the Gaussfit program to get relative parallax.

The other issue will effect the parallax error is the time line and frame number for your parallax data. More frames and fewer frames will have low parallax error. Short time line will have smaller error than the longer time line too. Therefore, there is not a very sharp guide line to de-select reference stars in order to lower the parallax error. It is very empirical and data dependent.

After finalizing your reference stars, you need to get the photometric parallax for the reference stars once again. Open the lhs1234.refphot file and delete any star you have deleted due to various reasons. Then re-run the **refdist** program. All of the main programs used in this reduction are summarized in the Figure E.3.

Currently, the final parallax requires

1. parallax error < 3 mas
2. 4 or more seasons
3. 40 or more useful frames
4. longer than 2.50 years baseline
5. VRI photometry done

**CTIOPI parallax
Reduction Flowchart**

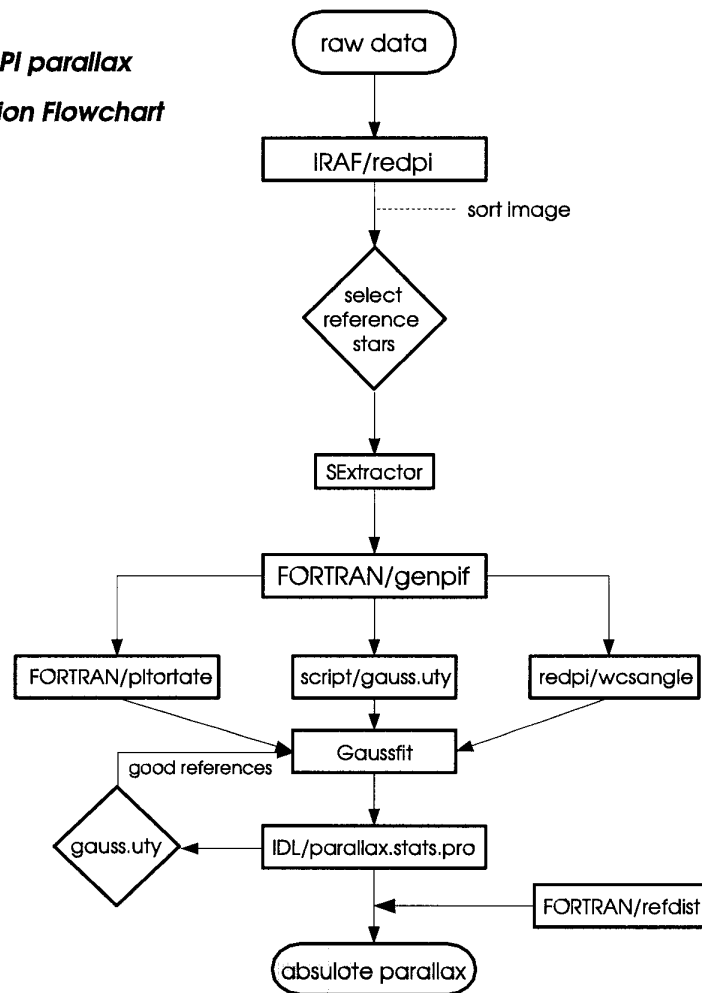


Figure E.3: The flow chart of parallax data reduction

E.9 Concerning gauss.uty and the IDL Program

1. For some reasons, you have found that one reference star is bad and you want to copy the back-up coord.* files under **coordbak**, then re-run Gaussfit. You HAVE TO run **gauss.uty/option1** to generate these utility files before you remove this bad star by using **gauss.uty/option2**.
2. Whenever you run **gauss.uty/option1**, it will create **coordbak** directory and copy all the coord.* to it. If you run it second time and **coordbak** exists, it will have a error message shown on the screen. You re-run the **genpif** to generate a new coord.* files. Those files under coordbak should be good.
3. After the first round of reduction, you should have results in muPar and piPar for every single star. When you remove those bad reference stars and re-run Gaussfit, the data for those removed stars will still in the muPar and piPar files.
4. If you science star is not in the last tagging sequence, **parallax.stats.pro** can't be applied for this case.
5. If the science star has a residual larger than 30 mas in either direction, you will see a * sign in the plot. It is always plotted on $y = 0.35$. You may also try to remove this frame then run Gaussfit once again to reduce the error.

Object:

Frame ID																				
1	2	3	4	5	6	7	8	9	10	11	12	13	14	15	16	17	18	19	20	
21	22	23	24	25	26	27	28	29	30	31	32	33	34	35	36	37	38	39	40	
41	42	43	44	45	46	47	48	49	50	51	52	53	54	55	56	57	58	59	60	
61	62	63	64	65	66	67	68	69	70	71	72	73	74	75	76	77	78	79	80	
81	82	83	84	85	86	87	88	89	90	91	92	93	94	95	96	97	98	99	100	
101	102	103	104	105	106	107	108	109	110	111	112	113	114	115	116	117	118	119	120	
121	122	123	124	125	126	127	128	129	130	131	132	133	134	135	136	137	138	139	140	
141	142	143	144	145	146	147	148	149	150	151	152	153	154	155	156	157	158	159	160	
161	162	163	164	165	166	167	168	169	170	171	172	173	174	175	176	177	178	179	180	
181	182	183	184	185	186	187	188	189	190	191	192	193	194	195	196	197	198	199	200	

ref star ID: 1 2 3 4 5 6 7 8 9 10 11 12 13 14 15 16 17 18 19 20

trail plate rotation angle=

Figure E.4: The parallax reduction sheet.

Quick References (Part 1)		
Main Blocks	Steps	what to do
Raw Data	1	fix99 (IRAF/redpi) (if necessary)
	2	fixname, gof and proc (IRAF/redpi)
	3	sort image by object name
Preparation	1	copy ctio.model, default.sex, default.param and parallax.stats.pro to lhs1234/
	2	make a link of de405.1980.2020.eph
	3	replace "default" to the object name (ex:lhs1234) reduce parallax field VRI photometry
	4	select reference stars with VRI photometry
	5	make lhs1234.phot file run sss/bbb option 0 to generate listfile displayexam(IRAF/redpi) to delete bad images
select references & science stars	1	
	2	make taglist file
	3	run taglist(IRAF/redpi) to tag stars (SPACE key:tag, ctrl-z:quit) NOTE: tag star in an order and pi star is always the last one.
		run (unix prompt>) wc -l *.list.* to check the number of stars tagged
run SExtractor	4	run sss/bbb option 1
	1	run sss/bbb option2
	2	run sss/bbb option 3 to fix the *.list.*
	3	run sss/bbb option 4 to execute SExtractor program
	4	run (unix prompt>) wc -l *.coord* to check any extra/missing stars in the *.coord* (if necessary, run these problematic images individually.)
	5	run sss/bbb option 6 to generate lhs1234.sexout

Table E.2: parallax data reduction quick reference 1

Quick References (Part 2)		
Main Blocks	Steps	what to do
get image header	1	run headmet (IRAF/redpi) open and organize lhs1234.hinfo file. double check image filter
get coordinate	1	get the coordinate and mean epoch from 2MASS all sky released version
generate coord.* lhs1234.pifonly	1 2	run genpif (FORTRAN)
trail plate	1	follow the prompt
	2	select one trail plate with small HA and seeing from lhs1234.hinfo run wcsangle (IRAF/redpi) to get trail plate angle relative to GSC2.2
	3	run pltrotate (FORTRAN) to rotate the trail plate
Gaussfit	1	run (unix prompt>)wc -l coord.* to remove frames with references less than 5
	2	rename these bad coord.* to *.coord
	3	modify ctio.model file
	4	run gauss.uty option 1
	5	run gaussfit
IDL	1	run (IDL prompt >).run parallax.stats.pro (run it twice)
	2	run (IDL prompt >) piplot, total.image, last.star_ID
	3	select any bad reference stars or bad images
	4	run gauss.uty option 2 to remove bad references
	5	remove all coord.* files
	6	copy coord.* from coordbak/ directory
		run gauss.uty option 1 to re-generate gaussfit utility files
		re-run gaussfit

Table E.3: parallax data reduction quick reference 2

Quick References (Part 3)		
Main Blocks	Steps	what to do
absolute parallax	1	copy lhs1234.phot to lhs1234.refphot
	2	remove pi star and only leave these good reference stars
	3	run refdist (FORTRAN) to generate lhs1234.refdistance
	4	final check on the reference stars
If necessary, return to the Gaussfit block to re-run gaussfit		
correct relative parallax to absolute parallax		
final parallax		

Table E.4: parallax data reduction quick reference 3

References

- Abell, G. O. (1959). The National Geographic Society-Palomar Observatory Sky Survey. *Leaflet of the Astronomical Society of the Pacific*, 8:121.
- Alonso, A., Arribas, S., and Martinez-Roger, C. (1994). Broad band JHK infrared photometry of an extended sample of late type dwarfs and subdwarfs. *A&A*, 107:365–383.
- Bakos, G. A., Sahu, K. C., and Nemeth, P. (2002). Revised coordinates and proper motions of the stars in the Luyten half-second catalog. *ApJS*, 141:187–193.
- Baraffe, I., Chabrier, G., Allard, F., and Hauschildt, P. H. (1998). Evolutionary models for solar metallicity low-mass stars: mass-magnitude relationships and color-magnitude diagrams. *A&A*, 337:403–412.
- Barbieri, C., Demarchi, G., Nota, A., Corrain, G., Hack, W., Ragazzoni, R., and Macchetto, D. (1996). First HST/FOC images of the low mass companion of the astrometric binary gliese 623. *A&A*, 315:418–420.
- Beaulieu, T. (2004). The spectroscopy observation for MOTION stars. *AJ*, in preparation.
- Benedict, G. F., McArthur, B., Chappell, D. W., Nelan, E., Jefferys, W. H., van Altena, W., Lee, J., Cornell, D., Shelus, P. J., Hemenway, P. D., Franz, O. G., Wasserman, L. H., Duncombe, R. L., Story, D., Whipple, A. L., and Fredrick, L. W. (1999). Interferometric Astrometry of Proxima Centauri and Barnard’s Star Using Hubble Space Telescope Fine Guidance Sensor 3: Detection Limits for Substellar Companions. *AJ*, 118:1086–1100.
- Bergeron, P., Leggett, S. K., and Ruiz, M. T. (2001). Photometric and Spectroscopic Analysis of Cool White Dwarfs with Trigonometric Parallax Measurements. *ApJS*, 133:413–449.

- Bertin, E., and Arnouts, S. (1996). SExtractor: Software for source extraction. *A&A*, 117:393–404.
- Bessell, M. S. (1990). BVRI photometry of the gliese catalogue stars. *A&AS*, 83:357–378.
- Bessell, M. S. (1991). The late-M dwarfs. *AJ*, 101:662–676.
- Bidelman, W. P. (1985). G. P. Kuiper’s spectral classifications of proper-motion stars. *ApJS*, 59:197–227.
- Binney, J., and Merrifield, M. (1998). *Galactic Astronomy*. Princeton University Press, Princeton, NJ.
- Burgasser, A. J., Kirkpatrick, J. D., Brown, M. E., Reid, I. N., Burrows, A., Liebert, J., Matthews, K., Gizis, J. E., Dahn, C. C., Monet, D. G., Cutri, R. M., and Skrutskie, M. F. (2002). The spectra of T dwarfs. I. near-infrared data and spectral classification. *ApJ*, 564:421–451.
- Burgasser, A. J., Kirkpatrick, J. D., Burrows, A., Liebert, J., Reid, I. N., Gizis, J. E., McGovern, M. R., Prato, L., and McLean, I. S. (2003). The First Substellar Subdwarf? Discovery of a Metal-poor L Dwarf with Halo Kinematics. *ApJ*, 592:1186–1192.
- Carney, B. W. (1983). A photometric search for halo binaries - part two - results. *AJ*, 88:623.
- Carney, B. W., Latham, D. W., Laird, J. B., and Aguilar, L. A. (1994). A survey of proper motion stars. XII: an expanded sample. *AJ*, 107:2240–2289.
- Cayrel de Strobel, G., Soubiran, C., Friel, E. D., Ralite, N., and Francois, P. (1997). A catalogue of [Fe/H] determinations: 1996 edition. *A&AS*, 124:299–305.
- Christy, J. W., and Walker, R. L., J. (1969). MK classification of 142 visual binaries. *PASP*, 81:643.
- CNS3-website (2004). The on-line database for CNS3. CNS3 website at <http://www.ari.uni-heidelberg.de/aricns/index.htm>.
- Dahn, C. C., Harrington, R. S., Kallarakal, V. V., Guetter, H. H., Luginbuhl, C. B., Riepe, B. Y., Walker, R. L., Pier, J. R., Vrba, F. J., Monet, D. G., and Ables,

- H. D. (1988). U.S. Naval Observatory parallaxes of faint stars - List VIII. *AJ*, 95:237–246.
- Dahn, C. C., Harrington, R. S., Riepe, B. Y., Christy, J. W., Guetter, H. H., Kallarakal, V. V., Miranian, M., Walker, R. L., Vrba, F. J., Hewitt, A. V., Durham, W. S., and Ables, H. D. (1982). U.S. Naval Observatory parallaxes of faint stars. VI. *AJ*, 87:419–427.
- Dahn, C. C., Harris, H. C., Vrba, F. J., Guetter, H. H., Canzian, B., Henden, A. A., Levine, S. E., Luginbuhl, C. B., Monet, A. K. B., Monet, D. G., Pier, J. R., Stone, R. C., Walker, R. L., Burgasser, A. J., Gizis, J. E., Kirkpatrick, J. D., Liebert, J., and Reid, I. N. (2002). Astrometry and photometry for cool dwarfs and brown dwarfs. *AJ*, 124:1170–1189.
- Dawson, P. C. (1986). The luminosity function of the halo population in the solar neighborhood. *AJ*, 311:984–1000.
- Dawson, P. C., and De Robertis, M. M. (2000). Optical/near-infrared spectroscopy of 10 late-type dwarfs: Comparison with models. *AJ*, 120:1532–1540.
- Dawson, P. C., and Forbes, D. (1989). BVRI photometry of 30 proper motion stars. *PASP*, 101:614.
- Delfosse, X., Forveille, T., Martin, E. L., Guibert, J., Borsenberger, J., Crifo, F., Alard, C., Epchtein, N., Fouque, P., Simon, G., and Tajahmady, F. (2001). New neighbours: II. An M9 dwarf at d=4 pc, DENIS-P J104814.7-395606.1. *A&A*, 366L:13–17.
- Dennis, T. R. (1965). On the Possibility of Determining the Helium Content of the Subdwarf μ Cassiopeiae. *PASP*, 77:283.
- Digby, A. P., Hambly, N. C., Cooke, J. A., Reid, I. N., and Cannon, R. D. (2003). The subdwarf luminosity function. *MNRAS*, 344:583–601.
- Duquennoy, A., and Mayor, M. (1991). Multiplicity among solar-type stars in the solar neighbourhood. II - Distribution of the orbital elements in an unbiased sample. *A&A*, 248:485–524.
- Eichhorn, H. (1974). *Astronomy of star positions; a critical investigation of star catalogues, the methods of their construction, and their purpose*. Ungar, New York.

- Eichhorn, H., and Jefferys, W. H. (1971). In Ianna, P., editor, *Proceedings of the Forth Astrometric Conf.*, volume 16, page 267, Schenectady, N.Y. Leander McCormick Obs.
- European Space Agency (1997). The Hipparcos and Tycho Catalogues (ESA 1997). *VizieR Online Data Catalog*, 1239.
- Filippenko, A. V. (1982). The importance of atmospheric differential refraction in spectrophotometry. *PASP*, 94:715–721.
- Fischer, D. A., and Marcy, G. W. (1992). Multiplicity among M dwarfs. *ApJ*, 396:178–194.
- Giampapa, M. S., and Liebert, J. (1986). High-resolution H-alpha observations of M dwarf stars Implications for stellar dynamo models and stellar kinematic properties at faint magnitudes. *ApJ*, 305:784–794.
- Giclas, H. L., Burnham, R., and Thomas, N. G. (1971). *Lowell proper motion survey Northern Hemisphere. The G numbered stars. 8991 stars fainter than magnitude 8 with motions > 0.26/yr.* Flagstaff, Arizona: Lowell Observatory, 1971.
- Giclas, H. L., Burnham, R., and Thomas, N. G. (1978). Lowell Proper Motion Survey - Southern Hemisphere Catalog 1978. *Lowell Observatory Bulletin*, 8:89.
- Gizis, J. E. (1997). M-subdwarfs: Spectroscopic classification and the metallicity scale. *AJ*, 113:806–822.
- Gizis, J. E., Monet, D. G., Reid, I. N., Kirkpatrick, J. D., Liebert, J., and Williams, R. J. (2000). New neighbors from 2MASS: Activity and kinematics at the bottom of the main sequence. *AJ*, 120:1085–1099.
- Gizis, J. E., and Reid, I. N. (1999). M Subdwarfs: The Population II Luminosity Function. *AJ*, 117:508–520.
- Gizis, J. E., and Reid, I. N. (2000). Hubble Space Telescope Observations of M Subdwarfs. *PASP*, 112:610–613.
- Gliese, W. (1957). Katalog der Sterne näher ALS 20 Parsek für 1950.0. *Astron. Rechen-Institut, Heidelberg*, 89 Seiten, 8.
- Gliese, W. (1969). Catalogue of Nearby Stars. Edition 1969. *Veroeffentlichungen des Astronomischen Rechen-Instituts Heidelberg*, 22.

- Gliese, W., and Jahreiß, H. (1979). Nearby Star Data Published 1969-1978. *A&AS*, 38:423–448.
- Gliese, W., and Jahreiß, H. (1980). The Use of Luyten’s Magnitude Estimates in the Selection of Red Nearby Star Suspects from His Proper Motion Catalogues LHS and NLTT. *A&A*, 85:350–352.
- Gliese, W., and Jahreiß, H. (1991). Preliminary Version of the Third Catalogue of Nearby Stars. Technical report.
- Gould, A., and Salim, S. (2003). Improved Astrometry and Photometry for the Luyten Catalog. I. Bright Stars. *AJ*, 582:1001–1010.
- Graham, J. A. (1982). UBVRI Standard Stars in the E-Regions. *PASP*, 94:244.
- Gray, D. F., and Nagar, P. (1985). The rotational discontinuity shown by luminosity class IV stars. *ApJ*, 298:756–760.
- Gray, R. O., Napier, M. G., and Winkler, L. I. (2001). The Physical Basis of Luminosity Classification in the Late A-, F-, and Early G-Type Stars. I. Precise Spectral Types for 372 Stars. *AJ*, 121:2148–2158.
- Greenstein, J. L. (1984). Spectrophotometry of the white dwarfs. *ApJ*, 276:602–620.
- Gunn, J. E., and Stryker, L. L. (1983). Stellar spectrophotometric atlas, wavelengths from 3130 to 10800 angstrom. *ApJS*, 52:121–153.
- Hambly, N. C., Henry, T. J., Subasavage, J. P., Brown, M. A., and Jao, W. C. (2004). The Solar Neighborhood VIII: Discovery of New High Proper Motion Nearby Stars Using the SuperCOSMOS Sky Survey. *AJ*, in preparation.
- Hambly, N. C., MacGillivray, H. T., Read, M. A., Tritton, S. B., Thomson, E. B., Kelly, B. D., Morgan, D. H., Smith, R. E., Driver, S. P., Williamson, J., Parker, Q. A., Hawkins, M. R. S., Williams, P. M., and Lawrence, A. (2001). The SuperCOSMOS Sky Survey - I. Introduction and description. *MNRAS*, 326:1279–1294.
- Hambly, N. C., Smartt, S. J., and Hodgkin, S. T. (1997). WD 0346+246: A Very Low Luminosity, Cool Degenerate in Taurus. *ApJ*, 489L:157.
- Harrington, R. S., and Dahn, C. C. (1980). Summary of U.S. Naval Observatory parallaxes. *AJ*, 85:454–465.

- Harrington, R. S., Dahn, C. C., Kallarakal, V. V., Guetter, H. H., Riepe, B. Y., Walker, R. L., Pier, J. R., Vrba, F. J., Luginbuhl, C. B., Harris, H. C., and Ables, H. D. (1993). U.S. Naval Observatory photographic parallaxes - List IX. *AJ*, 105:1571–1580.
- Harrington, R. S., Kallarakal, V. V., Christy, J. W., Dahn, C. C., Riepe, B. Y., Guetter, H. H., Ables, H. D., Hewitt, A. V., Vrba, F. J., and Walker, R. L. (1985). U.S. Naval Observatory parallaxes of faint stars - List VII. *AJ*, 90:123–129.
- Hartkopf, W. I., Mason, B. D., McAlister, H. A., Roberts, L. C., Turner, N. H., ten Brummelaar, T. A., Prieto, C. M., Ling, J. F., and Franz, O. G. (2000). ICCD Speckle Observations of Binary Stars. XXIII. Measurements during 1982-1997 from Six Telescopes, with 14 New Orbits. *AJ*, 119:3084–3111.
- Hartwick, F. D. A., Cowley, A. P., and Mould, J. R. (1984). Studies of late-type dwarfs. VI - Identification of Population II main-sequence stars at $M_v = +14$. *ApJ*, 286:269–275.
- Hawley, S. L., Gizis, J. E., and Reid, I. N. (1996). The Palomar/MSU Nearby Star Spectroscopic Survey II. The Southern M Dwarfs and Investigation of Magnetic Activity. *AJ*, 112:2799.
- Henry, T. J. (2004). The RECONS sample. *AJ*, in preparation.
- Henry, T. J., Franz, O. G., Wasserman, L. H., Benedict, G. F., Shelus, P. J., Ianna, P. A., Kirkpatrick, J. D., and McCarthy, D. W. (1999). The Optical Mass-Luminosity Relation at the End of the Main Sequence (0.08-0.20 M_\odot). *ApJ*, 512:864–873.
- Henry, T. J., Ianna, P. A., Kirkpatrick, J. D., and Jahreiß, H. (1997). The solar neighborhood IV: Discovery of the twentieth nearest star. *AJ*, 114:388–395.
- Henry, T. J., Johnson, D. S., McCarthy, D. W., J., and Kirkpatrick, J. D. (1992). Red / Infrared Observations of WOLF:424AB - are the Components Substellar. *A&A*, 254:116.
- Henry, T. J., Kirkpatrick, J. D., and Simons, D. A. (1994). The low-mass companion of Gliese 22A - First results of the Steward Observatory infrared speckle camera. *AJ*, 108:1437–1444.

- Henry, T. J., and McCarthy, D. W. (1990). A systematic search for brown dwarfs orbiting nearby stars. *ApJ*, 350:334–347.
- Henry, T. J., Walkowicz, L. M., Barto, T. C., and Golimowski, D. A. (2002). The Solar Neighborhood. VI. New Southern Nearby Stars Identified by Optical Spectroscopy. *AJ*, 123:2002–2009.
- Høg, E., Fabricius, C., Makarov, V. V., Urban, S., Corbin, T., Wycoff, G., Bastian, U., Schwekendiek, P., and Wicenec, A. (2000). The Tycho-2 catalogue of the 2.5 million brightest stars. *A&A*, 355:L27–L30.
- Houk, N. (1988). *Michigan Catalogue of two-dimensional spectral types for the HD star*. Ann Arbor: University of Michigan, Departement of Astronomy, 1975-1999.
- Ianna, P. A., Begam, M. C., and Mullis, C. R. (1994). Preliminary Parallaxes for Southern Nearby Stars. *Bulletin of the American Astronomical Society*, 26:1347.
- Ianna, P. A., Patterson, R. J., and Swain, M. A. (1996). Parallaxes and Proper Motions From the McCormick Observatory: List 47. *AJ*, 111:492.
- Ibata, R. A., and Irwin, M. J. (1997). Discrete Classification with Principal Component Analysis: Discrimination of Giant and Dwarf Spectra in K Stars. *AJ*, 113:1865–1870.
- Jahreiß, H., Scholz, R., Meusinger, H., and Lehmann, I. (2001). Spectroscopic distance estimates for fourteen faint red LHS and NLTT stars. *A&A*, 370:967–973.
- Jao, W., Henry, T. J., Subasavage, J. P., Bean, J. L., Costa, E., Ianna, P. A., and Méndez, R. A. (2003). The Solar Neighborhood. VII. Discovery and Characterization of Nearby Multiples in the CTIO Parallax Investigation. *AJ*, 125:332–342.
- Jefferys, W. H. (1979). On the overlapping plate method in astrometry. *AJ*, 84:1775–1777.
- Jefferys, W. H., Fitzpatrick, M. J., and McArthur, B. E. (1987). Gaussfit - a system for least squares and robust estimation. *Celestial Mechanics*, 41:39.
- Keenan, P. C., and McNeil, R. C. (1989). The Perkins catalog of revised MK types for the cooler stars. *ApJS*, 71:245–266.

- Kirkpatrick, J. D., Henry, T. J., and McCarthy, Donald W., J. (1991). A standard stellar spectral sequence in the red/near-infrared - Classes K5 to M9. *ApJS*, 77:417–440.
- Koen, C., Kilkenny, D., van Wyk, F., Cooper, D., and Marang, F. (2002). UBVR(I)_C photometry of Hipparcos red stars. *MNRAS*, 334:20–38.
- Kunkel, W. E., Liebert, J., and Boroson, T. A. (1984). Van Biesbroeck 3 - A low-luminosity white dwarf, not an M dwarf. *PASP*, 96:891–893.
- Landolt, A. U. (1992). UBVR photometric standard stars in the magnitude range 11.5–16.0 around the celestial equator. *AJ*, 104:340–371, 436–491.
- Leggett, S. K. (1992). Infrared colors of low-mass stars. *ApJS*, 82:351–394.
- Leggett, S. K., Ruiz, M. T., and Bergeron, P. (1998). The cool white dwarf luminosity function and the age of the galactic disk. *ApJ*, 497:294.
- Lépine, S., Rich, R. M., Neill, J. D., Caulet, A., and Shara, M. M. (2002a). Discovery of an M8.5 Dwarf with Proper Motion $\mu = 2''.38/\text{yr}$. *ApJ*, 581:47–50.
- Lépine, S., Rich, R. M., and Shara, M. M. (2003a). LSR 1610-0040: The First Early-Type L Subdwarf. *ApJ*, 591:L49–L52.
- Lépine, S., Rich, R. M., and Shara, M. M. (2003b). Spectroscopy of New High Proper Motion Stars in the Northern Sky. I. New Nearby Stars, New High-Velocity Stars, and an Enhanced Classification Scheme for M Dwarfs. *AJ*, 125:1598–1622.
- Lépine, S., Shara, M. M., and Rich, R. M. (2002b). New High Proper Motion Stars from the Digitized Sky Survey. I. Northern Stars with $0''.5 \text{ yr}^{-1} < \mu < 2''.0 \text{ yr}^{-1}$ at Low Galactic Latitudes. *AJ*, 124:1190–1212.
- Lépine, S., Shara, M. M., and Rich, R. M. (2003c). New High Proper Motion Stars from the Digitized Sky Survey. II. Northern Stars with $0''.5 \text{ yr}^{-1} < \mu < 2''.0 \text{ yr}^{-1}$ at High Galactic Latitudes. *AJ*, 126:921–934.
- Luyten, W. J. (1939). *Bruce Proper Motion Survey III. The Stars of Large Proper Motion and the Luminosity Function*. Minneapolis: University of Minnesota, 1939.
- Luyten, W. J. (1955). *A catalogue of 1849 stars with proper motions exceeding $0''.5$ annually*. Minneapolis, Lund Press, 1955.

- Luyten, W. J. (1963). *Bruce Proper Motion Survey. The general catalogue. Vol. I and II*. Minneapolis: University of Minnesota, 1963.
- Luyten, W. J. (1979a). *LHS catalogue. A catalogue of stars with proper motions exceeding 0.5 annually*. Minneapolis: University of Minnesota, 1979, 2nd ed.
- Luyten, W. J. (1979b). *New Luyten Catalogue of Stars with Proper Motions Larger than Two Tenths of an Arcsecond*. Minneapolis: University of Minnesota.
- Luyten, W. J., and Albers, H. (1979). *An Atlas of Identification of Charts For LHS stars*. Minneapolis: University of Minnesota, 1979.
- Martin, E. L., Delfosse, X., Basri, G., Goldman, B., Forveille, T., and Rosa, Z. O. M. (1999). Spectroscopic Classification of Late-M and L Field Dwarfs. *AJ*, 118:2466–2482.
- Mason, B. D., Gies, D. R., Hartkopf, W. I., Bagnuolo, W. G., Brummelaar, T. T., and McAlister, H. A. (1998). ICCD speckle observations of binary stars. XIX - an astrometric/spectroscopic survey of O stars. *AJ*, 115:821.
- Massey, P., Valdes, F., and Barnes, J. (1992). *A user's guide to reducing slit spectra with IRAF*. NOAO, Tucson, Arizona.
- McCaughrean, M. J., Close, L. M., Scholz, R.-D., Lenzen, R., Biller, B., Brandner, W., Hartung, M., and Lodieu, N. (2004). ϵ Indi Ba,Bb: The nearest binary brown dwarf. *A&A*, 413:1029–1036.
- McCook, G. P., and Sion, E. M. (1999). A catalog of spectroscopically identified white dwarfs. *ApJS*, 121:1–130.
- Monet, D., editor (1996). *USNO A - 1.0 a catalog of astrometric standards*.
- Monet, D. G. (1998). The 526,280,881 Objects In The USNO-A2.0 Catalog. *Bulletin of the American Astronomical Society*, 30:1427.
- Monet, D. G., Dahn, C. C., Vrba, F. J., Harris, H. C., Pier, J. R., Luginbuhl, C. B., and Ables, H. D. (1992). U.S. Naval Observatory CCD parallaxes of faint stars. I - Program description and first results. *AJ*, 103:638–665.
- Monet, D. G., Fisher, M. D., Liebert, J., Canzian, B., Harris, H. C., and Reid, I. N. (2000). A Survey for Faint Stars of Large Proper Motion Using Extra POSS II Plates. *AJ*, 120:1541–1547.

- Nstar-website (2004). The on-line database for nearby stars. Nstar website at <http://nstars.arc.nasa.gov/index.cfm>.
- Oja, T. (1985). Photoelectric photometry of stars near the north Galactic pole. II. *A&AS*, 61:331–339.
- Oort, J. H. (1926). *The stars of high velocity*. Groningen, Gebroeders Hoitsema, 1926.
- Oppenheimer, B. R., Hambly, N. C., Digby, A. P., Hodgkin, S. T., and Saumon, D. (2001a). Direct detection of galactic halo dark matter. *Science*, 292:698–702.
- Oppenheimer, B. R., Saumon, D., Hodgkin, S. T., Jameson, R. F., Hambly, N. C., Chabrier, G., Filippenko, A. V., Coil, A. L., and Brown, M. E. (2001b). Observations of ultracool white dwarfs. *ApJ*, 550:448–456.
- Patterson, R. J., Ianna, P. A., and Begam, M. C. (1998). The Solar Neighborhood. V. VRI Photometry of Southern Nearby Star Candidates. *AJ*, 115:1648–1652.
- Pokorny, R. S., Jones, H. R. A., and Hambly, N. C. (2003). The Liverpool-Edinburgh high proper motion survey. *A&A*, 397:575–584.
- Pokorny, R. S., Jones, H. R. A., and Hambly, N. C. (2004). The Liverpool-Edinburgh high proper motion survey II. *A&A*, submitted.
- Poveda, A., Herrera, M. A., Allen, C., Cordero, G., and Lavalley, C. (1994). Statistical studies of visual double and multiple stars. II. A catalogue of nearby wide binary and multiple systems. *Revista Mexicana de Astronomia y Astrofisica*, 28:43–89.
- Reid, I. N., Brewer, C., Brucato, R. J., McKinley, W. R., Maury, A., Mendenhall, D., Mould, J. R., Mueller, J., Neugebauer, G., Phinney, J., Sargent, W. L. W., Schombert, J., and Thicksten, R. (1991). The second Palomar Sky Survey. *PASP*, 103:661–674.
- Reid, I. N., Hawley, S. L., and Gizis, J. E. (1995). The Palomar/MSU Nearby-Star Spectroscopic Survey. I. The Northern M Dwarfs -Bandstrengths and Kinematics. *AJ*, 110:2838.
- Reid, I. N., Kilkenney, D., and Cruz, K. L. (2002). Meeting the Cool Neighbors. II. Photometry of Southern NLTT Stars. *AJ*, 123:2822–2827.

- Reyl , C., Robin, A. C., Scholz, R.-D., and Irwin, M. (2002). New nearby stars selected in a high proper motion survey by DENIS photometry. *A&A*, 390:491–499.
- R ser, S. (1996). IAU symp. In *Dynamics, Ephemerides, and Astrometry of the Solar system*, volume 172, page 481, Dordrecht. Kluwer.
- Ruiz, M. T., and Anguita, C. (1993). Newly identified cold subdwarfs - LHS 375, LHS 407, LHS 3181, and LHS 3555. *AJ*, 105:614–618.
- Ruiz, M. T., and Maza, J. (1987). Discovery of very low luminosity stars. *Revista Mexicana de Astronomiay Astrofisica*, vol. 14, 14:381–384.
- Ruiz, M. T., Maza, J., Wischnjewsky, M., and Gonzalez, L. E. (1986). ER 8 - A very low luminosity degenerate star. *AJ*, 304:L25–L28.
- Ruiz, M. T., Wischnjewsky, M., Rojo, P. M., and Gonzalez, L. E. (2001). Cal n-ESO Proper-Motion Catalog. *ApJS*, 133:119–160.
- Ryan, S. G. (1989). Subdwarf studies. I - UBVRI photometry of NLTT stars. *AJ*, 98:1693–1767.
- Ryan, S. G., and Norris, J. E. (1991). Subdwarf studies. II - Abundances and kinematics from medium resolution spectra. III - The halo metallicity distribution. *AJ*, 101:1835–1864.
- Salim, S., and Gould, A. (2003). Improved Astrometry and Photometry for the Luyten Catalog. II. Faint Stars and the Revised Catalog. *AJ*, 582:1011–1031.
- Sandage, A., and Kowal, C. (1986). New subdwarfs. IV - UBVI photometry of 1690 high-proper-motion stars. *AJ*, 91:1140–1188.
- Schmidt, M. (1975). The mass of the galactic halo derived from the luminosity function of high-velocity stars. *ApJ*, 202:22–29.
- Scholz, R.-D., Irwin, M., Ibata, R., Jahreiß, H., and Malkov, O. Y. (2000). New high-proper motion survey in the Southern sky. *A&A*, 353:958–969.
- Scholz, R.-D., McCaughrean, M. J., Lodieu, N., and Kuhlbrodt, B. (2003). varepsilon Indi B: A new benchmark T dwarf. *A&A*, 398:L29–L33.

- Scholz, R.-D., Szokoly, G. P., Andersen, M., Ibata, R., and Irwin, M. J. (2002). A new wide pair of cool white dwarfs in the solar neighborhood. *ApJ*, 565:539–544.
- Skrutskie, M. F., Schneider, S. E., Stiening, R., Strom, S. E., Weinberg, M. D., Beichman, C., Chester, T., Cutri, R., Lonsdale, C., Elias, J., Elston, R., Capps, R., Carpenter, J., Huchra, J., Liebert, J., Monet, D., Price, S., and Seitzer, P. (1997). The Two Micron All Sky Survey (2MASS): Overview and Status. In *ASSL Vol. 210: The Impact of Large Scale Near-IR Sky Surveys*, page 25.
- Smart, W. M. (1977). *Textbook on Spherical Astronomy*. Cambridge University Press, Cambridge, UK.
- Soderhjelm, S. (1999). Visual binary orbits and masses post Hipparcos. *A&A*, 341:121–140.
- Stone, R. C. (1996). An accurate method for computing atmospheric refraction. *PASP*, 108:1051–1058.
- Stone, R. C. (2002). A new method for computing differential color refraction. *PASP*, 114:1070–1086.
- Stryker, L. L., Hesser, J. E., Hill, G., Garlick, G. S., and Okeefe, L. M. (1985). The binary frequency of extreme subdwarfs revisited. *PASP*, 97:247–260.
- Subasavage, J. (2004). The nearby white dwarfs samples. *AJ*, in preparation.
- Teegarden, B. J., Pravdo, S. H., Hicks, M., Lawrence, K., Shaklan, S. B., Covey, K., Fraser, O., Hawley, S. L., McGlynn, T., and Reid, I. N. (2003). Discovery of a New Nearby Star. *ApJ*, 589:L51–L53.
- ten Brummelaar, T., Mason, B. D., McAlister, H. A., Roberts, Lewis C., J., Turner, N. H., Hartkopf, W. I., and Bagnuolo, William G., J. (2000). Binary Star Differential Photometry Using the Adaptive Optics System at Mount Wilson Observatory. *AJ*, 119:2403–2414.
- Tinney, C. G. (1993). The faintest stars: trigonometric and CCD paraallaxes. *AJ*, 105:1169–1178.
- van Altena, W. F. (1974). Correction to absolute parallax and proper motion. *AJ*, 79:826–831.

- van Altena, W. F., Auer, L. H., Mora, C. L., and Vilkki, E. U. (1986). Trigonometric parallaxes determined with the Yerkes Observatory 40 inch refractor. VI - Measurements made with PDS microdensitometers. *AJ*, 91:1451–1455.
- van Altena, W. F., Lee, J. T., Hanson, R. B., and Lutz, T. E. (1988). Parallax calibration of the population II main sequence, II. The effect of changes in the corrections to absolute parallax. In Philip, A. G. D., editor, *Calibration of stellar ages*, 7, pages 175–184, Schenectady, N.Y. Van Vleck Observatory and the Institute for space observations, L. Davis Press. A meeting held at the Van Vleck Observatory, Wesleyan University, in Middletown, Connecticut, May 13–14, 1988.
- van Altena, W., Lee, J. T., and Hoffleit, D., editors (1995). *Yale Parallax Catalogue*. L. Davis Press, Schenectady, New York.
- van de Kamp, P. (1940). *Popular Astronomy*, 48:297.
- van de Kamp, P. (1967). *Principles of Astrometry*. W. H. Freeman and Company, San Francisco, CA.
- Weis, E. W. (1996). Photometry of stars with large proper motion. *AJ*, 112:2300.
- Wroblewski, H., and Costa, E. (1999). New high proper motion stars with declinations between $-5(\text{deg})$ and $-30(\text{deg})$, and right ascensions between 13h 30m and 24h. *A&AS*, 139:25–28.
- Wroblewski, H., and Costa, E. (2000). Proper motions of Luyten Catalogue stars with declinations between $-5(\text{deg})$ and $-30(\text{deg})$ and right ascensions between 13h 30m and 24h. *A&AS*, 142:369–371.
- Wroblewski, H., and Costa, E. (2001). High proper motion stars with declinations between $-30(\text{deg})$ and $-40(\text{deg})$, and right ascensions between 00 h and 10 h 40 m. *A&A*, 367:725–728.
- Wroblewski, H., and Torres, C. (1989). New proper-motion stars south of declination -40 deg and right ascension between 00 H and 04 H 30 M. *A&AS*, 78:231–247.
- Wroblewski, H., and Torres, C. (1990). New proper motion determination of Luyten catalogue stars (LTT) south of declination -40 degrees and right ascension between 00 H and 04 H 30 M. *A&AS*, 83:317–329.

- Wroblewski, H., and Torres, C. (1991). New proper-motion stars south of declination -40 deg and right ascension between 04h 30m and 16h 00m. *A&AS*, 91:129–169.
- Wroblewski, H., and Torres, C. (1992). New proper motion determination of Luyten catalogue stars (LTT) south of declination -40 deg and right ascension between 04 H 30 M and 16 H 00 M. *A&AS*, 92:449–472.
- Wroblewski, H., and Torres, C. (1994). New proper-motion stars south of declination -40deg and right ascension between 16h and 24h. *A&AS*, 105:179–210.
- Wroblewski, H., and Torres, C. (1995). New proper motion determination of Luyten catalogue stars (LTT) south of declination -40deg and right ascension between 16h and 24h. *A&AS*, 110:27.
- Wroblewski, H., and Torres, C. (1996). New proper-motion stars with declination between -5deg and -30deg and right ascension between 0h and 9h. *A&AS*, 115:481–516.
- Wroblewski, H., and Torres, C. (1997). New proper-motion stars with declination between -5d and -30d and right ascension between 9h and 13h 30m. *A&AS*, 122:447–461.
- Wroblewski, H., and Torres, C. (1998). New proper motion determination of Luyten catalogue stars (LTT) with declination between -5(deg) and -30(deg) and right ascension between 0h and 13h 30m. *A&AS*, 128:457–458.